ACCURATE RELATIVE LOCATION OF SIMILAR EARTHQUAKES

Alan L. L. Logan
B.Sc. (Imperial, London)
M.Sc. (Birmingham)

Doctor of Philosophy
University of Edinburgh
1987

I, Alan Logan, declare that this thesis was entirely my own composition and that, except where expressly stated to the contrary, the work described herein was completely carried out and written by myself.

Acknowledgements

The work contained in this thesis was undertaken in the Global Seismology Research Group of the British Geological Survey whilst also a member of the Geophysics Department of the University of Edinburgh. For this, I would like to express my appreciation to Dr Chris Browitt for allowing me the use of the facilities at BGS and Prof Ken Creer for accepting me as a student in his department. I would also like to thank the Overseas Development Administration, not only for providing me with a three year studentship and funds to visit America, but also for their support of the Turkish Dilatancy Project without which this thesis would not have been possible.

I am extremely grateful to my supervisor Dr Russ Evans for his continual support, encouragement, criticism and willingness to discuss my problems at any time which has played a major role in the eventual completion of this thesis.

The Turkish Dilatancy Project was very successful, mainly due to the efforts of Russ Evans and John Lovell for which I would like to express my thanks. In addition, I would like to thank John for the work he put in on processing the data once we had returned and for his assistance with numerous other problems that occurred throughout my four years at BGS. There are also numerous other people who helped in the smooth running of the project. In particular, I would like to thank Alistair Miller for his expertise and experience in all matters and Balamir Ucer, his family and staff, for making our stay in Turkey very enjoyable. I would also like to thank Stuart Crampin, David Booth, Sheila Peacock, Martin Russell, John McDonald and David Beamish, all of whom helped in some way.

The excellence of the computing facilities at BGS has helped me enormously and for this I am particularly grateful to Russ Evans and Charlie Fyfe. I would also like to thank my fellow students and many other members of the Global Seismology Research Group for all their assistance over the years. In addition, I would like to thank my proof-readers - John Lovell, Pete Marrow, Iain Bush, Catherine Hadwin and Sara Cox - for the excellent job they did.

Finally, I would like to express my thanks to Catherine Hadwin for her support in the last few months when my enthusiasm started to wain and to my parents who have given me their full support throughout my eight years at university and without whom none of this would have been possible.

Abstract

During the summer of 1984 the third phase of the Turkish Dilatancy Project (TDP-3) was carried out for the purpose of investigating the hypothesis of extensive dilatancy anisotropy (EDA). A network of 9 three-component and 2 single-component stations was established over a section of the North Anatolian Fault in Northwestern Turkey and data was recorded over a six month period. In total, more than 4000 earthquakes of all types were recorded and, of these, 610 were well located within the network. Further detailed analysis of the data has shown that it is consistent with the idea of EDA. The project also included a geoelectric study of the same area and, in addition to the main network, seismic data was also collected on a closely spaced (200m) array and on two subsidiary networks situated over different tectonic regimes. All the data was collected on magnetic tape but, to supplement this, a computer based triggering system was also developed.

In the TDP-3 epicentral plot much clustering of the events can be seen and a closer examination of some of these clusters (or groups) has found that several of them contain events with very similar waveforms. Such a phenomena is attributed to the events having a common source and near-identical propagation paths and it is proposed that by accurately locating the relative position of each event within a group it should be possible to examine the source in detail. A relative location method is devised that enables two similar earthquakes to be located relative to each other using the change in the S-P time between them. A cross-correlation technique is then developed that is able to measure the change in the S-P time to a precision of 0.001 seconds for the TDP data (an order of magnitude better than the digitisation interval). This can

be done in either the time domain or the frequency domain but it is shown that the time domain is to be preferred because it is computationally simpler and less sensitive to changes in the size of the window, noise and signal saturation. When the cross-correlation technique is combined with the relative location method, the overall error of each location is no greater than 20-30m and is often less.

The method is then used to analyse three groups (one divided into two sub-groups) taken from the TDP data set. For each group, strike, dip, direction of elongation and source dimension are measured and then compared with the strike, dip and rake as best defined by the first motion data and the source dimension calculated using the spectral corner frequency. The two sets of results are, in general, consistent.

Contents

Page

Acknowledgements

Abstract

Contents

1. Turkish Dilatancy Project 1984 (TDP-3)

1.1 Introduction 1

1.2 Tectonics and Seismicity 6

1.2.1 Introduction 6

1.2.2 Tectonics 6

1.2.3 Seismicity on the North Anatolian Fault 8

1.3 MARNET 11

1.4 TDP-1 and TDP-2 14

1.5 TDP-3 19

1.5.1 Introduction 19

1.5.2 Preparation for Field Programme 20

1.5.3 Field Programme 22

1.5.4 Results 28

1.5.5 Buyukcekmece and Harmancik 31

1.5.6 Array 32

1.5.7 Trigger System 32

1.5.8 Geomagnetic Study 33

1.5.9 Other Studies 36

1.6 Conclusions 36

2. Seismic Source Studies and Similar Earthquakes

2.1 Introduction 38

2.2 Source Studies 39

2.2.1 Introduction 39

2.2.2 Source Models and Parameter Measurement 41
2.2.3 f_{max} 45
2.3 Barriers, Asperities, Characteristic Earthquakes and Swarms 47
2.3.1 Introduction 47
2.3.2 Barriers and Asperities 48
2.3.3 Characteristic Earthquakes or Earthquake Families 50
2.3.4 Swarms and Similar Earthquakes 51
2.3.5 Earthquake Families and their uses 58

3. Earthquake Location and the Relative Location Method
3.1 Introduction 63
3.2 Absolute Location Method 64
3.3 Relative Location Method 66
3.3.1 Introduction 66
3.3.2 Conversion of S-P Time into Apparent Hypocentral Separation 67
3.3.3 Computational Details 70

4. Cross-Correlation Method (Theory and Analysis)
4.1 Introduction 75
4.2 Cross-Correlation Method 76
4.2.1 Introduction 76
4.2.2 The Cross-Correlation Function and the Time Delay 77
4.2.3 Delay Measurement in the Time Domain 81
4.2.4 Delay Measurement in the Frequency Domain 82
4.3 Analysis of the Cross-Correlation Method 85
4.3.1 Introduction 85
4.3.2 Time Domain versus Frequency Domain 86
4.3.3 The Effect of Changing the Start Time 88
4.3.4 The Effect of Changing the Window Length 93
4.3.5 The Effects of Noise 98
4.3.6 The Effects of Saturation 108
4.3.7 Summary 114
4.4 Discussion of the Errors 114

5. Application of the Relative Location Method on Similar Earthquakes in Turkey

5.1 Introduction 117
5.2 General Procedure 117
5.3 Group One 119
5.3.1 Introduction 119
5.3.2 Group 1 - Relative Relocation 119
5.3.3 Group 1 - Fault Plane Solution 130
5.3.4 Group 1 - Spectral Determination of the Source Dimension 133
5.4 Group Two 147
5.4.1 Introduction 147
5.4.2 Group 2A - Relative Relocation 149
5.4.3 Group 2A - Fault Plane Solution 153
5.4.4 Group 2A - Spectral Determination of the Source Dimension 155
5.4.5 Group 2B - Relative Relocation 161
5.4.6 Group 2B - Fault Plane Solution 165
5.4.7 Group 2B - Spectral Determination of the Source Dimension 167
5.4.8 Comparison of Groups 2A and 2B 172
5.5 Group Three 177
5.5.1 Introduction 177
5.5.2 Group 3 - Relative Location 177
5.5.3 Group 3 - Fault Plane Solution 181
5.5.4 Group 3 - Spectral Determination of the Source Dimension 184

6. Summary and Conclusions

6.1 Summary 189
6.2 Conclusions 192
6.3 Improvements and Suggestions for Further Work 197

References 200
Appendix 1 - Computer Program Listing (RELOC) 213
Appendix 2 - Computer Program Listing (SERDEL) 221
Appendix 3 - Frequency Domain Method 245

Chapter 1

Turkish Dilatancy Project 1984 (TDP-3)

1.1 Introduction

Turkey is one of the most seismically active countries in the world and throughout history it has been devastated by a number of large earthquakes. However, their relative infrequency and ignorance of their origin has done nothing to deter civilisations from concentrating their populations in high risk areas. One such area is in Northwestern Turkey (see Fig. 1.1) where a branch of the North Anatolian Fault runs east-west beneath the Marmara Sea and close to the cities of Istanbul and Izmit (Evans *et al.*, 1985). This area, apart from containing a large percentage of modern Turkey's population, is also the country's major industrial region and its importance to the Turkish economy cannot be underestimated.

For this reason, there have been a number of seismic risk studies carried out in Western Turkey that attempt to pinpoint the more vulnerable regions and estimate likely recurrence times and ground accelerations that might be experienced. Such information can be used for the compilation of building codes and thereafter in the planning of future developments and for safety evaluation of existing structures. The recurrence times that are calculated are generally statistical measurements of the average time span between large earthquakes and have an accuracy of the order of many years. They are able to give some idea of when the next large earthquake is likely to occur and hence can be considered to be an elementary form of earthquake prediction. Improving upon

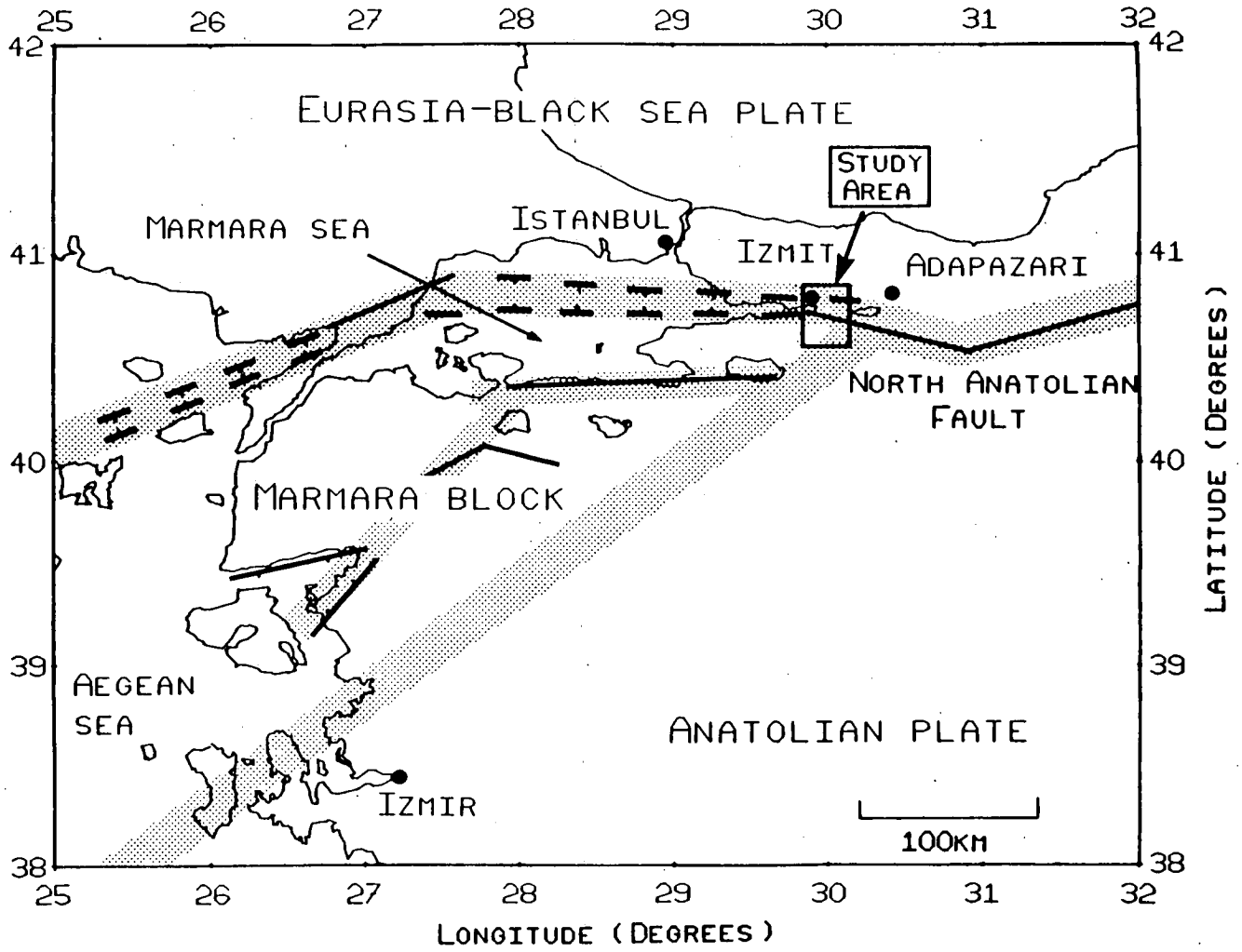

Fig. 1.1 - Major tectonic features of Northwestern Turkey. The North Anatolian Fault runs east-west through the Marmara Sea and into the Aegean Sea, separating the Eurasian-Black Sea plate from the Anatolian plate. Seismically active areas are shown stippled. The TDP-3 study area is also marked.

the accuracy of this prediction is a problem that geophysicists have been working on for many years.

The first serious attempt to investigate the possibilities of earthquake prediction was made by the Japanese who, in the early 1960's, set up a nationwide earthquake prediction programme. Soon afterwards the Americans began to encourage research into the subject which eventually led to the formation of their own nationwide programme in 1974. Several other countries have also made a significant step in this direction, most notably the USSR and China. As a result of the work carried out within these projects over the last twenty five years, there have been numerous theories developed, some surviving and some not, mostly based on observational data taken from a wide variety of geophysical disciplines. For a complete and relatively up-to-date review of the state of earthquake prediction the reader is referred to Rikitake (1976).

One of the more exciting discoveries was made in Garm, USSR, during a study of seismic wave velocities. It was found that the ratio of the P wave velocity (V_p) to the S wave velocity (V_s) decreased prior to a moderately large earthquake. Further work in the USSR and America revealed that the V_p/V_s ratio first drops and then recovers before the earthquake and that the length of the anomalous period closely correlates with the magnitude of the forthcoming earthquake. Similar observations were also reported from Japan and China. Attempts to explain the cause of these observations have led to the development of the dilatancy model (Scholz *et al.*, 1973).

Based on laboratory fracture studies it was suggested that rock under stress undergoes an inelastic volumetric increase due to the opening of microcracks parallel to the axis of maximum compression (dilatancy). This occurs when the stress at the crack tip reaches a critical point. In the dilatancy model it is proposed that the build up of tectonic stress prior to an earthquake produces a slow steady increase in the effective stress, eventually reaching the point where dilatancy occurs. As

the cracks grow, surrounding pore fluid will flow into them, but at a slower rate than that with which the cracks are growing. Consequently the rock becomes undersaturated which has the effect of decreasing V_p but not V_s (V_s is not dependant upon the fluid content). The resultant drop in pore pressure increases the effective stress which strengthens the rock and slows down the dilatancy (dilatancy hardening) until the rate of fluid flow into the region is greater than the rate of crack growth. V_p then begins to rise until saturation of the rock is achieved at a minimum pore pressure. Finally, the pore pressure builds up and it is thought that this triggers the earthquake. Apart from being able to explain the drop in the V_p/V_s ratio, the dilatancy model has also been able to account for other precursory effects such as land uplift, decrease in electrical resistivity and increase in radon emission.

In 1978 it was suggested that seismic anisotropy might exist in dilatant regions as a result of the crack alignment caused by the tectonic stress field (Crampin, 1978). It was proposed to investigate the anisotropy by monitoring the records of local earthquakes and examining them for evidence of shear wave splitting. A shear wave train passing through an anisotropic region is split into two components, each component travelling at a different velocity, with the leading component parallel to the crack alignment. The delay introduced between the two components is then preserved throughout the remainder of the propagation path in isotropic media. At the surface the split shear wave can be observed using polarisation diagrams (particle motion plots) and both the polarisation of the first arrival and the time delay between the two arrivals can be measured. The predominant direction of the local stress field can then be deduced from the polarisation of the first arrival since this is dependent upon the crack alignment which, in turn, is dependent upon the stress. The time delay between the two arrivals is determined by both the degree of anisotropy and the size of the anisotropic region. It is proposed that any change in the stress prior to an earthquake is most likely to show up as a change in the time delay since it is either the degree of anisotropy or its regional extent that

will change rather than the alignment of the cracks. Continuous monitoring of local earthquakes could prove to be useful for analysing the stress and looking for precursory effects prior to large earthquakes (Crampin *et al.*, 1984).

To test these ideas a project was designed to record local earthquakes on a section of the North Anatolian Fault in Northwestern Turkey. The first phase of the Turkish Dilatancy Project (TDP-1) took place during the summer of 1979 with a second phase (TDP-2) following on during the summer of 1980. The work was carried out by the Institute of Geological Sciences (now the British Geological Survey) in collaboration with Kandilli Observatory, Istanbul (now Kandilli Observatory and Centre for Research and Development in Space and Earth Sciences). It followed on from a joint project, financed by the Overseas Development Administration, in which MARNET, a telemetered seismic network spanning the Marmara Sea, was installed (Ucer *et al.*, 1985).

The dilatancy model, proposed above, relies upon the stress at the crack tip reaching a critical point, which implies that dilatant/anisotropic regions are likely to be very localised. However, shear wave splitting was observed on many of the records from TDP-1 and TDP-2 (Crampin *et al.*, 1984 & 1985) suggesting that anisotropy is fairly well distributed throughout the crust. To account for this observation, the theory of extensive dilatancy anisotropy (EDA) was developed. Laboratory studies have indicated that the growth of fluid-filled cracks can occur at sub-critical stress levels (Atkinson, 1979, 1982 & 1984). If this occurs within the crust then anisotropy is likely to be much more widespread (Crampin *et al.*, 1982 & 1984).

Another important discovery made during TDP-1 and TDP-2 was that shear waves meeting the free surface at angles greater than the critical angle ($\sin^{-1}(V_p/V_s)$, approximately 35^o) can be greatly distorted by mode conversions and phase and amplitude changes (Evans, 1984; Booth and Crampin, 1985). This discovery led to the concept of a shear wave window: an area on the surface

within which shear wave arrivals meet the surface at less than the critical angle and so will be free of surface effects. Stations outside the shear wave window will be of little use for looking at dilatancy since their records of shear wave splitting will be unreliable (Booth and Crampin, 1985). The shear wave window may also be locally distorted by topographic effects.

Bearing these developments in mind, a third phase of the project was planned (TDP-3) which took place during the summer of 1984. In addition to the seismic survey, an electromagnetic survey was also included which was carried out by the Geomagnetism Research Group of the British Geological Survey. The remainder of this chapter will look at TDP-3 in some detail, including a closer look at the background to the project and will present some preliminary results. It is the data set collected during this phase which will be predominantly used in the following chapters.

1.2 Tectonics and Seismicity

1.2.1 Introduction

The complex tectonic structure of the Eastern Mediterranean is a subject that is not easily summarised in a few sentences. Much research has been done on the subject over the last decade and although there is now general agreement on the more basic issues involved, there is still a certain amount of controversy over some of the details. The following is a brief review of some of the more established ideas on the tectonics relevant to Northwestern Turkey and will include a look at the seismicity of the area, past and present.

1.2.2 Tectonics

The general outline of the plates as they exist today is shown in Fig. 1.2 (based on McKenzie, 1972). The direction in which each plate is moving, relative to the Eurasian plate, is shown by an arrow and the length of each arrow is proportional to the magnitude of the relative velocity.

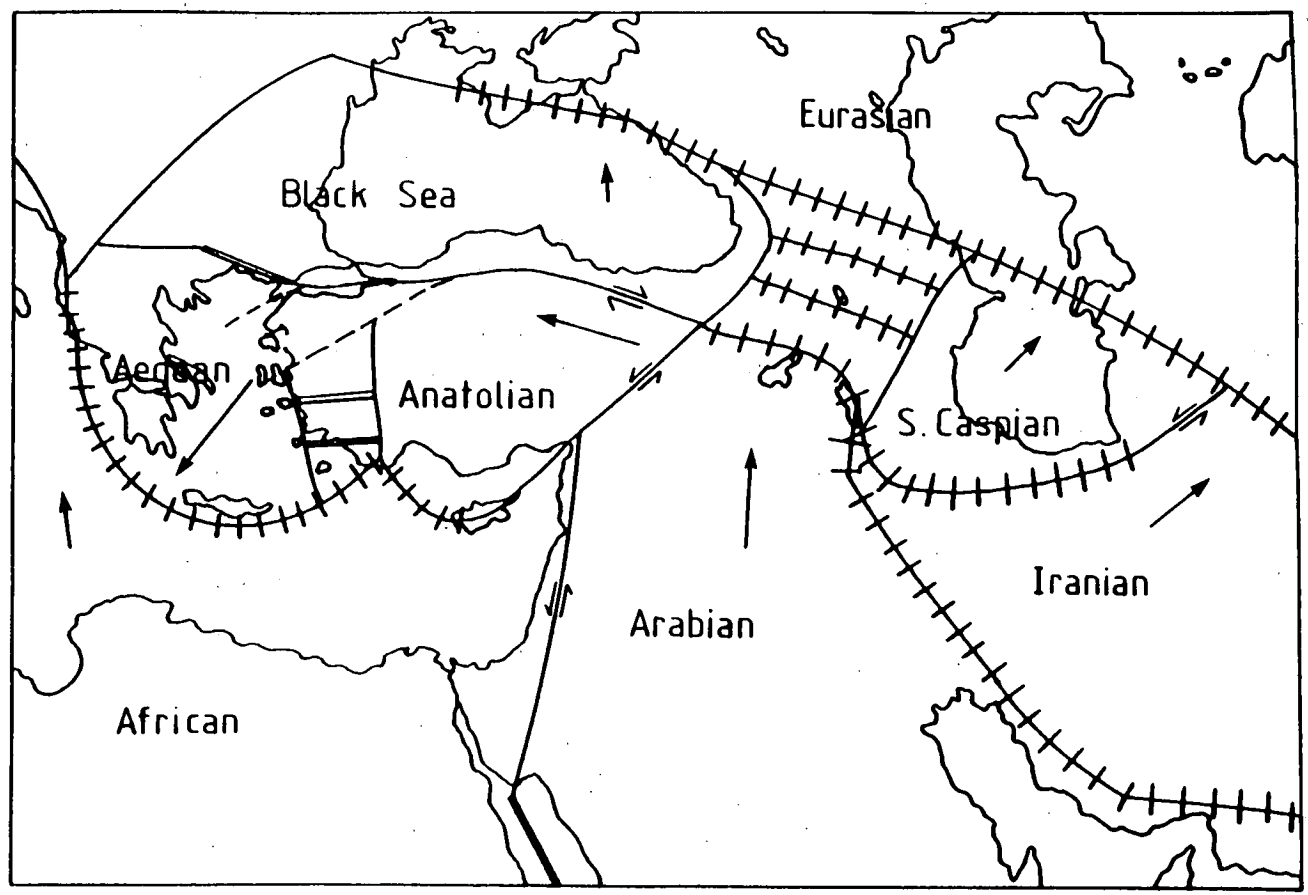

Fig. 1.2 - General outline of the plates in the Eastern Mediterranean region (based on McKenzie, 1972). The arrows indicate the direction of motion of each plate relative to the Eurasian plate with length proportional to the magnitude of the relative velocity. A single line indicates transcurrent faulting, a double line represents normal faulting and thrusting is represented by a single line with bars.

The driving force behind the movements in this area comes from the collision that took place in the early Tertiary between the northward moving African plate and the Eurasian plate. The collision had the effect of finally closing the Tethyan Ocean that had previously separated the two plates (Sengor, 1984). There also existed a Palaeotethyan plate that was gradually subducted prior to the collision, of which the Black Sea plate (Fig. 1.2) is thought to be the last remnant (Dewey *et al.*, 1973; Sengor, 1984). In addition, it is thought that the Anatolian plate may consist of several continental fragments gathered from the Tethyan Ocean.

After the African-Eurasian collision the Arabian plate to the east broke away from the African plate and continued in a northward direction until it collided with the Anatolian and Black Sea plates. As a result, the Anatolian plate was 'pinched out' and started moving rapidly westwards. This was the start of the North Anatolian Fault and occurred about ten million years ago, during the middle to late Miocene (Dewey and Sengor, 1979). The westward movement of the Anatolian plate is still relatively rapid and takes it into an area being vacated by the Aegean plate.

It is this area (Western Turkey and the Aegean) and its relation to the surrounding regions that has caused much of the controversy over the years. The faulting in the area is predominantly normal which is an unexpected feature of a collision zone since normal faulting would usually imply an extensional regime. Several theories have been put forward to try and fit this into the regional pattern but the complexity of the problem means that no single theory has been able to overcome all of the inconsistencies. The most widely accepted theories put forward so far include those of McKenzie (1972, 1978), Makris (1976) and Le Pichon and Angelier (1979, 1981). A review can be found in Main (1985).

1.2.3 Seismicity on the North Anatolian Fault

The North Anatolian Fault runs east-west across Northern Turkey starting at 41^{o}E at the junction with the East Anatolian

Fault and forms a well defined band of strike-slip faulting as far as Mudurnu at 31°E. Here it divides into a number of branches: at least one running southwestwards past the city of Bursa and on into Western Anatolia; and one continuing the east-west line into the Marmara Sea and south of Istanbul before fading away into the Aegean Sea. To the west of Adapazari, the east-west running branch is quite clearly defined by a half graben type feature which has resulted in the formation of Lake Sapanca and Izmit Bay (the eastern arm of the Marmara Sea).

The North Anatolian Fault is seismically very active and over the centuries has produced many large and devastating earthquakes with an average period of 10 - 20 years. In the eastern Marmara region there have been several major earthquakes including the Cinarcik earthquake of 1963 (Dewey, 1976) and the Adapazari earthquakes of 1878 and 1894 (Ambraseys and Zatopek, 1969; Karnik, 1971), suggesting that the region is currently being deformed. To the east it has been widely noted that a series of large earthquakes starting in 1939, at Erzincan in eastern Turkey (39°E), and ending in 1967, at Mudurnu (31°E), form a westward migrating sequence (Pamir, 1944; Ambraseys and Zatopek, 1969; Dewey, 1976; Toksoz *et al.*, 1979). Together, this evidence led Toksoz *et al.* (1979) to suggest that the Izmit Bay region is a seismic gap between the westward migrating sequence to the east and the Cinarcik earthquake of 1963 to the west. In other words, unless strain is being released by some other process, such as aseismic creep, the area may experience a large earthquake sometime in the relatively near future. All earthquakes mentioned in the text are listed in table 1.1.

It is within this seismic gap that the study area for the Turkish Dilatancy Projects was chosen. It is centred in the mountains just south of the half graben containing Lake Sapanca and Izmit Bay, southeast of the city of Izmit and approximately 100km east of Istanbul. The location of the study area is shown in fig. 1.1.

Locality	Date	Time (h m)	Lat. (^{o}N)	Long. (^{o}E)	M_s	Source
Adapazari	1878.04.19	(0900)	(40.8)	(29.0)	(6.7)	Karnik (1971)
Adapazari	1894.07.10	(1233)	(40.6)	(28.7)	(6.1)	Karnik (1971)
Erzincan	1939.12.26	2357	39.8	39.4	8.0	Dewey (1976)
Niksar	1942.12.20	1403	40.7	36.4	7.0	Dewey (1976)
Combiri	1943.11.26	2220	41.0	33.2	7.3	Dewey (1976)
Bolu	1944.02.01	0322	41.1	33.2	7.3	Dewey (1976)
Kursunlu	1951.08.13	1833	40.9	32.7	6.8	Dewey (1976)
Abant	1957.05.26	0633	40.6	31.0	7.0	Dewey (1976)
Cinarcik	1963.09.18	1658	40.7	29.1	6.2	Dewey (1976)
Mudurnu	1967.07.30	1656	40.6	30.8	6.9	Dewey (1976)

Table 1.1 - List of all major earthquakes mentioned in the text.

The general level of seismicity in this area, relative to the rest of Western Turkey, can be judged from the epicentral plot of the earthquakes recorded by Kandilli Observatory between 1976 and 1981 (Fig. 1.3). It should be noted that the locations are slightly biased in favour of the northwest since there is a higher density of stations there (see fig. 1.4). There are two trends within the epicentres that can be seen in fig. 1.3 and these are marked by two lines (AB and CD). The upper one of these trends (AB) follows the line of the North Anatolian Fault into the Marmara Sea and beyond, whilst the other, more obvious, trend (CD) runs southwestwards to the Aegean coast. It has been suggested that this second seismic lineation runs down another branch of the North Anatolian Fault (Ucer *et al.*, 1985). In the southwest (below line CD) the seismic activity is generally extensional in nature as it is beneath a large part of the Aegean Sea.

The study area for the Turkish Dilatancy Project is above the eastern most swarm that can be seen on line AB.

1.3 MARNET

As mentioned in section 1.1, the Marmara Sea region is Turkey's major industrial area and the prospect of a large earthquake is of great concern because of the havoc it could cause to the Turkish economy. It is, therefore, desirable to be able to assess the seismic risk in the area and for this the regional seismicity needs to be known in some detail.

Between 1970 and 1974, a network of twelve short period instruments was set up over Western Turkey. In 1978, in collaboration with the British Geological Survey and funded by the Overseas Development Administration, a second network of six stations was developed by Kandilli Observatory (Ucer *et al.*, 1985). These stations spanned the Marmara Sea and were radiolinked to the observatory in Istanbul. The network was given the name MARNET and the distribution of its stations is shown in figure 1.4, along with the original network.

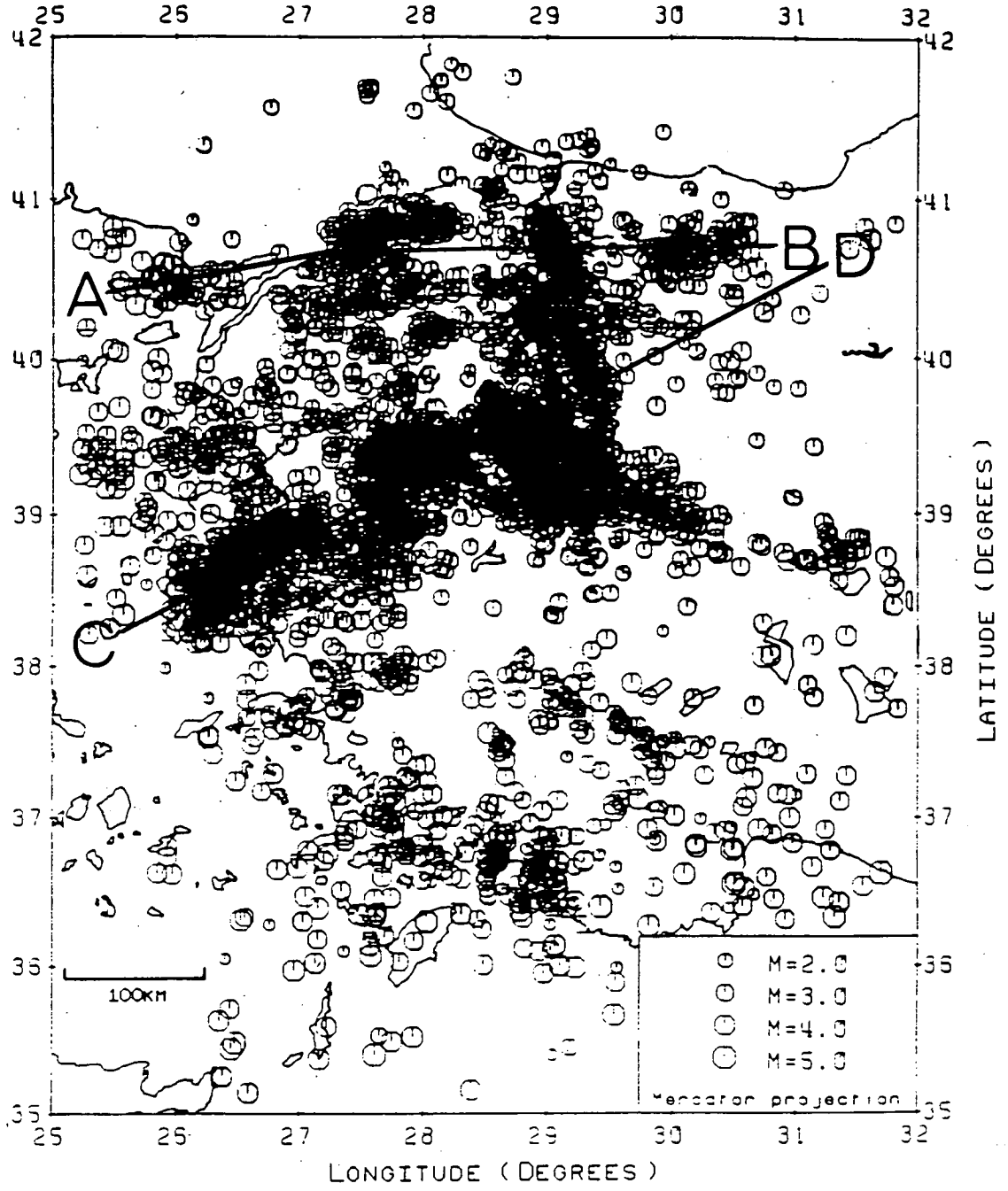

Fig. 1.3 - Epicentral plot of all well located earthquakes recorded by Kandilli Observatory in Western Turkey between 1976 and 1981. There is a slight bias in favour of the NW due to the greater concentration of stations there.

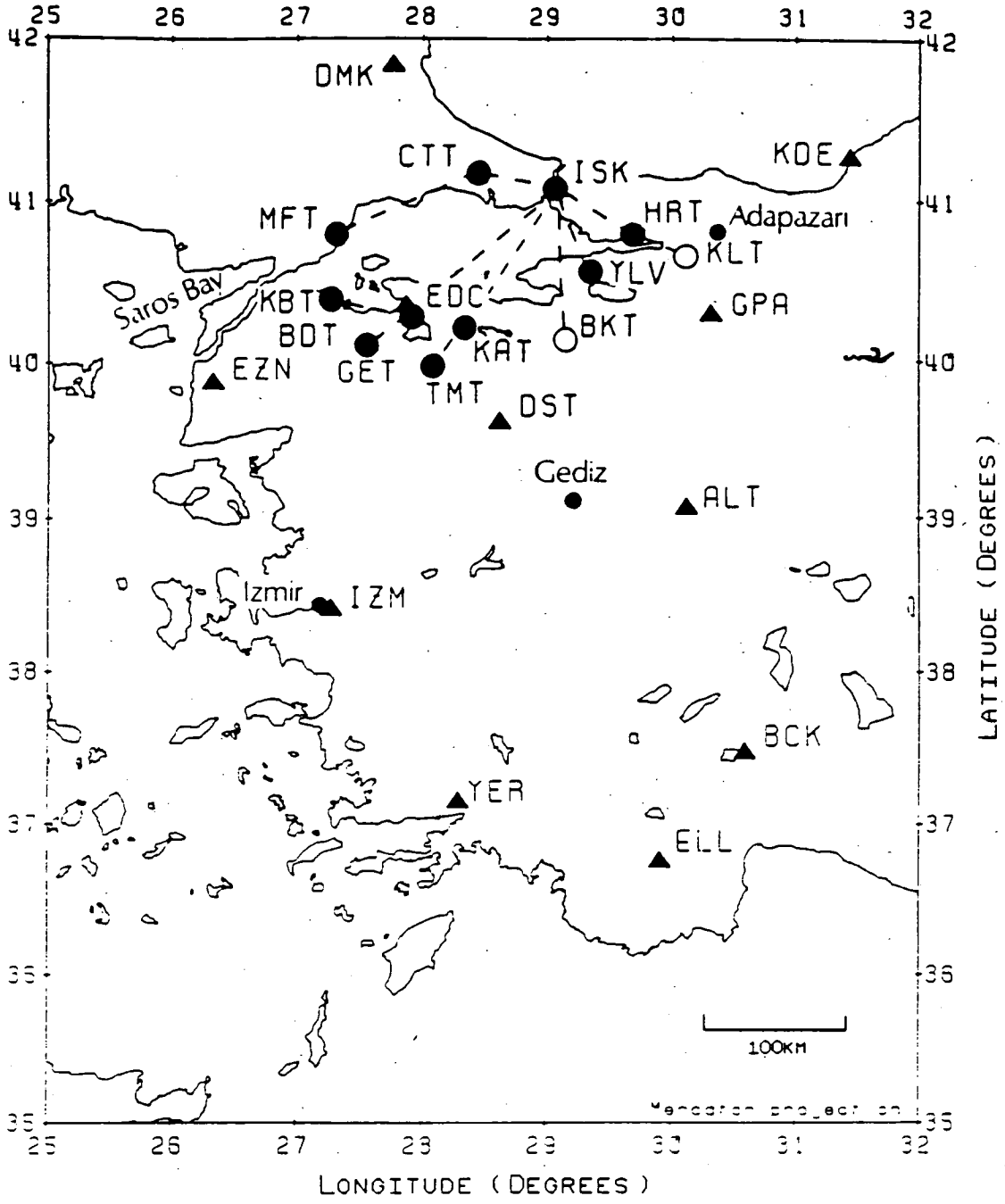

Fig. 1.4 - Seismic stations operated by Kandilli Observatory in Western Turkey. Circles are stations of the Marmara Sea network (MARNET) telemetered to the station in Istanbul (ISK), and tiangles are ISK stations that record on paper drums. Open symbols indicate stations that have now been dismantled.

It was by using the records from MARNET in conjunction with the known regional seismicity and local tectonics that the area for the Turkish Dilatancy Projects was selected. An active swarm of small earthquakes was detected near the station of Keltepe (KLT in Fig. 1.4) which appeared to be suitable for the study. A more accurate location for the swarm was established by setting up two manned temporary stations in the area for one day and monitoring all local seismicity. From these results the layout of the main network was worked out.

1.4 TDP-1 and TDP-2

The first phase of the Turkish Dilatancy Project (TDP-1) took place during the summer of 1979 in the area described in section 1.2.3. The network was operational for six weeks and consisted of 8 three-component stations, the layout for which is shown in Fig. 1.5. For the second phase (TDP-2), the coverage of the focal sphere was improved by increasing the number of stations to nine, while the operational time was increased to nine weeks. The layout is shown in Fig. 1.6. In both projects the stations were telemetered to a base station where the analogue signals were recorded on magnetic tape.

From the TDP-1 data set 145 local events could be located using HYP071 (Lee and Lahr, 1975) and their epicentres are shown in Fig. 1.7. For TDP-2 205 events were located and these are shown in Fig. 1.8.

The model used in the location procedure was determined during TDP-1 by timing several nearby explosions. The model is a relatively simple one since the waves from the explosions would not have sampled particularly great depths. Fortunately, for the analysis of shear wave splitting accuracy in the hypocentral location is not too important.

Shear wave splitting was clearly observed in both sets of data, leading to further developments on the hypothesis of EDA as explained in the introduction (section 1.1). Unfortunately, the

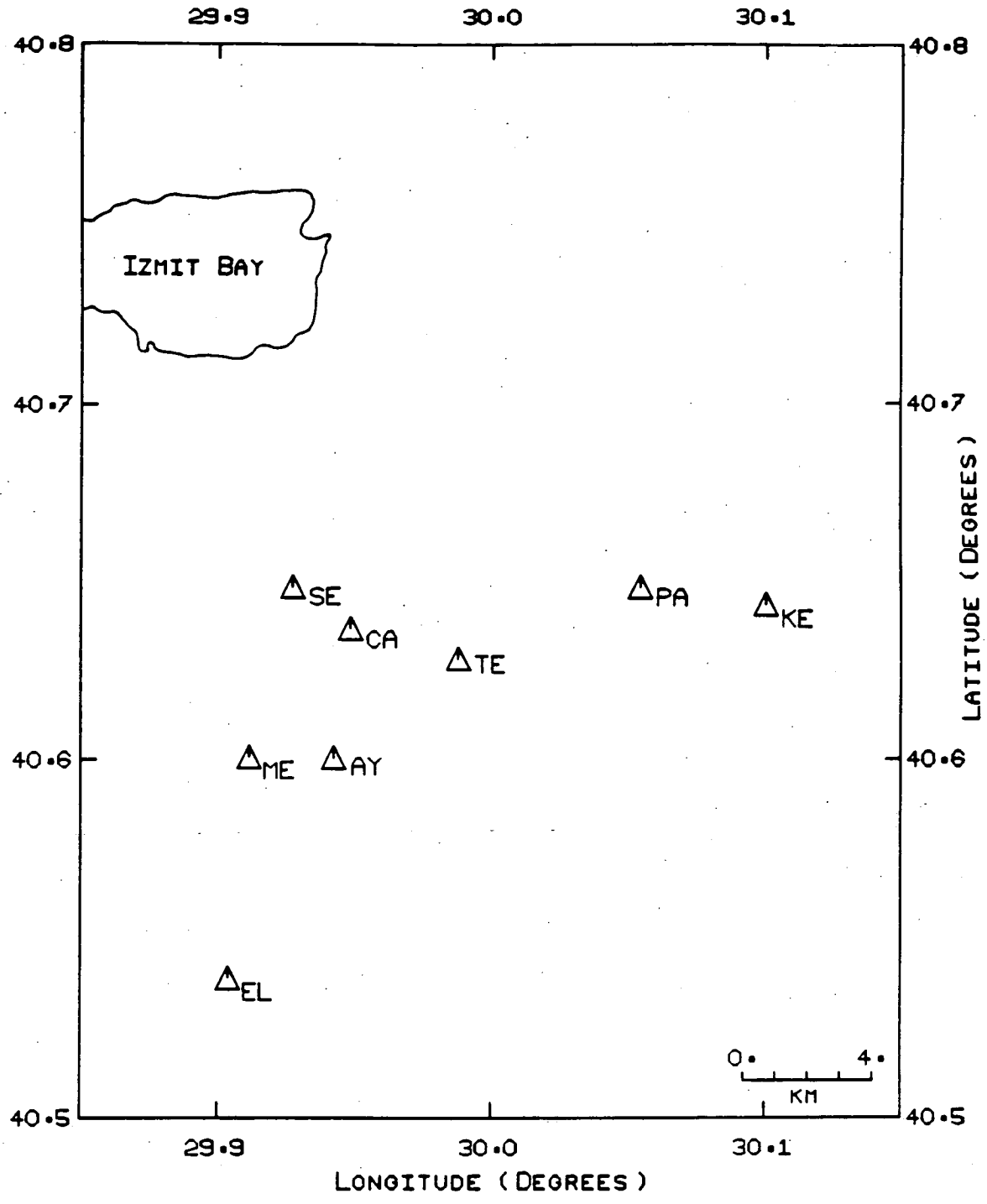

Fig. 1.5 - Station layout for TDP-1 (1979).

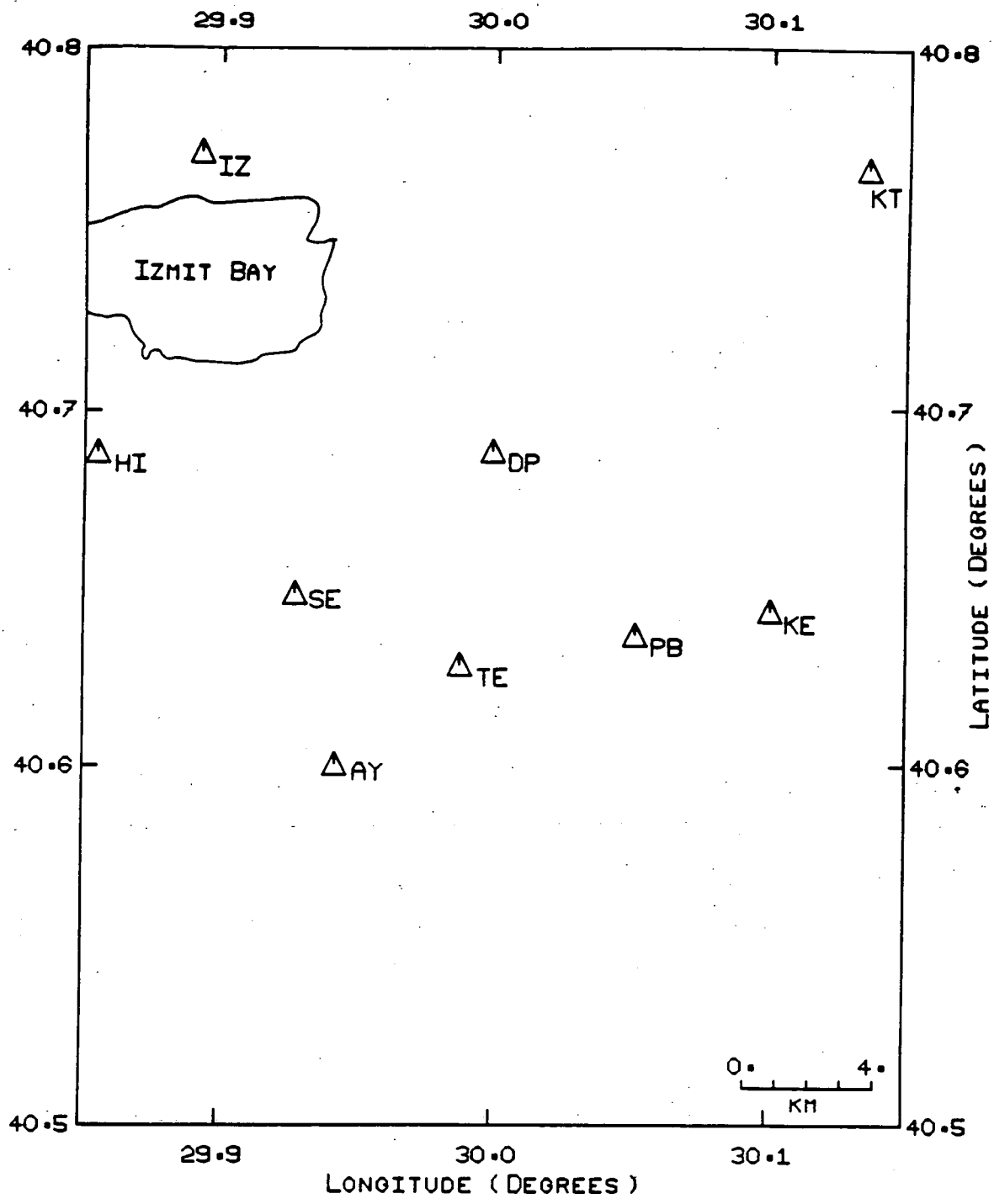

Fig. 1.6 - Station layout for TDP-2 (1980).

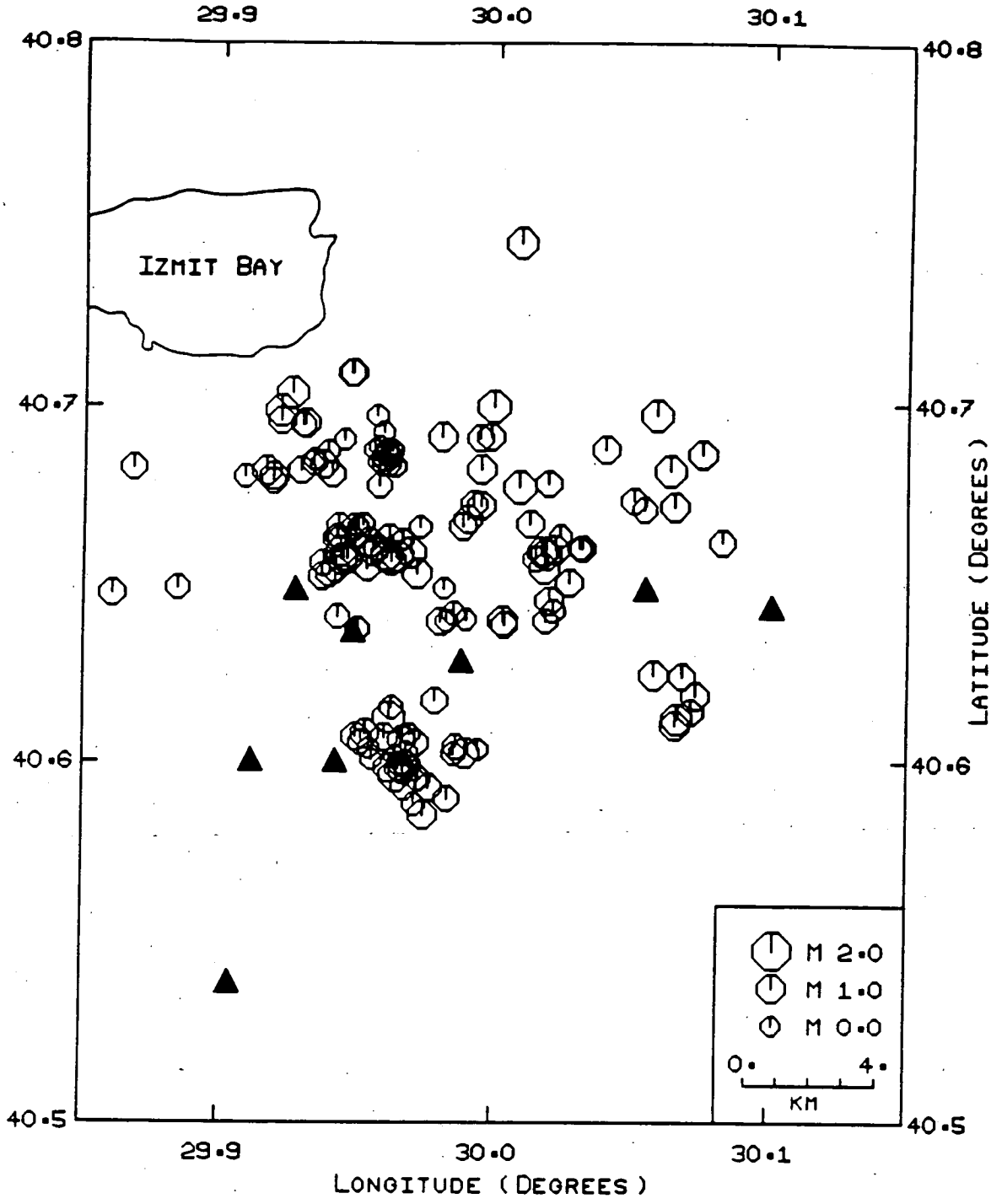

Fig. 1.7 - Epicentral plot of the 145 events recorded during TDP-1 (triangles indicate the station locations).

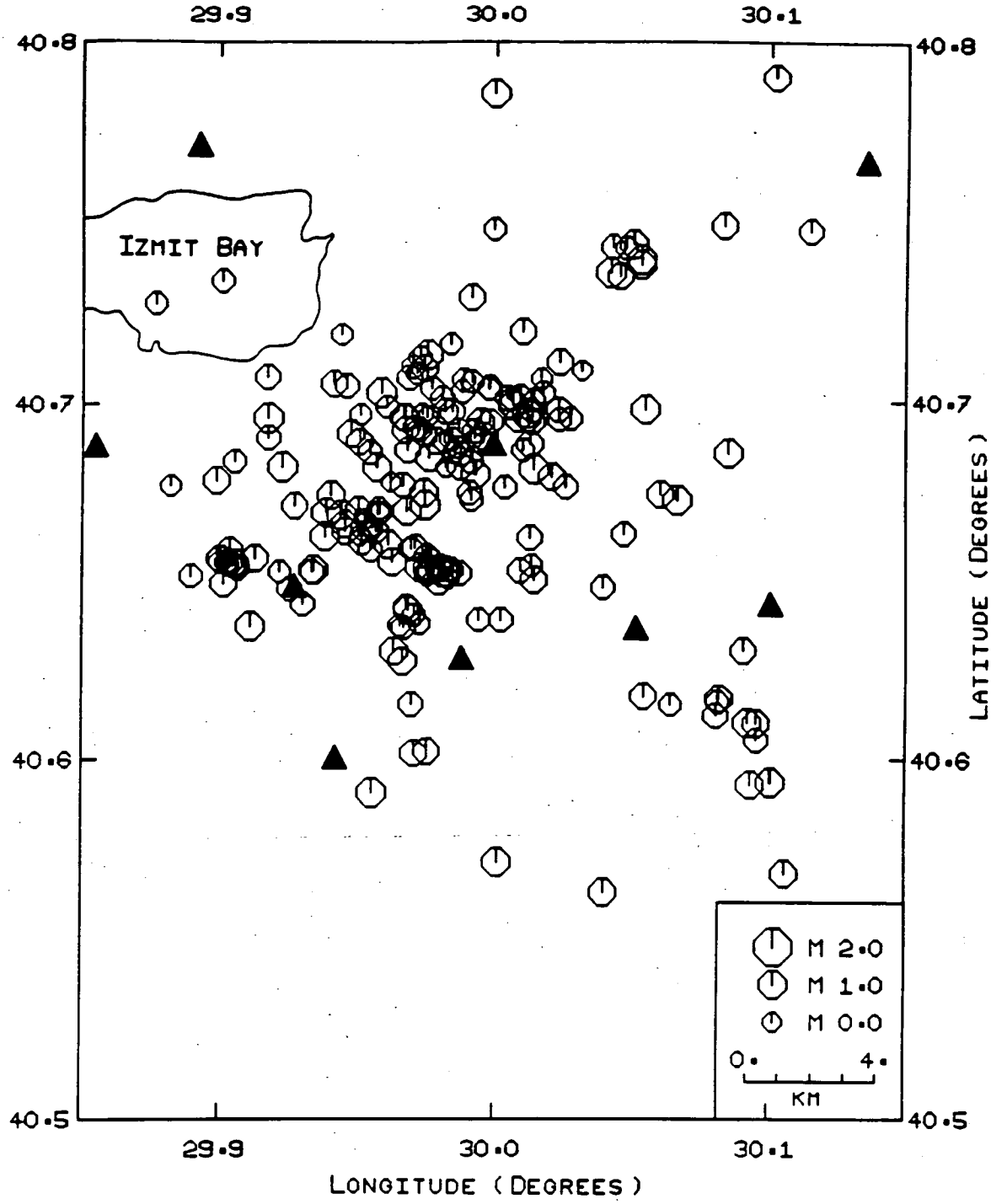

Fig. 1.8 - Epicentral plot of the 205 events recorded during TDP-2 (triangles indicate the station locations).

TDP-2 data set is somewhat limited because the significance of the shear wave window had not yet been realised and the network was too widely spread.

1.5 TDP-3

1.5.1 Introduction

The first two phases of the Turkish Dilatancy Project (TDP-1 and TDP-2) were very successful in helping to develop ideas on seismic anisotropy and how best to observe it. To follow up on this, a third phase was planned to study the same area for a longer period, using a greater variety of geophysical methods (TDP-3). Funding was provided by the Overseas Development Administration for a budget scheduled over a three year period.

The area has been designated a seismic gap (Toksoz *et al.*, 1979) and a sizeable earthquake is expected in the near future (section 1.2.3). Theory predicts that prior to an earthquake the stress in the area will build up and it is hoped that some form of earthquake prediction method can be developed by monitoring the stress and observing this build up. One of the aims of the project is to try and observe changes of stress with time by monitoring the resultant changes in the geophysical parameters.

The study took place from April to November 1984. The main project team was comprised of three staff members from the Global Seismology Research Group (Dr. J.R.Evans, J.Lovell, A.Miller), two staff members from the Geomagnetism Research Group (Dr. D.Beamish, J.McDonald) and two students (A.Logan, M.Russell). Additional assistance was kindly given by S.Crampin, D.Booth and S.Peacock at various times throughout the project. Whilst in Turkey, all work was carried out in collaboration with colleagues at Kandilli Observatory, Istanbul, in particular, B.Ucer and N.Kafadar. The main network was run continuously throughout the whole period of the study and more than 4000 earthquakes were recorded, approximately half of which had epicentres within, or very close to, the study area. Eliminating events that were too small to be

located reduced the number of well determined events to 610.

Other work carried out during the project included the development of a computer based triggering system (see section 1.5.7). It was able to monitor several input channels at once and trigger by looking for amplitudes well above the norm. If a certain number of the channels triggered at the same time then the computer would record the assumed event on disk. The system was tested on the main network, MARNET and on a small array of six stations that was established within the study area. This array ran for a period of two months and it is hoped that the data will be of use for looking at topographic and site effects (see section 1.5.6).

In addition to the main network, two small subsidiary studies were carried out for short periods in the Buyukcekmece and Harmancik areas, shown in Fig. 1.9. These networks were situated over different fault structures and it was hoped that they would yield data for comparison with the main study area. Unfortunately, in both areas the seismicity levels were low and the only useful data were recorded from local quarry blasts and from regional and teleseismic earthquakes.

1.5.2 Preparation for Field Programme

The project started officially in March 1983. In October 1983, Drs. J.R. Evans and D. Beamish spent two weeks in Turkey finalising some of the details of plans laid down in the previous six months. They were able to inspect facilities at Kandilli Observatory and spent seven days in the field looking at potential field sites, both for field stations and for a base. Discussions with British Council staff helped clear the way for the haulage and importation of project equipment and numerous other discussions helped to ensure the goodwill necessary for the smooth running of the project.

The six months prior to the start of the field programme in April 1984 were spent checking, repairing and calibrating

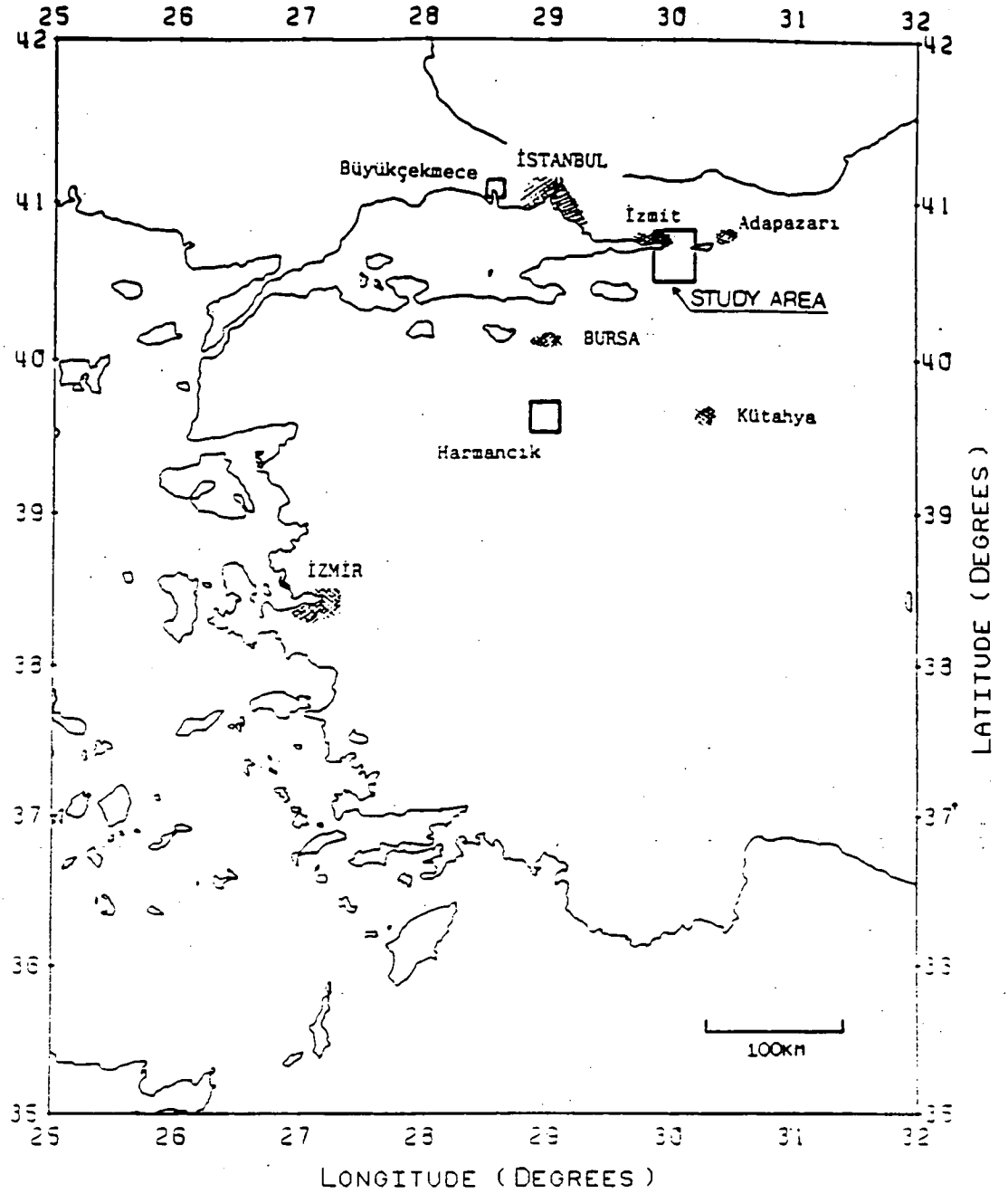

Fig. 1.9 - Western Turkey showing the location of two subsidiary networks at Buyukcemece and Harmancik in relation to the main study area.

equipment for the field and in the preparation of software for data collection, analysis and presentation of the data. In total, 45 seismometer systems were taken out, each system consisting of a seismometer (Willmore Mk. III), amplifier modulator, radio transmitter and receiver with aerials and a power supply. The data were to be recorded on four Geostores and replayed through a Store14, filter bank and jetpen recorder. All of this equipment had to be checked to see that it was functioning correctly, that the seismometers were set to a period of one second and that the amplifier modulators and radios were tuned to the correct frequencies. The equipment was drawn from both the NERC equipment pool and the stock of equipment held by the Global Seismology Research Group.

Three PDP-11 computer systems were purchased for the project. Two of the computers were to be used as triggering systems and the third for data analysis and quality control. The programs used by the triggering systems were tested for several months on LOWNET - an eight station network in Central Scotland telemetered to the BGS office in Edinburgh (Crampin *et al.*, 1970; Turbitt *et al.*, 1985). For the data analysis system most of the software that was needed had already been written. The location program HYP071 (Lee and Lahr, 1975) had to be converted from a program designed to work on a main frame computer to one suitable for the PDP-11. This program, as well as the analysis system as a whole, was thoroughly tested before being sent out.

All of this equipment and more (tool kits, test bench facilities, etc.) was then packed up and dispatched overland to Turkey in March 1984. In total, 6.5 tonnes of equipment, worth approximately £500,000, was sent, including a consignment from the Geomagnetism Group. It arrived in Turkey at the beginning of April without any problems occurring at customs.

1.5.3 Field Programme

For the duration of the project Kandilli Observatory was able to provide several buildings for use as laboratories and living

accommodation. The Observatory, which has recently been attached to Bogazici University, sits on a hill on the eastern side of Bosphorus, allowing easy access to the motorway and then on to the study area, Istanbul or the airport. The Observatory was able to provide personnel who could accompany trips into the field to act either as translators and/or to carry out negotiations, as well as provide backup vehicles with drivers for use during busy periods.

Two laboratories (one for seismology, one for geomagnetism) and a store room were set up in one of the buildings. The rooms were reasonably large and being north-facing meant that they stayed relatively cool during the heat of the summer. The seismology laboratory was set up to contain the replay system, data analysis computer and repair benches, with excess space being used for storage of computer equipment and tapes. The geomagnetism laboratory was similarly set up with analysis system and repair bench.

The study area lay approximately 100km east of Istanbul just off the main Istanbul-Ankara road and so access to it was relatively easy. On extended trips to the field, accommodation could be found in the city of Izmit.

The network was set up during April 1984. Initially, seven three-component stations were installed and radiolinked to the base station at Hereke, a little way outside the study area on the road to Istanbul (HRT in fig. 1.4). During the study period two further three-component and two single component stations were installed to make a total of eleven. Fig. 1.10 shows the layout of the stations and table 1.2 lists their details (location and the dates when they were installed and dismantled).

Each component in the network was set up identically, as shown diagrammatically in Fig. 1.11. The signal produced by the seismometer was fed into the amplifier modulator where it was amplified and frequency modulated to a centre frequency of 676Hz. The modulated signal then went to the radio transmitter where it was frequency modulated again using a frequency of several hundred

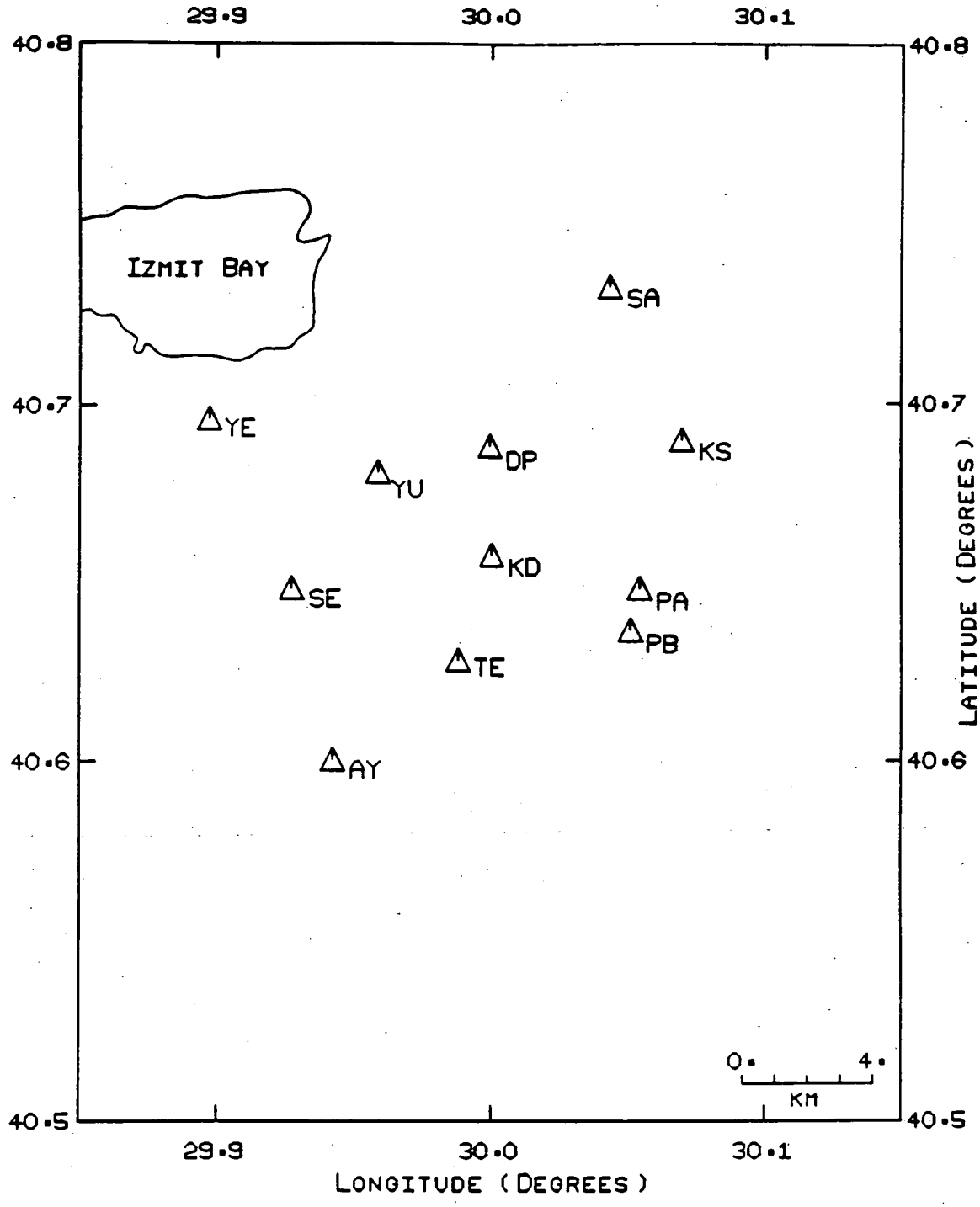

Fig. 1.10 - Station layout for TDP-3 (1984).

Station	Lat. (°N)	Long. (°E)	Ht. (m)	No. of compts.	Installed	Dismantled
AY	40.6005	29.9425	995	3	30 Apr	28 Oct
DP	40.6992	29.9995	190	3	29 Apr	28 Oct
KD	40.6577	30.0002	593	3	30 Jun	25 Aug
KS	40.6900	30.0700	140	3	2 May	28 Oct
PA	40.6485	30.0547	990	3	21 Jun	18 Jul
PB	40.6368	30.0515	847	3	2 May	27 Oct
SA	40.7325	30.0438	44	1	12 May	28 Oct
SE	40.6485	29.9275	614	3	29 Apr	27 Oct
TE	40.6283	29.9880	648	3	3 May	27 Oct
YE	40.6960	29.8973	47	1	4 Jun	25 Aug
YU	40.6810	29.9587	380	3	15 May	27 Oct

Table 1.2 - Details of all TDP-3 stations including the location, number of components and the dates on which they were installed and dismantled.

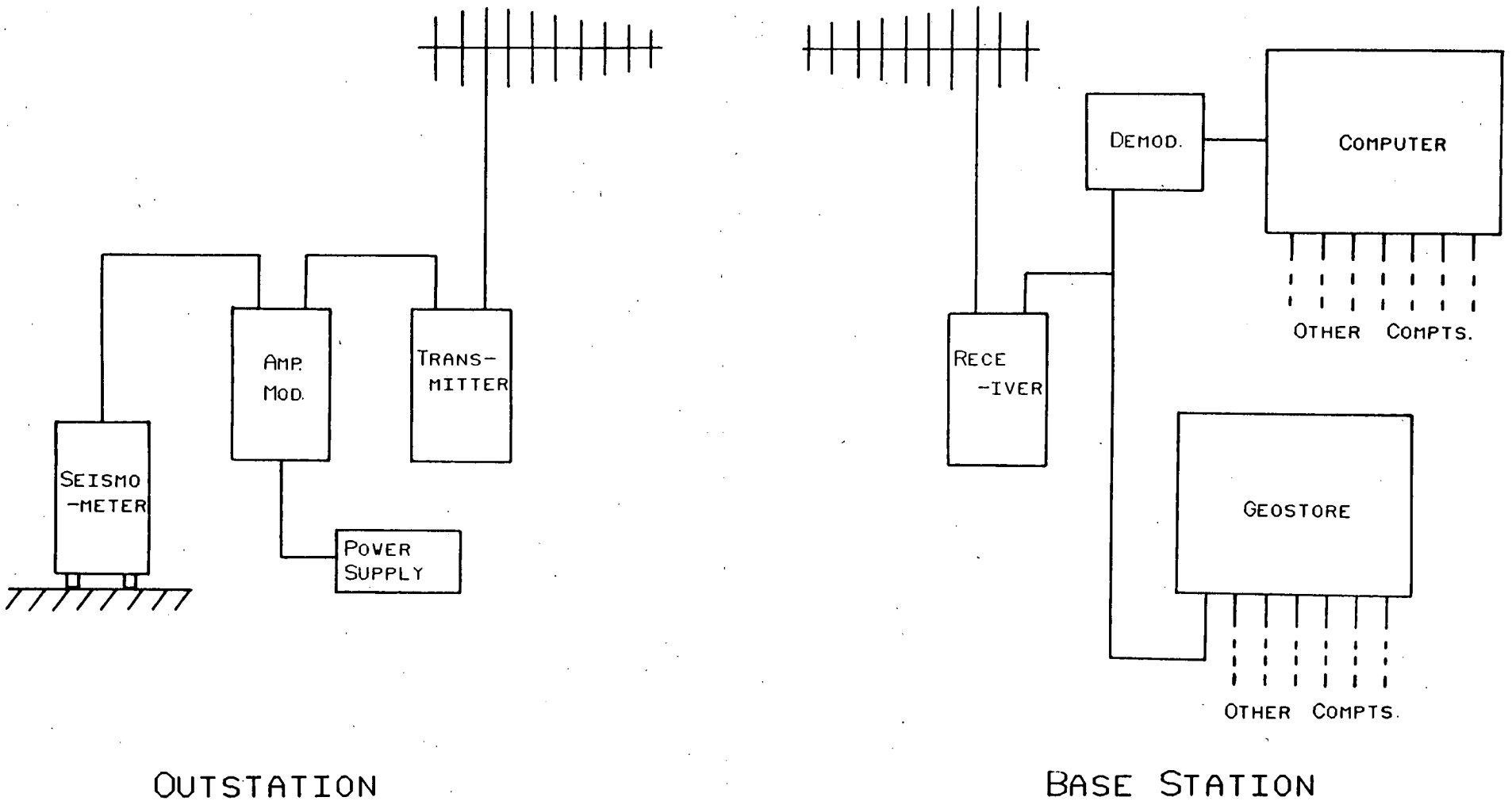

Fig. 1.11 - Diagrammatic representation of a single component system. The signal from the seismometer is passed to an amplifier modulator where it is frequency modulated at 676Hz. It then goes to the transmitter where it is modulated again at 458MHz (components spaced at 0.25MHz intervals) and transmitted to the base station. The signal is then demodulated back to the 676Hz modulated signal by the receiver and either recorded on a Geostore tape recorder or demodulated again and passed to the computer.

megahertz. This enabled transmission to the base station where the receiver demodulated the signal back to the 676Hz modulated signal. It was then recorded on the Geostore as a modulated signal or fed to the computerised trigger system via a demodulator card. The transmission frequencies that were used started at 458.000MHz and went up at 0.250MHz spacing.

On the Geostore one channel was reserved for an external time signal. Initially this was connected to an MSF receiver but poor reception led to it being abandoned. The OMEGA receiver had a similar problem. Eventually the signal from Radio Moscow was used and a small circuit built to convert the signal to one that could be recorded.

The base station was situated in a Turkish PTT (Post,Telephone and Telegraph) microwave relay station that sat on a hill above the town of Hereke, approximately 20kms outside the network . The site is also used as a MARNET station (HRT) and its location can be seen on fig. 1.4. The Turkish PTT kindly provided a room and storage facilities. The room was used as a laboratory, housing the computer and the three Geostores needed to record all the stations. The power needed to run the systems was taken from the PTT power supply. Before being passed to the recorders and radio receivers it was fed through a power conditioner which smoothed out any irregularities in the supply. In the event of a power cut the recording system would have kept going for over a day since it was backed up by 20Ah batteries. The power supply to the computers was fed through an uninterruptable power supply (UPS) which acted as both a power conditioner and as a backup capable of running the computer for approximately one hour in the event of a power cut. Outside the building a large mast was constructed to hold all the aerials and radio receivers. Signals were fed inside through insulated two core cables.

In addition to the conventional seismometer system described above, the new Earth Data 9690 digital acquisition system was first employed during the project. With this system each station only needs one amplifier modulator, transmitter and receiver,

regardless of whether it is a three-component or single component station. In the case of it being a three-component station, all three seismometer signals are fed into the amplifier modulator where they are multiplexed into a single signal and transmitted. At the receiving end, the signal is fed from the receiver to an interface unit where the signal is demultiplexed and either an analogue (frequency modulated) or digital signal can be taken from it.

The Geostores were run at 15/160 inches per second and each tape ran for approximately three and a half days. This meant that regular visits to the base station were required to change tapes and check the state of the signals being received from the outstations. In the event of a poor or non-existent signal, it would be necessary to visit the relevant station.

1.5.4 Results

Data were recorded continuously on analogue magnetic tapes (150 in all) from April to November 1984. In addition, many digital magnetic tapes were used to store files produced by the trigger system.

Throughout the field programme some preliminary data analysis was carried out. Two out of every set of three tapes were listened to and an event list made up. Then, for every fourth set, the local events that were listed were played out on the jetpen recorder, their times picked by hand and their locations calculated using HYP071 (Lee and Lahr, 1975). This type of analysis was useful for both checking on data quality and for identifying problems with the network that were undetectable at the base station, such as a radio receiver going off frequency and picking up an adjacent channel.

The bulk of the data analysis, however, was done by John Lovell in Edinburgh, after returning from Turkey. The tapes were re-listened to and paper copies made on the jetpen recorder of all interesting events. These events were then digitised using a

program specially developed by Evans (1980, 1986a), and once in digital form the arrival times could be picked with relative ease using a new picking program (Evans, 1986b).

Altogether 4000 earthquakes of all types (local, regional, teleseismic) were identified from the records. Of these approximately 1500 were local events (those with epicentres within or very close to the network). However, they could not all be located since some events were too small to be detected at more than one or two stations. This left 610 earthquakes that could be located satisfactorily and the epicentres are shown in Fig. 1.12. The level of seismicity did not differ very much from TDP-1 and TDP-2.

The magnitudes of the local events were calculated as

$$M = \log_{10}(A) + F$$

where A is the mean of the maximum ground velocity at each station and F is a scale factor that is added so that the magnitudes approximate M_L and are consistent with the previous projects (TDP-1 and TDP-2). On this scale the largest magnitude event recorded within the study area was approximately $3.5M_L$ although a magnitude of over $4.0M_L$ was recorded near to Adapazari, a few kilometres outside the network. Both events were widely felt in the area.

Further processing of the data was carried out to produce polarization diagrams (particle motion plots) and fault plane solutions. Shear wave splitting was widely observed in the polarization diagrams and, as described in the introduction (section 1.1), could be interpreted as being due to extensive dilatancy anisotropy (EDA). In general, stress measurements obtained from observations of EDA were found to agree with those from TDP-1 and TDP-2. The small differences that were found can now be looked at in more detail to see if they are of any significance. Also, a closer look can be made at stations KD (Fig. 1.10), which has shown a high degree of scatter in

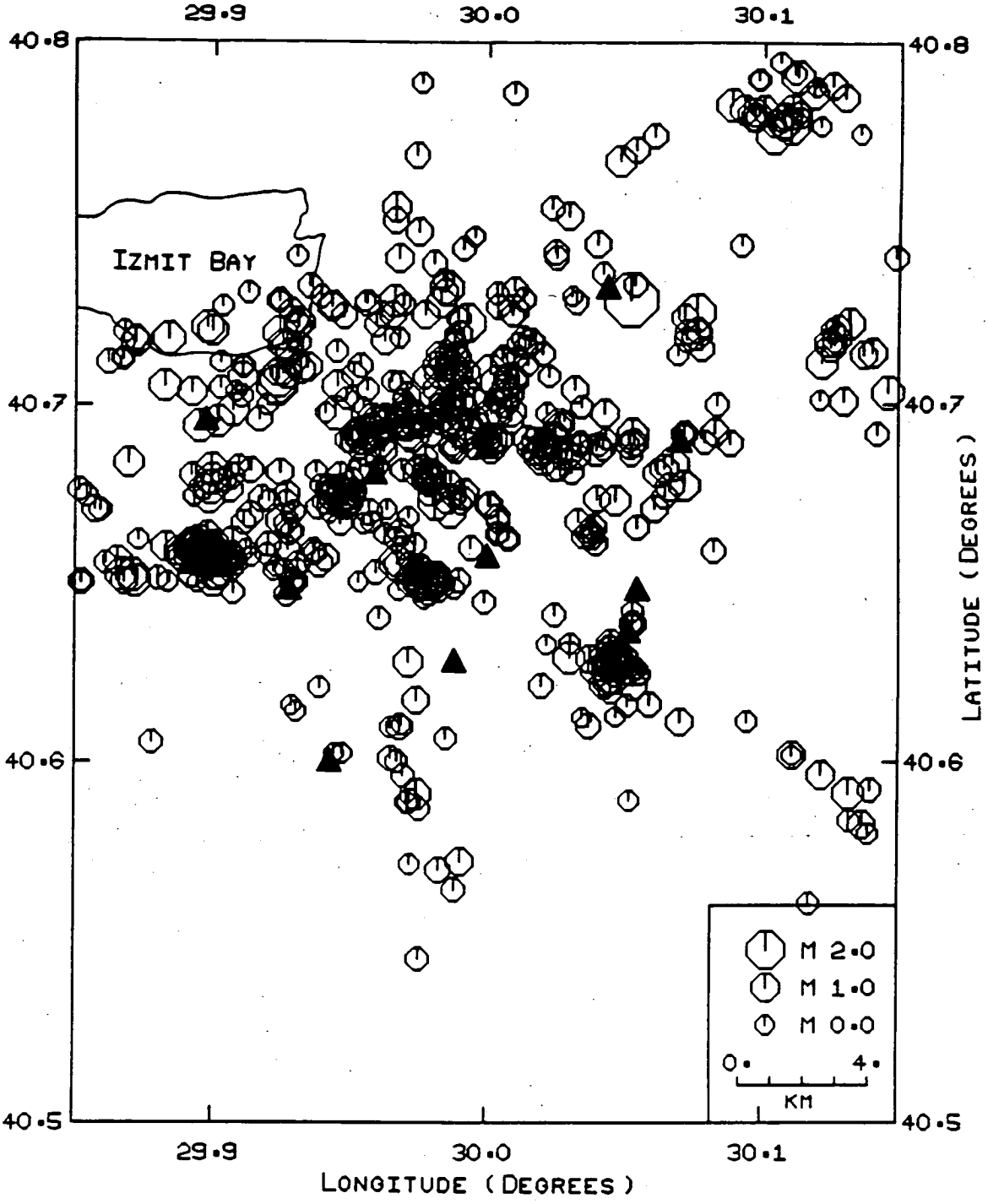

Fig. 1.12 - Epicentral plot of the 610 local events recorded during TDP-3 (triangles indicate the station locations).

polarization, and PA, which has results inconsistent with the rest of the network.

1.5.5 Buyukcekmece and Harmancik

One of the subsidiary aims of the project was to find a swarm of earthquakes that originated from a different tectonic regime than that of the main network. By using the MARNET records, two potential swarms were found near Buyukcekmece and Harmancik (Fig. 1.9) and these were investigated.

Buyukcekmece is approximately 40kms west of Istanbul. It was thought that the swarm detected at the nearby MARNET station of Catalca (CTT in Fig. 1.4) might have originated on a fault that can be traced through the area on geological maps. To get a better idea of the seismicity pattern in the area, a small preliminary network of three stations was installed, each station being radiolinked to Kandilli Observatory where it was recorded on a Geostore. If the swarm could have been located it is likely that the network would have been enlarged or repositioned, but unfortunately, during the two months that it was operating, no earthquakes were recorded, only quarry blasts.

Harmancik lies approximately 60kms south of Bursa and 150kms south of Istanbul. It was thought that the origin of the swarm might lie on a branch of the North Anatolian Fault that runs down from Mudurnu into Western Anatolia (see section 1.2.3). A network of four stations was installed and over a two month period many events were recorded, but it is thought that most of these were quarry blasts. Only one recognised earthquake was located in the area, and several well outside. Eventually this network had to be abandoned because of an untimely and unforeseen loss of manpower. Further investigations in this area or any other area were not possible because of the lack of time.

1.5.6 Array

For a two month period, a small array of six stations was laid out on a roughly flat piece of land near the station at Yuvacik (YU in Fig. 1.10). The stations were set out in the shape of a crucifix at a spacing of 200m and were linked by cable to a central recording van borrowed from the pool at Kandilli Observatory. For this exercise the digital equipment (amplifier modulator and interface box) and a computer were used to monitor the stations and record the events. The main advantage of using the digital equipment was that only one cable was required for each station, even though all six stations contained three components.

The purpose of this array was to analyse the arrivals in detail and to look at possible site and topographic effects. The analysis has yet to be carried out.

1.5.7 Trigger System

Outside the United States good automatic triggering systems are rare. This is despite the advantages they offer in terms of improved precision of timing, signal linearity and dynamic range. One of the aims of the TDP-3 project was to develop a triggering system based on the PDP-11 series of mini computers and Dr. J.R. Evans spent much of his time on the development of both the hardware and the software for such a system.

At the base station up to sixty channels could be fed into the computer through a demodulator rack and A/D convertor. Each channel could be continuously monitored so that when an event is detected on more than a preset number of channels, an event file is created for as long as the event keeps triggering the system. The file is then stored on an internal disk which has to be archived on to magnetic tape every two to three days because of the limited storage capacity of the disk.

The program that controlled the system could have used a variety of different algorithms for judging when an event had occurred. The system was first developed whilst still in Edinburgh using an algorithm that looked for large gradients in the signal (i.e. accelerations). This proved reliable for detecting quarry blasts but unpredictable when looking for earthquakes. So a second algorithm was introduced which compared the short term average ground velocity to the long term average of the signal and this proved to be much more reliable in the particular circumstances. The system also had to be tuned to discriminate between noise and earthquake triggered events, but not to the extent that it would miss small earthquakes.

At the end of the project the triggering system was working reasonably well and was tested on MARNET for a short while. Since returning to Edinburgh further development has taken place and it has been satisfactorily tested on LOWNET and on a small network installed in Kenya. It is hoped that future development will include the attachment of automatic picking and location programs, both of which are in the development stage.

1.5.8 Geomagnetic Study

Analysis of electromagnetic data recorded before and after the 1979 Carlisle earthquake showed a marked change in the earth's conductivity structure (Beamish, 1982). It was postulated that this was caused by the change in stress that must have accompanied the earthquake and it is proposed that this might be of use in the quest to predict earthquakes.

The conductivity of rock is very much dependant upon microcracks, the pore fluid contained within them and the permeability. It is proposed in the hypothesis of EDA that, under stress, microcracks will grow parallel to the principal axis of compression, even at low stress levels. The possible effect of this is to produce variations in the conductivity due to a change in the permeability as the cracks start to run into each other. It is likely that the conductivity will change such that it is

greater parallel to the cracks than perpendicular to them and hence introduce anisotropy into the conductivity structure.

As part of TDP-3, it was proposed that the Geomagnetism Research Group of the British Geological Survey should run an experiment to examine the conductivity structure beneath the study area. This would enable an independent estimate of stress direction to be made which may or may not support the hypothesis of EDA. Also it would be possible to look for changes in the conductivity structure over the duration of the study period and look to see if there is any correlation with changes observed in the velocity structure or the seismicity.

In the study, conducted by Dr. D. Beamish, M. Russell and J. McDonald, five stations were installed, four of which are shown, in relation to the seismic network, in Fig. 1.13. The fifth station needed to be remote from the study area so that it could be used as a control station. It was therefore positioned at the base station at Hereke where all the data including that transmitted from the four field stations were recorded on a magnetic cartridge. Each station was designed to record the two horizontal components of the earth's electric field (E field), using copper sulphate ($CuSO_4$) pots buried in the ground to measure the potential difference, as well as the three components of the earth's magnetic field (B field), measured using a fluxgate magnetometer. A reading was taken from each of the five components every five seconds and transmitted to the base station.

The conductivity structure can be estimated from the earth response function given by the ratio of the electric to magnetic fields (E/B). This can be done because it is the magnetic field that induces the currents in the crust that set up the electric field. Different depths can be examined by considering different periods in the data. The shorter period components of the magnetic field are not able to penetrate very far into the crust and so the corresponding response function is only dependent upon conductivities near the surface. As the period increases, conductivities at greater depths are brought into the response

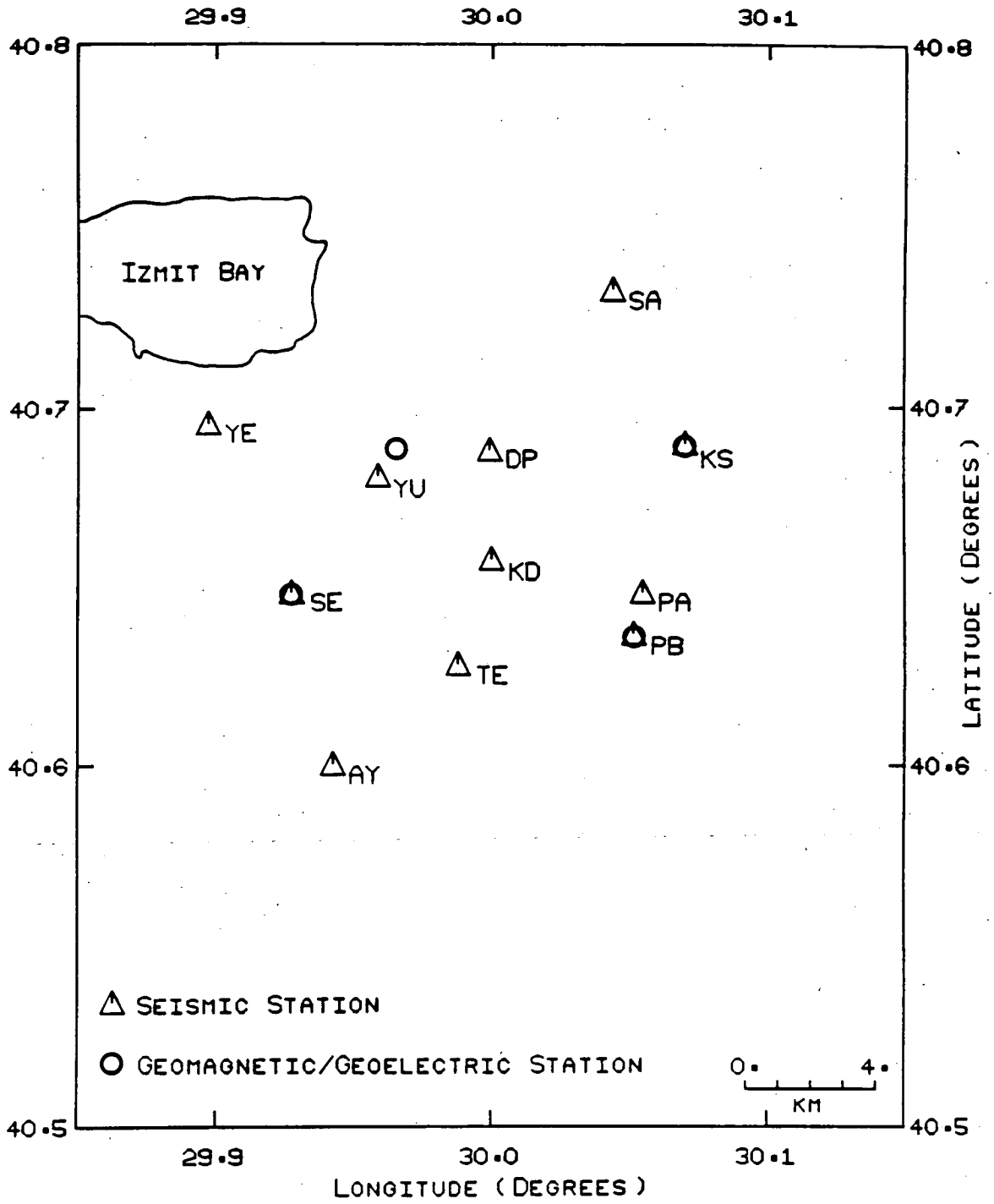

Fig. 1.13 - The layout of the geomagnetic/geoelectric stations in relation to the seismic network.

function. In this way the conductivity structure can be built up.

In addition to the main project, the Geomagnetism Group also carried out development work on a portable system that works at much shorter periods. However, the results obtained using this system have proved to be unsatisfactory and the whole system has undergone review since returning to Edinburgh.

Results obtained so far in the main study show a highly conductive top layer over a substantial, north-dipping, geoelectric boundary. The geoelectric anisotropy broadly agrees with measurements made by looking at shear wave splitting and so supports the hypothesis of EDA. Further work is being carried out to examine the variations that were measured during the project to see if they are of any significance.

1.5.9 Other Studies

In addition to the seismic and geoelectric studies mentioned above, several independent studies were carried out during the same period. The University of Edinburgh, in collaboration with Istanbul Technical University (ITU), have set up a regional microgravimetric network over an area stretching from Istanbul and Bursa to Bolu (approximately 300km). ITU have also carried out a magnetotelluric traverse over the area and in collaboration with the University of Kiel (Germany), the Institute of Oceanographic Sciences and Kandilli Observatory have recently started a long-term study of earth tilt. This last project is taking place as part of a joint German-Turkish investigation of the area to the east of the TDP study area.

1.6 Conclusions

The third phase of the Turkish Dilatancy Project has now been completed as far as the original project aims are concerned. A large volume of seismological and geoelectrical data has been collected and the routine processing and analysis of this dataset has been carried out. With the introduction of a geoelectric

study, support for the hypothesis of EDA has increased and further detailed studies should enable significant advances to be made in this area. The use of EDA for predicting earthquakes has still to be proven since reliable observations of changes of stress with time have yet to be made, but joint studies of the data sets from all three phases of the project, spanning five years, may throw up such observations.

Other aspects of the project had varying amounts of success. The development of the triggering system whilst in Turkey proved to be quite satisfactory and since returning, further development work has greatly improved it. The small array set out near Yuvacik was very successful although little has been done with the data that were collected. Lastly, the attempt to collect data from a different tectonic regime did not go as well as was hoped, although it was not a complete failure since the data recorded for teleseismic and regional events could be used to help determine crustal structure.

There is still much that can be done with a data set from such a comprehensive three component network. It is already being put to a variety of uses outside the original aims of the project and the remainder of this thesis is an example of one such case.

Chapter 2

Seismic Source Studies and Similar Earthquakes

2.1 Introduction

In chapter 1 the third phase of the Turkish Dilatancy Project is described in detail. The main aim of the project was to investigate seismic anisotropy by monitoring shear wave splitting in the records of local earthquakes and, in the long term, to use this as a means with which to predict earthquakes. The task of analysing all of the data recorded for this purpose is a large one and, at the time of writing, had still to be completed. However, an excellent data set was collected and there are many different ways in which it could be used.

For analysing seismic anisotropy a network of closely spaced, three-component stations, sitting immediately above the source was required. All local, regional and teleseismic earthquakes were then recorded over a six month period, producing one of the most comprehensive data sets available from an area of such intense seismic activity. In total, over 1500 local earthquakes were detected (610 of those have since been reliably located) along with over 2500 regional and teleseismic events. One possible study that could be carried out and which would be of some interest to the Turkish Dilatancy Project is a study of the crustal structure beneath the project area. At present, knowledge of the structure is very limited, but by analysing either the surface waves from regional and teleseismic events or P-wave teleseismic residuals a better understanding could be achieved. The teleseismic events could also be used in conjunction with

records from around the world for studying the Earth's core. Turkey is particularly well situated for this since it lies on the opposite side of the Earth from the Pacific Ocean where there is a relative abundance of large earthquakes. The opportunities open for using the local events are numerous and include, for example, studies of the source, propagation effects (attenuation, scattering, etc.), seismic risk, frequency-magnitude relationships as well as further structural studies and it is the first of these options (source studies) that the remainder of this thesis is concerned with.

Over the years many ideas have been put forward to try and explain how an earthquake originates and models have been set up that try to explain how a fault behaves and how it relates to the observed seismogram. In this chapter those theories that have proved most popular are reviewed, showing how source parameters and mechanisms may be derived from seismic records. In comparison, a new method is introduced in the following chapters that is able to examine the source in detail for its dimensions and mechanism. It uses groups of similar earthquakes (earthquakes with near-identical waveforms) that have been observed in many of the swarms found during the Turkish Dilatancy Project. These similar earthquakes have also been widely observed by other seismologists around the world and the last section of the chapter outlines some of the work that they have been doing.

2.2 Source Studies

2.2.1 Introduction

The seismic source is an area of seismology that has only recently started to receive the attention it deserves. Part of the problem is that most of the information about the source has to be obtained from the seismogram and in most cases any physical examination of the source is not possible. The two notable exceptions to this are the rare examples of earthquakes occurring at the surface and very deep mine studies (for example, Spottiswoode and McGarr, 1975; McGarr *et al.*, 1981). However, the

waveform of each seismogram is not only determined by the source but also by the propagation path. The amplitude and phase content of the signal, as originally emitted by the source, are distorted by high frequency attenuation, phase changes and reverberations on their way to the surface. Separating these effects is not an easy task.

There have been many attempts to try and explain what is happening at the source, with each idea leading to a model that tries to match the theoretical radiated signal with that observed at the surface. Most models are based on the faulting process, as observed in surface geology, which is generally accepted to be the most valid physical description of a shallow earthquake (Johnson, 1979). In general, the problem has been approached in two different ways. In the kinematic approach the time history of the slip is specified *a priori*, whereas in the dynamic approach the stress system of the fault is specified *a priori*. As the theories have developed, it is the dynamic approach that has received the greater emphasis (Johnson, 1979) since it is able to give a more complete solution (Randall, 1973). In addition to these theoretical models there have also been numerous observational studies (Bakun *et al.*, 1976; Bakun and Lindh, 1977; Hanks, 1977; Boatwright, 1978) carried out to try and check the theoretical results or to investigate the consequences of interpreting earthquakes in terms of a specific model (Johnson, 1979).

In this section, those ideas and models that have proved most popular are reviewed. Attention, throughout the review, is focussed upon the measurement of the source dimension since emphasis will be placed upon it in the following chapters. The section will then end with a discussion of an upper frequency limit that has occasionally been observed in seismograms and which may have some bearing on the corner frequency analysis of chapter 5.

2.2.2 Source Models and Parameter Measurement

In studies prior to 1967 it was established that seismic source parameters such as fault length, rupture velocity and stress drop could be obtained from the spectra of seismic waves (for example, Matumoto, 1960; Berckhemer, 1962). However, up to that point the only physical parameter used to specify most earthquakes was the magnitude (defined as a logarithm of the amplitude of a specified seismic wave recorded on a specified seismometer). It was already well known that larger earthquakes were able to generate longer period waves more efficiently (for example, Honda *et al.*, 1939; Asada, 1953; Kanai *et al.*, 1953) but it was not until 1967 that the two different approaches could be combined (Aki, 1967). In his paper, Aki used a dislocation model, and the assumption that large and small earthquakes satisfy a similarity condition, to find a first approximation to the relationship between the seismic spectrum and the magnitude. The model was able to explain satisfactorily the discrepancy found between the magnitude scale based on short period body waves and that based on long period surface waves, as noted by Gutenberg and Richter (1956). In addition, the theory also suggested an inverse linear relationship between the source dimension (a measure of the size of the active part of the fault from which the earthquake originated) and the corner frequency (where the high frequency roll-off departs from the flat long period base level of the amplitude spectrum):

$$f_c \propto 1/r \qquad (1)$$

where f_c = corner frequency
r = source radius

This relationship was then further quantified by Brune (1970, 1971). Brune based his theory on a dislocation model with the time function related directly to the effective stress available (unlike Aki (1967) who assumed a step function in time) and the model has proved to be quite successful in explaining some of the

features observed in near and far-field spectra. The theory derives the relationship between the source dimension and corner frequency using the S wave spectra only:

$$f_c(S) = \frac{2.34\ V_s}{2\pi r} \qquad (2)$$

where V_s = S wave velocity. In addition, the model also enables estimates to be made of other source parameters such as the amount of slip, the seismic moment (a form of magnitude related to fault area, amount of slip and fault rigidity) and stress drop (the difference between the initial and final equilibrium stresses). Brune's paper became the basis for much of the work on this subject that was to follow and the model is still widely used today. It is a theory that has obtained the maximum information on the nature of the spectrum without having a complete dynamical solution (Randall, 1973).

In Brune's theory no expression, equivalent to equation (2), relating P wave corner frequency to the source dimension was given. Hanks and Wyss (1972), therefore, proposed substituting the P wave velocity (V_p) for the S wave velocity (V_s) in equation (2) to give

$$f_c(P) = \frac{2.34\ V_p}{2\pi r} \qquad (3)$$

An explanation to support this proposal was given by Molnar *et al.* (1973). He suggested that the corner frequency was due to spatial finiteness. The time domain pulse received at the surface will be broadened as a result of the seismic energy being emitted from different parts of the fault plane. In addition, it will also produce a roll-off in the spectrum at high frequency. The size of the effect will depend on both the source dimension and the seismic velocity and since $V_p > V_s$ the P wave pulse will be narrower and thus have a higher corner frequency. $f_c(P) > f_c(S)$ is a phenomena referred to as the corner frequency shift and which has been widely observed in many studies (Hanks, 1981). It should

also be pointed out, however, that there are other studies that have observed the opposite (Bakun *et al.*, 1976) although these are few in number. In fig. 2.1 idealised P and S wave far-field displacement spectra are shown, indicating how $f_c(P)$ and $f_c(S)$ should be related to each other.

In 1973 Randall (1973) demonstrated that the principal results of Brune's theory are not strongly dependent upon the model he uses. He also points out that observational studies have found spectra consistent with the Brune model for both large and small earthquakes with either low or high stress drops. All this, Randall suggests, shows how powerful the theory is, but it does not automatically imply that the dislocation-type source is correct.

The above theory gives a ratio of the P and S wave corner frequencies (equation (3)/equation (2)) that should be equal to the ratio of the P and S wave velocities

$$R_c = \frac{f_c(P)}{f_c(S)} = \frac{V_p}{V_s} \simeq 1.75 \qquad (4)$$

However, this has not always been found to be correct. Madariaga (1976) developed a theory that modelled the far-field radiation in terms of an expanding circular fault. In this theory he derives equations for the P and S wave corner frequencies in terms of the source radius

$$f_c(S) = \frac{1.32\ V_s}{2\pi r} \qquad (5)$$

and

$$f_c(P) = \frac{2.01\ V_s}{2\pi r} \qquad (6)$$

(note the use of V_s instead of V_p)

which gives a corner frequency ratio of

$$R_c = \frac{f_c(P)}{f_c(S)} = 1.52 \qquad (7)$$

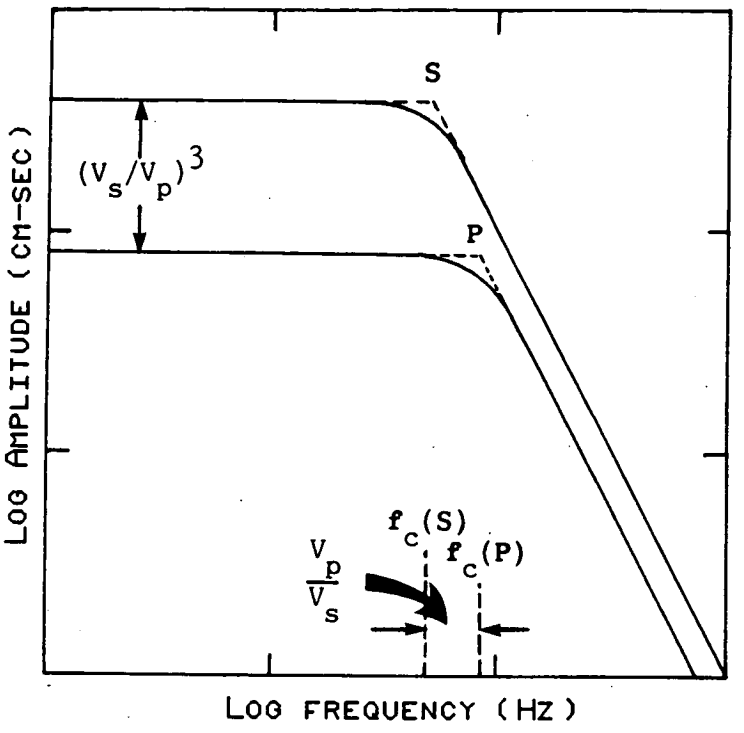

Fig. 2.1 - Idealised P and S-wave far-field displacement spectra showing how the P and S-wave corner frequencies ($f_c(P)$ and $f_c(S)$) are related to each other (Brune, 1970; Hanks and Wyss, 1972).

He also found data to support his theory.

Different corner frequency ratios should make it possible to distinguish between the two models when analysing data for a source radius. However, the errors involved in measuring the corner frequency mean that this may not be possible. In such a case, both models could be used from which a range of source radii would be determined.

In 1976 a different approach was made by Backus and Mulcahy (1976a, 1976b) who presented a thorough analysis of the seismic source within which a description of the source was given by a polynomial moment expansion of the excess stress. From this expansion moments of differing orders of degree could be extracted with each order representing a different aspect of the source such as the seismic moment or source dimension. The idea was further developed by Silver (1983, 1985) to allow statistical measurements of the source dimension, duration and directivity to be made from measurements of either the curvature of the amplitude spectrum at low frequency or the variance of the normalised time domain pulse (these are equivalent measurements in different domains).

This approach appears to be one of the most promising although there have been several other notable studies including those of Boatwright (1980, 1982, 1984) and Hanks (1979, 1982a). Brune (1976) and Johnson (1979) have both attempted to review general source theory and the reader is referred to these papers for a more broad examination of some of the ideas mentioned here.

2.2.3 f_{max}

The idealised far-field S wave acceleration spectra of the Brune model (Brune, 1970) should be flat for all frequencies above the corner frequency. However, observations of strong motion records would seem to indicate that some limit exists (referred to as f_{max}) above which the amplitudes diminish (Hanks, 1982a & 1982b). Fig. 2.2 shows an idealised acceleration spectrum indicating both the corner frequency and f_{max}. Most of the

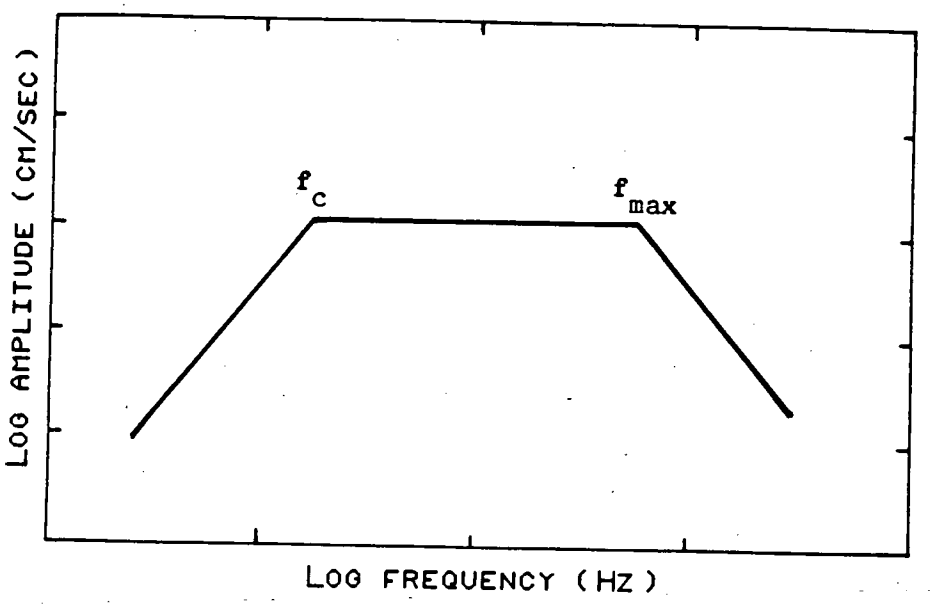

Fig. 2.2 - An idealised acceleration spectrum showing the relationship between the corner frequency (f_c) and f_{max}.

observations noted by Hanks (1982b) were made in California and were generally restricted to a band of 10-20Hz although he does not seem to think that there is anything special about this band (Hanks, 1982a). Indeed, Papageorgiou and Aki (1983a) found sharp cut-off frequencies in a much lower range (2.5-5Hz). In both studies measurements were taken close to the epicentre although f_{max} was observed for both large and small earthquakes (Hanks, 1982a). In addition, it was noted that f_{max} is usually greater than the corner frequency for the same spectrum (as in fig. 2.2).

The cause of this upper limit is uncertain and has been attributed to the source, the path, recording site effects or a combination of all three. For example, Ida (1973) interpreted f_{max} as a source effect from which an estimate of the slip could be made. Hanks, on the other hand, first attributed it to anelastic attenuation along the total travel distance (Hanks, 1979) but later (Hanks, 1982a) decided that it was a local recording site effect. Several other people have also had a say in the matter (Day, 1982; Papageorgiou and Aki, 1983a,b; Anderson and Hough, 1984; Aki, 1987).

In chapter 5 the spectra of several small earthquakes are analysed for their corner frequency. As would be expected the corner frequencies are relatively high and so it is important to check that there is no upper frequency limit in these spectra which may cause uncertainty in the corner frequency measurements. Consequently, the acceleration spectra for these same events are analysed.

2.3 Barriers, Asperities, Characteristic Earthquakes and Swarms

2.3.1 Introduction

A swarm is the name given to any group of earthquakes that are clustered about a particular point in space and, maybe, time as well. They may or may not be associated with a large earthquake which led Mogi (1967) to classify swarms into three types: type 1 are main shock - aftershock sequences; type 2 are foreshock - main

shock - aftershock sequences; and type 3 are sequences with no obvious main shock. Types 1 and 2 have been widely observed for many years, due to the attention drawn to large earthquakes, but the extent of type 3 was not properly realised until microearthquake studies became common. An example of a typical microearthquake study is TDP-3 (see chapter 1). In total, 610 well located events were found within the study area, with all magnitudes less than 3.5 M_L and the majority less than 2.0M_L. The epicentres of all these events are plotted in fig. 1.12 of chapter 1 and the extent of the swarm activity can be clearly seen. Since no large earthquakes were recorded during the study, all the swarms can be classified as type 3.

All three types of swarm can be explained using a theory that has been developed over the last 10 years. The distribution of earthquakes over a fault plane is thought to be controlled by strong patches which, in turn, determine how the stress is released. The type of swarm activity depends on the kind of role played by the strong patch. An outline of the theory is given in the following sub-section.

It has been observed in studies of both palaeoseismic and recent earthquakes that individual faults often generate swarms of earthquakes (of all three types mentioned above) that show a similarity in their waveform and little variation in their magnitude. Such a fault is, therefore, said to generate a characteristic earthquake and this phenomenon can be explained by the theory mentioned above. Over the last 10 years similar earthquakes have been used in a variety of ways, a review of which is contained at the end of the chapter. This then leads on to another method that makes use of swarms of similar earthquakes of type 3 and which is explained in detail in the following chapters.

2.3.2 Barriers and Asperities

A simple model used to describe fault motion during an earthquake is of either a uniform slip or a uniform stress drop over the entire fault plane and, for many years, such a model has

proved adequate for most seismologists. However, it has been unable to explain observed high-frequency radiation and the occurrence of swarms of earthquakes. Therefore, it has been necessary to consider an irregular slip motion over a heterogeneous fault plane (Aki, 1984). The heterogeneity is generally thought to occur as the result of strong patches being distributed around the fault surface. These strong patches are referred to as either barriers or asperities, the exact term depending on the role being played by the strong patch.

It has been shown that the rupture mechanism of an earthquake can be modelled by an in-plane shear crack propagating along a fault. The stress associated with the P and S waves travelling ahead of the crack tip causes slip on the fault which maintains the propagation of the crack (Burridge, 1973; Andrews, 1976; Das and Aki, 1977a). If the distribution of strength over the fault plane is heterogeneous then the rupture process will be greatly complicated (Das and Aki, 1977b) and can thus be used to explain various seismic source phenomena including the occurence of swarms.

When the stress over the fault is homogeneous, the strong patches on the fault (in this case referred to as barriers) will effect the propagation of a shear crack in one of four ways (Das and Aki, 1977b). If the areal extent of the barrier is large then the propagation will be stopped, but if it is small then the barrier can interact in three different ways depending on the local level of the tectonic stress:

(i) if it is high the barrier will be broken as the crack passes;

(ii) if it is low the crack will proceed beyond the barrier leaving it unbroken;

(iii) at intermediate levels the barrier may remain unbroken as the crack passes but the increase in dynamic stress may cause it to break at a later time.

Thus the occurence of aftershocks can be explained by the release of stress at barriers that are initially left unbroken by

the passage of the main shock and it is considered to be a stress-roughening process (Aki, 1984).

Alternatively, the stress surrounding a strong patch maybe released by aseismic creep and foreshocks, resulting in the concentration of stress at the strong patch (now referred to as an asperity). The main shock occurs when the asperity breaks and this is considered to be a stress-smoothing process since the stress distribution prior to the main shock is heterogeneous (Aki, 1984).

Foreshocks and aftershocks can, therefore, be explained by two different model types, but since aftershocks are much more abundant than foreshocks it would appear that the barrier-type model dominates. However, it is thought that the asperity-type model plays a major role in both rupture initiation and the occurrence of major earthquakes (Aki, 1984). Despite their differences, it is thought that the different model types are indistinguishable in their waveform.

2.3.3 Characteristic Earthquakes or Earthquake Families

The occurrence of earthquakes over large areas can usually be modelled by the log linear frequency-magnitude relationship ($\log N = a - bM$) as described by Gutenberg and Richter (1954). However, paleoseismic studies have suggested that individual faults and fault segments tend to generate a *characteristic earthquake* with a relatively narrow range of magnitudes which do not follow the Gutenberg-Richter relationship (Schwartz and Coppersmith, 1984). This idea has been reinforced by instrumental studies of recent events that have recorded groups of earthquakes with similar waveforms and with little variation in their magnitudes. These groups are often referred to as *earthquake families*, following the work of Hamaguchi and Hasegawa (1975), and may consist of all three types of swarm activity.

Aki (1984) suggests that there are two types of earthquake family which may be modelled in terms of the stability of either

asperities or barriers on the fault. The asperity-type model is characterised by constant fault length and slip whilst the barrier-type model has a constant fault length but variable slip. Evidence for this distinction can be found in the studies of Okada *et al.* (1981) and Takeo (1983), who analysed the seismicity associated with the Usu Volcanic eruption of 1977. The rapid uplift of a dacite dome resulting in the generation of numerous earthquakes from the same fault area and a study of 300 earthquakes, produced over a five day period, found that over a third of them could be classified into one of eight groups by similarity of waveform.

These groups consisted of two types. In one type, the absolute amplitudes within the group never varied by more than a factor of two and this type has been attributed to a stable asperity located on the crater wall along which the dacite dome slid during the uplift. The constant slip is thought to be due to nearly constant dynamic friction and asperity strength. In the other type of earthquake family, the waveforms of each event are similar but the absolute amplitudes vary by an order of magnitude which can be explained by a barrier model. Two strong stable barriers determine the fault length of the group while the slip is determined by the distribution of weaker barriers over the fault plane. This model supports the observation of Tsujiura (1983a) that the largest earthquake in a group would be expected to occur at a late stage since, after the propagation of the event, few barriers would be left unbroken.

In the following chapters, groups of similar earthquakes will be accurately relocated and it is hoped that the results may be interpreted in terms of the theory described above.

2.3.4 Swarms and Similar Earthquakes

All three types of swarm sequence, described at the beginning of this section (2.3.1), can thus be modelled using the concept of barriers and asperities. The similarity of the waveforms within a swarm is very much dependant upon the size of the causative fault

and the resulting separation between the events. For the case of the aftershocks of a large event, the fault area broken by the main rupture may be several kilometres long and the subsequent distribution of unbroken barriers will be spread over this length. Aki (1984) has listed the estimated barrier interval and maximum slip for several notable earthquakes. The barrier intervals range from 1km for Parkfield, 1966 (Papageorgiou and Aki, 1983a,b) to 30km for Gobi-Altai, 1957 (Florensov and Solonenko, 1963). Assuming the aftershocks to be spread over these lengths, the waveforms, and hence the similarity, would be expected to change progressively along the fault. The contents of the emitted signal of each event would be determined by the properties of the fault surrounding the barrier that is broken and will be limited by intermediate strength barriers spread along the fault.

For type 3 swarms, where there is no main shock, the active area of the fault will be relatively small and it is likely that the same strong barriers will determine the contents of the seismic wave for each event. Hence, the waveforms will all be similar but the groups will be smaller in their areal extent.

Fig. 2.3 is an example of a group of aftershocks, recorded at one station, that occurred after the North Wales earthquake of 1984. The eight events shown are selected from a group totalling over 300 that were recorded by the British Geological Survey after the occurence of the main shock (Marrow and Walker, 1986). The locations of the whole group, as calculated by HYP071 (Lee and Lahr, 1975), are shown in Fig. 2.4. The locations are all considered to be of a high quality and are estimated to have an error of approximately 1km (Marrow and Walker, 1986). Even allowing for this error, the spread of the locations is constrained to an area of no more than a few kilometres across and, by using the barrier model (section 2.3.2), it can be assumed that this is a fair estimate of the barrier interval for the main shock. The eight chosen events of fig. 2.3 are comprised of four pairs of similar earthquakes (or doublets).

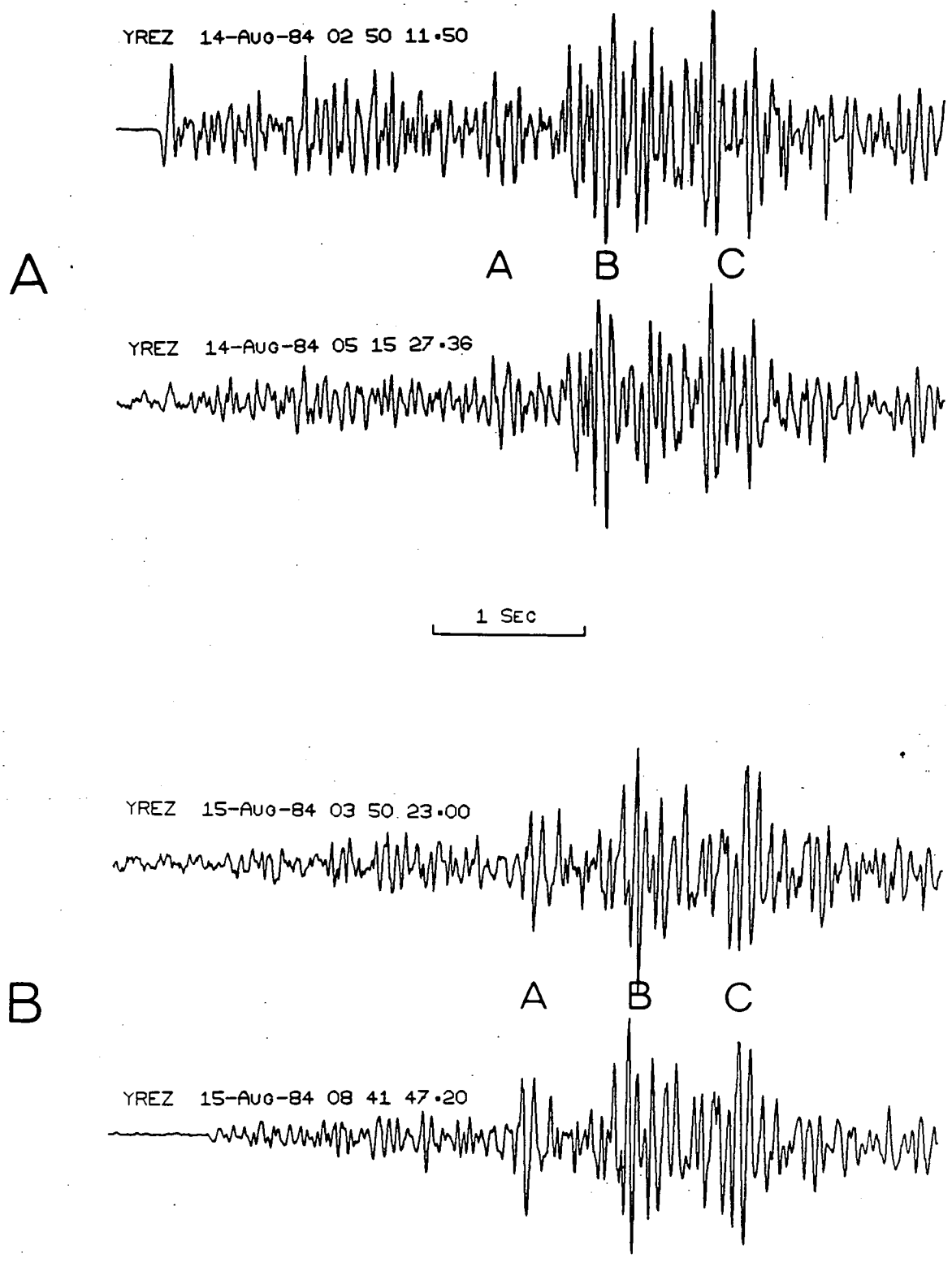

Fig. 2.3 - Two pairs of similar earthquakes taken from the aftershocks recorded after the North Wales earthquake of 1984.

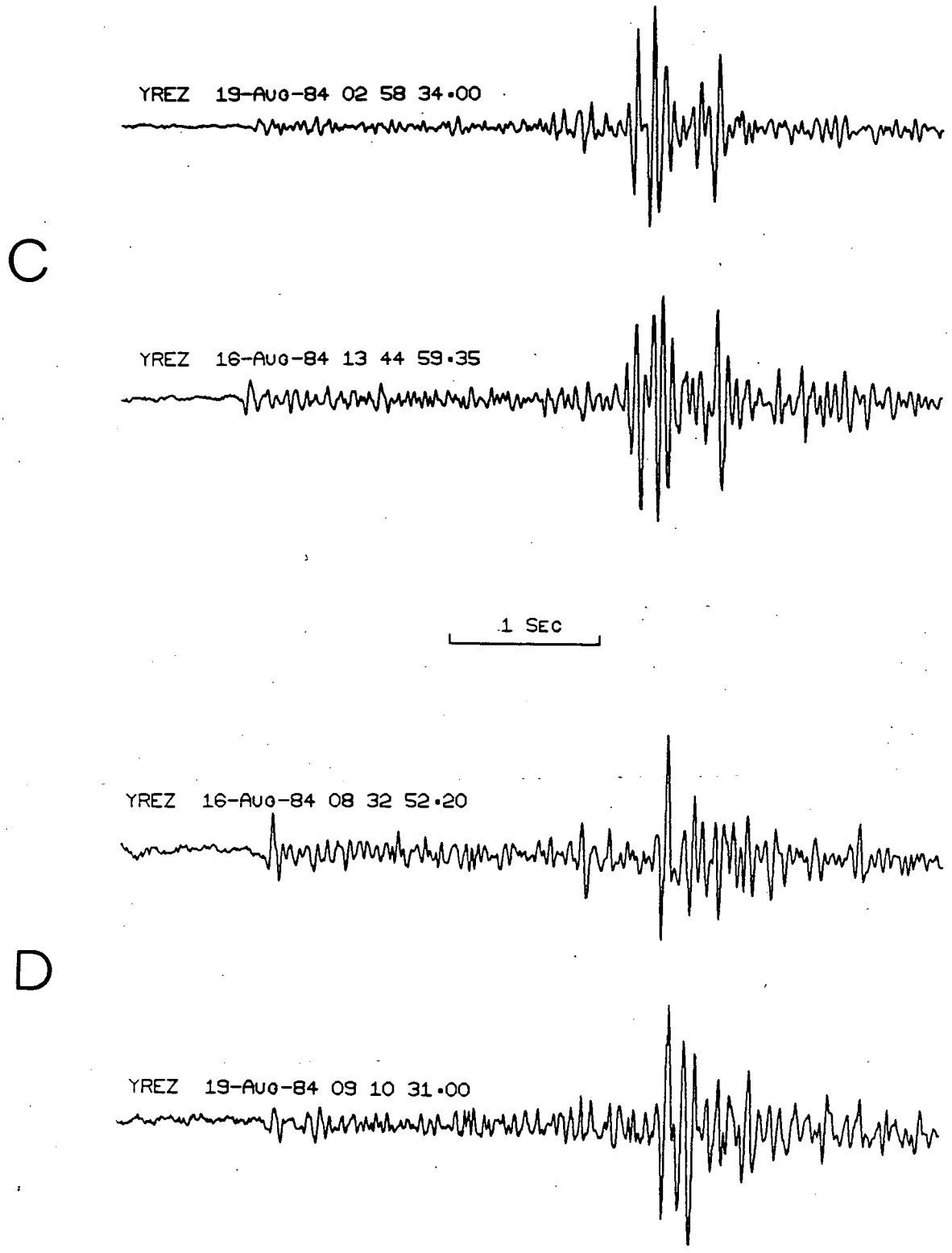

Fig. 2.3(cont) - Two pairs of similar earthquakes taken from the aftershocks recorded after the North Wales earthquake of 1984.

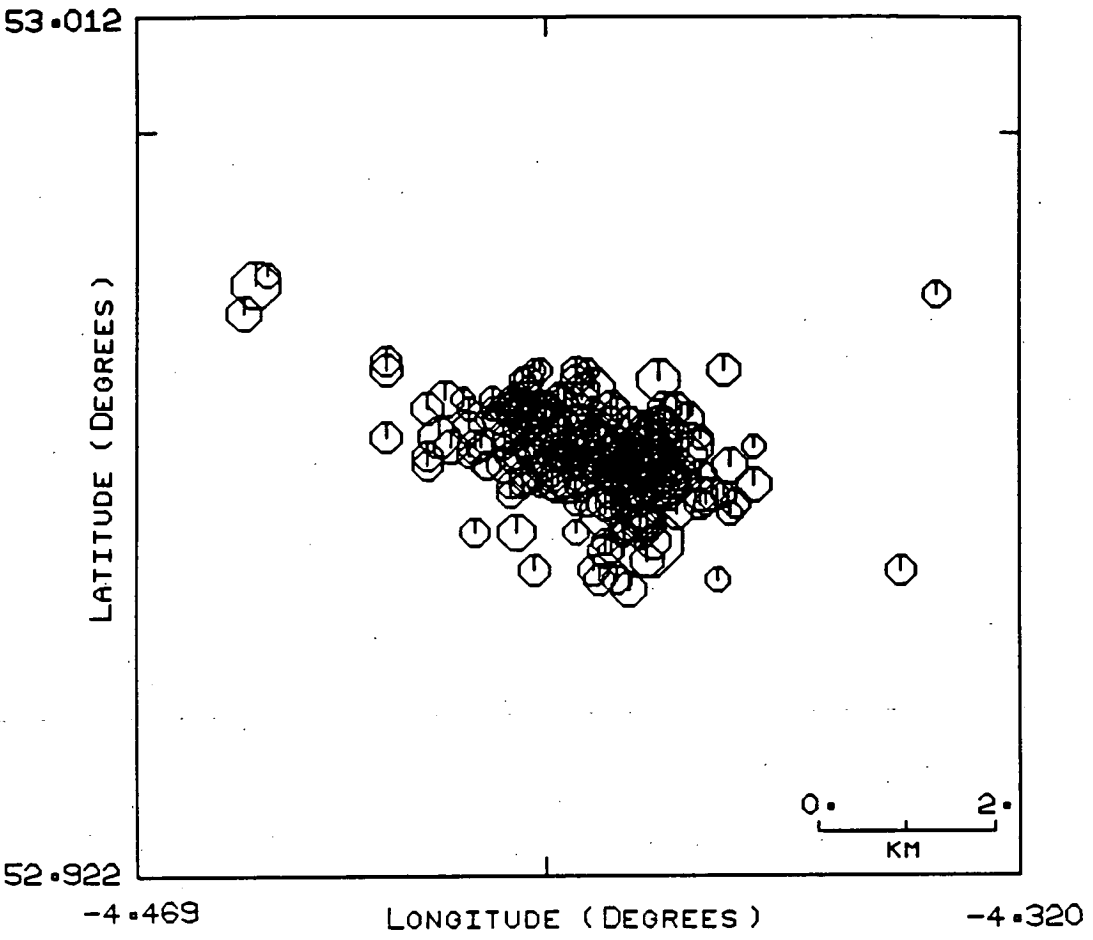

Fig. 2.4 - The HYPO71 locations of all aftershocks of the North Wales earthquake of 1984.

To sidetrack briefly. In 1980 Geller and Mueller (1980) examined four earthquakes from central California that were recorded on the USGS local array (CALNET). The basic seismograms only displayed some general similarity but when low-pass filtered below 5Hz the signals became almost identical. Geller and Mueller suggested that this meant that all four events were within a radius of no more than a quarter of a wavelength or 200 - 400m. In other words, similarity is retained in the lower frequencies of seismograms as the separation between the events becomes greater.

For the eight events in Fig. 2.3, the similarity between each event in a pair suggests that they are very close to each other. There is also some similarity between the seismograms of pairs C and D, especially at the lower frequencies, which suggests that they may be within a few hundred metres of each other. To a lesser extent, the same applies to pairs A and B. In both pairs the S arrival is comprised of three phases, marked A,B and C in Fig. 2.3, indicating some similarity at very low frequencies and implying a likely separation of several hundred metres.

Many other events from the same group of aftershocks could be classified into earthquake families which supports the barrier model idea of a rupture between two strong barriers leaving hundreds of weaker barriers unbroken. However, for a large earthquake such as this (M_L=5.4), it is possible that the change of stress accompanying the main rupture may have affected adjacent faults. In this case, no similarity would be expected in the seismograms which may account for some of the events observed.

In comparison to this, Fig. 2.5 shows a selection of seismograms taken from a group of over twenty similar events. These were recorded during the Turkish Dilatancy Project and are all less than 1.4M_L in magnitude. There are no large events associated with the group which is, therefore, a type 3 swarm. The similarity between the events is much more striking than anything found within the group of North Wales aftershocks and the similarity is also consistent throughout the whole group. This implies that the group is very tightly constrained to a small area

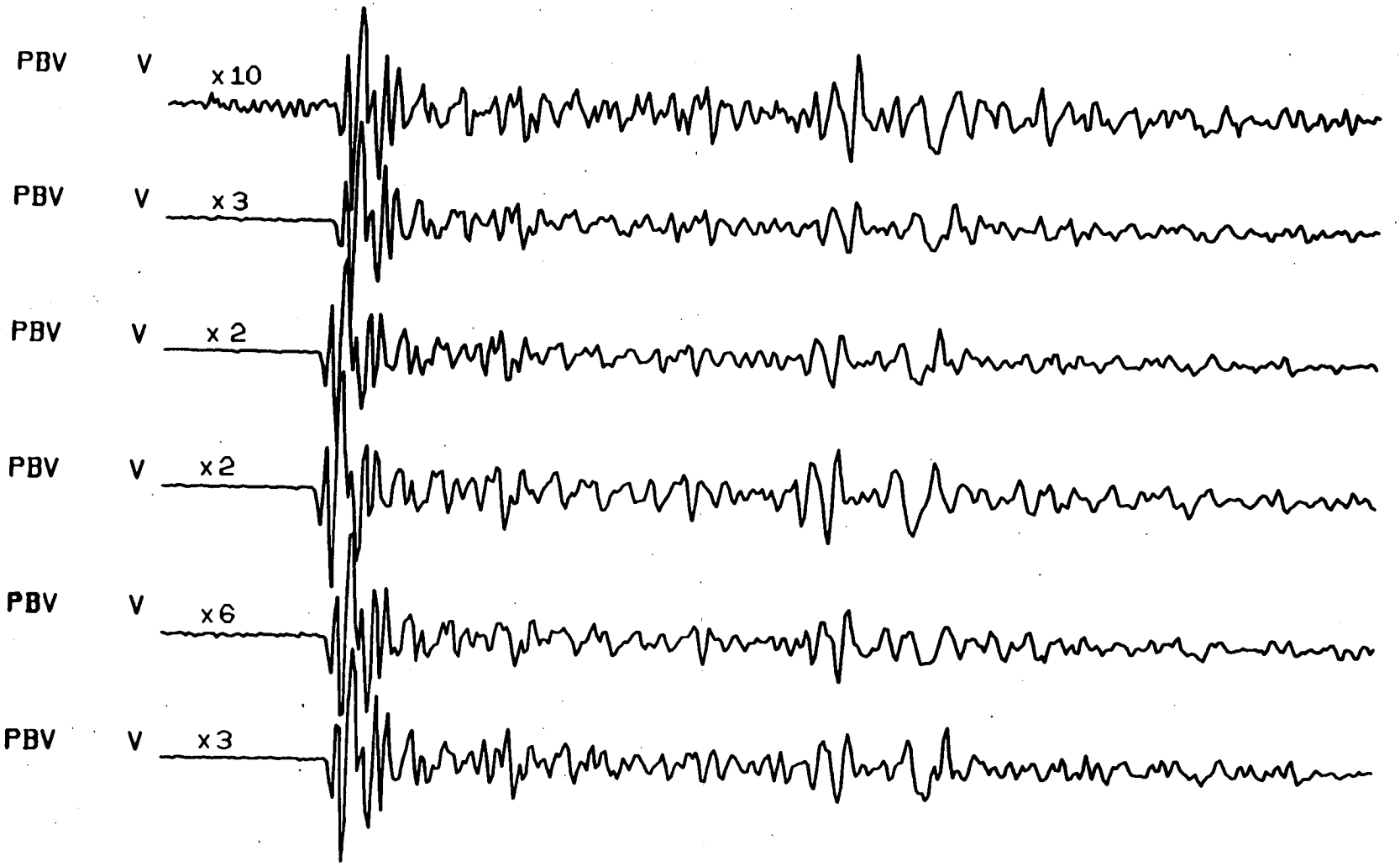

Fig. 2.5 - Six similar earthquakes recorded during TDP-3 at station PB. The relative gain for each trace is shown at the start of the trace.

on the fault.

2.3.5 Earthquake Families and their uses

Prior to 1975, similar earthquakes had only been observed in small groups of two or three spread over a few days. Little importance was attached to these few observations and so the amount of research carried out on them was limited.

In 1975 Hamaguchi and Hasegawa (1975) reported finding a group of seventy-two similar earthquakes that occurred over a period of about fifty days. They were found whilst sorting the data from 50,000 earthquakes recorded after the Tokachi-oki earthquake of 1968. It was Hamaguchi and Hasegawa that termed the phrase *earthquake family*, for any group of earthquakes having a similar wave character. Also around this time other observations of earthquake families were being made such as the study of the Bear Valley, California, earthquake sequence of 1972 (Ellsworth, 1975).

In 1978, Ishida and Kanamori (1978) looked at all the earthquakes which occurred in the epicentral region of the 1971 San Fernando earthquake during the period from 1960 to 1970. Five of the events were found to be located within a small area around the main shock hypocentre and since they were spatially separated from the surrounding activity they were considered to be foreshocks. The waveforms of these five events were found to be very similar and further analyses, including a look at their spectra, suggested that it might be possible, sometime in the near future, to be able to distinguish foreshock sequences from ordinary swarms that have no associated main shock. Unfortunately, further research has been unable to clarify the situation. The original idea is based upon the assumption that foreshocks and swarms will have distinct and consistently different characteristics which will enable them to be separated. However, the characteristics are not consistent, as is highlighted by the observations of Tsujiura (1983b) who came to the conclusion that swarms show similarity but foreshocks do not. This does not agree with the observations of Ishida and Kanamori (1978) as noted

above.

It was mentioned in the previous section that Geller and Mueller (1980) had looked at four similar earthquakes from central California. They found that by low-pass filtering the seismograms, the similarity could be improved and an estimate of event separation could be made. Several other people have since made use of this method. Frankel (1982) found a change in the focal mechanism of events two months prior to a sizeable earthquake in the Virgin Islands. He also observed that events within this period tended to occur in pairs, each pair with similar waveforms, which he estimated to be about 100m apart using the method of Geller and Mueller. Frankel also suggests that since doublets are very unusual in the Virgin Island region they may be indicative of high stress in the vicinity of the impending shock. This again highlights the uncertainty of whether or not foreshocks and clusters can be separated. Pechmann and Kanamori (1982) have examined foreshocks and aftershocks of the Imperial Valley earthquake of 1979. The seismograms of the foreshocks, which are all very similar, are well correlated at frequencies up to 4Hz, suggesting a separation of 200-400m. For the aftershocks, the correlation is not as good suggesting a slightly higher separation.

This type of analysis is not very precise but it can be improved upon by using a relocation method as will be described in the following chapters. Tsujiura (1980, 1981) made use of such a method for several groups of similar earthquakes recorded around the northern Tokyo Bay and Izu Peninsula. Using S-P times, measured by eye, a measure of the focal region was obtained. The error in the measurement is very much determined by the precision with which the S-P time is measured and, in this case, is likely to be of the order of 100m since times are only read to one hundredth of a second.

Similar earthquakes have also been used to analyse the collapse of a caldera in the Galapagos Islands (Kaufman and Burdick, 1980) and to investigate triggering mechanisms in

subduction zones such as the Solomon Islands (Lay and Kanamori, 1980).

There is also one other major use to which similar earthquakes have been put and that is the measurement of changes in velocity. It has long been believed that changes in the seismic wave velocity and the V_p/V_s ratio occur prior to an earthquake (for example: Semenov, 1969; Anderson and Whitcomb, 1975; Rikitake, 1976). It is necessary, therefore, to be able to measure changes in the velocity very accurately, but uncertainty in the crustal structure and hypocentral location make this very difficult.

Until recently, the most accurate methods being used were those involving artificial sources such as airguns, explosives or vibrators (Peake *et al.*, 1977; Buchbinder and Keith, 1979; Leary *et al.*, 1979; Clymer and McEvilly, 1981). The timing precision was of the order of a few milliseconds but the methods are both costly and time consuming as well as being unable to sample very great depths. These methods may, therefore, be of use in areas such as California where the majority of earthquakes are relatively shallow, but in areas where the earthquakes are deeper, they are unlikely to penetrate the hypocentral regions where velocity changes are expected to occur.

In order to sample greater depths, earthquakes have to be used. Unlike artificial sources, the earthquake position and origin time are not known and this makes it impossible to observe travel time changes. However, similar earthquakes can be used since it is known that they originate from the same place and sample the same propagation path each time. Poupinet *et al.* (1982) used a cross-correlation method (as described in the following chapter) to measure the changes in P arrival time between two events that occurred on the Calaveras Fault, California, before and after the Coyote Lake earthquake of 1979. The timing precision was estimated to be four milliseconds. The relative positions of the events were calculated by minimising the sum of the squared differences between the observed and calculated P arrival time differences. The final residuals were then plotted

against azimuth (station relative to epicentre) and interpreted in terms of a change in the velocity anisotropy. This seems plausible since there would have been a significant change in stress accompanying the main shock which would have affected the velocity anisotropy in the region.

Poupinet *et al.* (1984, 1985) developed this further by using a moving window analysis to cross-correlate the whole seismogram (P arrival, S arrival and coda); with the timing precision increased to about one millisecond. A similar analysis to their original work was carried out on a different pair of earthquakes associated with the Coyote Lake earthquake of 1979. In addition to this, they were able to make use of the information in the coda. The coda is believed to consist mainly of scattered S waves reaching the station along numerous different paths and so it is very sensitive to variations in velocity. Should there be a general change in the V_p/V_s ratio between the two events, then the delay of one coda relative to the other would be expected to increase with time along the seismogram. The slope of this increase is proportional to the velocity change. Poupinet *et al.* (1984, 1985) measured the slope on many stations and they came to the conclusion that the S wave velocities had decreased by only 0.2% between the two events. This is very small when compared to the 5% obtained when the change in the V_p/V_s ratio was first measured (Rikitake, 1976, for a review) although later studies in California suggested that it should be 1% or smaller (Boore *et al.*, 1975; Kanamori and Fuis, 1976; Wesson *et al.*, 1977).

Pointing (1985) also attempted a study of three groups of similar earthquakes recorded in the Suguta Valley, Kenya, based on the method used by Poupinet. Unfortunately, the events were only recorded on one or two stations which meant that he was unable to distinguish hypocentral movement from a change in the velocity. Using the ideas put forward by Geller and Mueller (1980) did give some measure of the hypocentral separation but it did not really resolve the problem. This study illustrates very well the problems that may be encountered in the analysis outlined in the following chapters.

Earthquake families are now being observed on networks worldwide, both teleseismically and locally. The individual seismograms are of no more use than any other seismogram, but as a group they hold much more information that can be utilised for looking at both the source and the propagation path. They also open yet another new path towards the ultimate aim of being able to predict earthquakes.

Chapter 3

Earthquake Location and the Relative Location Method

3.1 Introduction

Earthquake families are introduced in the previous chapter as swarms of earthquakes that produce seismograms with similar waveforms and it is assumed that this similarity occurs as a result of the earthquakes having a common source and following near-identical propagation paths. In this and the following chapters, a method is introduced that enables these similar earthquakes to be located, relative to each other, to an accuracy of a few tens of metres and thus allow the source to be examined in detail. Chapter 4 describes and analyses the method used to obtain the required timing precision, but first, chapter 3 considers the problem of determining earthquake locations and goes on to describe the relative location method that is to be used in chapter 5.

Nearly all earthquakes, whether they are local, regional or teleseismic, are routinely located almost as soon as they have been recorded. These locations are referred to as absolute since, for each one, latitude, longitude, depth and origin time are determined. However, the errors involved are large, due to the complexity of the crust which cannot be accurately modelled, and hence the locations will be of little use for probing the source. To get around the problem, a location method is used that calculates the location of one event relative to another. It can be used for any pair of earthquakes that are assumed to have near-identical propagation paths since all crustal errors will be common to both events and can thus be ignored. The method is ideal for use with similar

earthquakes but it can also be used for any earthquakes, such as aftershocks or foreshocks, that are thought to have originated from the same area. In such a case, the error involved in their absolute location will still be greater than any error induced in the relative location method by the break down in the assumption of identical propagation paths. For those events where the assumption is valid the location accuracy is no longer restricted by the method itself but by the precision with which the arrival times can be measured (see chapter 4). In the remainder of this chapter the theory behind the relative location method is explained, preceded by a review of the location method used in this study for obtaining absolute locations.

3.2 Absolute Location Method

Once a data set has been collected, one of the first operations to be carried out is the location of the events within it. The arrival times of the P and S waves are picked directly from the seismogram and passed into a computer program that can calculate the hypocentre and origin time. Many such programs have been written and the choice for a particular application will depend on several factors. For example, different algorithms are needed for different types of earthquake (local, regional or teleseismic) to allow for such things as the Earth's curvature. Also, the programs vary in their complexity and the choice will, therefore, depend on the computing facilities available.

All the earthquakes used in this study are local events for which the most popular program in use is HYP071 (Lee and Lahr, 1975). The input required for the program, apart from the P and S arrival times, is comprised of a crustal model and the coordinates of the recording stations. The crustal model consists of a series of horizontal, isotropic layers each with a specified thickness and velocity. If required, it is also possible to allow for some lateral variation by using a variable first layer. To start the calculation a trial hypocentre is chosen (latitude, longitude, depth and origin time) and the travel times from this to each of the stations are computed. As a rough guide to the error in the

location of the trial hypocentre, the RMS sum of the differences between the observed and computed travel times is calculated. The trial hypocentre is then moved so that the sum of the differences is reduced and the whole calculation is iterated until one of several termination criteria is exceeded. The iteration is stopped if the movement of the trial hypocentre is less than a specified distance or if the RMS sum of the travel time differences cannot be reduced within four attempts or if the number of iterations exceeds a specified number. The final position reached by the trial hypocentre defines the location of the earthquake.

The error involved in the method, as with all absolute location methods, may be very large and can be attributed to imprecision in the arrival times and, more significantly, over-simplification in the crustal model.

For the data used in this study, the arrival times are usually measured to a hundredth of a second which is equivalent to picking to the nearest data point. In terms of the distance travelled by a seismic wave, one hundredth of a second corresponds to several tens of metres and this gives the lower limit obtainable. It is possible to lower the limit if data with a high signal to noise ratio is used. Such data will allow some degree of interpolation between the data points and hence enable more precise arrival times to be picked.

The problem of over-simplification in the crustal model is more difficult to overcome. It is not possible to evaluate the size of the error produced as a result of the simplification because the true structure of the crust is not known. Even if a better, or more reliable, estimate of the structure could be made it would be difficult to use because there is a limit on the complexity that the computer can handle. As a result, absolute locations will never be very accurate, regardless of how precisely the arrival times are measured.

In general, absolute location methods are adequate for most applications since accuracy is not a high priority, but for

examining the source, or for any other case where detail is required, they are totally unsuitable. The following section introduces a method that is able to get around these problems.

3.3 Relative Location Method

3.3.1 Introduction

The relative location method can be used on any group of earthquakes that have a similar origin and which have been recorded at enough stations to give a good azimuthal coverage. One event from the group is chosen to be the master event and all the others are then located relative to it. The absolute location of the group will only be known to the same accuracy as that determined routinely for the master event although within the group itself the accuracy of the relative locations will be vastly superior. The method assumes that the paths from source to receiver are the same for all the events within a group. For fairly widespread groups, such as aftershocks and foreshocks, this is not necessarily the case, but if the method is deemed to be valid up to the point where the accuracy of the relative locations is equal to that of the absolute locations, then it could be justifiably used on any group of earthquakes that cluster within a radius of a few kilometres. The best results, however, are obtained from groups of similar earthquakes since their sources can be considered to be nearly identical and any differences in the propagation path will be negligible.

Absolute location methods use the arrival times of the P and S phases which can be clearly recognised on most seismograms. The difference between the two arrivals (the S-P time) depends on the distance travelled from source to receiver, either of the P or S velocities (V_p or V_s) and their ratio (V_p/V_s). For two events originating from the same region the small difference in the S-P time, measured at any one station, can be attributed to either a difference in location or a change in the V_p/V_s ratio. For the groups of similar earthquakes that are to be analysed later in the thesis, the magnitudes are all small (less than $1.5M_L$) and the time

span only a few days. Hence any changes in stress are likely to be very small and restricted to an area close to the source. Consequently, if there are any changes in velocity they will be restricted to the source area and will not be very big. On this basis it seems unlikely that there will be any change in the V_p/V_s ratio large enough to noticeably alter the S-P time since a significant change over such a small area would be needed. Alternatively, a small change in the V_p/V_s ratio over a large area could be measured but as suggested above there is no reason to assume that there will be any change in the stress, and hence the velocity, outside the source region. All changes in the S-P time can, therefore, be converted into a distance at the source equal to the difference in the propagation paths for the two events. This is the basis of the relative location method.

3.3.2 Conversion of S-P Time into Apparent Hypocentral Separation

Consider two events (A and B) at distances d_1 and d_2 from station X, as shown in Fig. 3.1 (the separation between the events is exaggerated for clarity). The difference that would be observed in the S-P time between the two events could be converted into a difference in hypocentral distance of $d_2 - d_1$ (BB'). The apparent position of event B, as 'seen' by the station and with respect to event A (the master event), will be defined by a sphere centred on the station with radius d_2 (d_1 is taken from the HYPO71 location of event A). The true location will lie somewhere, unknown, on the sphere (shown by the arc in Fig. 3.1). The calculated path difference ($d_2 - d_1$) is referred to as the apparent hypocentral separation and will only be equal to the true hypocentral separation if both events lie on the one raypath. To calculate the true hypocentral separation it is necessary to determine the apparent hypocentral separation at a minimum of three stations. The true location will then be given by the point where the three resultant spheres cross each other.

In practice the data is never perfect and it is likely that the spheres will have no common point. The location is, therefore, calculated as the point that best fits the data using a least

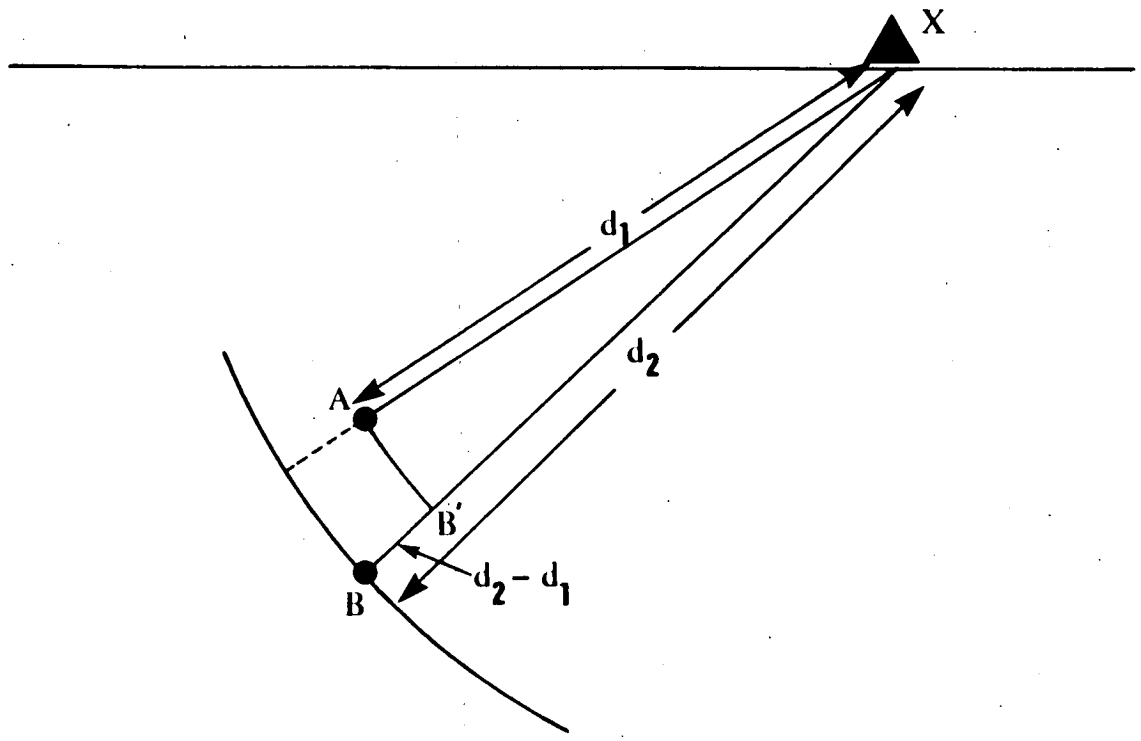

Fig. 3.1 - Two similar earthquakes (A and B) at distances d_1 and d_2 from station X (earthquake separation exaggerated). The change in the S-P time measured at X is due to the apparent hypocentral separation d_2-d_1 (BB') and event B will appear to lie on a sphere of radius d_1+ d_2-d_1) centred on X as indicated by the arc (d_1 taken from the HYPO71 location of event A).

squares procedure and it would help to constrain the solution if more than three stations were to be used.

The factor needed for converting the difference in S-P time to apparent hypocentral separation is defined in terms of the P and S velocities (V_p and V_s) within the source region. Consider two events, distances d_1 and d_2 from the station. The P and S travel times for each event will be

$$T_{p1} = d_1 / V_p \qquad T_{s1} = d_1 / V_s$$

$$T_{p2} = d_2 / V_p \qquad T_{s2} = d_2 / V_s \qquad 3.1$$

where T_{p1} is the P travel time for event 1, and so on. The S-P time for each event will therefore be

$$(S\text{-}P)_1 = (T_{s1} - T_{p1}) = d_1(1/V_s - 1/V_p)$$

$$(S\text{-}P)_2 = (T_{s2} - T_{p2}) = d_2(1/V_s - 1/V_p) \qquad 3.2$$

and hence the difference in S-P time will be

$$T_{s\text{-}p} = [(S\text{-}P)_2 - (S\text{-}P)_1] = (d_2 - d_1)(1/V_s - 1/V_p) \qquad 3.3$$

which reduces to

$$T_{s\text{-}p} = d(V_p - V_s)/V_pV_s \qquad 3.4$$

where $d = d_2 - d_1$. Rearranging equation 3.4 to define the difference in distance in terms of the difference in S-P time gives

$$d = T_{s\text{-}p}V_pV_s/(V_p - V_s) \qquad 3.5$$

or

$$d = FT_{s\text{-}p} \qquad 3.6$$

where $F = V_pV_s/(V_p - V_s)$. In practice, it is not necessary to carry out this calculation since it is incorporated into the next step which is the calculation of the true hypocentral separation.

At this stage it should be pointed out that the crustal model being used here is a simple half-space with P and S velocities equal to those in the source region. Obviously this is not very realistic but it can be shown that the error produced by the simplification does not greatly affect the method and can be ignored. In equation 3.1 the travel times could be divided into travel times inside and outside the source region with those outside cancelling in equation 3.3 (assuming the propagation paths to be identical) leaving equation 3.5 unaffected. Where the error is introduced is after the apparent hypocentral separation has been calculated. It is assumed that the second event lies somewhere on a sphere centred on the station with radius $r = d_1 + d$. However, layering in the crust will cause the waves to refract with the result that they will deviate from the assumed straight line and the sphere will no longer represent the change in distance. To get some idea of the magnitude of the error for the TDP-3 network the change in the S-P time was calculated for two events, placed at a typical depth of 10km and a maximum epicentral distance of 8km, in a crust containing one layer and a half-space with a large velocity contrast between them. For this relatively extreme case the change in the S-P time was negligible (0.2ms compared to a timing precision of 1ms). For most stations the effect would be even smaller, so, unless the crust contains many layers with large velocity contrasts, it would seem reasonable to ignore the effect and proceed to use a half-space.

3.3.3 Computational Details

From each pair or group of events a master event is chosen and its absolute location determined by HYP071 (Lee and Lahr, 1975). The change in S-P time is then measured for all the other events at all possible stations and the results stored in a file ready for input to the relative location program. With additional data, such as station and master event coordinates, the relative locations can now be determined.

First, changes in the distance to each event are calculated for small movements (100m) of the master event in three orthogonal directions (north, east and vertically up). Using equation 3.4, and

assuming values for V_p and V_s in the source region, these distances are then converted to changes in the S-P time. Each station will thus have three readings and with n stations the data can be arranged in a (3 x n) matrix (M).

The problem is now assumed to be a linear one. The matrix M is only valid within the region where V_p and V_s remain unchanged but it is not possible to say just how far this region extends. For the groups of similar earthquakes analysed in chapter 5, event separations are rarely greater than a few hundred metres. It seems unlikely that over this range there will be any significant change in the velocity. Therefore, the assumption of linearity would appear to be justified for similar earthquakes. In chapter 4 support for this assumption is given in the discussion on errors where three earthquakes are located relative to each other in a closed loop. Discrepancies in the closure are used as a measure of the error in the method. If the assumption of linearity is invalid the error would be expected to be large, but it is not.

The S-P time for any point in the vicinity of the master event can now be defined using the matrix M. To facilitate the calculation, the vectors corresponding to the small movements of the master event, as described above, are deemed to be unit vectors which can be used to define any point in space. These points will be displayed as row vectors

$$\mathbf{a} = (a_1, a_2, a_3) \qquad 3.7$$

For example, **a** = (1,0,0) corresponds to a position 100m north of the master event while **a** = (0,1,2) is a point 100m east and 200m above the master event.

To calculate the difference in the S-P time for an event at **a**, the position vector is post-multiplied by the matrix M

$$\mathbf{a}.M = \mathbf{R} = (R_1, R_2 \ldots R_n) \qquad 3.8$$

where n is the number of stations and R_i is the calculated difference in S-P time at the i^{th} station.

However, in this study the reverse is required: given a set of differences of the S-P time, a point in space is needed that best fits the observed data. The observed data can be expressed as a row vector

$$\mathbf{O} = (O_1, O_2 \ldots O_n) \qquad 3.9$$

where O_i is the observed difference in the S-P time at the i^{th} station. Ideally, a vector (**a**) is required such that the calculated differences in S-P time (**R** of equation 3.8) are equal to the observed differences (**O**). In practice, it is unlikely that such a vector can be found because of errors in the observed differences, so the aim is to obtain the best approximation.

Mathematically, this is done by minimizing the sum of the squares of the differences between **O** and **R** (otherwise referred to as a chi-squared function):

$$\sum_i (R_i - O_i)^2 = \text{minimum} \qquad 3.10$$

From equation 3.8 R_i can be expressed as

$$R_i = \sum_j a_j m_{ij} \qquad 3.11$$

and substituting equation 3.11 into equation 3.10 gives

$$\sum_i (\sum_j a_j m_{ij} - O_i)^2 = \text{minimum} \qquad 3.12$$

The aim is to find values of a_j to satisfy equation 3.12. Computationally, this is done by using the condition that the value of the derivative of such a function is zero at any extremum:

$$\frac{\partial}{\partial a_k}\sum_i\left(\sum_j a_j m_{ij} - O_i\right)^2 = 0 \qquad \text{for } k = 1, 2, 3 \qquad 3.13$$

Rearranging equation 3.13 gives

$$\sum_i \frac{\partial}{\partial a_k}\left(\sum_j a_j m_{ij} - O_i\right)^2 = 0 \qquad 3.14$$

and

$$\sum_i \left[\ 2\left(\sum_j a_j m_{ij} - O_i\right).\frac{\partial}{\partial a_k}\sum_j a_j m_{ij}\ \right] = 0 \qquad 3.15$$

$$\text{for } k = 1, 2, 3$$

Equation 3.15 can be simplified to

$$\sum_i \left[\ \left(\sum_j a_j m_{ij} - O_i\right)m_{ik}\ \right] = 0 \qquad \text{for } k = 1, 2, 3 \qquad 3.16$$

since

$$\frac{\partial}{\partial a_k}\sum_j a_j m_{ij} = m_{ik} \qquad 3.17$$

Equation 3.16 gives a set of simultaneous equations which have to be solved for a_j (j = 1, 2, 3). Rearranging equation 3.16 gives

$$\sum_i \left[\ \left(\sum_j a_j m_{ij}\right)m_{ik}\ \right] = \sum_i \left[\ O_i m_{ik}\ \right] \qquad k = 1, 2, 3 \qquad 3.18$$

which can be expressed in terms of the matrices **a**, **M** and **O**, as set out earlier

$$\mathbf{a}.\mathbf{M}.\mathbf{M}^T = \mathbf{O}.\mathbf{M}^T \qquad 3.19$$

where $\mathbf{M}^T$ is the transpose matrix of **M**. Calculating the inverse of the product $\mathbf{M}.\mathbf{M}^T$ and post multiplying both sides by the result

finally gives

$$a = O.M^T(M.M^T)^{-1} \qquad 3.20$$

where $(\ )^{-1}$ indicates the inverse matrix.

Hence equation 3.20 can be used to convert observed changes in the S-P time into relative locations and it has been incorporated into a computer program (RELOC) which is listed in appendix 1 along with sample input and output files.

3.4 Error Analysis

The location method developed in the previous section is a least squares problem and, by following the theory described by Bevington (1969, 150pp)[1], an error matrix can be derived from which it is possible to evaluate the error in 'a' given the reading error in 'O'.

A χ^2 function is defined in its general form as

$$\chi^2 = \sum_i \frac{1}{\sigma_i^2}(R_i - O_i)^2 \qquad 3.21$$

In the previous section the '$1/\sigma_i^2$' term has been omitted from equation 3.10 since σ_i is considered to be constant for all readings and so has no effect on the evaluation of 'a'. Following the same derivation as before, but retaining σ_i, we get

$$\sum_i \frac{1}{\sigma_i^2} O_i m_{ik} = \sum_j a_j \sum_i \frac{1}{\sigma_i^2} m_{ij} m_{ik} \qquad 3.22$$

This is the general form of equation 3.18. Expressing this in matrix form gives

$$\beta = a.\alpha \qquad 3.23$$

1. Bevington, P., R., 1969. Data reduction and error analysis for the physical sciences, McGraw-Hill, New York.

where $\beta = \sum_i \frac{1}{\sigma_i^2} O_i m_{ik}$ and $\alpha = \sum_i \frac{1}{\sigma_i^2} m_{ij} m_{ik}$

The error in a_j is given as the products of the errors in each data point multiplied by the effect that data point has on the determination of a_j :

$$\sigma_j(a)^2 = \sum_i \sigma_i^2 \left(\frac{\partial a_j}{\partial O_i}\right)^2 \qquad 3.24$$

From equation 3.20 we can see that the derivative term will be

$$\left(\frac{\partial a_j}{\partial O_i}\right) = \sum_k (\alpha_{jk})^{-1} \frac{1}{\sigma_i^2} m_{ik} \qquad 3.25$$

and therefore

$$\sigma_j(a)^2 = \sum_k \sum_m \left[(\alpha_{jk})^{-1}(\alpha_{jm})^{-1} \sum_i \frac{1}{\sigma_i^2} m_{ik} m_{im}\right]$$

$$= \sum_k \sum_m \left[(\alpha_{jk})^{-1}(\alpha_{jm})^{-1} \alpha_{km}\right]$$

$$= (\alpha_{jj})^{-1} = \varepsilon_{jj} \qquad 3.26$$

The inverse matrix $\varepsilon = \alpha^{-1}$ is called the error matrix since it contains most of the information needed to estimate the errors. Assuming σ_i to be constant over the whole data set (i.e. $\sigma_i = \sigma$), ε can be expressed in matrix form as

$$\varepsilon = \left[\frac{1}{\sigma^2} MM^T\right]^{-1} = \sigma^2 \left[MM^T\right]^{-1} \qquad 3.27$$

and therefore

$$\sigma_j(a) = \sigma\left(([MM^T]^{-1})_{jj}\right)^{1/2} \qquad 3.28$$

As an example, the location errors for event A4 from appendix 1 have been determined. The reading error for each data point in this event is one millisecond ($\sigma = 1$). σ is given in milliseconds since the location program (RELOC) converts all input times to milliseconds before calculating '**M**'. Also, the locations initially calculated by the program are in units of 100m (hectometres, hm) and are converted to kilometres by dividing by ten. The same must also be done for the location errors produced by equation 3.28. The values for $([MM^T]^{-1})_{jj}$, as extracted from the program, are

$$([MM^T]^{-1})_{11} = 0.0153$$

$$([MM^T]^{-1})_{22} = 0.0183$$

$$([MM^T]^{-1})_{33} = 0.0151$$

and passing these values into equation 3.28 gives final location errors of

$$\sigma_1(a) = 0.124\text{hm} = 0.0124\text{km} = 12.4\text{m}$$

$$\sigma_2(a) = 0.135\text{hm} = 0.0135\text{km} = 13.5\text{m}$$

$$\sigma_3(a) = 0.123\text{hm} = 0.0123\text{km} = 12.3\text{m}$$

Chapter 4

Cross-Correlation Method (Theory and Analysis)

4.1 Introduction

In the previous chapter a method was described for the relative location of groups of earthquakes that are assumed to originate from the same area and follow similar propagation paths. The limit on the accuracy of the method is determined by the precision with which the P and S arrival times can be measured. For events from the TDP data set all arrival times are quoted to the nearest hundredth of a second (the digitisation interval) although this is not necessarily a good indication of the precision of the reading. It should be possible in ideal conditions (i.e. noise free) to increase the precision by interpolating between data points, but in practice this is rarely possible. Therefore, the resultant spatial uncertainty for each reading is approximately 50-60m (the distance travelled by a seismic wave in 0.01 seconds at a typical velocity of 5-6km/s). As noted in the previous chapter, the relative location method can be applied to groups of aftershocks and foreshocks for which routine P and S arrival times are used. If the location method was error free it would be possible to lower the location accuracy below the 50-60m spatial uncertainty of each reading by increasing the number of stations. However, in reality, aftershocks and foreshocks are likely to be fairly widespread leading to errors in the location method introduced by a breakdown in the assumptions of linearity and similar propagation paths. In such a case it would be difficult to estimate the true error in the location although it is still likely to be better than the corresponding absolute locations.

However, for one particular class of earthquakes, it is possible to get the location accuracy down to less than 20-30m. In chapter 2 it was noted that swarms of earthquakes often contain numerous events with waveforms that are very similar. To achieve this the events must be very tightly clustered and, therefore, more likely to justify the assumptions of linearity and similar propagation paths made in the location method. In addition, the waveform similarity allows a cross-correlation technique to be used that can improve the timing precision by at least an order of magnitude over the digitisation interval (regardless of any noise, unless it is so great as to totally swamp the signal). For the TDP data sets this will give a reading precision of 0.001 seconds and a corresponding spatial error of less than 10m.

In the remainder of this chapter the cross-correlation technique is explained in both the time and frequency domains. It is then analysed to compare the two different domains and to examine the effects of changing the window length, noise and signal saturation. Finally, the errors are discussed for the method as a whole, combining the cross-correlation technique with the relative location method.

4.2 Cross-Correlation Method

4.2.1 Introduction

In the relative location method groups of earthquakes are relocated using changes in the S-P time. For groups such as foreshocks or aftershocks, P and S arrival times are measured routinely and S-P times calculated for each event at each station. Any changes in the S-P time are easily measured and the events can then be relocated

$$\text{Change in S-P Time} = (S_2 - P_2) - (S_1 - P_1) \qquad 4.1$$

Alternatively, by rearranging equation 4.1 the change in the S-P time can be expressed as the difference between the relative delay times of the corresponding P and S arrivals

$$\text{Change in S-P Time} = (S_2 - S_1) - (P_2 - P_1) \qquad 4.2$$

In this form the timing precision can now be improved since the relative delay times can be measured using a cross-correlation technique. In the remainder of this section the theory behind the cross-correlation technique is examined.

4.2.2 The Cross-Correlation Function and the Time Delay

Cross-correlation is a mathematical operation that enables two signals to be compared for similarity and, if they are similar, to measure the time delay between them. The actual mathematics of the operation, which can be carried out in either the time domain or the frequency domain, will be explained later in the section. In fig. 4.1a,b two pairs of similar earthquakes are shown as recorded on two different components of the TDP-3 network. Even though the lower event has 2-3 times the amplitude of the upper one (an observation hidden by the fact that the seismograms are normalised) the similarity between them is good at all frequencies, suggesting that the events are very close (chapter 2). For both pairs, sections of the seismograms are extracted and the cross-correlation function calculated (in this case it is in the time domain). Each section (in future referred to as a window) contains 65 samples and its position is marked by bars above and below the seismograms. The cross-correlation function is plotted out below the seismograms and has been smoothed using a cubic spline.

From the cross-correlation function, the similarity is measured by the height of the central peak relative to the background level of the function (the absolute height can be ignored since it is largely dependant upon the amplitude of the seismograms). It should be noted that the background level cannot always be taken to be the level of the signal on either side of the central peak. As in fig. 4.1a (and less so in fig. 4.1b) the cross-correlation function has several other peaks that gradually diminish in amplitude away from the central peak. These peaks are caused by the presence of a dominant frequency within the S phase, a point that will become clearer once the theory has been presented. The background level

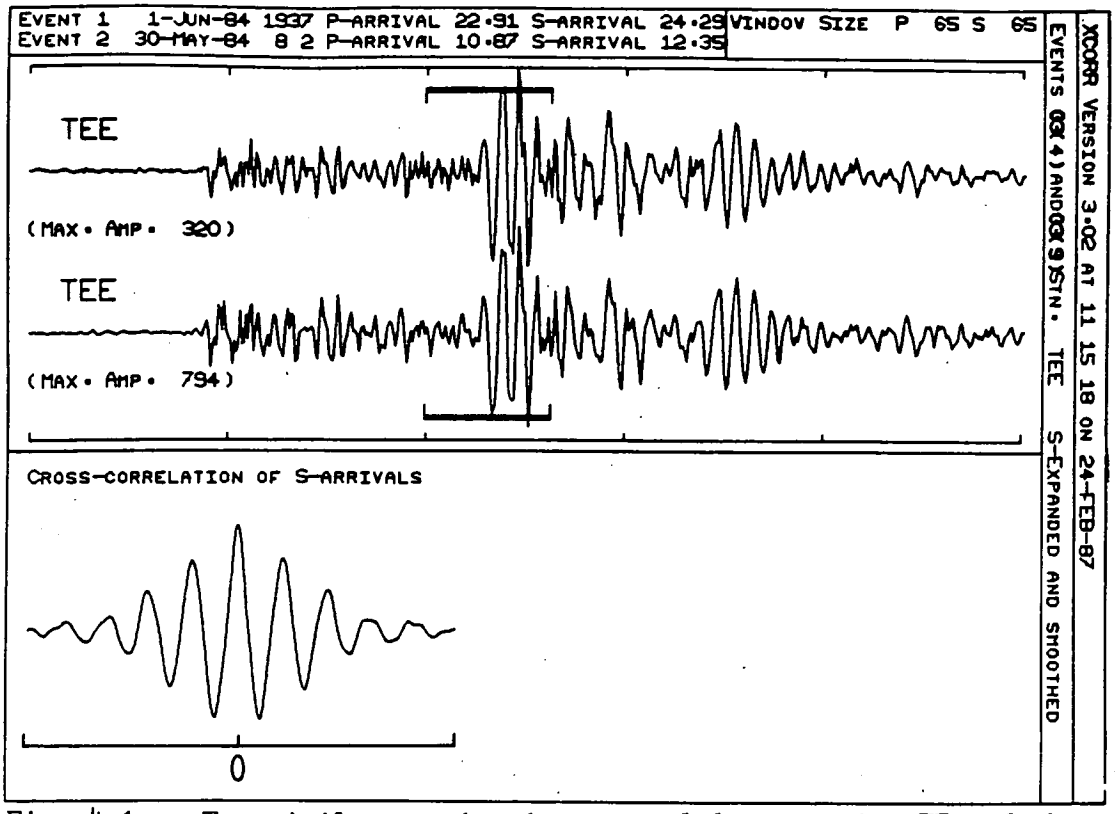

Fig. 4.1a - Two similar earthquakes recorded at station TE and the cross-correlation function calculated for sections of the seismograms containing the S-arrival (as indicated by the bars above and below the seismograms).

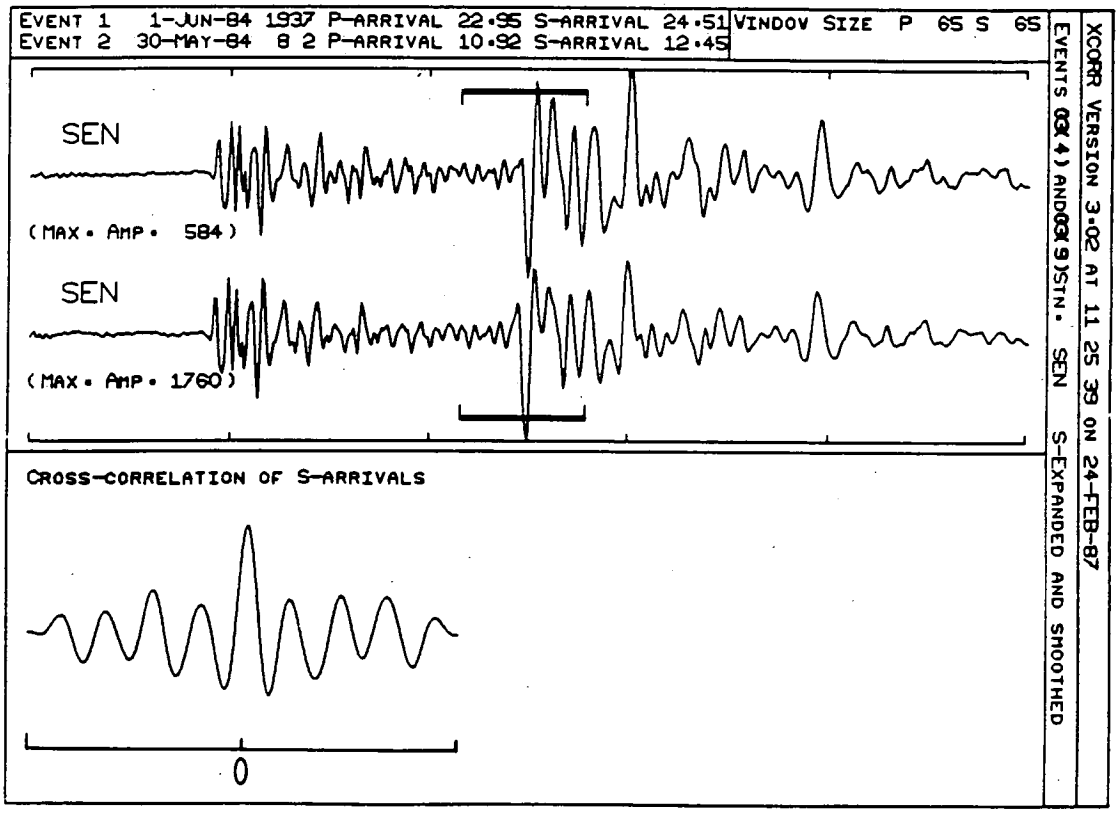

Fig. 4.1b - Two similar earthquakes recorded at station SE and the cross-correlation function calculated for sections of the seismograms containing the S-arrival (as indicated by the bars above and below the seismograms).

can thus be measured at the point where the peaks die away. In fig. 4.1a this would appear to be at the very extreme of the cross-correlation function as plotted, but in fig. 4.1b it does not appear to have been reached.

The other, more quantitative, measure that can be taken from the cross-correlation function is the time delay between the seismograms. If the seismograms were perfectly aligned within the window then the central peak would lie exactly over the middle (marked by a zero). Any amount it is offset is a measure of the misalignment of the seismograms. The calculation of this offset is dealt with in the following section. To obtain the absolute time delay between the two S arrivals would require knowing the start times of the two windows. However, for the purpose of the present study this is not necessary. Providing the relative positions of the seismograms do not change for the P arrival time delay measurement, the change in the S-P time is simply given by the change in the position of the central peak of the cross-correlation functions.

In practice, the time delay is not only calculated for the P and S arrivals but for the whole seismogram using a moving window analysis. A window of set length is moved along the seismogram two samples at a time. At each point the cross-correlation function is calculated and the offset of the central peak measured which is then plotted, as a function of time, below the midpoint of the window. In fig. 4.2 an example is shown of two seismograms above a plot of the time delay as calculated using the window shown.

The length of the window is very important. If it is too short, the window may not contain sufficient signal for the delay to be properly evaluated. If it is too long, the window may pick up more than one phase, each phase with a different time delay and an ill-defined overall time delay that is an average over the whole window. In section 4.3.4 the effects of changing the window length will be analysed in greater detail. For the rest of the analysis the window is set to a length of 0.64 seconds (64 samples).

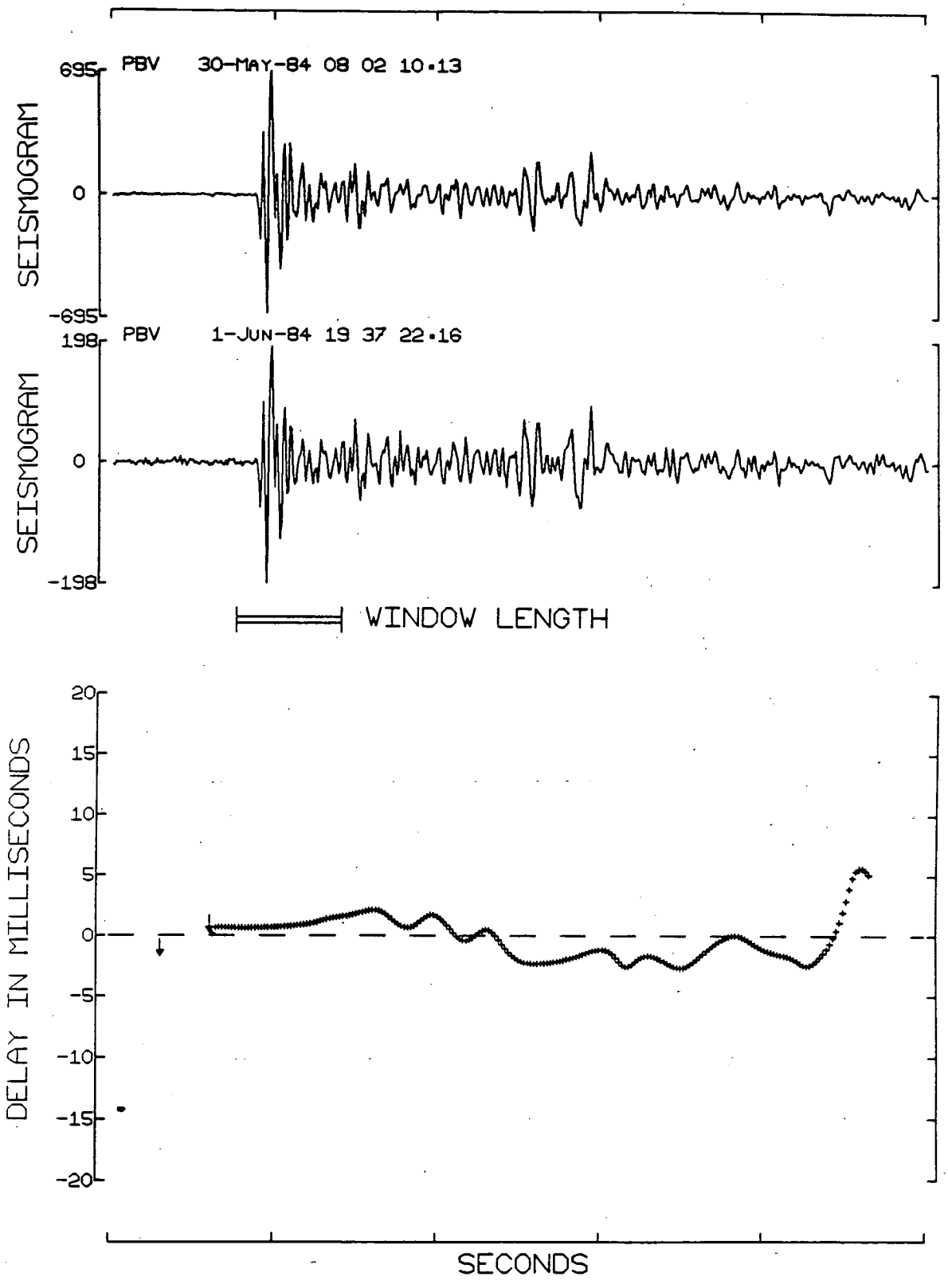

Fig. 4.2 - Two similar earthquakes recorded at station PB and the time delay function calculated in the time domain using the window shown.

Before calculating the cross-correlation function it is important to reduce the windowed signal to a mean zero level. The presence of any DC bias would result in a meaningless cross-correlation function. In addition, the window may also be cosine tapered in order to reduce the effects of the cut-off at either end.

The next stage is to calculate the cross-correlation function. Up to now the examples that have been shown have all been in the time domain and in the following section (4.2.3) the theory behind it will be expanded upon. It is also possible to carry out the calculations in the frequency domain and this will be explained in section 4.2.4. Each domain has its own advantages and disadvantages and these will be discussed later.

4.2.3 Delay Measurement in the Time Domain

In the time domain, the cross-correlation function, c(t), for two continuous series, a(t) and b(t), is given by

$$c(t) = \int_T a(T)\ b(T-t)\ dT \qquad 4.3$$

For discrete data, such as that used in this study, equation 4.3 can be written as

$$c_t = \sum_T a_t\ b_{T-t} \qquad 4.4$$

Computationally, the value of the cross-correlation function at time t involves displacing one of the series by the number of samples corresponding to t and summing the products of the newly aligned data points. For the complete cross-correlation function, this is repeated for all values of t.

If the series are similar, the cross-correlation function will peak when the series are most closely aligned. At this point, peaks will line up with peaks and troughs with troughs, resulting in a large positive correlation. However, the discrete nature of the series and of the resultant cross-correlation function means that it

is unlikely that the alignment will be perfect and the true peak will lie somewhere between the calculated points. Fig. 4.3 shows an example of two series and their cross-correlation function with the middle twenty points expanded to show the actual data points (crosses) superimposed upon the smoothed curve. The smoothing is done using a cubic spline for presentational purposes only.

To calculate the true position of the peak it is necessary to interpolate between the data points. Although the position could be found by measuring the peak of the smoothed function, in practice, it is done by finding the zero crossing of the differences between the data points on either side of the peak (the two methods can be shown to be equivalent). An increase in the reading precision by an order of magnitude over the digitisation interval is thus easily obtained. The value determined for the position of the peak is then used to construct the time delay plot as described in the previous section.

4.2.4 Delay Measurement in the Frequency Domain

The time delay measurement can also be carried out in the frequency domain and the method used here follows that of Poupinet *et al.* (1984). First, it is necessary to calculate the Fourier transforms of the signals a(t) and b(t)

$$a(t) \longrightarrow A(f)$$

$$b(t) \longrightarrow B(f)$$

The cross-spectrum is then calculated as

$$C(f) = B(f)^{*}.A(f) \qquad 4.5$$

where $B(f)^{*}$ is the complex conjugate of B(f). This operation is the frequency domain equivalent of cross-correlation and C(f) is the Fourier transform of the cross-correlation function

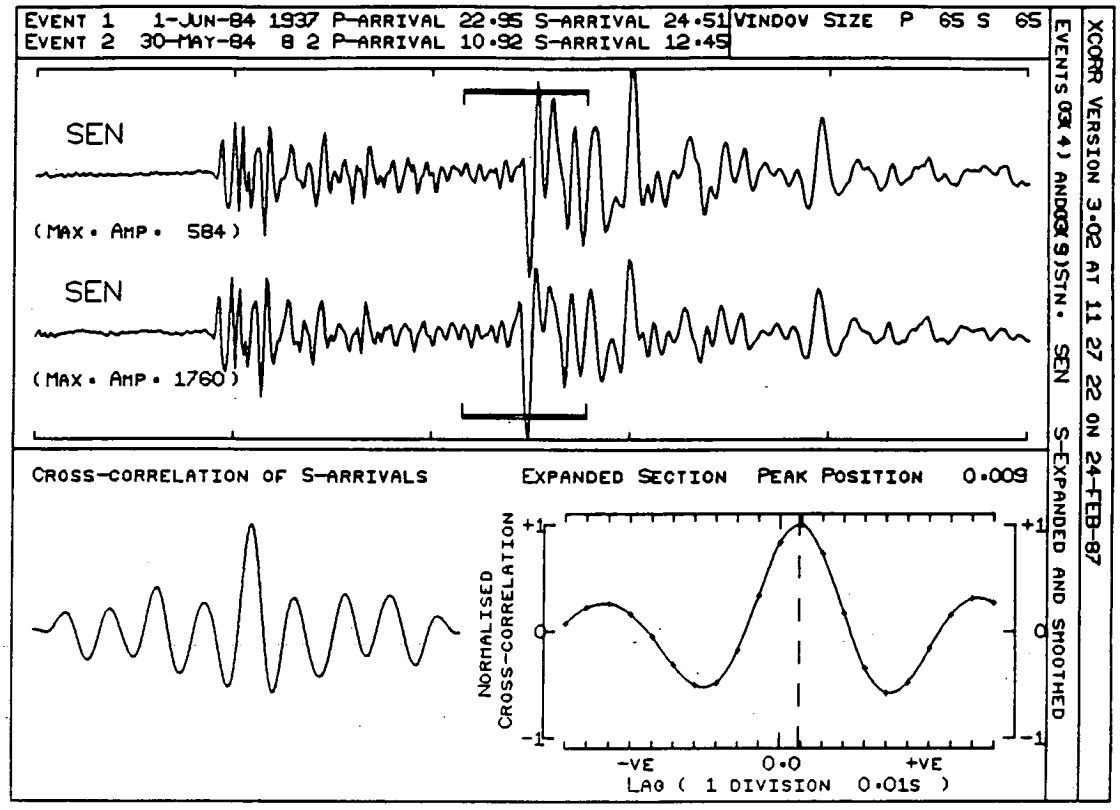

Fig. 4.3 - Two similar earthquakes recorded at station SE and the cross-correlation function, calculated for the window shown, with the middle twenty points of the function expanded. The crosses mark the actual data points to which a smoothed curve has been fitted using a cubic spline.

$$C(f) \longrightarrow c(t)$$

C(f), which is a complex series, can be divided into separate amplitude and phase components. The time delay (δ) and the phase ($\phi(f)$) are related by

$$\phi(f) = 2\delta\pi f \qquad 4.6$$

which means that if the phase is plotted against frequency the result will be a straight line with gradient $2\delta\pi$. Using a least squares procedure the gradient can be determined and the time delay measured. However, there are problems.

The presence of noise will result in the signals being incoherent, particularly at high frequencies. This will affect the phase calculation and cause the plot of phase against frequency to deviate from a straight line. To help eliminate the effects of this on the delay calculation, the coherency is computed.

First, the amplitudes of the input signals (A(f) and B(f)) and the square root of the amplitude of the cross spectrum (C(f)) are determined. The resultant series are then smoothed using a centred five point triangular operator and are represented by $A(f)'$, $B(f)'$ and $C(f)'$. The coherence, H(f), is then calculated as

$$H(f) = \frac{C(f)'}{A(f)'.B(f)'} \qquad 4.7$$

The range of H(f) is from zero (no coherence) to one (total coherence) and it is a measure of the similarity of the frequency content of each series.

The coherence is then used to calculate a weighting factor, W(f), defined as

$$W(f) = \frac{H(f)^2}{1 - H(f)^2} \qquad 4.8$$

With an equation such as this a small drop in the coherence will result in large drop in the weight. For example, H(f) = 0.99 gives W(f) = 49.3 whereas H(f) = 0.95 gives W(f) = 9.3 and H(f) = 0.8 gives W(f) = 1.8.

In the least squares procedure for measuring the gradient, W(f) is used to weight each point in the phase - frequency plot. The less coherent any particular frequency then the less the phase at that frequency will influence the calculation. The value of the time delay determined from the gradient is then used to construct the time delay plot as described in section 4.2.2.

A single computer program has been written that encompasses both the time and frequency domain methods (SERDEL) and this is listed in appendix 2.

4.3 Analysis of the Cross-Correlation Method

4.3.1 Introduction

Previous studies that have used a cross-correlation technique on groups of similar earthquakes have tended to carry out all calculations in the frequency domain (for example: Poupinet *et al.*, 1982, 1984; Pointing, 1985). However, it is not obvious why the frequency domain should be better to use than the time domain, or vice versa, since theory suggests that they should be equal. In practice, computational difficulties and the resulting effects of noise mean that differences do exist. By comparing the results obtained using the two different domains, this section attempts to look more closely at these differences and to outline the respective advantages and disadvantages of the two methods.

The precision with which the time delays are measured can be affected by a number of factors such as the length of the window, the presence of noise or a saturated signal. In general, both domains are affected although the magnitude of the effect can vary between them. The remainder of this section looks closely at these effects and the errors they introduce into the measurement.

4.3.2 Time Domain versus Frequency Domain

The theory of how time delay measurements are carried out in both the time and frequency domains is described in the previous section (4.2). For comparison, fig. 4.4a,b shows the plots of time delay against time along the seismogram for one pair of similar earthquakes in both the time domain (fig. 4.4a) and frequency domain (fig. 4.4b). Each point (cross) represents the time delay for a window (size as indicated on the diagram) centred on that point.

From these plots the time delays that correspond to the P and S arrivals can be read off and the difference calculated. These arrivals are usually quite easy to identify from the seismograms and are characterised on the time delay plot by a certain amount of stability in the function. The reason for this is that the P and S arrivals are coherent and dominate the seismogram, thus giving a very stable cross-correlation function as the window traverses the phase. On the other hand, the P and S codas contain arrivals that have been scattered and that have undergone phase and amplitude changes during propagation. They are, therefore, much more sensitive to changes in the propagation path and, as a result, lose some of their coherency. Their presence, together with any incoherent noise, leads to a less stable cross-correlation function and hence time delay function.

In fig. 4.4a,b it can be seen that the time delay functions in both the time and frequency domains are similar in character but differ in their degree of scatter. However, from the descriptions of the methods given earlier it is not obvious as to why there should be such a difference. For this reason, appendix 3 has been written to analyse and illustrate the frequency domain method in more detail.

In brief, the increased scatter in the frequency domain is caused by incoherency between the signals which gives high weighting values to unstable sections of the phase and results in a distortion of the estimation of the phase gradient. In the time domain method no direct weighting system is used, but, in calculating the time

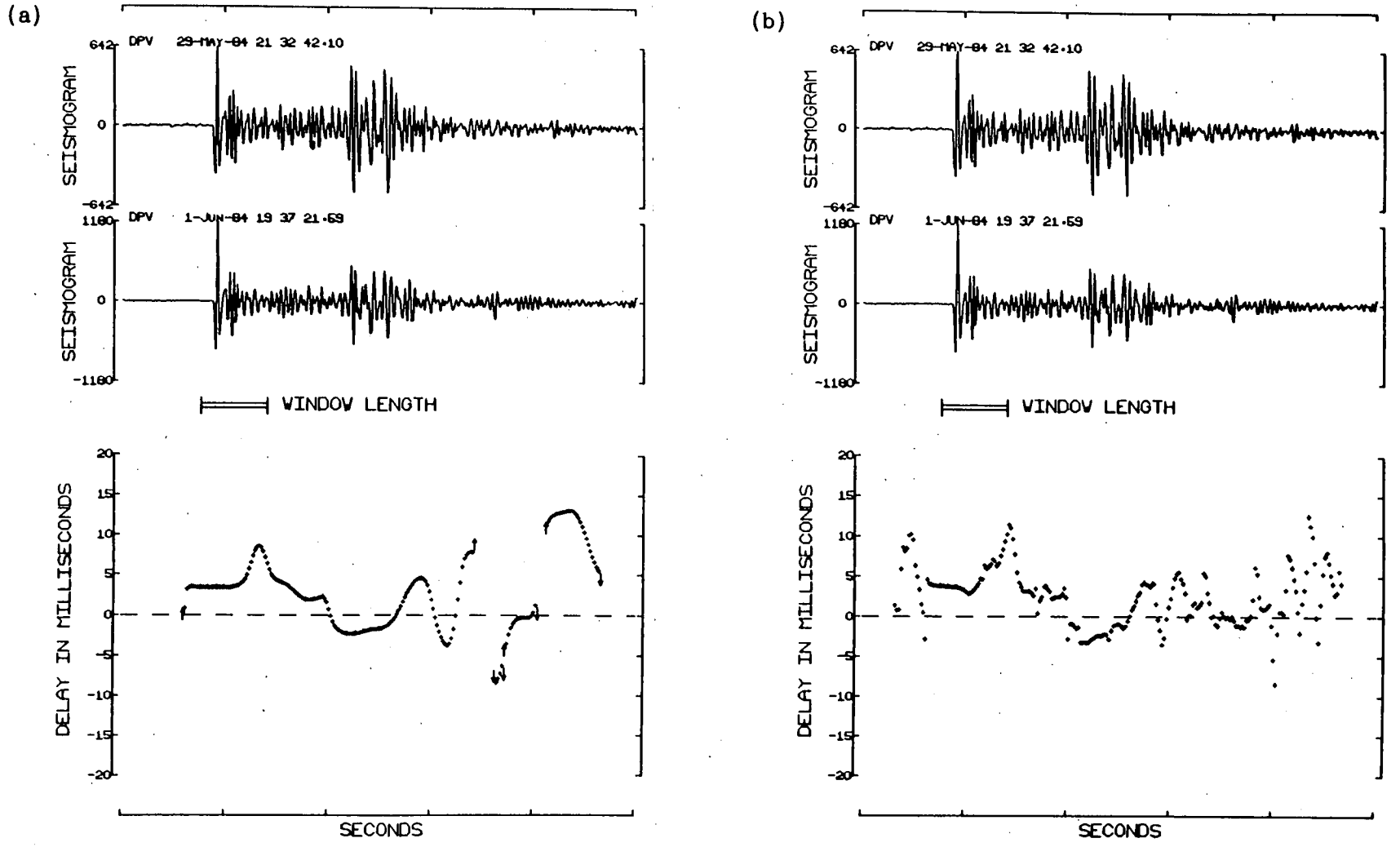

Fig. 4.4a,b - The time delay function for a pair of similar earthquakes calculated in (a) the time domain and (b) the frequency domain.

delay, the results are implicitly weighted by the cross-spectral amplitude. It is shown in appendix 3 that, by implementing a similar weighting system, the frequency domain method can produce time delay functions which are very similar to the corresponding functions in the time domain.

One difference that still exists, regardless of the weighting system used, is the way in which the time delay shoots off scale in the time domain plot. The delay measurement is taken from the peak of the cross-correlation function which is stable when the correlation is good. However, when it is poor the central peak descends into the background level such that it is no longer the highest peak. As a result, the time delay measurement suddenly jumps by an amount related to the dominant period of the seismogram, which may be as much as one tenth of a second. The presentational effect of this can be seen at the end of the time domain plot where the arrows indicate that the time delay has gone off scale.

Finally, it is worth pointing out that although the two methods frequently produce slightly different results, the difference is rarely more than 1ms and can be regarded as negligible.

4.3.3 The Effect of Changing the Start Times

The program that carries out the cross-correlation (as listed in appendix 2) has one major drawback at the time of writing. When the phase of the cross-correlation function is calculated in the frequency domain no attempt is made to unwrap it. All phase values are calculated to lie within the bounds of 180^{o} to -180^{o}. If the delay between the signals becomes sufficiently large, the phase will either increase or decrease rapidly and on reaching $+/-180^{o}$ will wrap itself around (for example 190^{o} will become -170^{o}). This will have the effect of decreasing the magnitude of the gradient and making nonsense of the delay.

To ensure that this is not a problem, the two seismograms must be lined up to within 0.02 seconds before starting. In fig. 4.5a-h

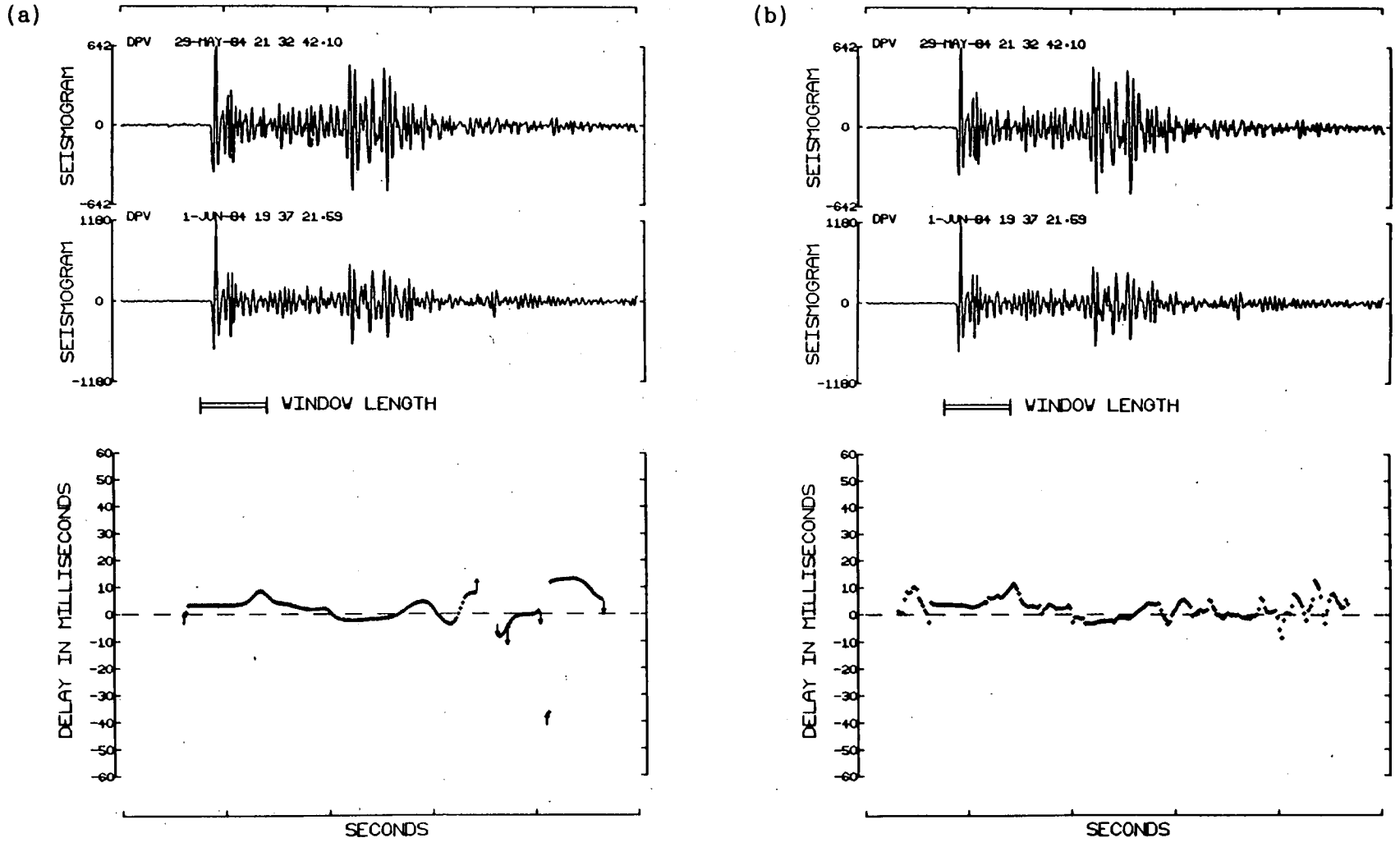

Fig. 4.5a,b - The time delay function for a pair of similar earthquakes with the seismograms aligned to the nearest 1/100 of a second in (a) the time domain and (b) the frequency domain.

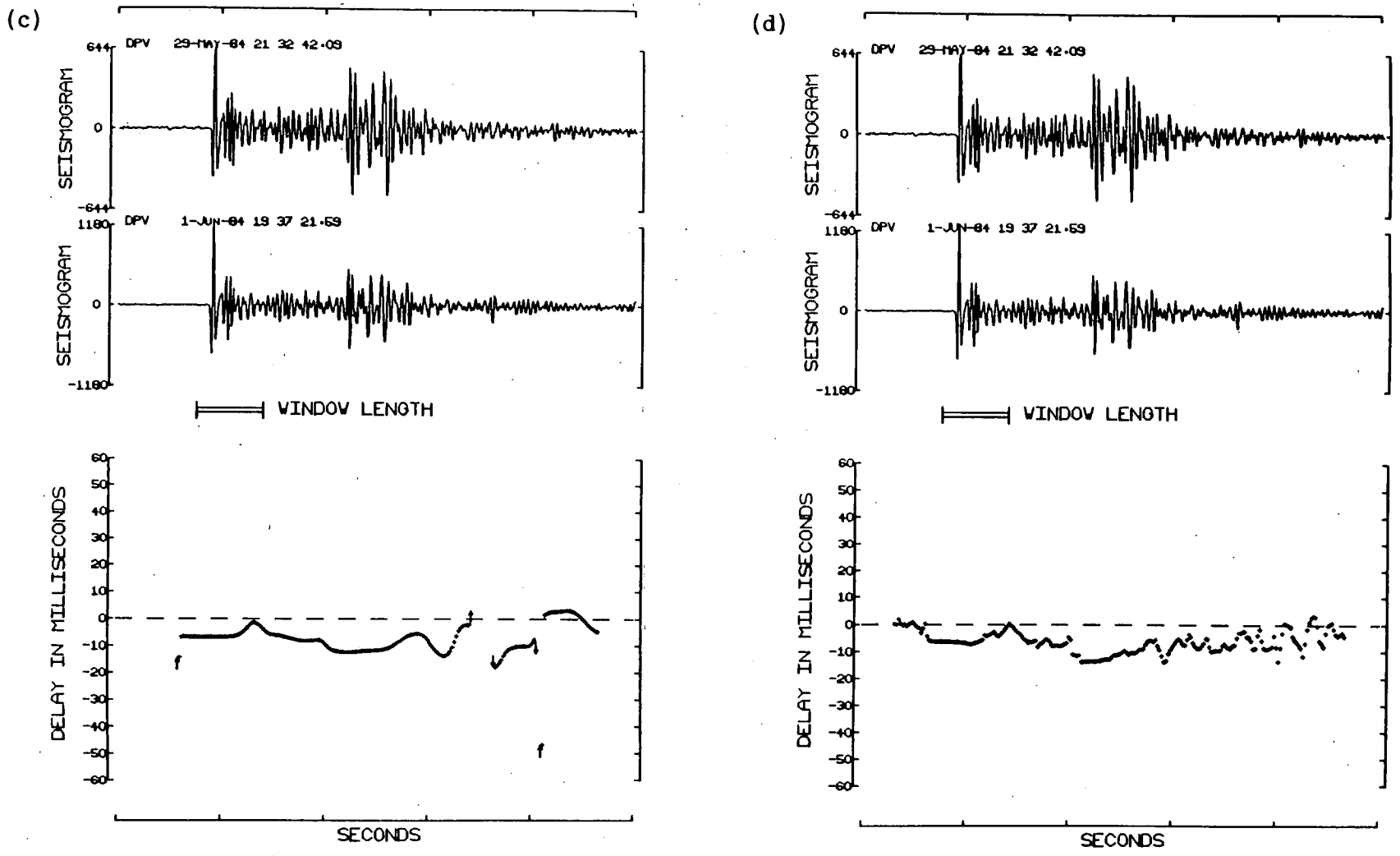

Fig. 4.5c,d - The time delay function for a pair of similar earthquakes with the seismograms displaced by 1/100 of a second in (c) the time domain and (d) the frequency domain.

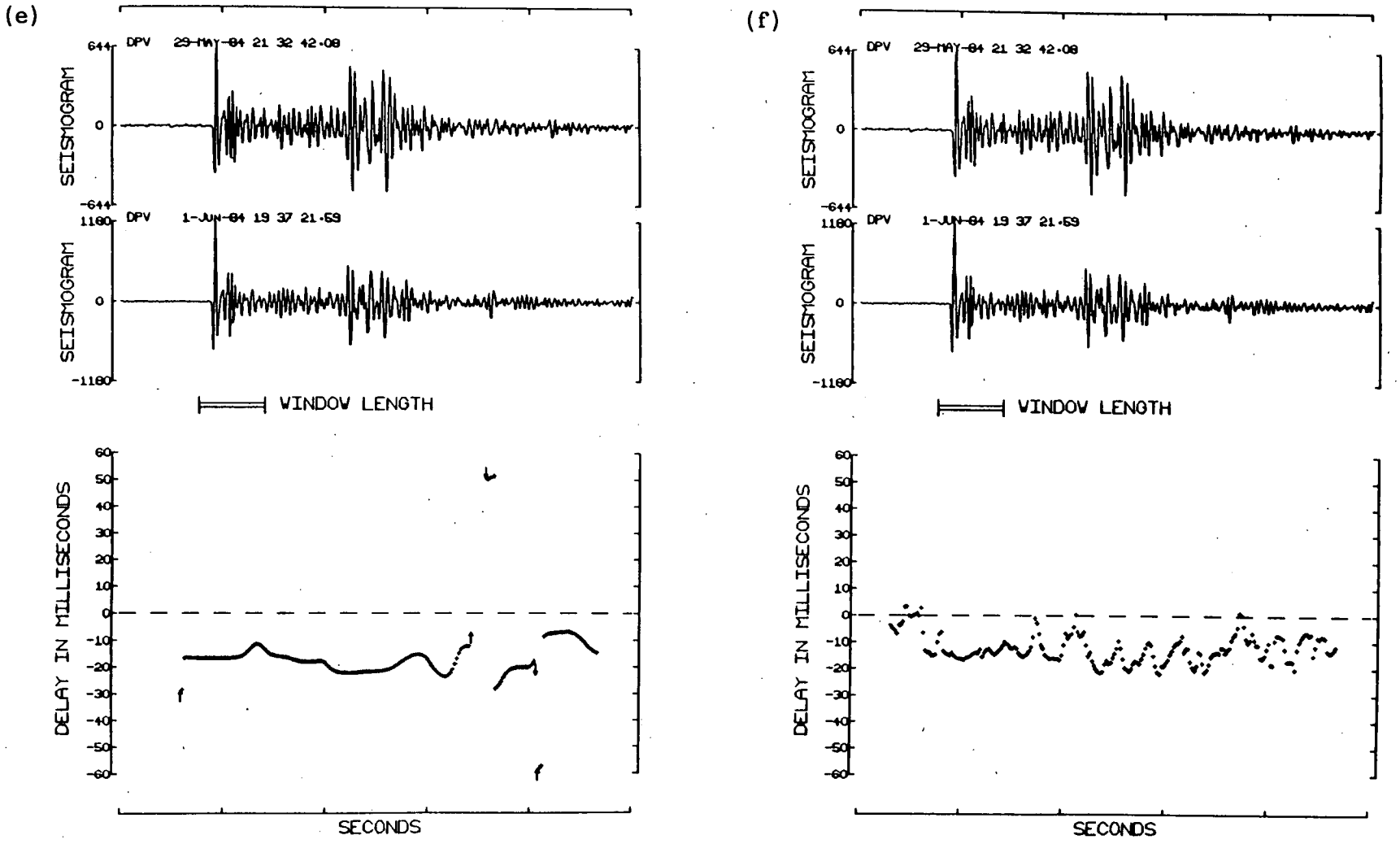

Fig. 4.5e,f - The time delay function for a pair of similar earthquakes with the seismograms displaced by 2/100 of a second in (e) the time domain and (f) the frequency domain.

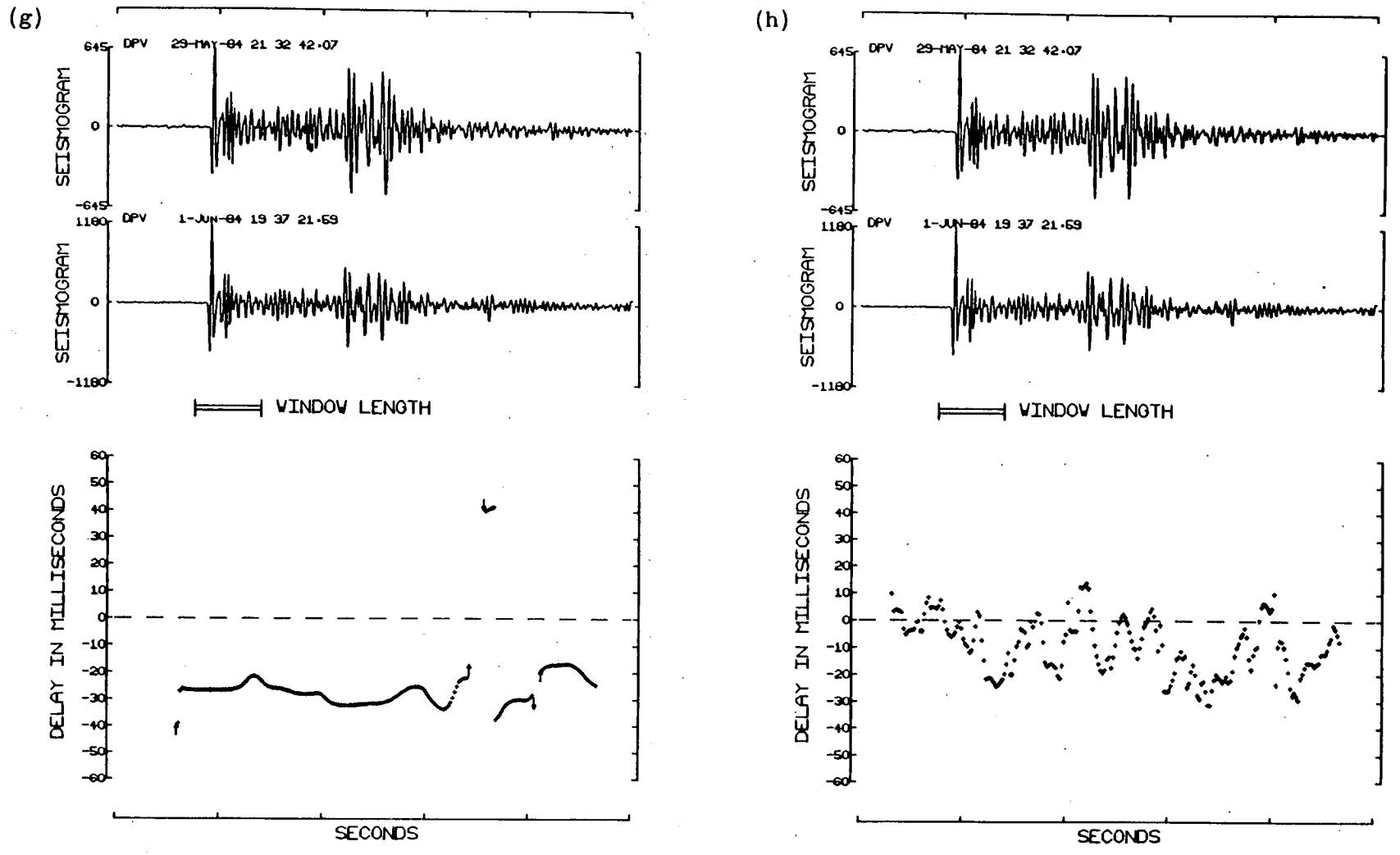

Fig. 4.5g,h - The time delay function for a pair of similar earthquakes with the seismograms displaced by 3/100 of a second, in (g) the time domain and (h) the frequency domain.

the effects of not unwrapping the phase are demonstrated. Fig. 4.5a,b shows the time delay function with the seismograms lined up to the nearest hundredth of a second and in fig. 4.5c,d with one of the seismograms displaced by 0.01 seconds. In both cases the time and frequency plots are very similar. In fig. 4.5e,f the displacement is increased to 0.02 seconds and the time delay plot calculated in the frequency domain begins to lose its structure although the time domain plot remains unaffected. With the displacement increased again to 0.03 seconds (fig. 4.5g,h) the frequency domain plot becomes very scattered, having lost all its previous structure. From here on the time delay function will oscillate about the zero line as the phase keeps wrapping itself with increasing delay.

As can be seen, the time domain does not have an equivalent problem. Displaced signals will only be a problem when the displacement becomes a significant proportion of the sample window (i.e. several tenths of a second), which is very unlikely to happen.

4.3.4 The Effects of Changing the Window Length

The window length is a critical parameter in the cross-correlation calculation since it determines how many data points are to be used. In the following study a window length of 0.64 seconds (64 samples) is used and an example of the time delay function produced by this window is shown in fig. 4.6a,b for both the time and frequency domains. The functions are both relatively stable and similar over a major part of the seismogram. However, in fig. 4.6c,d the window length is cut to 32 samples and the time delay functions begin to lose their stability and similarity. In both domains the time delay plots show a higher degree of scatter, although the regions corresponding to the P and S arrivals are still relatively stable. With the window halved again to 16 samples (fig. 4.6e,f) the structure in the time delay function is almost totally lost. There is still some stability in the P arrival delay in both domains, but the S arrival delay is totally lost in the frequency domain plot and can only be read from the time domain plot with prior knowledge of its position.

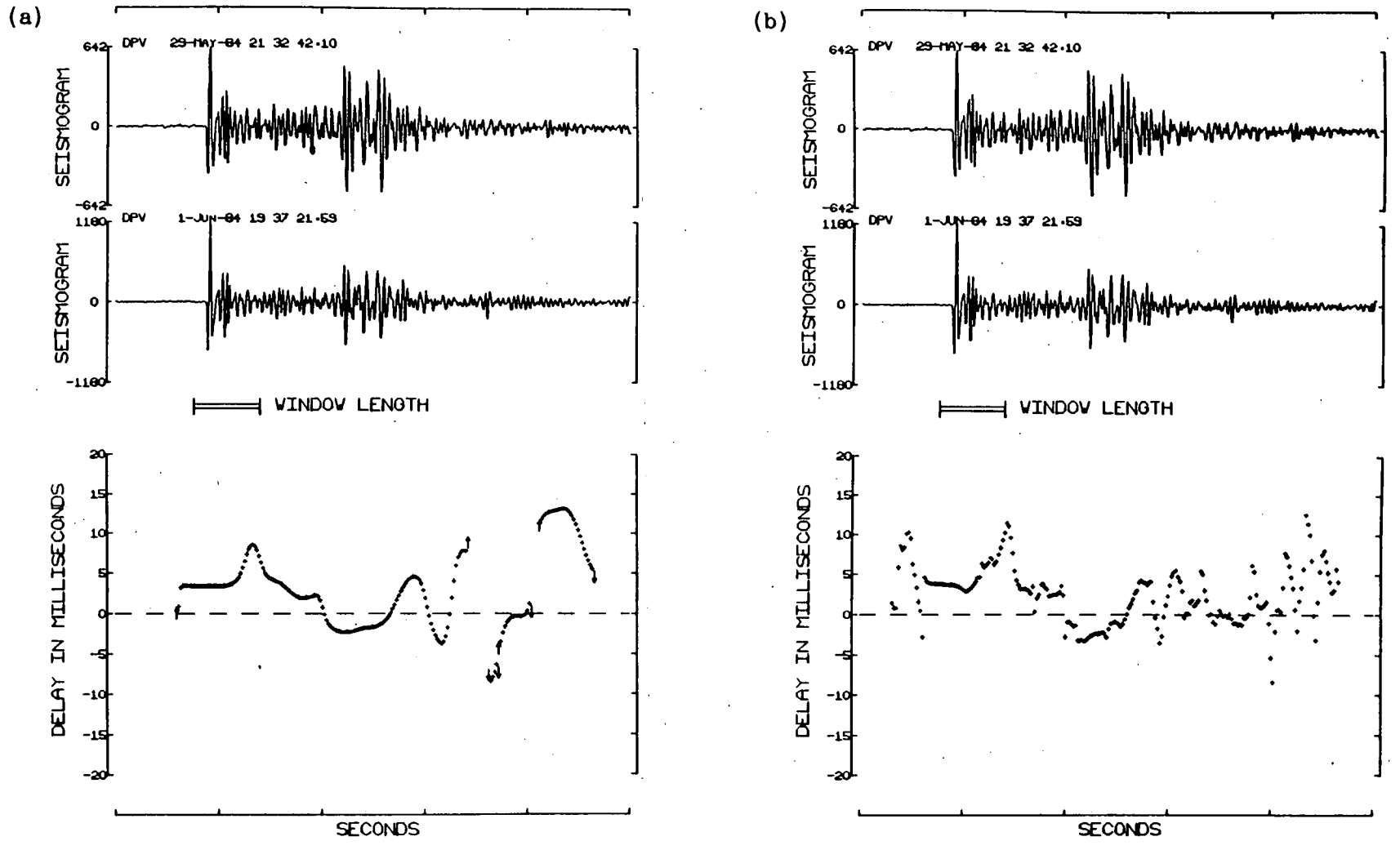

Fig. 4.6a,b - The time delay function for a pair of similar earthquakes calculated using a window length of 64 samples in (a) the time domain and (b) the frequency domain.

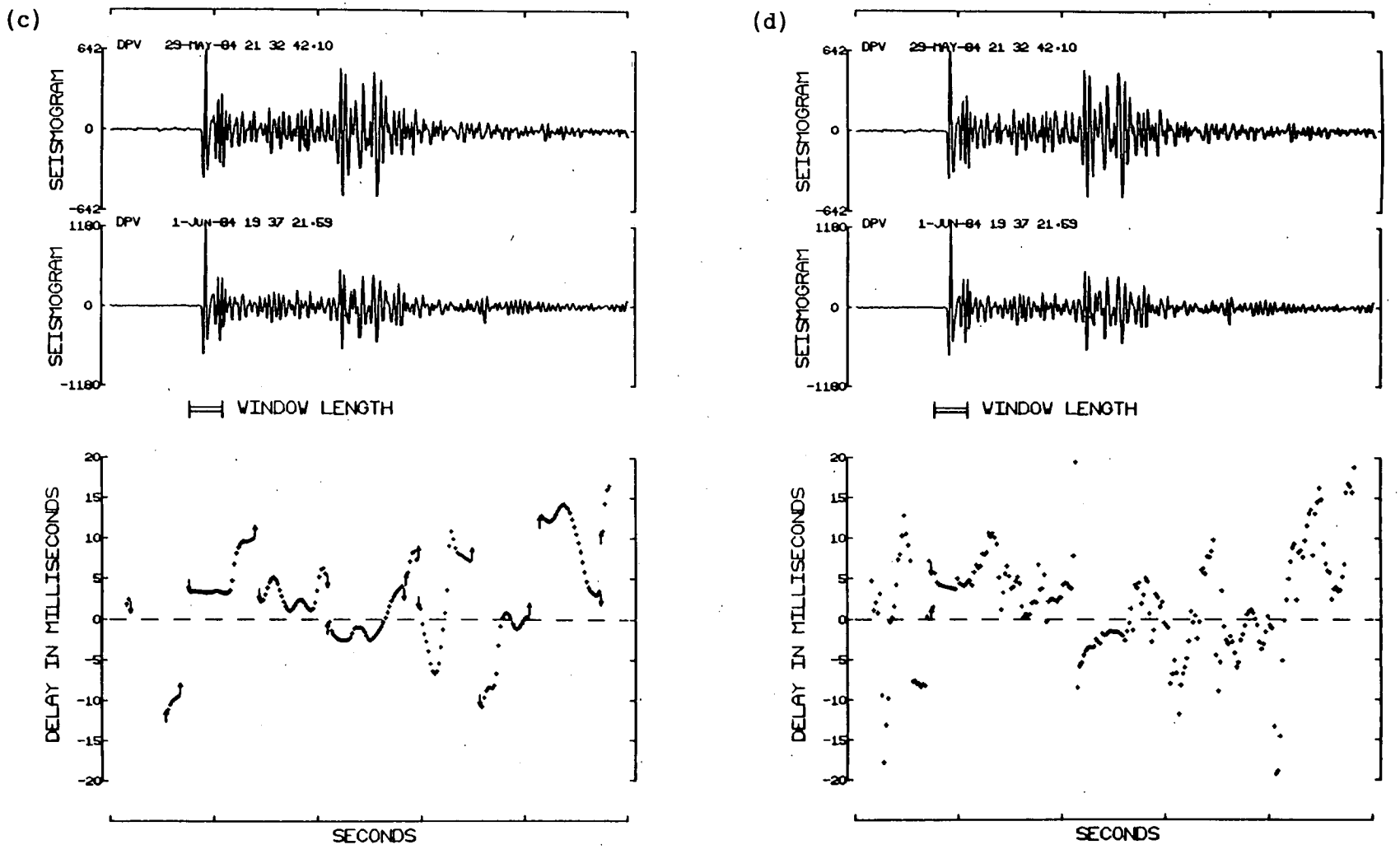

Fig. 4.6c,d - The time delay function for a pair of similar earthquakes calculated using a window length of 32 samples in (c) the time domain and (d) the frequency domain.

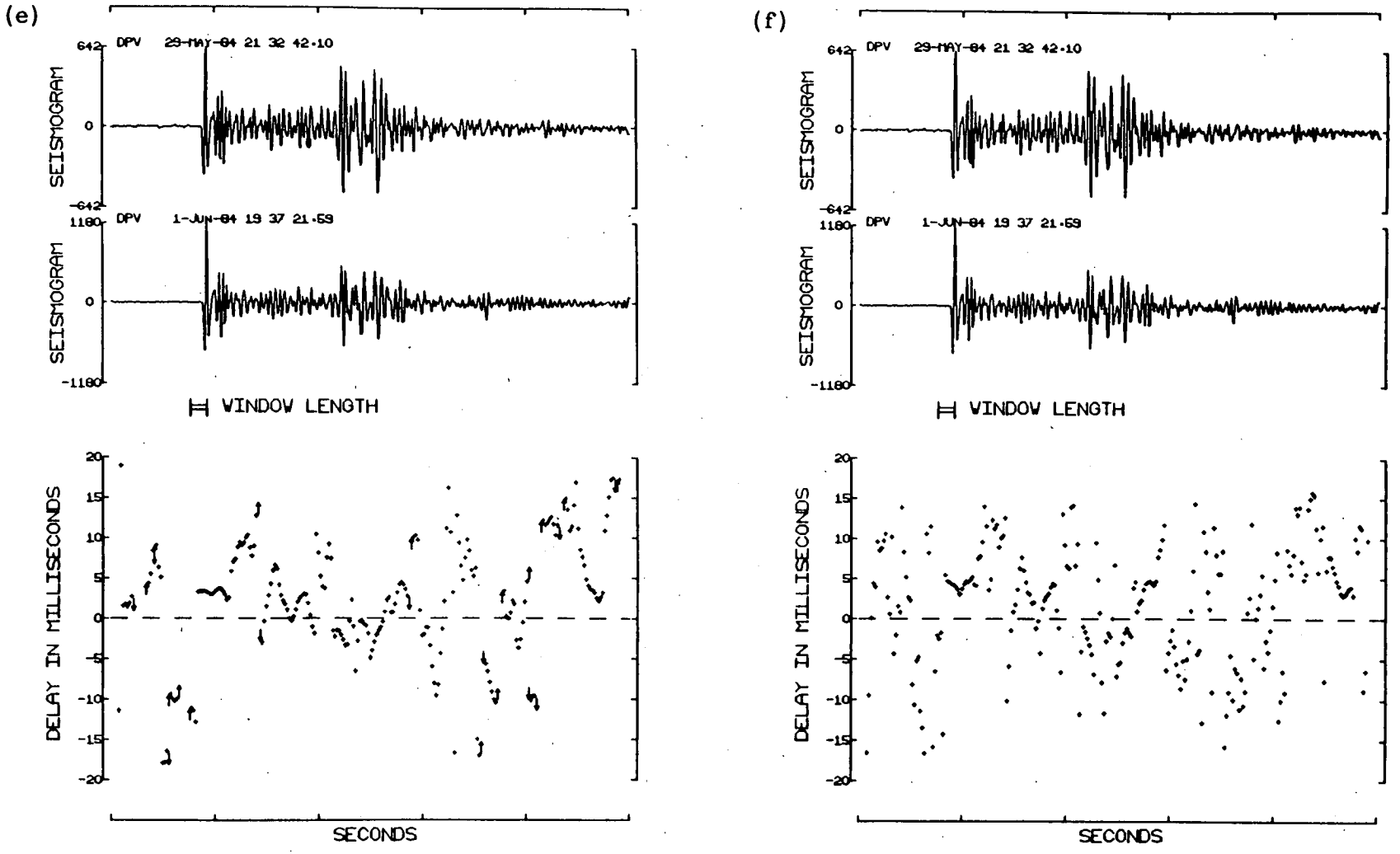

Fig. 4.6e,f - The time delay function for a pair of similar earthquakes calculated using a window length of 16 samples in (e) the time domain and (f) the frequency domain.

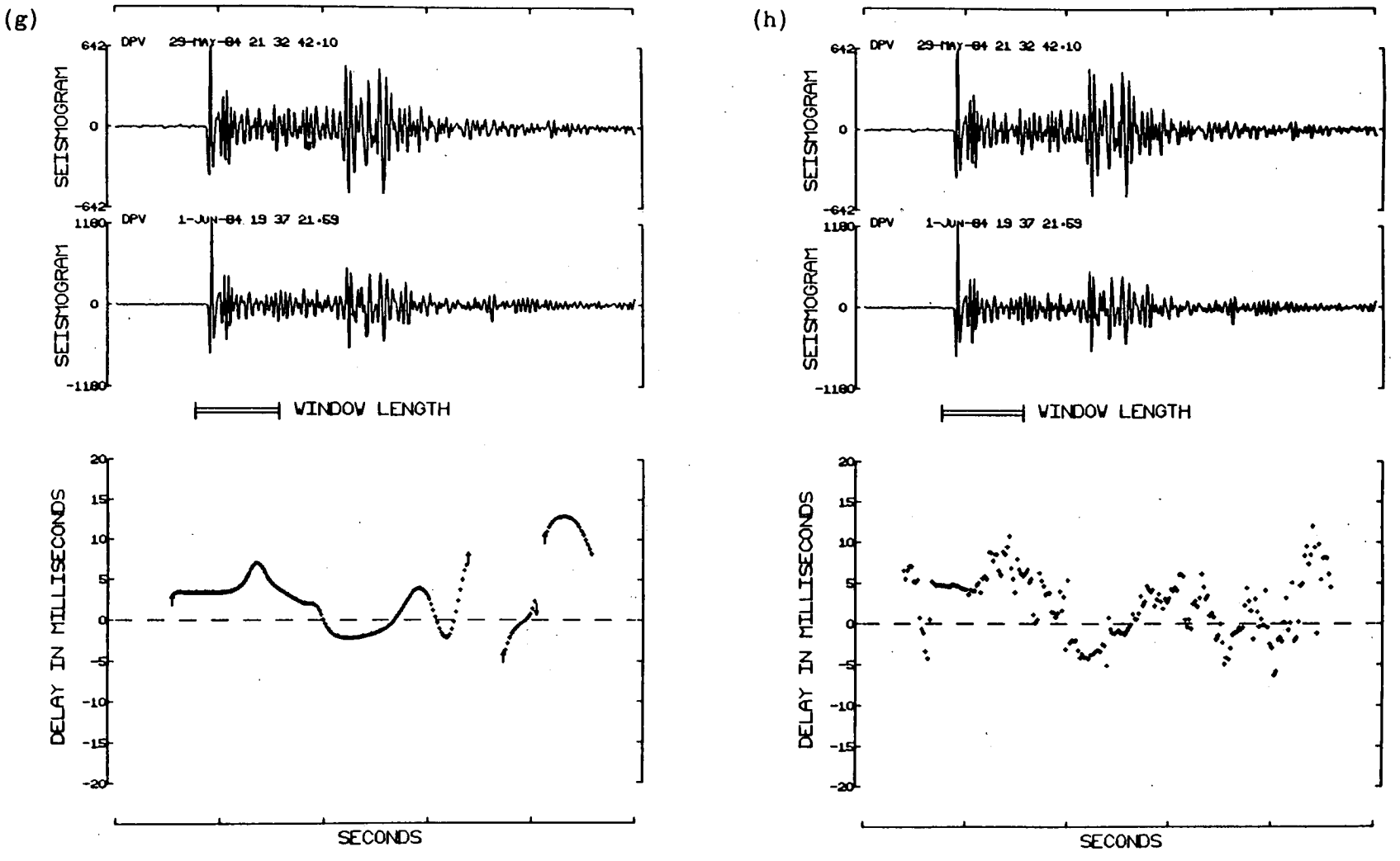

Fig. 4.6g,h - The time delay function for a pair of similar earthquakes calculated using a window length of 80 samples in (g) the time domain and (h) the frequency domain.

On this evidence it would appear to be better to use a longer window but there is a limit as to how far you can go. Fig. 4.6g,h shows the same pair of earthquakes with the window now set to 80 samples. In the time domain it would appear to be an improvement since the time delay function is smoother than for 64 samples with the P and S arrival delays well defined, but in the frequency domain it is quite the opposite with a higher degree of scatter. The problem that arises when increasing the size of the window is that the measured delay will be an average over the whole window and if this should happen to include two separate phases then the delay may be distorted. This has a greater effect in the frequency domain calculation than in the time domain.

Hence, when choosing a window size, a compromise has to made between making it larger so as to avoid instability and making it smaller so as to improve the resolution. The choice is likely to be largely determined by the separation between the P and S arrivals. In this study, with S-P times of one second or more, 64 samples has proved to be about right.

4.3.5 The Effects of Noise

Within a large group of similar earthquakes, such as the ones looked at in this study, there are bound to be small magnitude events that are obscured or partially obscured by noise. It is important to understand the effects that this noise will have on the measurement of time delay and the magnitude of the error incurred. In order to study the effects, an option has been added to the cross-correlation program to take five seconds of noise from either the beginning or the end of the event file, to amplify it and add it to the seismogram.

To demonstrate the effects the same pair of earthquakes is used as has been used in the previous three sub-sections. Fig. 4.7a,b shows the seismograms and their time delay functions in both the time and frequency domains without the addition of noise. This pair has been chosen because the signals are clean, well above the natural noise level and they produce reasonably clean and continuous

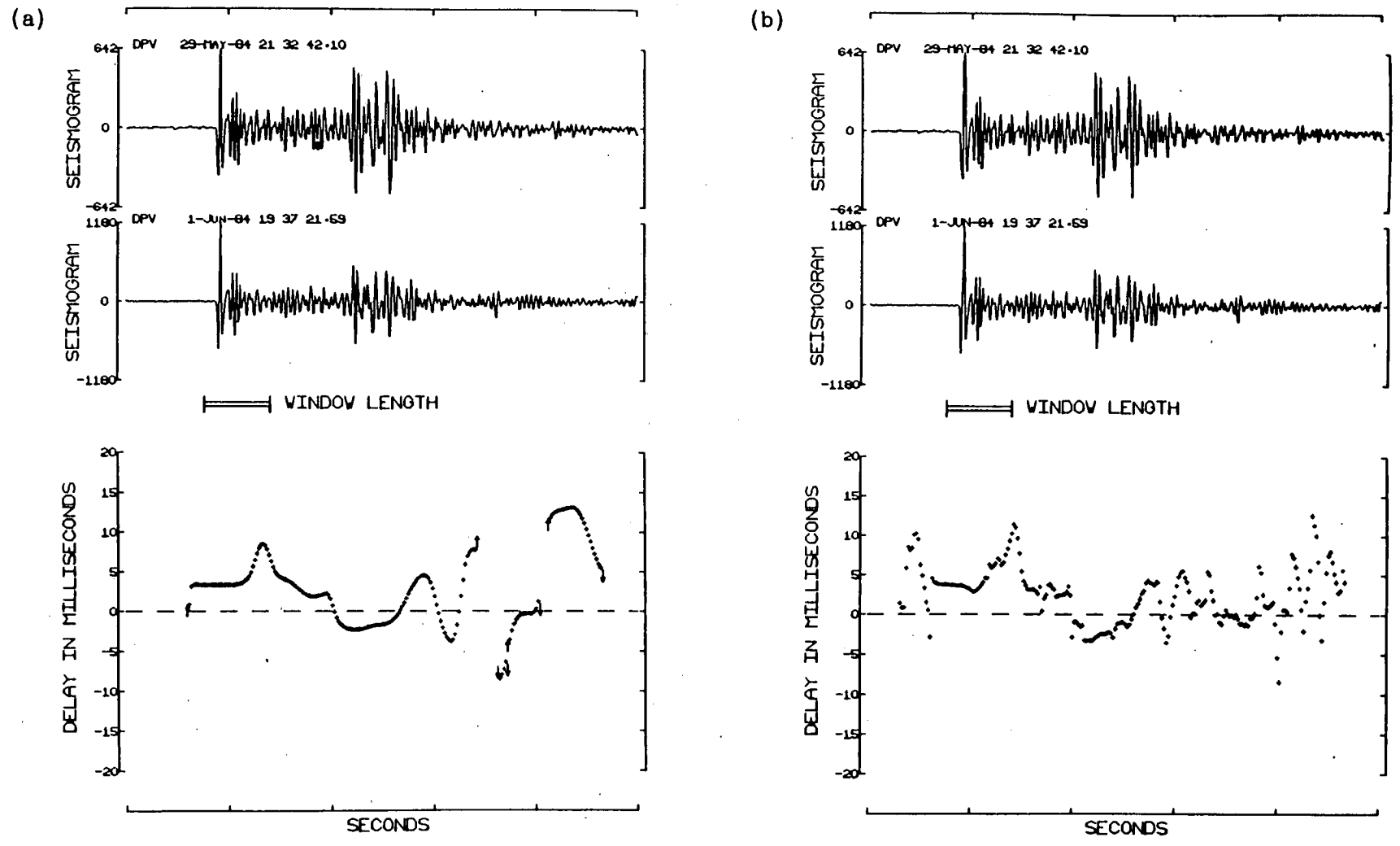

Fig. 4.7a,b - The time delay function for a pair of similar earthquakes with no noise added to the signals in (a) the time domain and (b) the frequency domain.

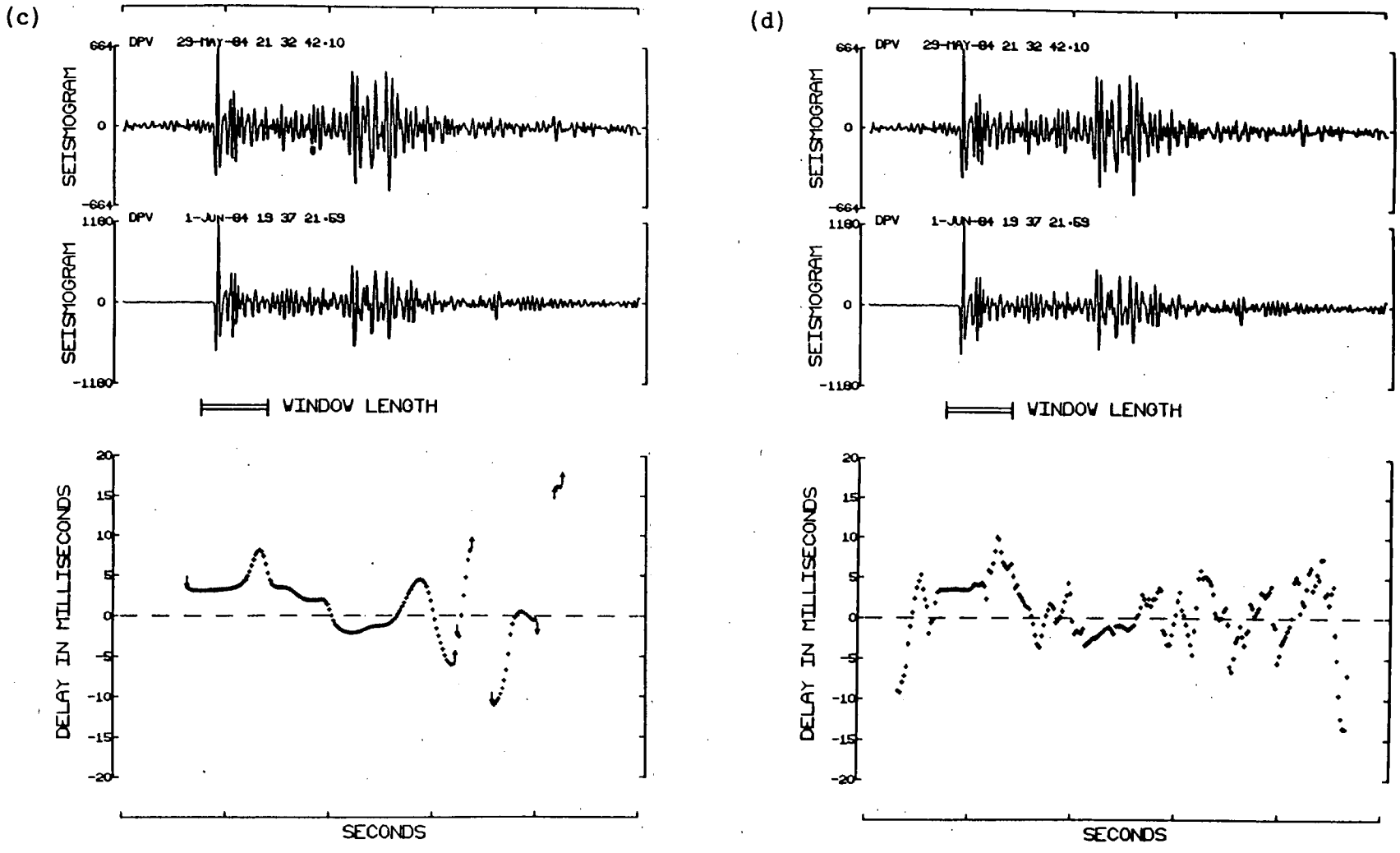

Fig. 4.7c,d - The time delay function for a pair of similar earthquakes with noise (amp. factor 2) added to the top signal in (c) the time domain and (d) the frequency domain.

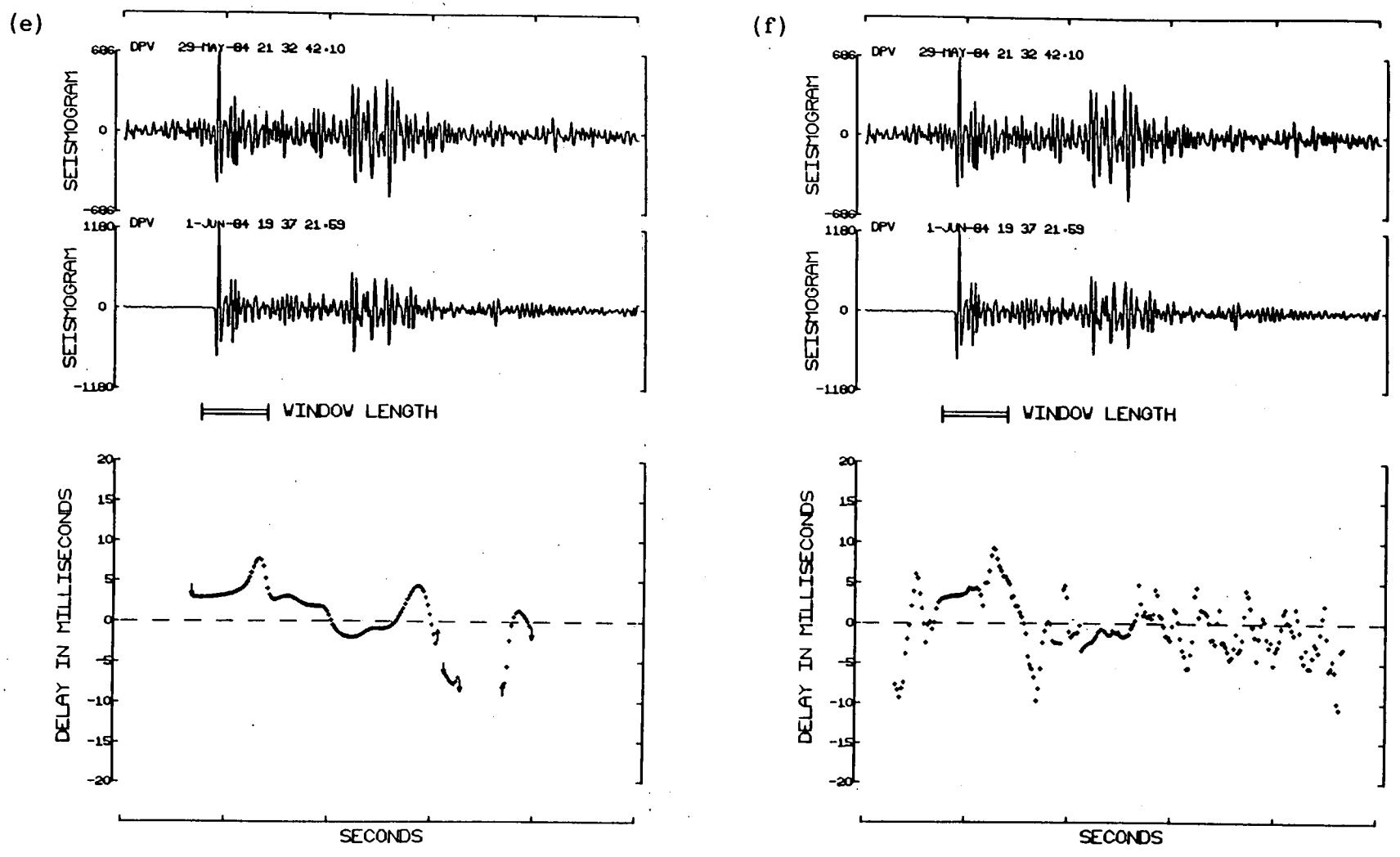

Fig. 4.7e,f - The time delay function for a pair of similar earthquakes with noise (amp. factor 4) added to the top signal in (e) the time domain and (f) the frequency domain.

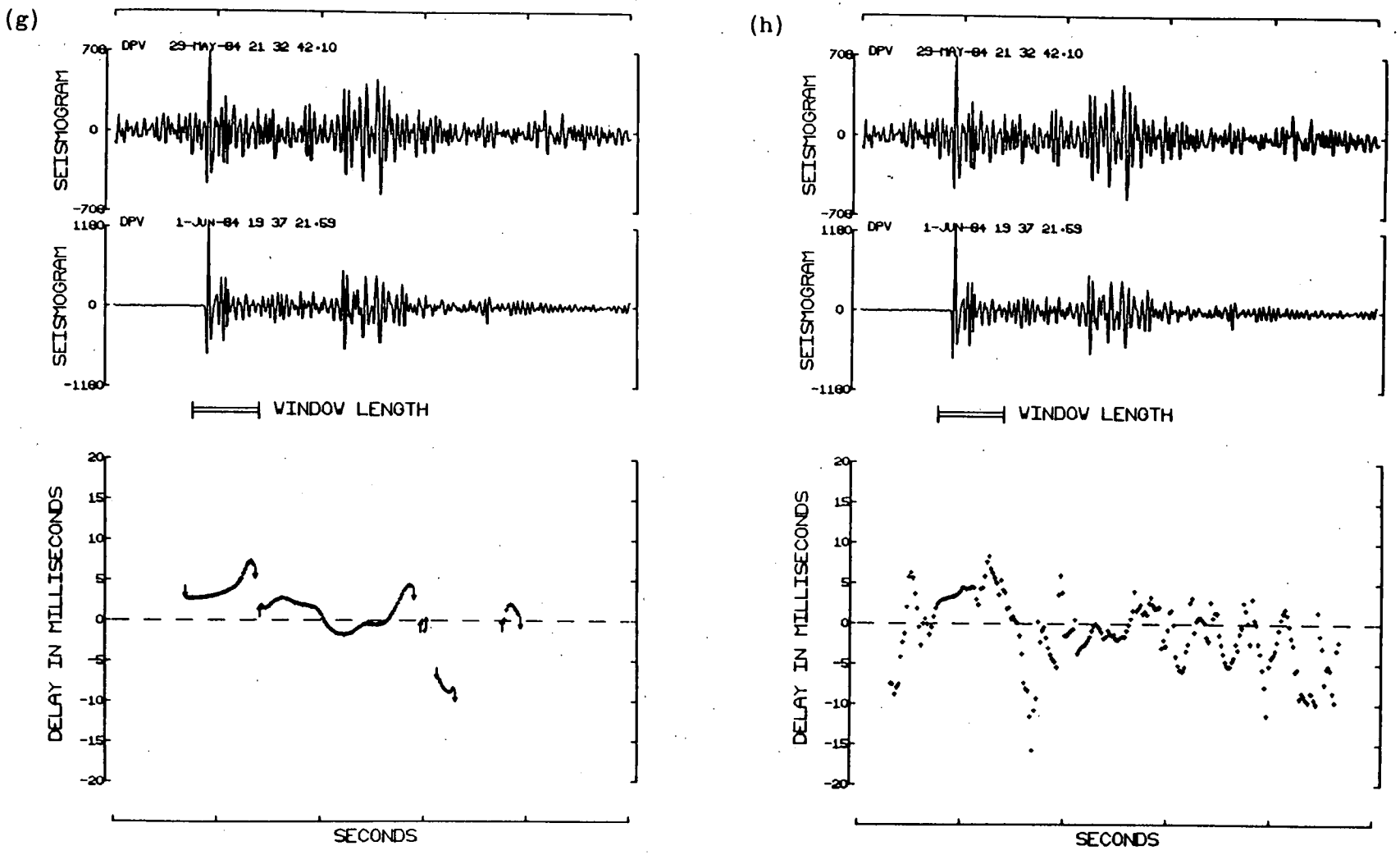

Fig. 4.7g,h - The time delay function for a pair of similar earthquakes with noise (amp. factor 6) added to the top signal in (g), the time domain and (h) the frequency domain.

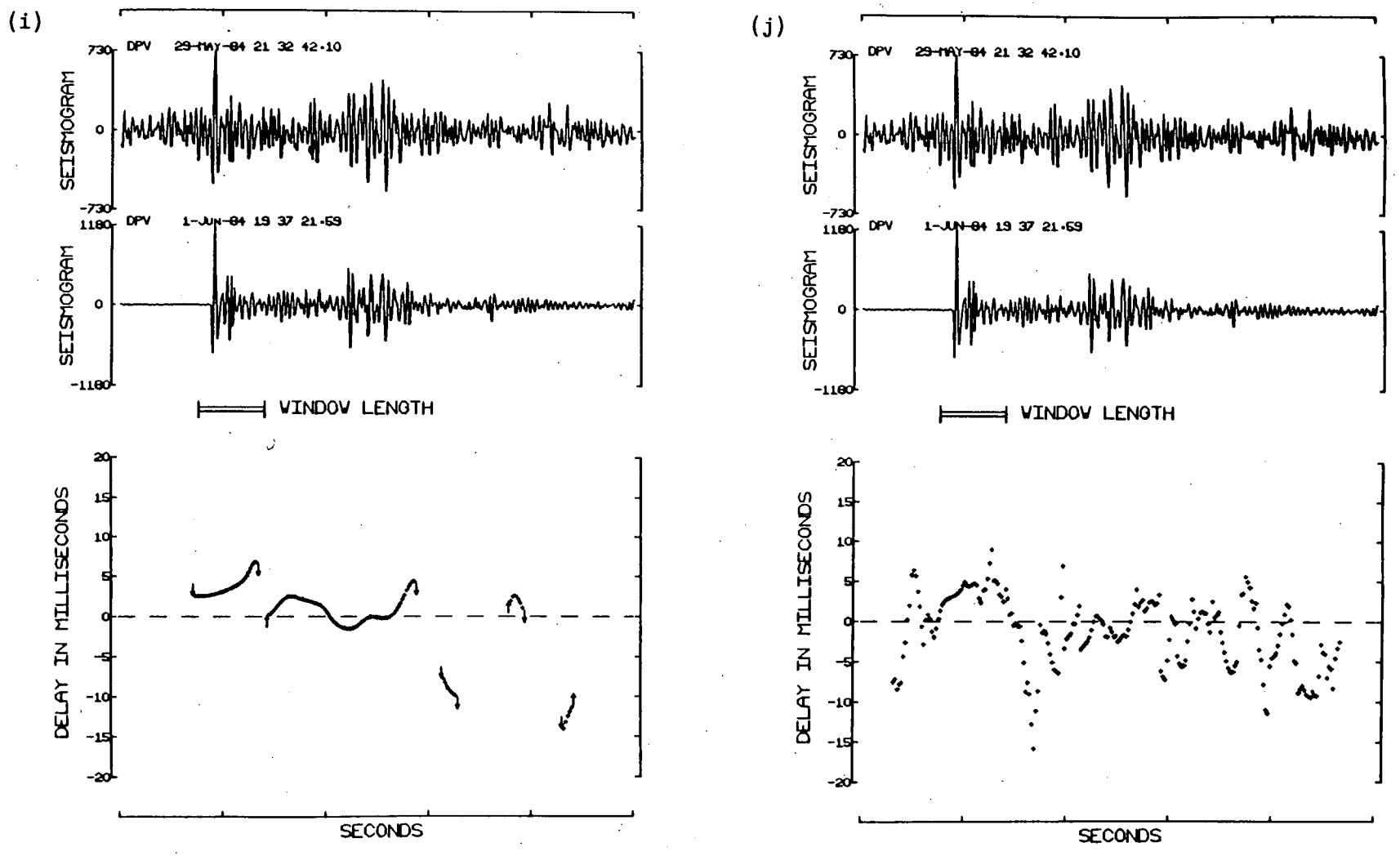

Fig. 4.7i,j - The time delay function for a pair of similar earthquakes with noise (amp. factor 8) added to the top signal in (i) the time domain and (j) the frequency domain.

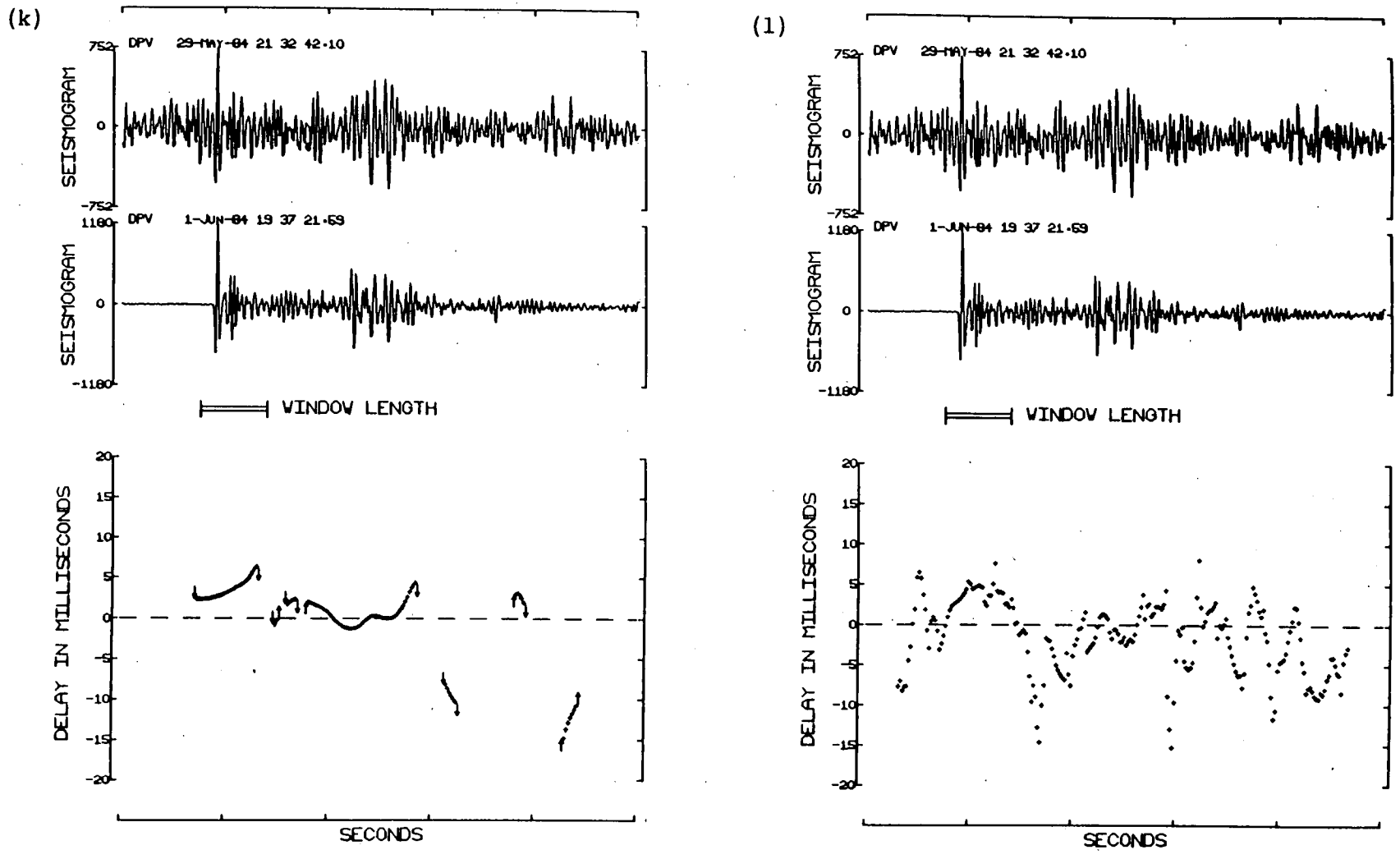

Fig. 4.7k,l - The time delay function for a pair of similar earthquakes with noise (amp. factor 10) added to the top signal in (k) the time domain and (l) the frequency domain.

time delay functions. The time delays for the P and S arrivals are stable at 3 and -2 milliseconds respectively. Fig. 4.7c-1 shows the change in the time delay function as noise is progressively added to the top signal.

As the noise increases, the time delay functions gradually change, with the frequency domain being affected to a greater extent than the time domain. At twice the noise level (fig. 4.7c,d) the top signal is still very clear and the time delay functions are not very different from the originals (fig. 4.7a,b). With noise at four times the initial level (fig. 4.7e,f) changes in the time delay functions become more noticeable. The continuity is reasonably good but those areas associated with the P and S arrivals have started to lose their stability and there is a slight decrease in the absolute values of the delays. This general deterioration continues as the noise is increased to six and eight times its initial value (fig. 4.7g,h and fig. 4.7i,j) with the S region in the frequency domain almost totally losing its stability. The last figure with the noise at ten times its initial value (fig. 4.7k,l) shows the top signal with a signal-to-noise ratio that is lower than any encountered during the main study. The time delay functions have now lost much of their continuity although in the time domain the areas associated with the P- and S-arrivals have not totally lost their stability. The time delays for these two regions are now 2 and -1 milliseconds which differ from the original values by only 1 millisecond.

The above examples deal with the case of only one seismogram in a pair being affected by noise. In the main study this is a fairly realistic occurence since the master event is chosen to be a clean signal of large magnitude. However, with some groups or in other applications it may be necessary to cross-correlate two noisy signals. In such a case the same effects as those observed above will occur but at lower noise levels. For example, fig. 4.8a-d shows the same pair of seismograms with two times and four times the initial noise level added to both signals. This compares with fig. 4.7c,d and fig. 4.7e,f and as can be seen there is a much greater distortion in the time delay functions with changes in the time delay for the P and S arrivals of about one millisecond again.

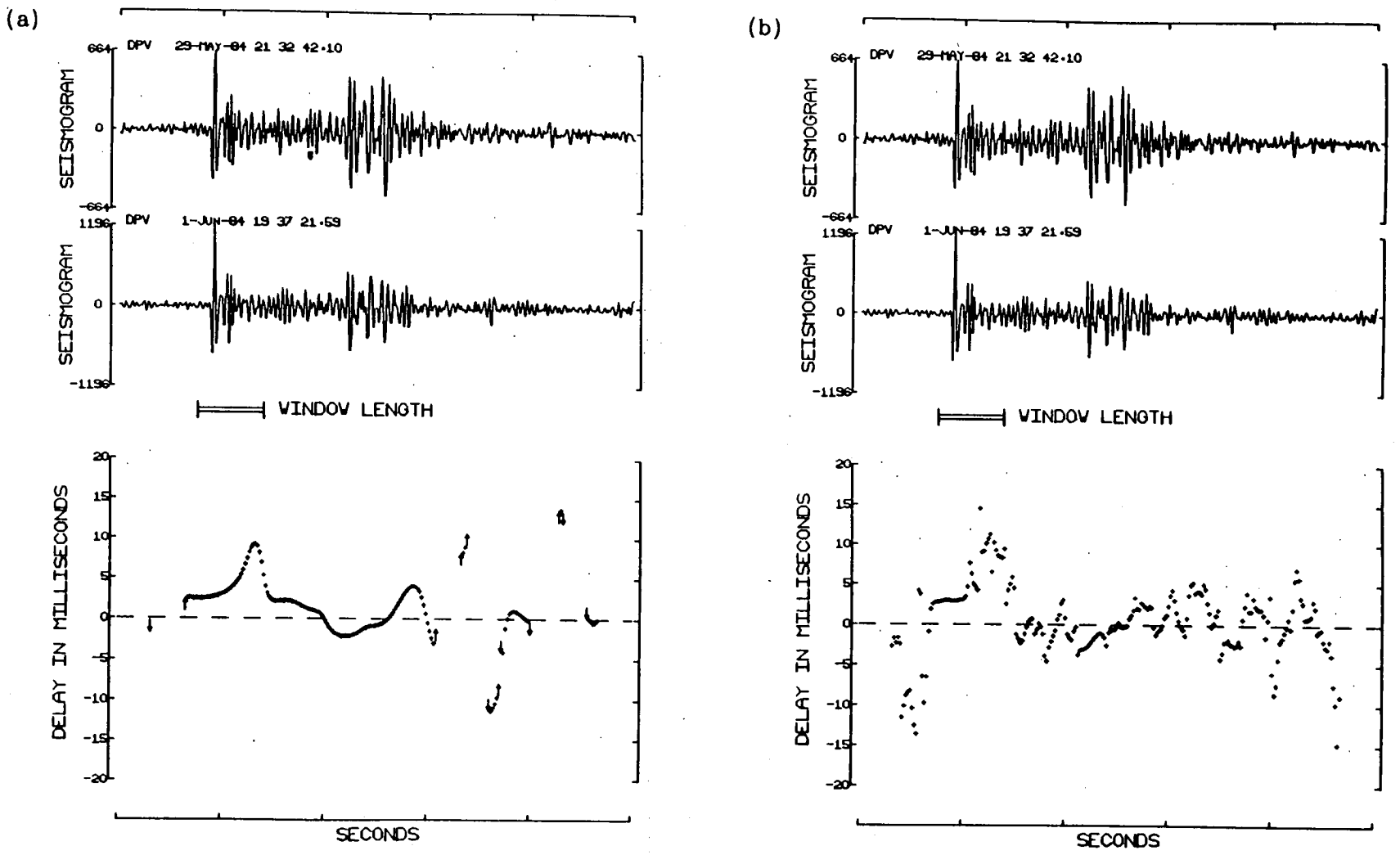

Fig. 4.8a,b - The time delay function for a pair of similar earthquakes with noise (amp. factor 2) added to both signals in (a) the time domain and (b) the frequency domain.

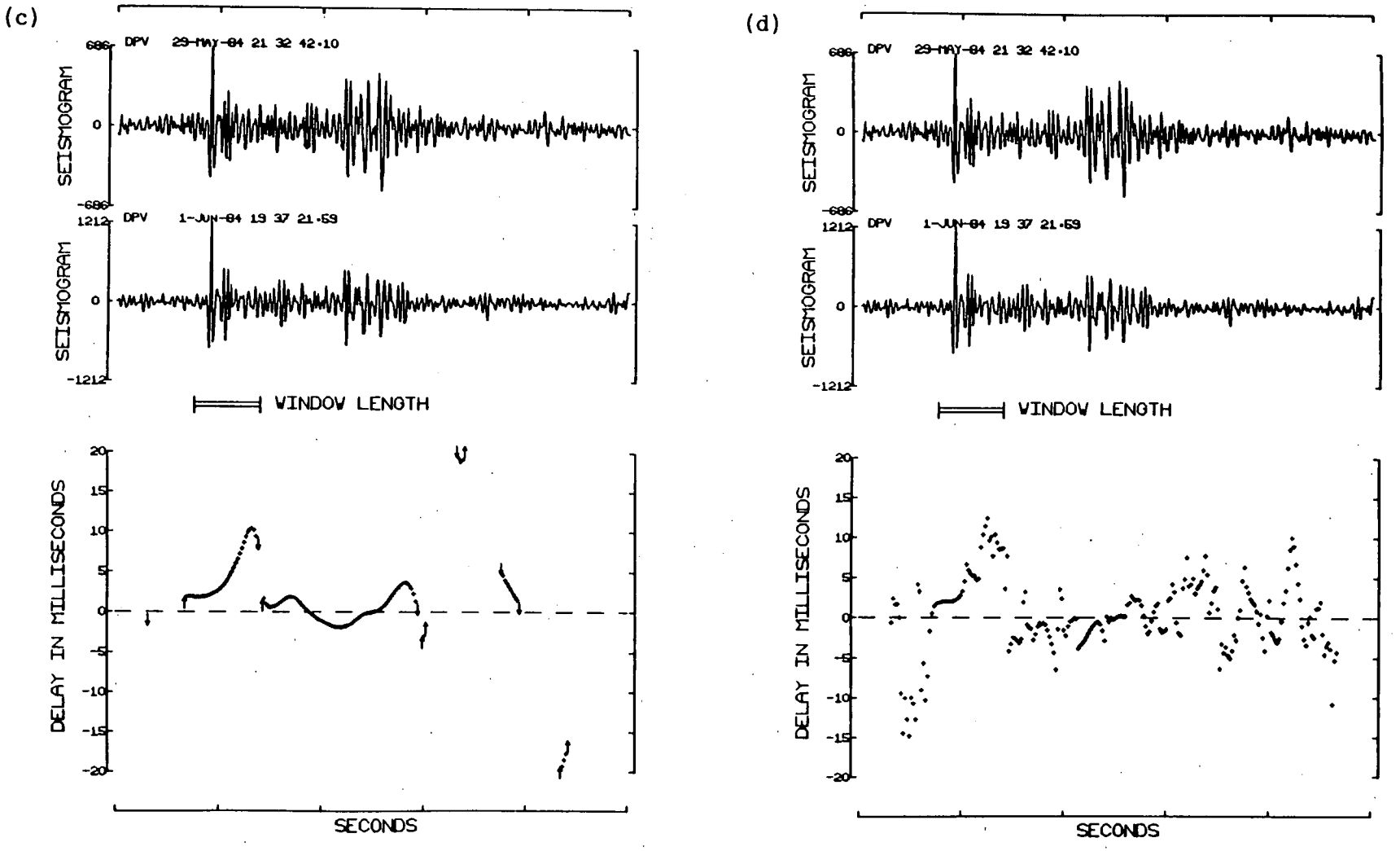

Fig. 4.8c,d - The time delay function for a pair of similar earthquakes with noise (amp. factor 4) added to both signals in (c) the time domain and (d) the frequency domain.

These results are very encouraging since the presence of noise does not seem to have a very significant effect on the time delay readings for the P and S arrivals.

4.3.6 The Effects of Saturation

The occurrence of large magnitude earthquakes may cause the recording equipment to saturate, particularly in the amplifier modulator. This will have the effect of distorting the seismogram by truncating the peaks and troughs which, in turn, may affect the calculation of the time delay function. To see exactly what effect it does have, the cross-correlation program was adapted to allow for the amplification of one or both of the signals and to set all points that lie above a certain value equal to that value (i.e. to saturate the signal).

Using the same pair of earthquakes as before, the top signal was progressively saturated and the time delay function calculated in both the time and frequency domains. The results are displayed in fig. 4.9a-j. Fig. 4.9a,b shows the original unsaturated seismograms and their time delay functions. With the top signal amplified six times (fig. 4.9c,d) the amount of saturation is not very great and the time delay functions do not change by very much. The saturation becomes more significant at an amplification of ten (fig. 4.9e,f) but the time delay functions are still not greatly affected. The distortion in the frequency domain is slightly worse than that in the time domain but the error is still much less than one millisecond. This distortion gets worse as the amount of saturation increases, particularly in the frequency domain where stability in the S region is almost totally lost. Fig. 4.9g,h and fig. 4.9i,j show the top signals amplified by factors of fifteen and fifty respectively.

These results show that even in cases of extreme saturation the time delay functions are still reliable when calculated in the time domain. In the frequency domain more care must be taken if there is a significant amount of saturation, although at low levels it is still reliable. Overall the errors induced by saturated signals are

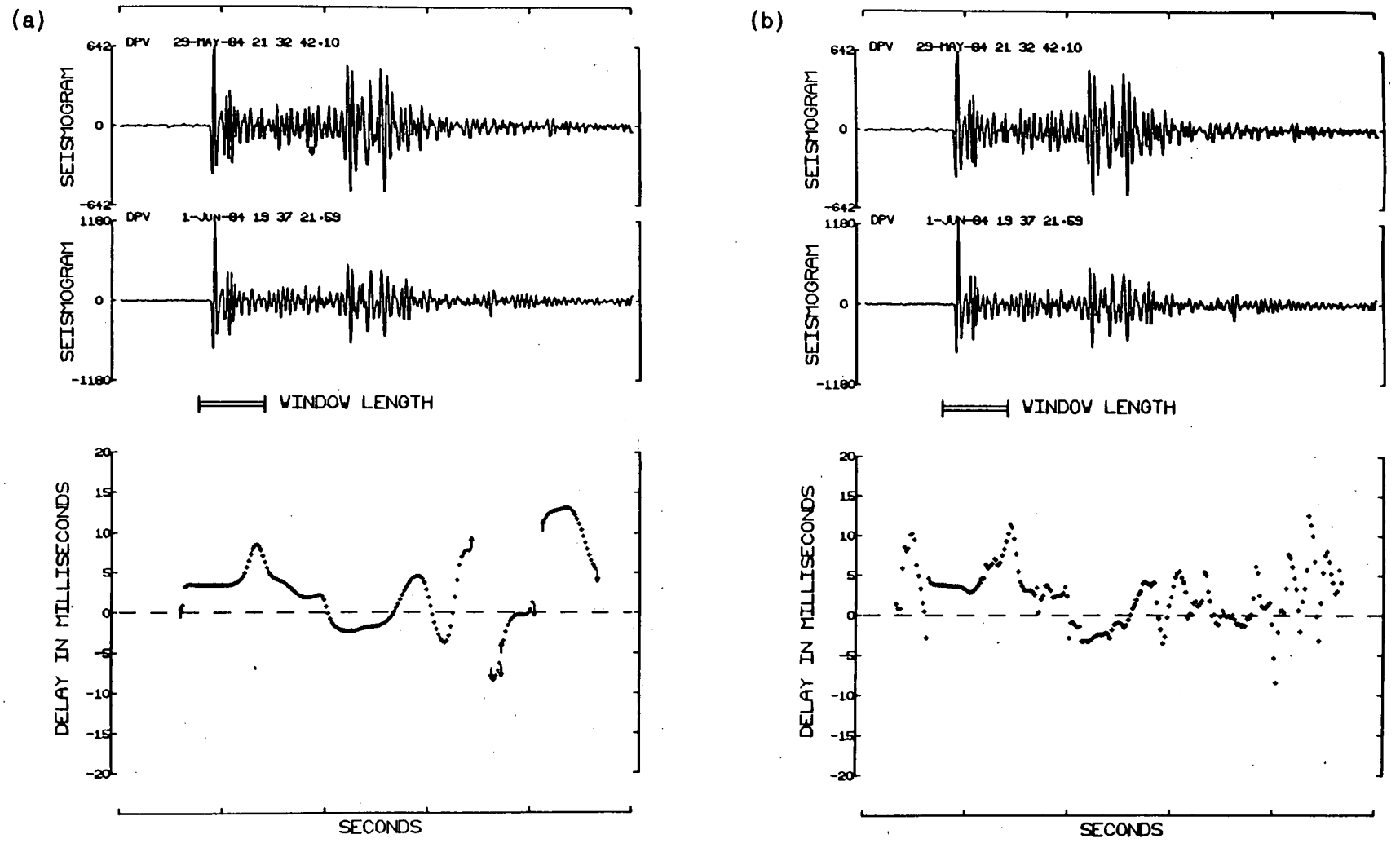

Fig. 4.9a,b - The time delay function for a pair of similar earthquakes with no amplification in (a) the time domain and (b) the frequency domain.

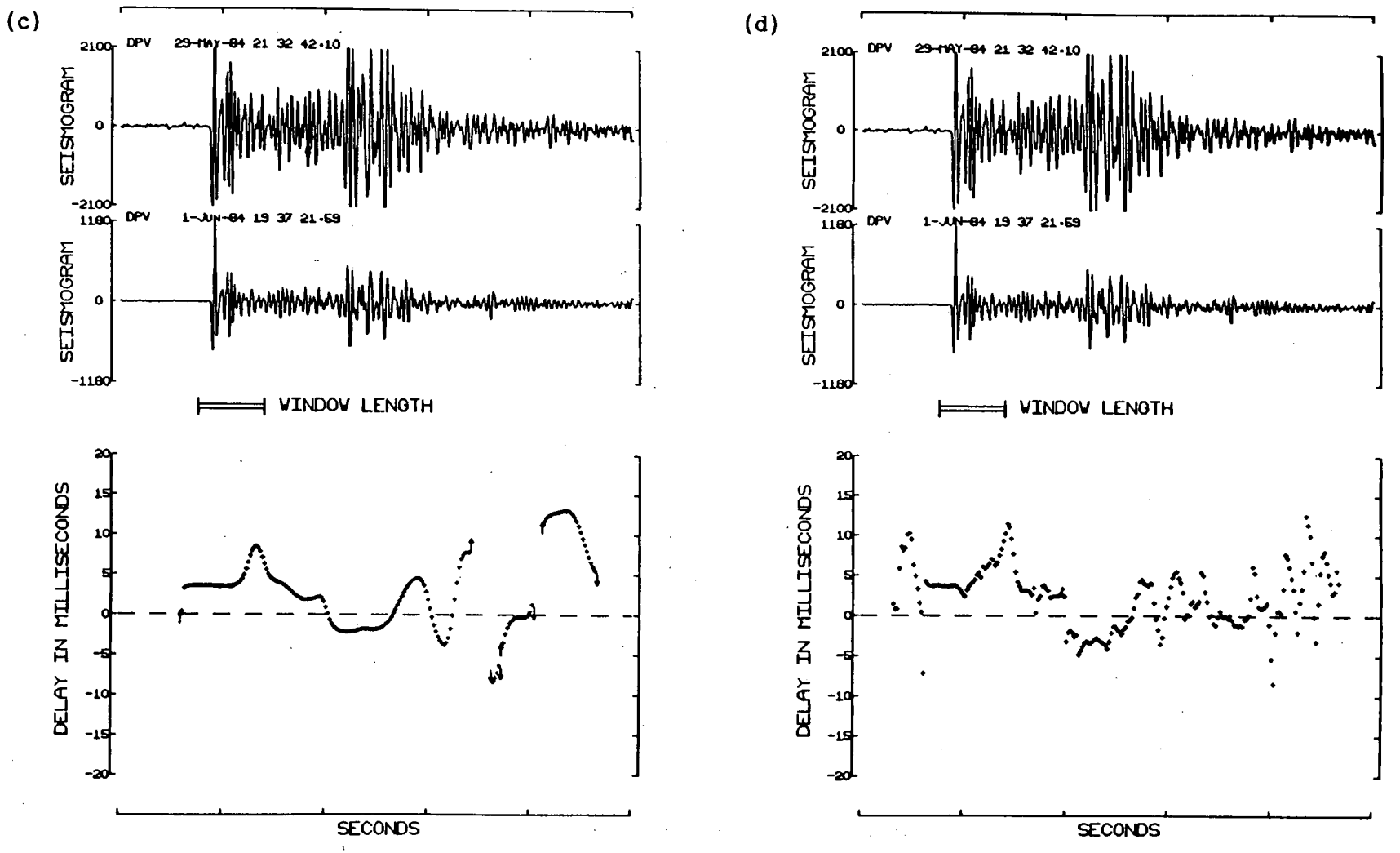

Fig. 4.9c,d - The time delay function for a pair of similar earthquakes with the top signal amplified by a factor of 6 in (c) the time domain and (d) the frequency domain.

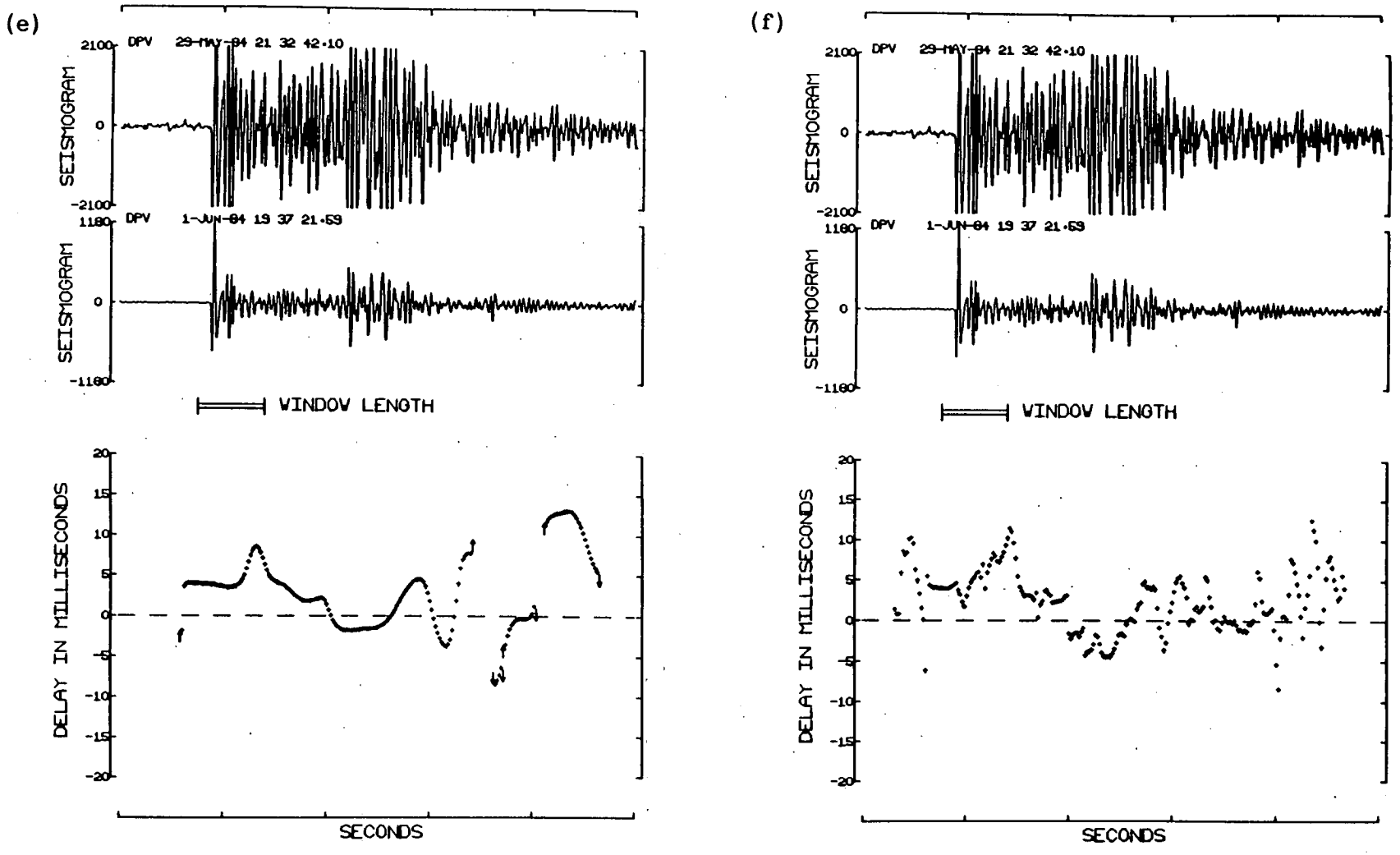

Fig. 4.9e,f - The time delay function for a pair of similar earthquakes with the top signal amplified by a factor of 10 in (e) the time domain and (f) the frequency domain.

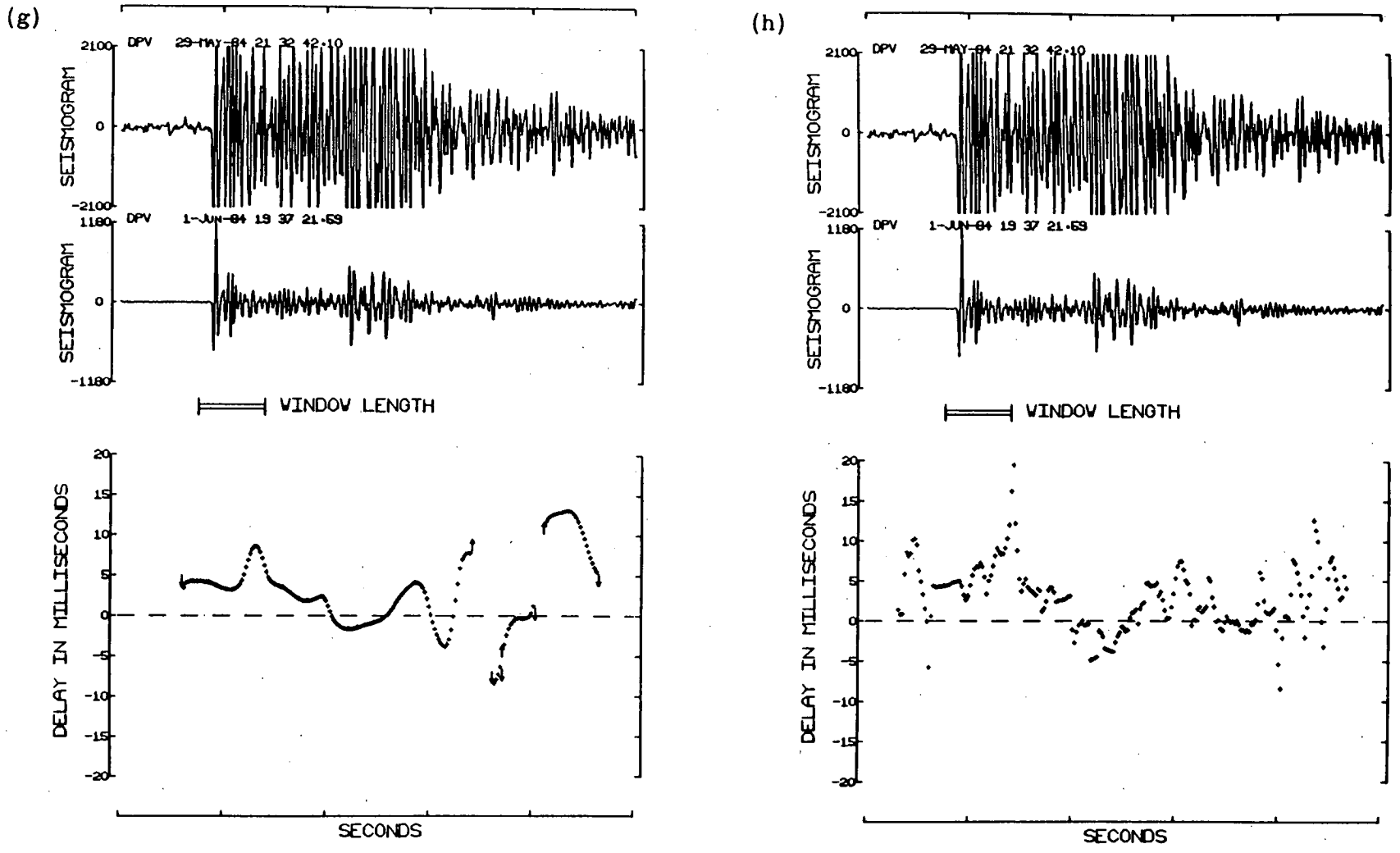

Fig. 4.9g,h - The time delay function for a pair of similar earthquakes with the top signal amplified by a factor of 15 in (g) the time domain and (h) the frequency domain.

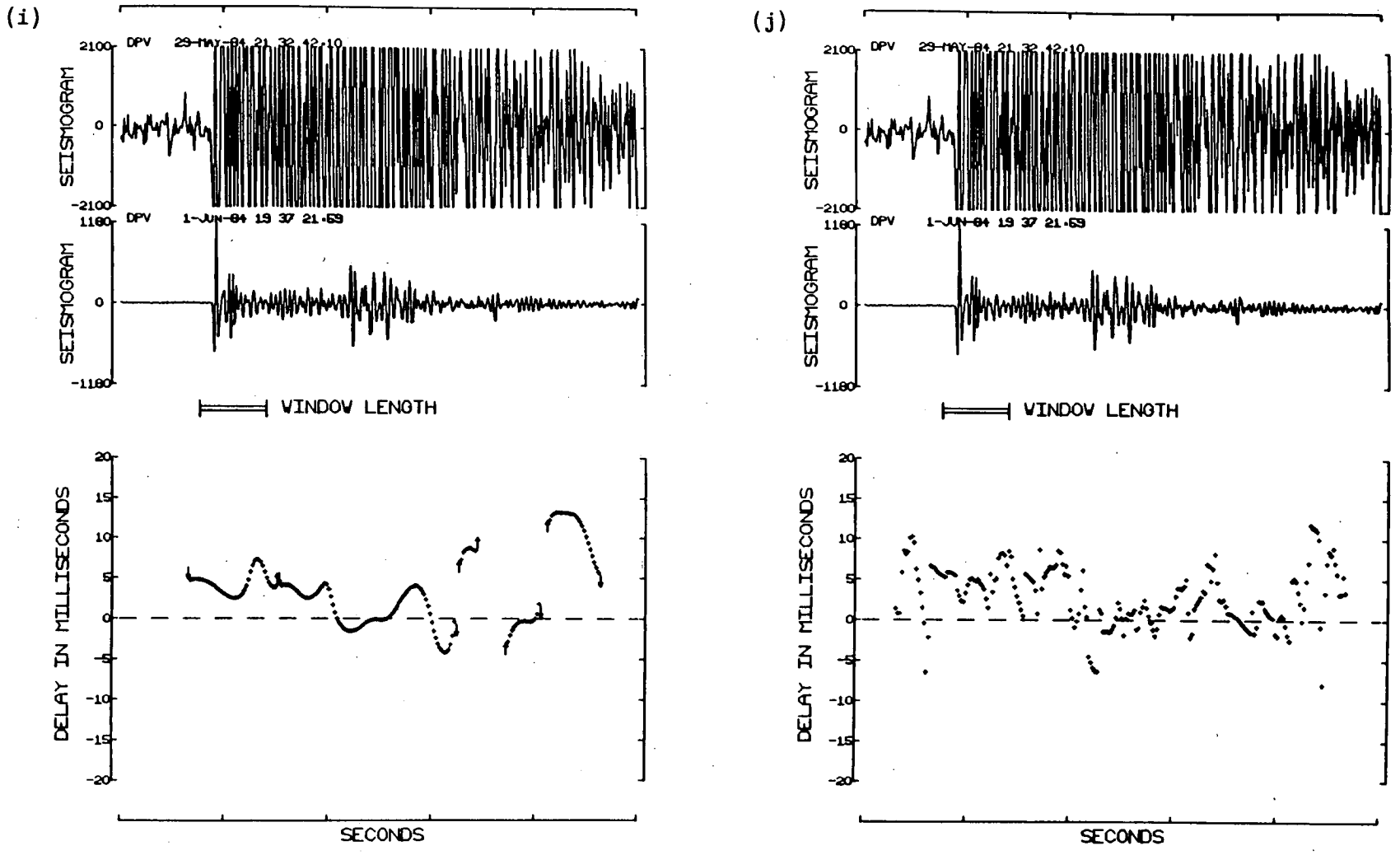

Fig. 4.9i,j - The time delay function for a pair of similar earthquakes with the top signal amplified by a factor of 50 in (i) the time domain and (j) the frequency domain.

no more than one or two milliseconds.

4.3.7 Summary

It would appear that for the majority of seismograms it makes no real difference whether the cross-correlation calculation is carried out in the time or frequency domain. Using the program as listed in appendix 2 does have the problem that the seismograms must be properly lined up if the frequency domain calculation is not to be distorted by phase wrapping. However, this problem could be corrected if a phase unwrapping routine was to be developed and included in the program.

When the cross-correlation calculation is complicated by either the presence of noise or by a saturated seismogram the time domain calculation appears to be less affected than in the frequency domain, although the difference is generally negligible if the noise or saturation is not too extreme. This is a little surprising bearing in mind that the frequency domain method incorporates a weighting system based on coherency which should allow it to cope with noise and saturated signals since these effects will be incoherent. It may be that the weighting is insufficient to overcome the bias introduced by the incoherency.

4.4 Discussion of the Errors

In chapter 5 groups of similar earthquakes are analysed using both the cross-correlation technique, as described above, and the relative location method of chapter 3. The main aim of the study is to examine the source in detail by locating each event within a group to a very high degree of accuracy and then using the resultant event distribution to extract such information as source dimension, orientation and event sequences. It is important, therefore, to have some idea of the error of each location. In this section the errors involved in both measuring the change in the S-P time and the relative location method are discussed and at the end an attempt is made to gain an estimate of the overall error.

The change in the S-P time is measured from a plot of the time delay function (see fig. 4.2 for an example). The function is calculated by moving a window along both seismograms and, at each point, computing the cross-correlation function from which the time delay is determined. In the time domain this is done by measuring the position of the central peak of the function (see fig. 4.3) whereas in the frequency domain it is done by measuring the slope of the phase. In either case the reading error is small (of the order of 1ms) although the higher degree of scatter of the time delay function as calculated in the frequency domain (see section 4.3.2) would suggest that the measurement has a slightly larger error in the frequency domain than in the time domain. To actually measure the change in the S-P time the values of the time delay function corresponding to the P and S arrivals are taken and the difference between them determined. Fig. 4.4 contains a variety of examples and it can be seen that the time delay function tends to stabilise around the P and S phases. The error involved in reading the time delay of either phase is usually 1-2ms although it may occasionally be as high as 3 or 4ms. Therefore, the overall error in the measurement of the change in the S-P time will be 2-3ms (the combination of two readings each with an error of 1-2ms) with an associated spatial uncertainty of 10-15m (spatially, 1ms may be equated to approximately 5m since that is the distance travelled by the wave in that time).

In the relative location method there are several potential sources of error. The model used in the location is, in effect, a half-space with a velocity equal to that assumed for the source region. In reality, however, the waves will pass through many layers on their way to the surface but, as noted in section 3.3.2 for groups typical of those found in the TDP data set, the effects of any refraction will be negligible and can be ignored. An error may also be introduced into the location if the events being analysed are too far apart causing a breakdown in the assumptions of linearity and similarity of propagation paths. For groups of similar earthquakes, such as those analysed in chapter 5, this should not be a problem since the very fact that they are similar suggests that they must be closely spaced. Should either of the

above errors occur, it would be very difficult to estimate the magnitude of the effect. Lastly, it should be noted that the locations are dependant upon the velocity assumed for the source region. As the velocity increases the separation between any two events will also increase but their relative positions will not change. In other words, the velocity that is chosen will determine the scale of the event distribution. Fortunately, the effect is not too large and a reasonable estimate of the velocity can usually be made. To demonstrate the effect, the first group to be analysed in chapter 5 will be located over a wide range of velocities. It will show that for events separated by several hundred metres the separation will only change by approximately 50m over the whole velocity range and for lesser separations the error will be proportionally smaller. In the interpretation the only noticeable effect will be in the measurement of the source dimension. Any other observable structure within the distribution will remain unaltered.

So, it would appear that errors in measuring the change in the S-P time and in the velocity chosen for the source region are the only significant contributors to the error in the final location. To get an estimate of the overall error a set of three similar events are chosen (A, B and C) which are then located relative to each other in a closed loop. Any discrepancy in the closure can be considered to be a measure of the error in the location. First, B and C are located relative to A and from this the location of B relative to C can be calculated. Then, B is located relative to C using the location method and the two locations are compared. This procedure was carried out on 10 sets taken from group 2A of chapter 5. The errors were generally found to be dependent upon the separation of the events (i.e. the greater the separation the greater the error) and ranged from 0-30m with an average of 12m. From this it would seem reasonable to quote an error of 20-30m as an upper limit which should present no problem in extracting detailed information about the source. The error analysis also supports the assumption of linearity made in the location method. If the assumption was invalid the closure errors would be expected to be large, but they are not.

Chapter 5

Application of the Relative Location Method on Similar Earthquakes in Turkey

5.1 Introduction

In chapters three and four a method has been described that allows groups of similar earthquakes to be located, relative to each other, with an error no greater than 20-30m. In chapter 5 this method is used to analyse four such groups, one from the TDP-2 and three from the TDP-3 data sets. From the results of this analysis it is possible to examine the source in detail and to extract such information as source dimension, orientation and event sequences. For comparison, the fault plane solutions are calculated for each group and corner frequencies, obtained by spectral analysis, are used to estimate the source dimension.

Before describing these groups and the result of the analysis, the next section will outline how the relative location method and the cross-correlation technique are incorporated into a general procedure that is used in the main study.

5.2 General Procedure

Before proceeding with the cross-correlation the groups of similar earthquakes that are to be analysed have to be found. The routine location of earthquakes from large data sets often reveals clustering of events in both space and time, albeit on a coarse scale, and these are quite easily spotted on epicentral plots of the events. Clusters that are thought to be interesting are played out

so that a visual inspection can be made. For this purpose it is only necessary to look at the records of one component since the similarity will exist at all stations. When selecting a cluster for inspection it is important to include events that occur within the vicinity of the cluster. It is possible that a mistake could be made in picking the phase data and this may result in an erroneous location.

Having selected a group, the next stage is to decide which event within the group is to be the master event. It is important to note that if a station does not record the master event, whether it is because it is too far away or faulty, then it cannot be used to calculate any of the locations, even if it records all the other events within the group. It is advisable, therefore, to choose a master event that is recorded at as many stations as possible. In general, this will be one of the larger magnitude events which, in addition to being able to reach the more remote stations, also has the advantage that it will be recorded at a higher signal to noise ratio at all the other stations.

All events within the group must now be cross-correlated with the chosen master event. When running the program, a time must be specified at which the cross-correlation will start. For this purpose, the P arrival times, as picked by hand, can be used with one second subtracted from them. In total, five seconds of data will be extracted from the data files, which is usually ample for local earthquakes with S-P times of less than three seconds. On inspecting the output it may be found that the seismograms were not adequately aligned and that the delay plot is either off scale (if in the time domain) or incoherent (if in the frequency domain). If this is the case, the cross-correlation should be repeated using start times adjusted accordingly.

From the delay plots, the changes in the S-P time are measured by taking the difference between the time delay readings of the P and S arrivals. The measurements have to be done by hand since a certain amount of judgement is needed to identify the P and S arrivals and their corresponding delays. This is because the time

delay function is not always stable throughout an entire phase. It may have a slight slope on it or contain a small jump and so choosing the right point is best done by eye. The error produced by such instability is very rarely greater than a few milliseconds.

Finally, having measured the change in the S-P time at each station for each event, the relative positions of the events can be calculated. All readings are read into a file which is then run through the relocation program. Appendix 1 includes sample input and output files along with a listing of the program.

5.3 Group One

5.3.1 Introduction

Following the second phase of the Turkish Dilatancy Project (TDP-2) Balamir Ucer and Stuart Crampin made a detailed examination of records from about one hundred earthquakes whose epicentres spanned the surface break of the southern fault of the North Anatolian Fault graben. As a result they found that 95% of the events could be classified into one of about ten groups with almost identical records and very close hypocentres. The largest of these groups was selected for analysis in this section.

The chosen group contains twenty-one events occurring over a period of nineteen days with seventeen of the events occuring within a period of only two days. The approximate location of the cluster is at 40° 42' N, 30° 00' E and at a depth of approximately 10kms.

5.3.2 Group 1 - Relative Relocation

The event codes and filenames of the 21 events comprising group 1 are listed in table 5.1. All the events have been located routinely using HYP071 (Lee and Lahr, 1975) and the locations are also listed in table 5.1. In fig. 5.1 the HYP071 locations are plotted in relation to the station layout for TDP-2 and, so that this group can be related to the other groups, fig. 5.2 shows the locations in relation to the station layout for TDP-3.

			Location (HYP071)			
Event Code	Filename	Date	Time	Latitude (Deg/min)	Longitude (Deg/min)	Depth (km)
G1(1)	TD0232.B51	800819	151 31.09	40-41.84	30- 0.80	10.21
G1(2)	TD0232.E46	800819	446 18.15	40-41.72	29-58.06	11.28
G1(3)	TD0247.F07	800903	5 7 38.97	40-42.02	30- 0.85	9.95
G1(4)	TD0247.J27	800903	927 1.84	40-42.29	30- 0.05	11.73
G1(5)	TD0247.J38	800903	938 47.45	40-42.03	30- 0.18	12.00
G1(6)	TD0247.J44	800903	944 24.20	40-41.94	30- 0.39	10.36
G1(7)	TD0247.J54	800903	954 5.84	40-42.05	30- 0.28	9.77
G1(8)	TD0247.K45	800903	1045 46.21	40-41.71	30- 0.71	9.71
G1(9)	TD0247.R13	800903	1713 1.82	40-41.93	30- 0.39	10.46
G1(10)	TD0247.R45	800903	1745 47.60	40-41.69	30- 0.49	10.27
G1(11)	TD0248.A04	800904	0 4 19.11	40-42.20	29-59.87	9.11
G1(12)	TD0248.R06	800904	17 6 50.29	40-42.09	30- 0.55	9.09
G1(13)	TD0248.X07	800904	23 7 39.37	40-42.04	30- 0.37	10.03
G1(14)	TD0249.A00	800905	0 0 19.69	40-42.07	30- 0.02	9.83
G1(15)	TD0249.E24	800905	424 33.13	40-42.35	29-59.32	9.78
G1(16)	TD0249.E46	800905	446 16.40	40-41.92	30- 0.19	11.31
G1(17)	TD0249.E50	800905	450 17.64	40-42.32	29-59.50	9.67
G1(18)	TD0249.G29	800905	629 36.37	40-41.80	30- 0.34	11.12
G1(19)	TD0249.M47	800905	1247 12.87	40-41.80	30- 0.70	10.38
G1(20)	TD0250.F17	800906	517 11.17	40-41.88	30- 0.38	11.41
G1(21)	TD0251.P41	800907	1541 8.11	40-41.66	30- 0.81	10.27

Table 5.1 - Group 1. Event codes, filenames (GSRG standard files) and HYP071 locations (origin time and hypocentre).

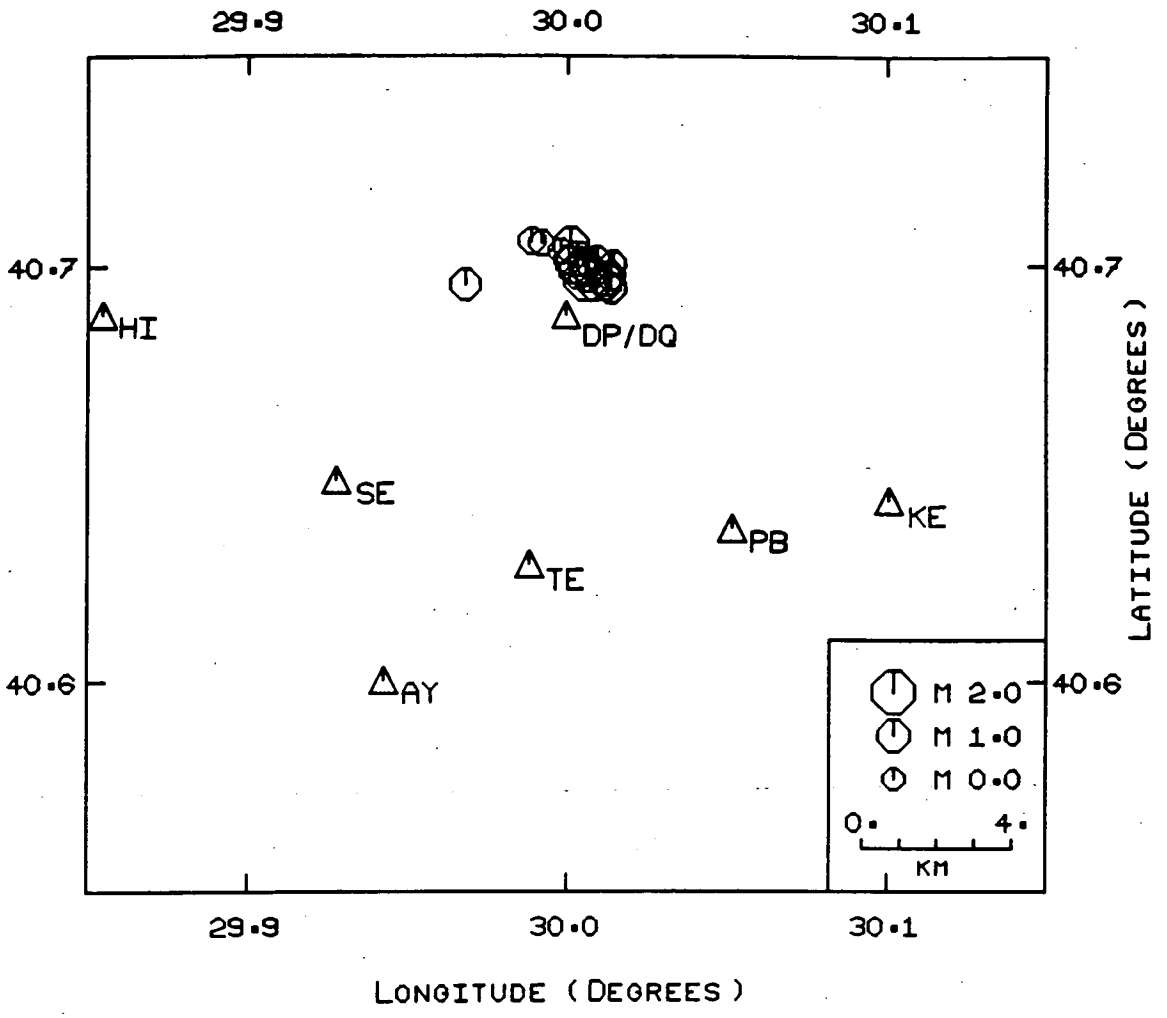

Fig. 5.1 - Epicentral plot of the Group 1 HYP071 locations (listed in table 5.1) superimposed upon the TDP-2 station layout (IZ and KT are off the edge of the map).

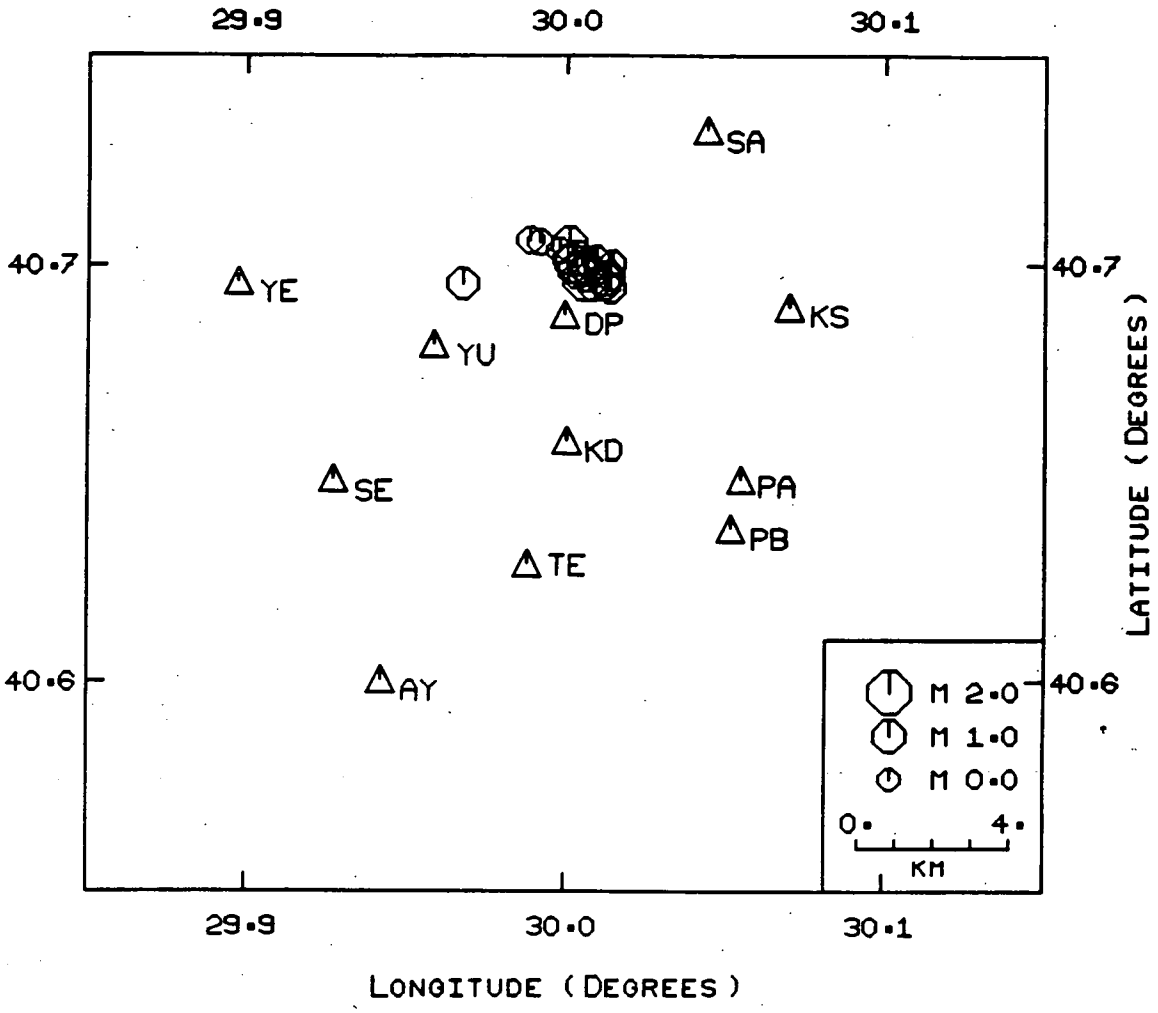

Fig. 5.2 - Epicentral plot of the Group 1 HYP071 locations (listed in table 5.1) superimposed upon the TDP-3 station layout.

Of the twenty-one events only two could not be relocated. G1(2) is a small magnitude event that was only recorded on two of the stations (a minimum of three is required). G1(18) is a large magnitude event that saturated the equipment on several channels which led to a distortion of the signals and a loss of similarity.

G1(4) was chosen to be the master event because it was cleanly recorded on six of the stations (TE, SE, AY, IZ, DQ and KT). The remaining eighteen events were then located relative to the master event. As indicated in the previous chapter, the velocity chosen for the source region is not a critical parameter since it only affects the size of the separation between the events and not the relative position. At a depth of ten kilometres the P velocity is likely to be somewhere around 6-7 km/s and to demonstrate the above point the relative locations have been calculated at four different velocities (Vp = 7.0, 6.5, 6.0, 5.5km/s and Vp/Vs = 1.75). Fig. 5.3a-d displays the epicentral plot for each velocity and two orthogonal cross-sections through it. Each event has been numbered according to its position within the group.

The most striking feature of the epicentral plot, regardless of the velocity used, is the apparent alignment of the events in a roughly NW-SE direction. Chronologically, the epicentres show no real pattern except for a slight clustering of events in groups of two or three (for example 13, 14, 15). To see if there is any alignment of the events outside the epicentral plane the two cross-sections were taken as shown in fig. 5.3a-d. Section A-B is in the preferred NW-SE direction with section C-D at right angles to it. There is no vertical exaggeration. From section C-D there appears to be quite a strong alignment at 45^{o} to the vertical suggesting that the relocated hypocentres lie on a plane striking N141^{o}E with a dip of 45^{o}. However, in section A-B there is also some alignment of the events, albeit very weak, with those events near to B higher than those at A. It might therefore be possible to fit the group to a line rather than a plane but the physical implications of such a fit are difficult to realise.

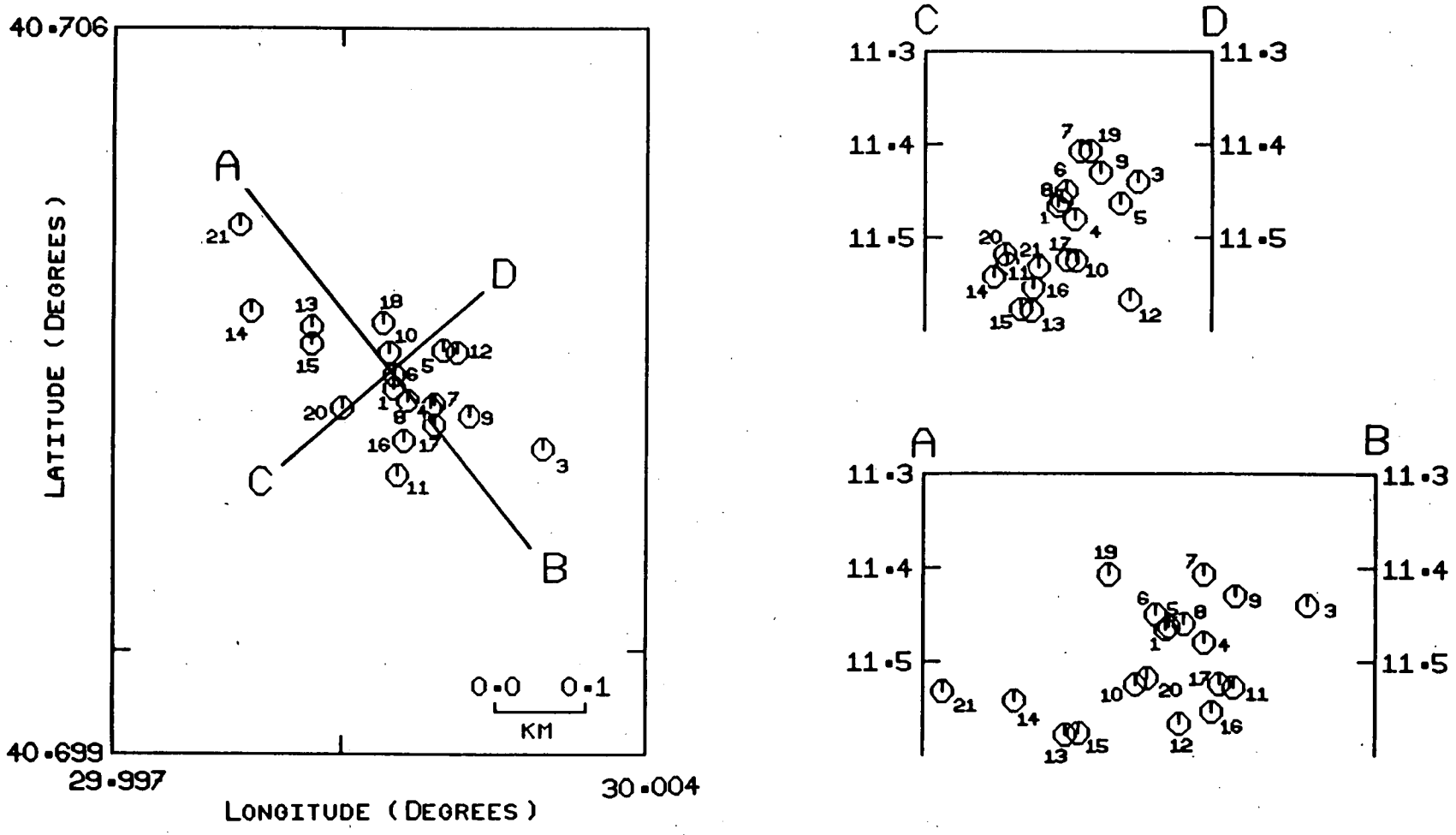

Fig. 5.3a - Epicentral plot and two orthogonal cross-sections of the events in Group 1 relocated at a velocity of Vp = 7.0km/s and Vs = 4.0km/s.

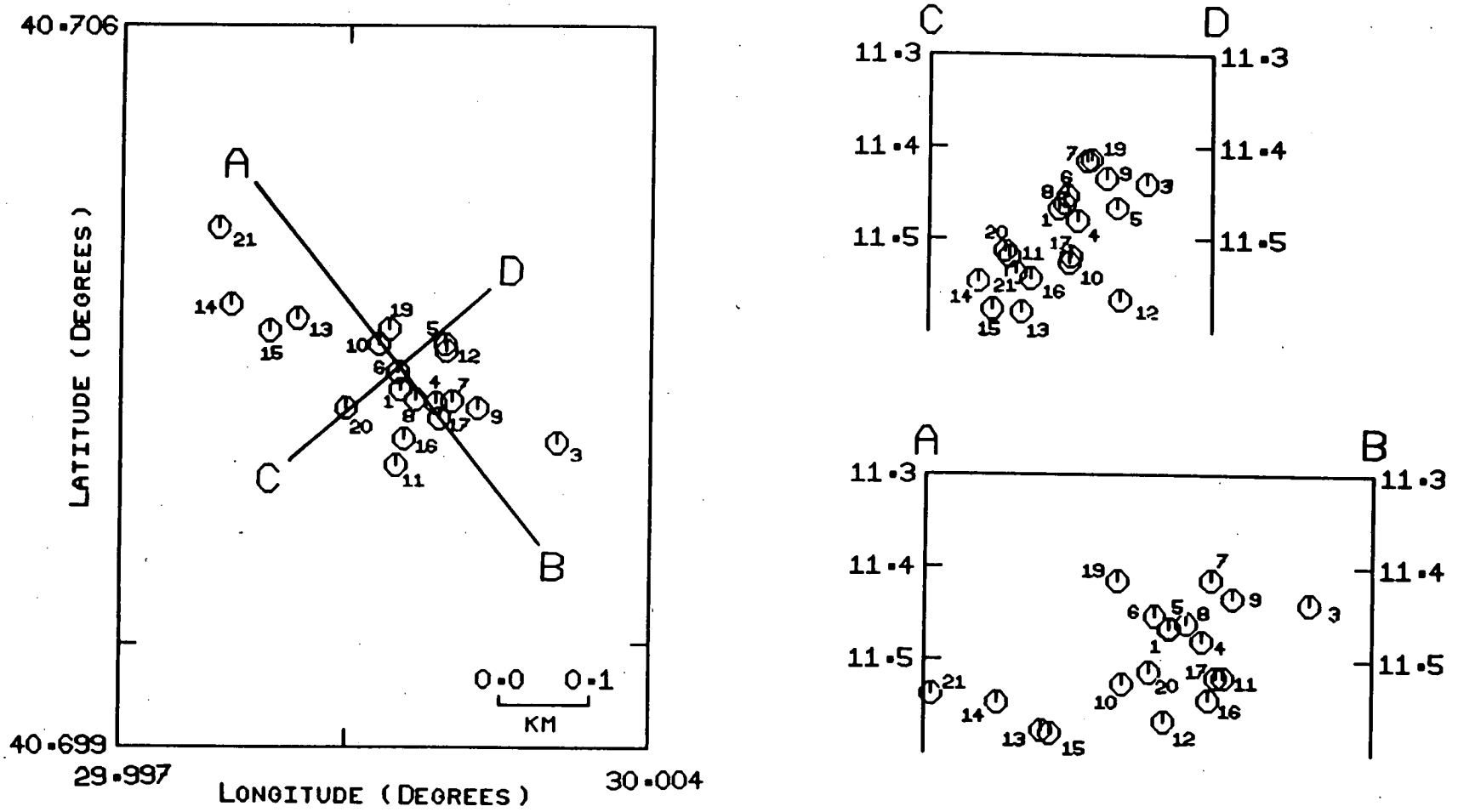

Fig. 5.3b - Epicentral plot and two orthogonal cross-sections of the events in Group 1 relocated at a velocity of Vp = 6.5km/s and Vs = 3.7km/s.

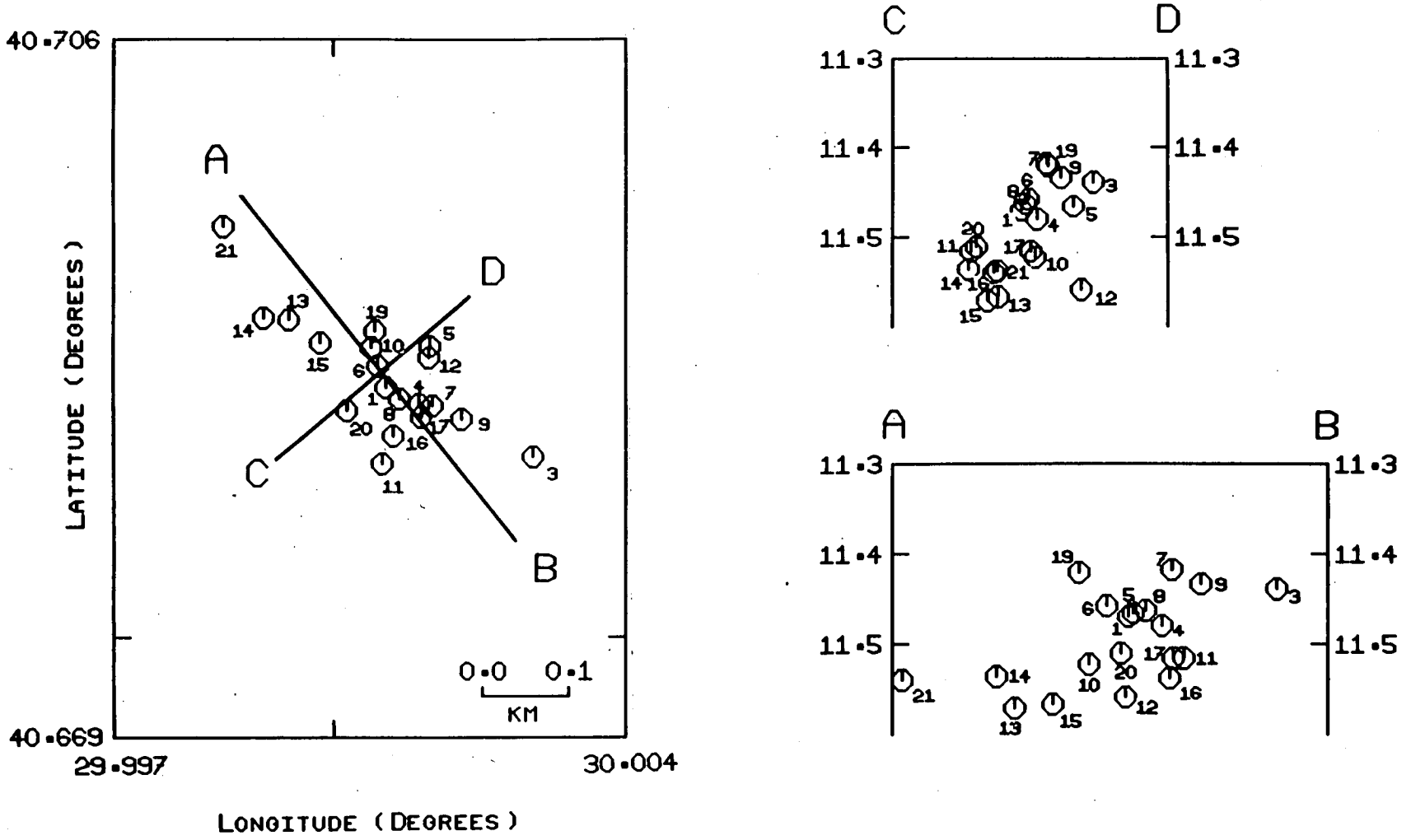

Fig. 5.3c - Epicentral plot and two orthogonal cross-sections of the events in Group 1 relocated at a velocity of Vp = 6.0km/s and Vs = 3.4km/s.

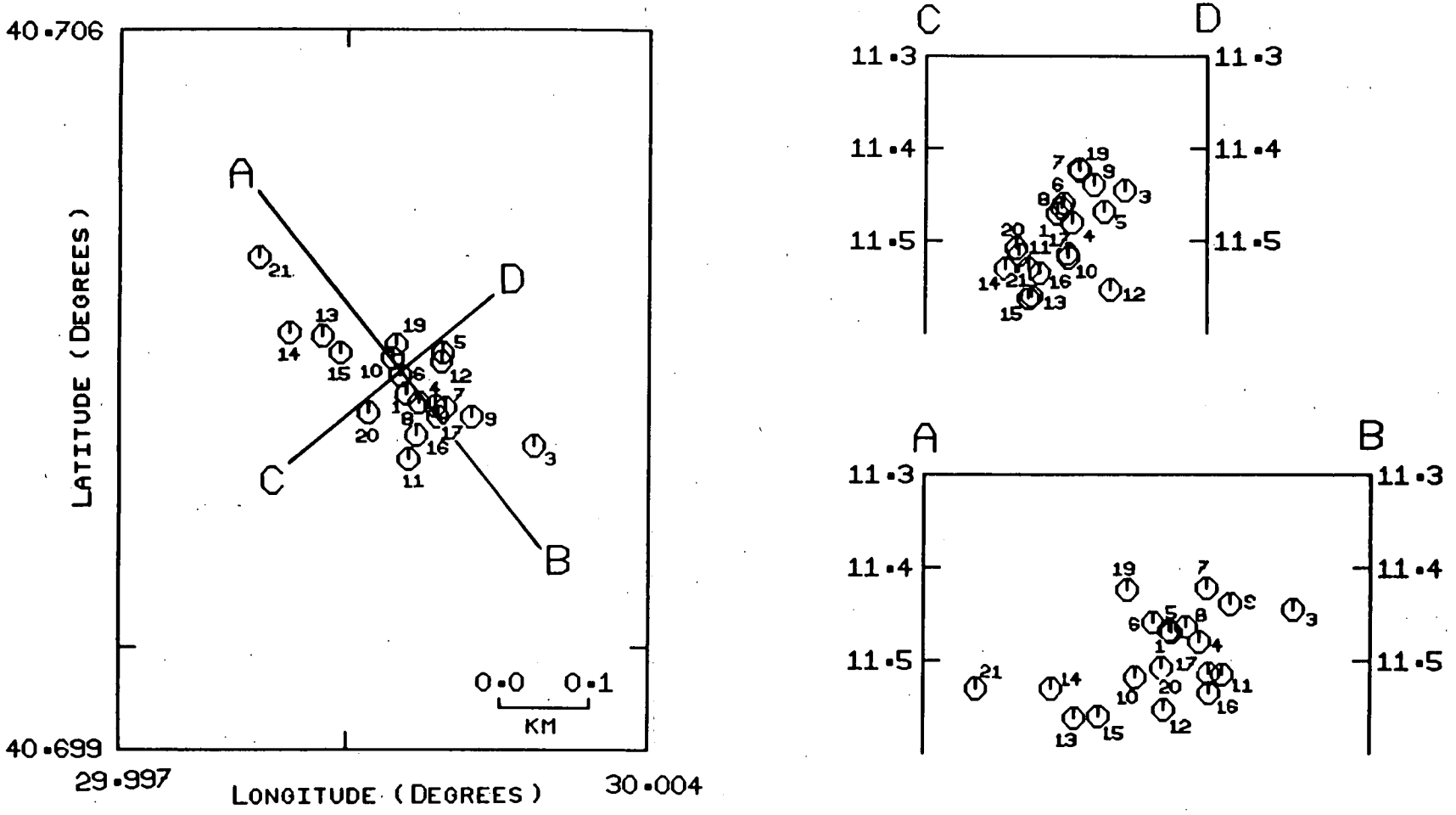

Fig. 5.3d - Epicentral plot and two orthogonal cross-sections of the events in Group 1 relocated at a velocity of Vp = 5.5km/s and Vs = 3.1km/s.

The only feasible geophysical interpretation of such a line, at this depth, is some kind of magmatic intrusion. However, other evidence would suggest that this is not likely to be the case. At depths of the order of 10kms the temperature will be relatively low and small magmatic bodies (less than a few hundred metres across) would cool and crystallise unless they were associated with a much larger body. Geoelectric studies carried out by the Geomagnetism Research Group during TDP-3 (see chapter 1) have produced a resistivity structure for depths down to 50km (further analysis could extend this limit to 100km). Magmatic bodies are very hot and therefore very conductive but no such body appears to exist within the crust below the network (Russell, 1987). Heat flow measurements would also be very useful but as yet there have been no heat flow studies carried out in the area.

So from the geoelectric information alone it seems unlikely that the finger-like seismic distribution that we are seeing is magmatic in origin. A fault-type source is therefore assumed and the remainder of the section looks at this a little more closely.

Chapter 2 outlines the theory put forward by Aki (1984) which suggests that earthquake families can be modelled in terms of the stability of either asperities or barriers on a fault. It is proposed that the asperity-type model is characterised by constant fault length and slip whilst the barrier-type model has constant fault length but variable slip. In both cases similar waveforms are produced but for the asperity-type model the absolute amplitudes will be approximately equal whereas for the barrier-type model they will vary by at least an order of magnitude. For group 1 the ratio of the largest to the smallest amplitude at any one station is about one hundred (saturated records of the largest event make accurate measurement impossible) and this is consistent with the barrier-type model. For such a model the source can be considered to be an area of weakness on the fault, bounded by strong patches or barriers where large stresses are needed to cause any movement of the fault. Between these strong barriers there may be many weaker barriers that can be broken at much lower stresses and it these weaker barriers that determine the distribution of earthquakes within a group. The

effective fault length and the frequency content of the transmitted waveform are determined by the strong barriers since they remain unchanged for the whole group. It might, therefore, be expected that any weak barriers that remain unbroken after the last event in a group has occurred, might be visible in a plot of the relocated hypocentres. In fig. 5.3 many of the events are clustered in small groups. Most of the unoccupied areas between the events are quite small and the resolution of the plot is such that we can not positively identify them as barriers. There are, however, several larger gaps but it maybe that these lie outside the area of weakness since there is no reason to assume the area to have a regular or smooth boundary. If they are caused by weak barriers the group may reactivate itself in the relatively near future. In fig. 5.3 the two cross-sections show that the group can be split into two sub-groups, the upper sub-group containing events 1-9 and 19 while the lower sub-group contains events 10-21 (except 19). It would seem, therefore, that before event 10 the group was prevented from expanding downwards by a barrier that was not big enough or strong enough to affect the fault length but large enough to absorb the change in stress. In the cross-sections there is still a small break between the sub-groups which may be all that is left of the barrier.

Earlier in the section it was noted that a slight alignment of the events could be seen in section A-B of fig. 5.3. Using the barrier-type model this is easily explained as an elongation of the area of weakness. The direction of this elongation can be expressed in terms of an angle taken with respect to the strike of the fault plane. However, the angle cannot be measured directly from fig. 5.3 since cross-section A-B is a vertical projection of the inclined fault plane and as a result all projected angles will be reduced. For a plane dipping at an angle 'a' and with the cross-section running parallel to the strike, the true angle 'b' (on the inclined plane) and the measured angle 'c' (on the cross-section) are related by

$$\tan (b) = \tan (c)/\sin (a) \qquad 5.1$$

For group 1, a = 45^{o} c = 20^{o} - 25^{o} giving a true angle of b = 27^{o} - 33^{o} (these angles follow the convention used to define angles of rake). The direction of elongation is most likely to be dependant upon the distribution of barriers over the fault rather than the direction of slip (rake). In the following section the rake will be calculated as part of the fault plane solution so that this assumption may be checked.

The dimensions of the plane depend upon the velocity used in the relocation. At V_p = 6.0km/s and V_s = 3.4km/s the extreme dimensions of the group are 450m by 180m by 125m with the main body of events confined to a volume 230m by 180m by 65m (this does not include events 3, 12 and 21 which lie in solitary positions away from the others). Higher or lower velocities would increase or decrease the dimensions respectively.

5.3.3 Group 1 - Fault Plane Solution

The first motion (up or down) recorded on a correctly calibrated vertical seismometer can be directly converted to initial ground motion (up or down). The initial ground motion is determined by the motion of the P wave as it arrives at the station; compression pushing the ground up and dilation pulling it down. If the location of the earthquake is known, then the path taken by the wave can be traced back to the source where the first motion can be plotted on the focal sphere at the correct azimuth and take-off angle. This can then be repeated for all stations that record the event. On paper these results can be represented by plotting an equal area projection of either the upper or lower focal hemisphere, with closed circles representing compression and open circles dilation. For local earthquakes, such as those recorded during the Turkish Dilatancy Projects which have epicentres that lie within or close to the network, all arrivals will originate from the upper focal hemisphere. All plots to follow will be of the upper focal hemisphere.

From a plot of the first motion data and modelling the source as a double couple source, it should be possible to plot out the fault

plane and its auxilliary plane (focal planes), although they cannot be distinguished by this method alone and so need independent evidence (Aki and Richards, 1980). In practice, the fault plane solution obtained is often badly constrained because of either a lack of or a poor distribution of the data. Sometimes it is possible to get around this by plotting and solving several events at the same time - a composite solution. This is justifiable if the events can be shown to be closely grouped and are likely to have similar solutions. Where this may not be possible there are other ways of improving the solution. The most widely used is to look for stations that lie on or near one of the nodal planes. These can be found by looking at the relative amplitudes of the P and S waves. On either of the nodal planes the P will have negligible amplitude while the S has a large amplitude and so the S/P amplitude ratio should be large. On first motion plots such stations are shown by putting a cross through the normal symbol. One other convention used is that small circles indicate when there is uncertainty in the direction of the first motion.

In the previous sub-section a fault plane striking N141^{o}E and dipping 45^{o} was revealed using the relative location method. To see if the fault plane solution is consistent with this, the first motion data has been plotted in fig. 5.4. Six of the stations showed very clear arrivals and there was no doubt as to the first motion, but for stations PB and KT this was not so. The signals were intermittent and often very noisy. The readings for these two stations were obtained by considering eight of the largest magnitude events within the group and taking what appeared to be the most consistent value. The results were independently checked by John Lovell.

The range of fault plane solutions that can be obtained from this set of data is quite large and would be even larger but for the reading at KT which is both compressional and nodal. One of the nodal planes is quite well constrained since it must separate the dilational and compressional readings of DP and SE respectively and must strike in a roughly E-W direction. The other nodal plane is less well constrained but must lie orthogonal to the first and close

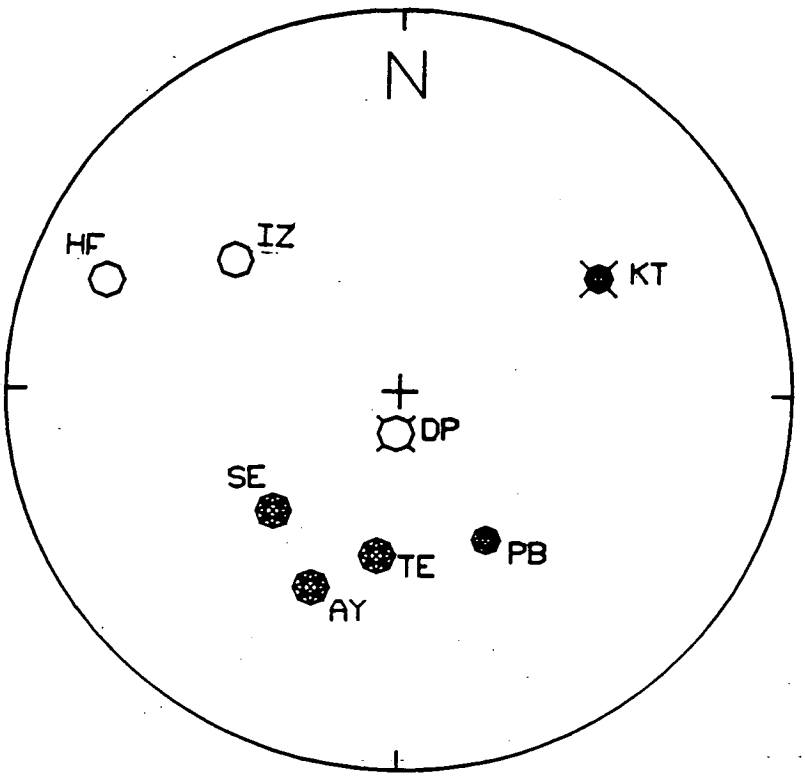

Fig. 5.4 - Equal area upper hemisphere projection of P-wave first motion for Group 1, centred on the HYP071 location of the master event ($40^{o}42.29'$, $30^{o}00.05'$, 11.73km).

to KT. Two possible solutions are shown in fig. 5.5a and fig. 5.5b. As mentioned earlier, the fault plane cannot be distinguished from the auxilliary plane and so some other information is required. An examination of the surface geology may reveal the direction of strike for faults breaking the surface and which may be used to infer the strike direction at depth. In this particular case the dominant fault system in the area is the E-W striking North Anatolian Fault which would fit one of the nodal planes quite well. However, there is no guarantee that what goes on at the surface is continued at depth. Evidence to suggest that other fault orientations do exist can be found in the fault plane solutions calculated by Evans *et al.* (1985) for the same set of data (TDP-2). He found several events that ran in a roughly N-S direction and which contained a significant normal component. This would agree quite well with the second nodal plane.

We may conclude from this that it is not possible to say which of the planes is the fault plane. However, the purpose of this section was to look for consistency between the fault plane solution and the fault plane outlined in the previous section. If the strike and dip that have been derived are used to define one of the nodal planes then a perfectly acceptable fault plane solution can be found and this is shown in fig. 5.5c. Therefore, it would appear to be reasonable to interpret the roughly N-S trending nodal plane as the fault plane.

In the previous section the area of weakness on the fault was found to be elongated at an angle of between 27^{o} - 33^{o} to the strike. In fig 5.5c the rake of the assumed fault plane is -14^{o}, a difference of approximately 45^{o}. This suggests that the direction of elongation is not dependent upon the direction of slip and lends support to the idea that it is determined by the distribution of the barriers over the fault plane.

5.3.4 Group 1 - Spectral Determination of the Source Dimension

Section 5.3.2 established a source dimension of 450m by 180m by 125m for group 1. As explained in chapter two a measure of the

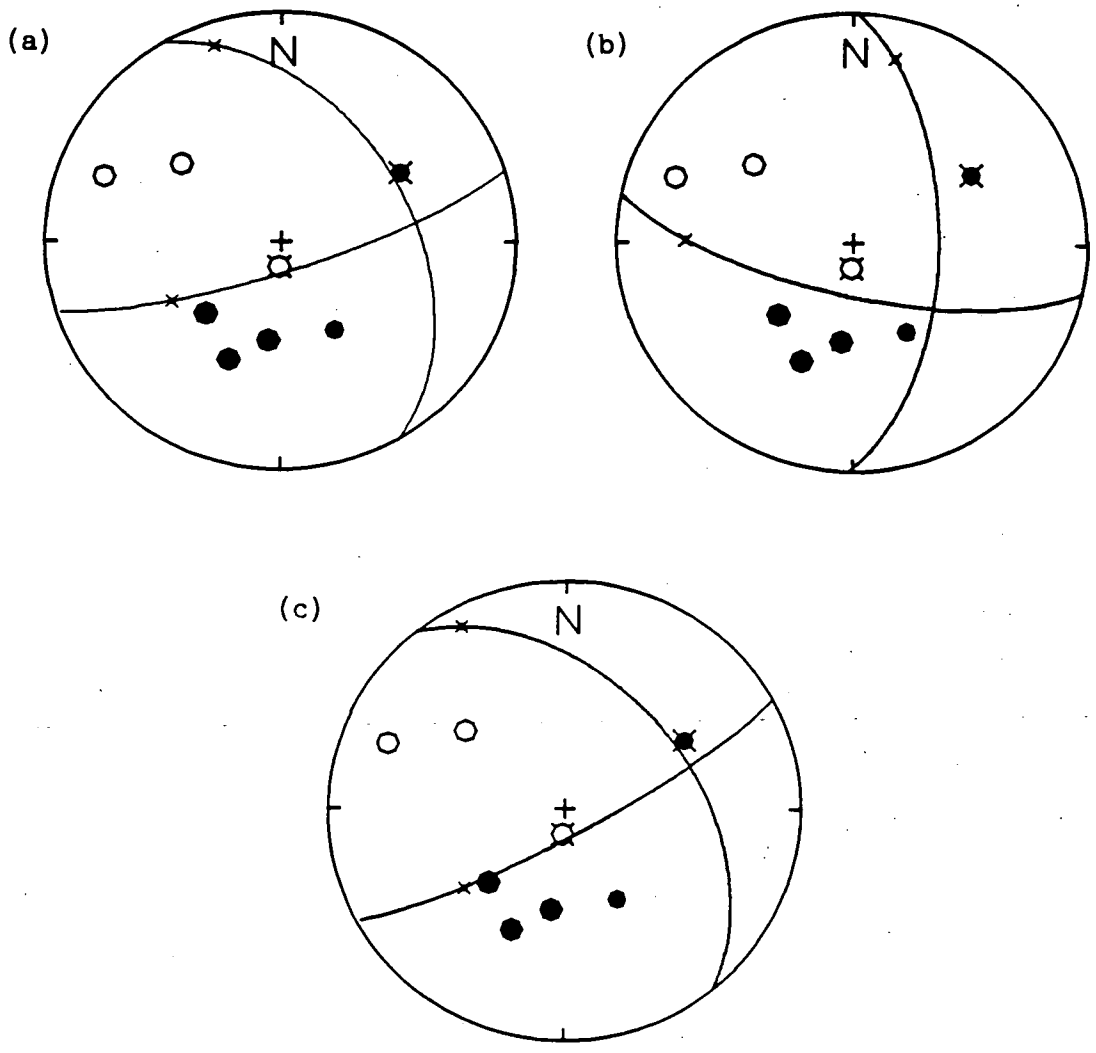

Fig. 5.5 - Three fault plane solutions superimposed upon the first motion plot of fig. 5.4. In (a) strike=150°, dip=44°, rake=-16°, (b) strike=181°, dip=60°, rake=-22° and (c) strike=141°, dip=45°, rake=-14° (the fault plane revealed in section 5.3.2).

source dimension can also be obtained through other indirect means, the most popular of these being a spectral technique based on the seismic-source model proposed by Brune (1970, 1971). This section aims to calculate the source dimension using this method for comparison with the above results. Before proceeding with the analysis a summary is made of the major points and equations given in chapter two.

The model proposed by Brune predicts that the S wave far-field displacement spectra will consist of a flat low-frequency spectral level followed by a high-frequency roll-off that starts at a characteristic frequency usually referred to as the corner frequency ($f_c(S)$). Brune was able to derive the following expression for the corner frequency

$$f_c(S) = \frac{2.34\ V_s}{2\pi r} \qquad \text{(Brune (1970), Brune (1971))}$$

where V_s = S wave velocity
r = source radius

For the P wave spectra Hanks and Wyss (1972) suggested that the above equation can be adapted by substituting the S wave velocity for the P wave velocity (V_p) giving

$$f_c(P) = \frac{2.34\ V_p}{2\pi r}$$

Fig. 2.1 of chapter two shows the relationship between the S wave and P wave spectra. If the Brune model is valid, then the ratio of the S and P corner frequencies should be equal to the ratio of the S and P velocities

$$R_c = \frac{f_c(P)}{f_c(S)} = \frac{V_p}{V_s} = 1.75$$

but, in practice, this has not always been found to be true. Madariaga (1976) put forward a model that predicted different

formulae for the P and S corner frequencies and a maximum ratio of about 1.5

$$f_c(S) = \frac{1.32\ V_s}{2\pi r}$$

$$f_c(P) = \frac{2.01\ V_s}{2\pi r} \qquad \text{(note use of } V_s \text{ instead of } V_p\text{)}$$

To help decide which of these formulae to use the following analysis of the group 1 data will include a calculation of the corner frequency ratio.

To measure the spectral source dimension from a group of similar earthquakes it should only be necessary to analyse one event, since the corner frequency should not change from one event to another. In practice, the presence of noise and the absence of some channels due to equipment failure means that more reliable results will be obtained if several events are looked at. Also, the measurement of corner frequency on real spectra is not always as straightforward as the theory suggests and there can be a sizeable error in the measurement. Hence, for statistical reasons, it is wise to inspect more than one event.

From the events of group 1 three of the largest were selected, as these were most widely recorded across the network (G1(2), G1(4) and G1(5)). For each component of each station that recorded the events the S wave displacement spectrum was calculated and the corner frequency picked. Fig. 5.6 shows a selection of seismograms and their spectra taken from all three events. These examples were selected to illustrate the range of corner frequencies that were measured both across the network and from one event to another at the same station. In each case the spectrum is calculated both for a window containing the S arrival (solid line) and for one containing noise only (dashed line) which is taken from a section of the seismogram prior to the first arrival. The respective windows are shown above the seismograms. For those stations furthest from

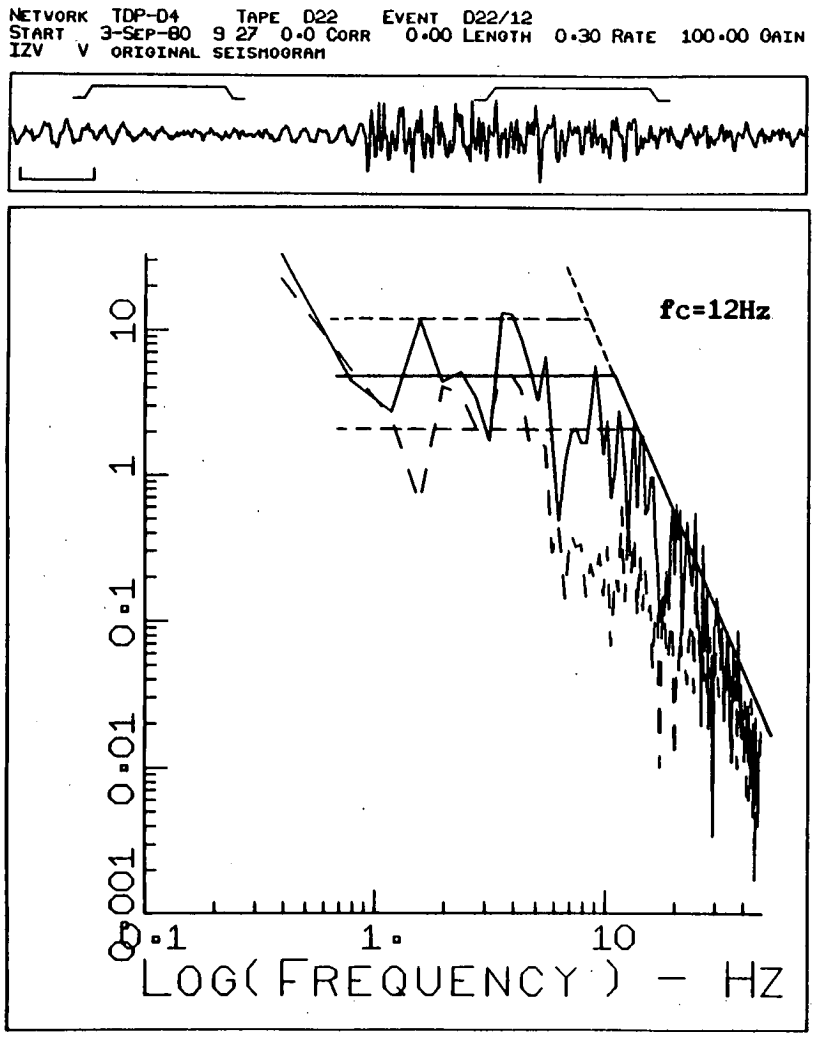

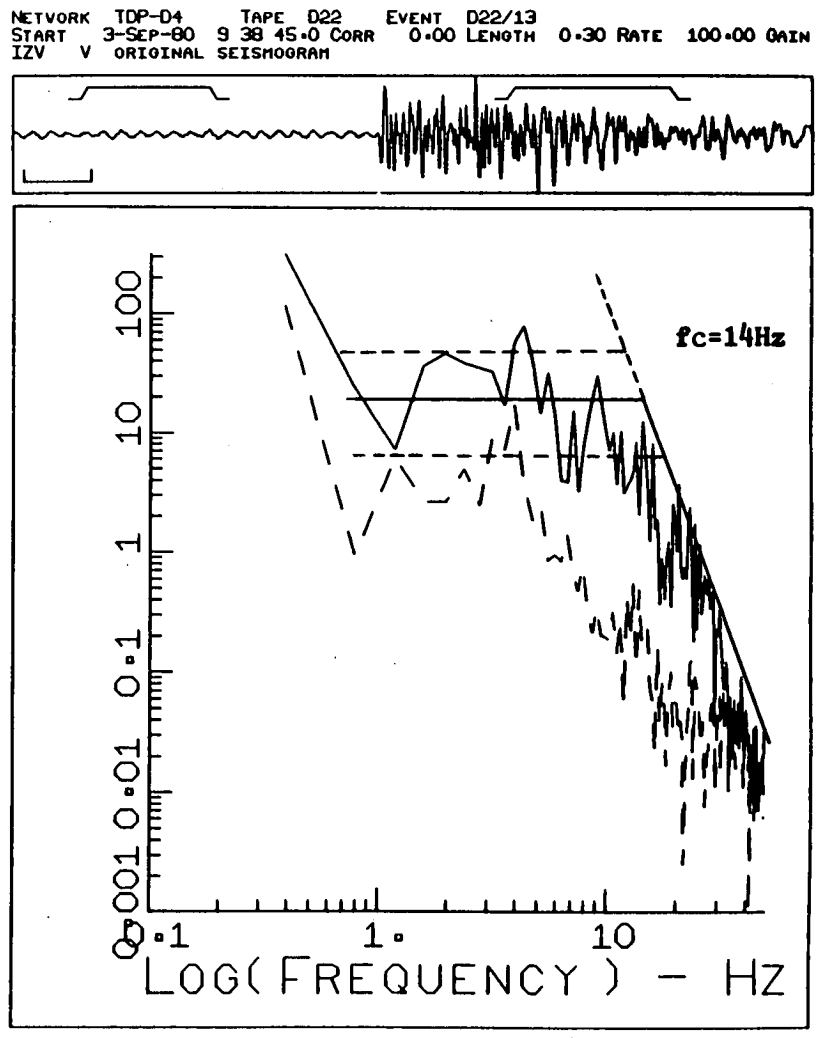

Fig. 5.6a,b - S-wave displacement spectra for different events recorded at one station (IZ). Corner frequency (fc) is estimated as shown by the solid line. The straight dotted line gives an indication of the error involved in this measurement. The noise spectra (dotted) is taken from a window prior to the first arrival.

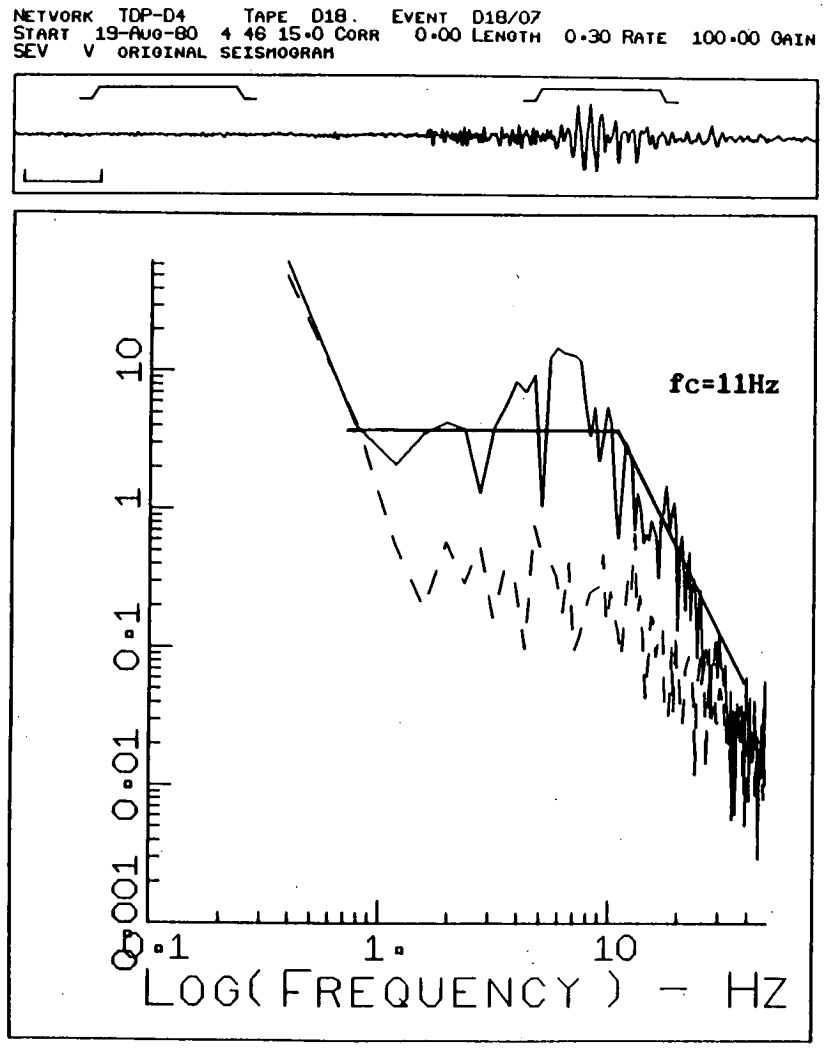

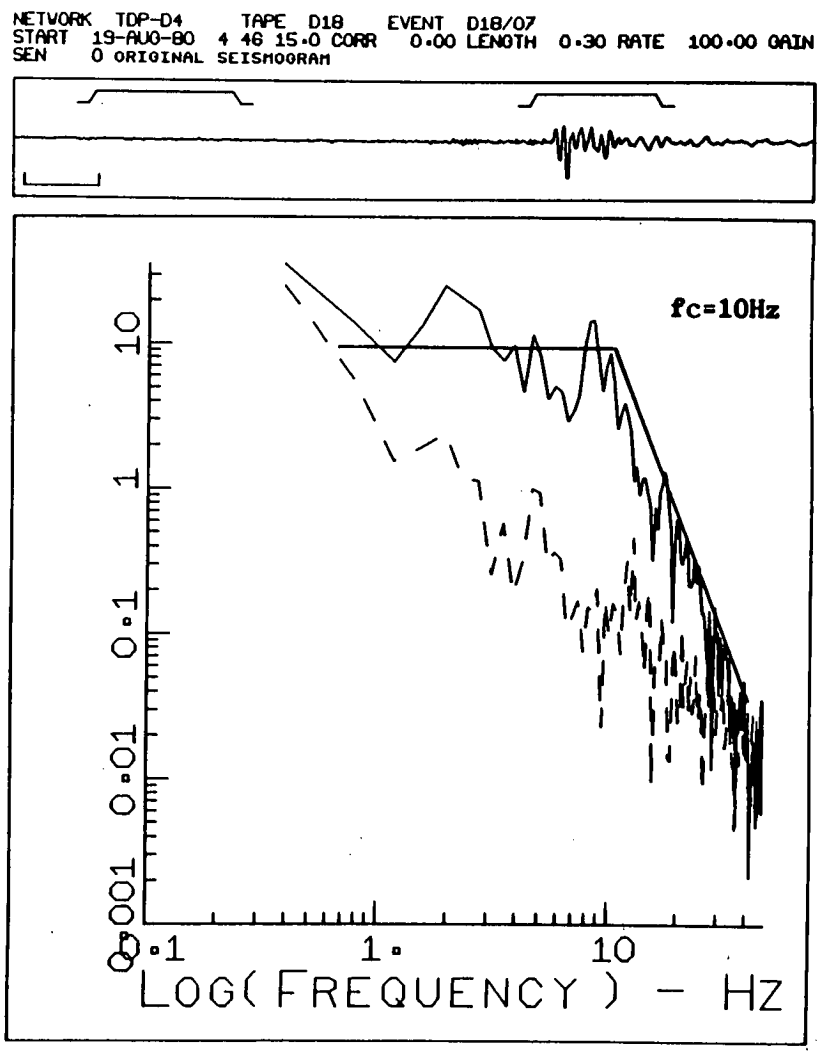

Fig. 5.6c,d - S-wave displacement spectra for one event recorded on two different components at the same station (SE). The estimated corner frequency (fc) is shown. The noise spectra (dotted) is taken from a window prior to the first arrival.

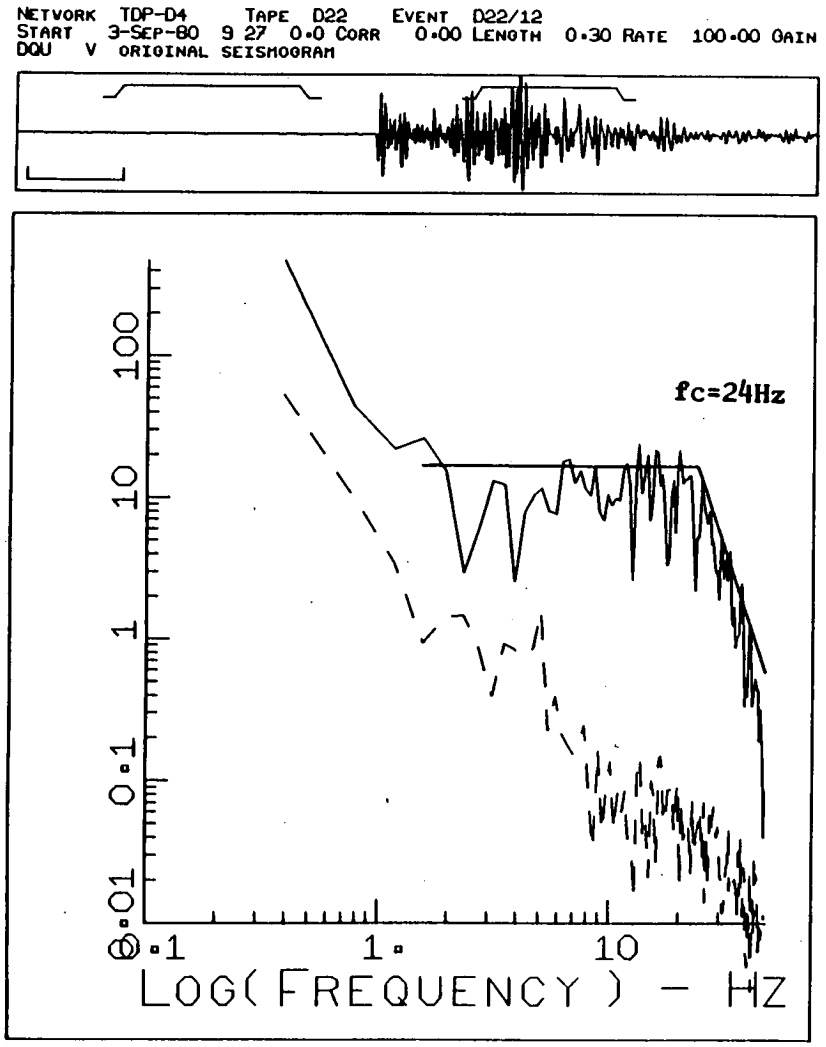

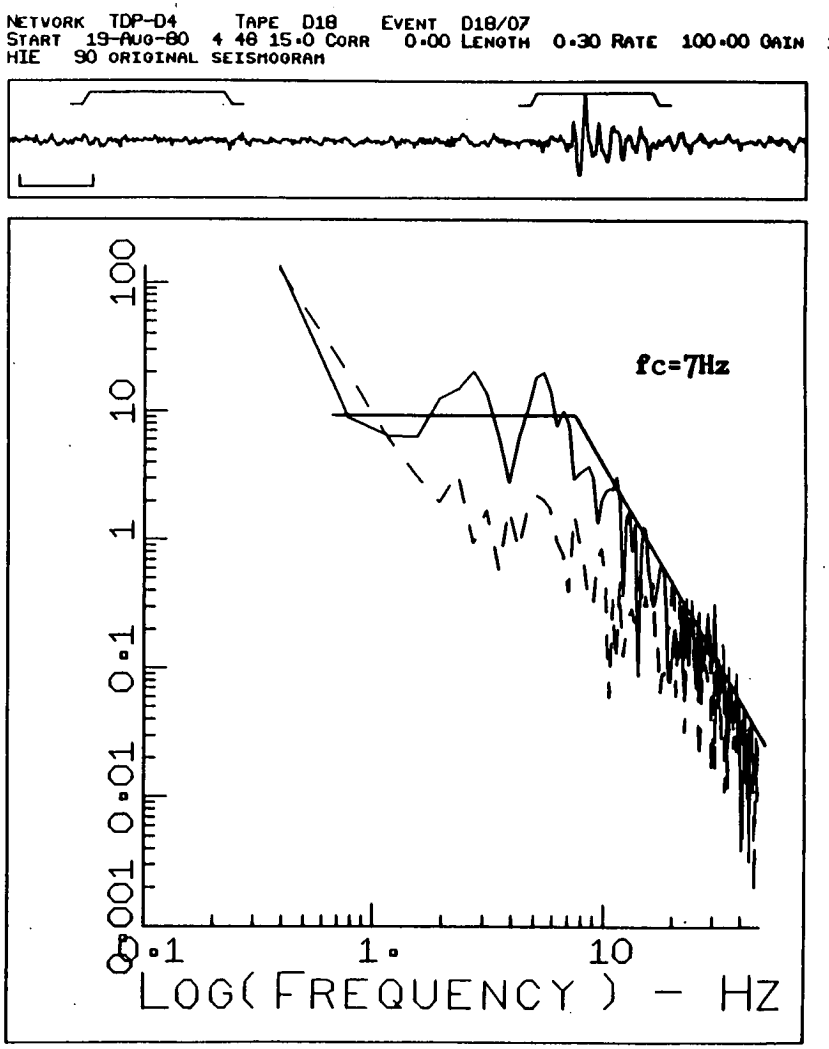

Fig. 5.6e,f - S-wave displacement spectra from Group 1 showing two extremes in the corner frequency (fc) measurement. In (e) 'ringing' in the seismogram at approx. 20Hz causes the corner frequency to be increased. In (f) the corner frequency is low, probably a result of the low signal to noise ratio. The noise spectra (dotted) is taken from a window prior to the first arrival.

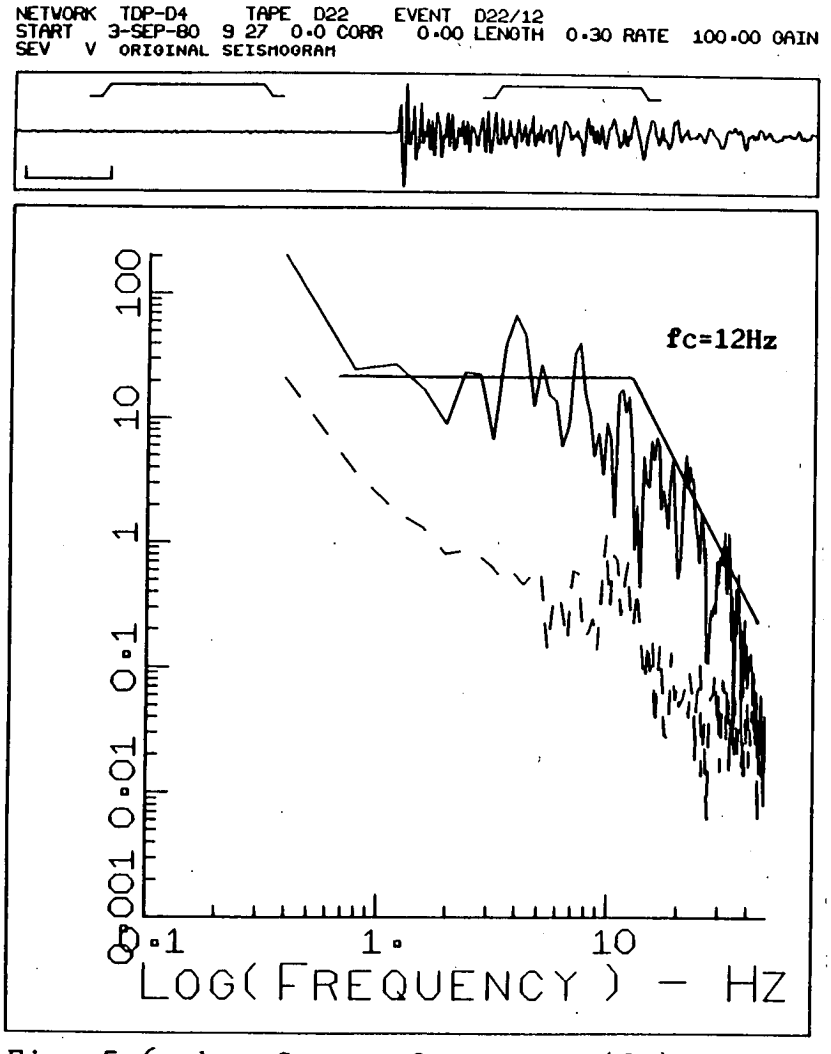

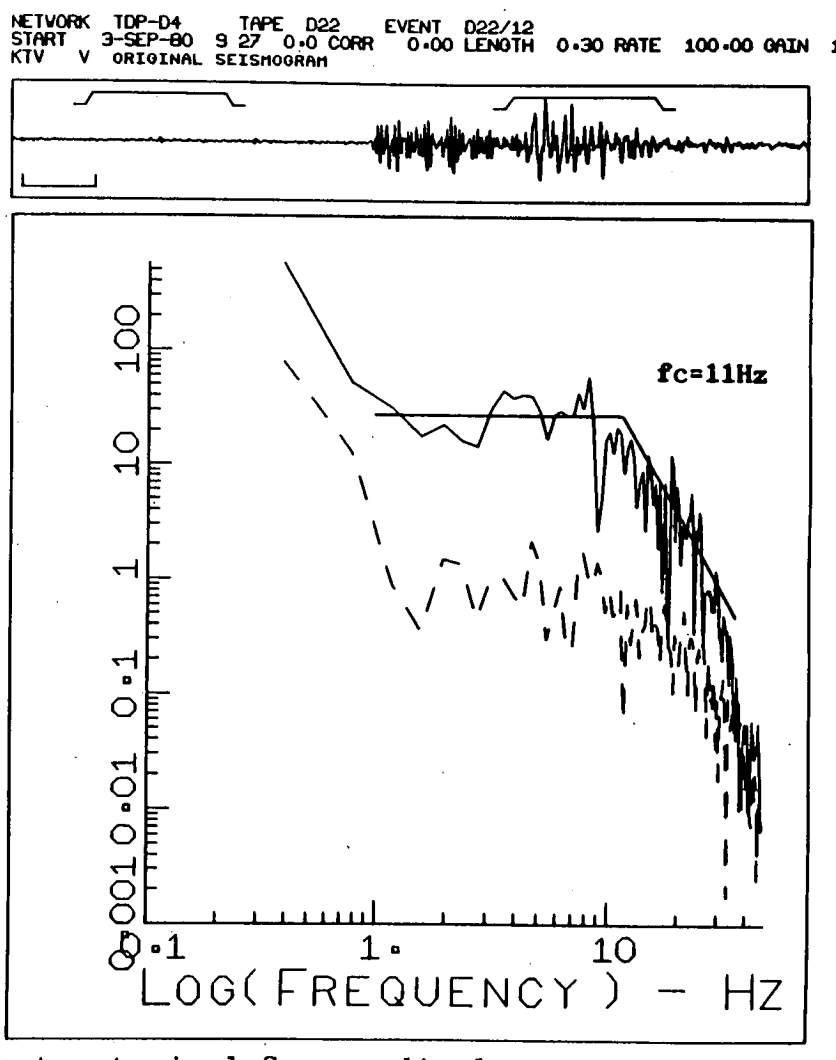

Fig. 5.6g,h - Corner frequency (fc) measurements for two typical S-wave displacement spectra from Group 1. The noise spectra (dotted) is taken from a window prior to the first arrival.

the epicentre (IZ,HI of figs. 5.6a,b,h) the noise is relatively high and the spectral level appears to be close to that of the signal. The true spectral levels, however, have been distorted by plotting on a log scale and so the noise is not as significant as it may seem. For the other stations in fig. 5.6 the signal and noise spectral levels differ by at least a factor of ten for all frequencies up to a point well above the corner frequency.

The position or size of the window is not crucial. It is important that the window contains only the one phase and does not, for example, contaminate the S window with the tail of the P coda. Moving the window does not affect the position of the corner frequency although the finer detail of the spectrum is affected. A thorough check of all this was made prior to processing the data.

To pick the corner frequency the real spectrum needs to be interpreted in terms of the model case (i.e. a flat low frequency level and a high frequency roll-off). The conversion is done by smoothing the spectrum by eye and estimating the model spectral lines. From the intersection of these lines the corner frequency is measured. In fig. 5.6 the interpretation has been superimposed upon the spectra.

Figs. 5.6a,b show two events recorded at one station. As can been seen, the error involved in picking the corner frequency is quite large but, despite this, the agreement between the readings is good and this is true for all stations. Figs. 5.6c,d demonstrate the agreement that exists between two different components at the same station. Fig. 5.6e shows an example of how a local site effect can distort the reading of the corner frequency. 'Ringing' in the seismogram, measured at a frequency of approximately 20Hz, has increased the amplitude of the frequencies just above the corner frequency and thus moved it along. This effect can be seen on any event recorded at station DP/DQ. Hence all measurements of the corner frequency from this station have been ignored. Figs. 5.6f,g,h are typical of the spectra obtained.

Table 5.2 contains the readings made for all three events and from these results $f_c(S) = 12 \pm 2$ Hz was obtained by calculating the mean and standard deviation of all the valid readings.

Before using this result to calculate the source dimension the corner frequency ratio needs to be evaluated. The above procedure was repeated for one of the events (TD0247.J27 - the master event) but with the window placed over the P arrival. Fig. 5.7 shows two examples for comparison with figs. 5.6g,h. Table 5.3 contains the readings made at each station and from these results $f_c(P) = 21 \pm 3.5$ Hz was obtained in the same way as for $f_c(S)$.

Using the P and S corner frequency results gives a corner frequency ratio of

$$R_c = \frac{f_c(P)}{f_c(S)} = \frac{21 \pm 3.5}{12 \pm 2} = 1.75 \pm 0.41$$

This value suggests that the data would best fit the Brune model, but the error is such that it is not really possible to distinguish between this and the Madariaga model. As a result, both models are used to evaluate the source dimension and the range of values obtained can then be compared to the relative location results.

Using the Brune model, velocities of $V_p = 6.0$km/s and $V_s = 3.4$km/s and errors in the velocity of 10% we get

$$r = \frac{2.34\ V_p}{2\pi f_c(P)} \quad \text{or} \quad r = \frac{2.34\ V_s}{2\pi f_c(S)}$$

$$r = 106 \pm 21 \text{ m} \qquad r = 105 \pm 20 \text{ m}$$

This gives an average of $r = 106 \pm 20$ m.

Using the Madariaga model we get

$$r = \frac{2.01\ V_s}{2\pi f_c(P)} \quad \text{or} \quad r = \frac{1.32\ V_s}{2\pi f_c(S)}$$

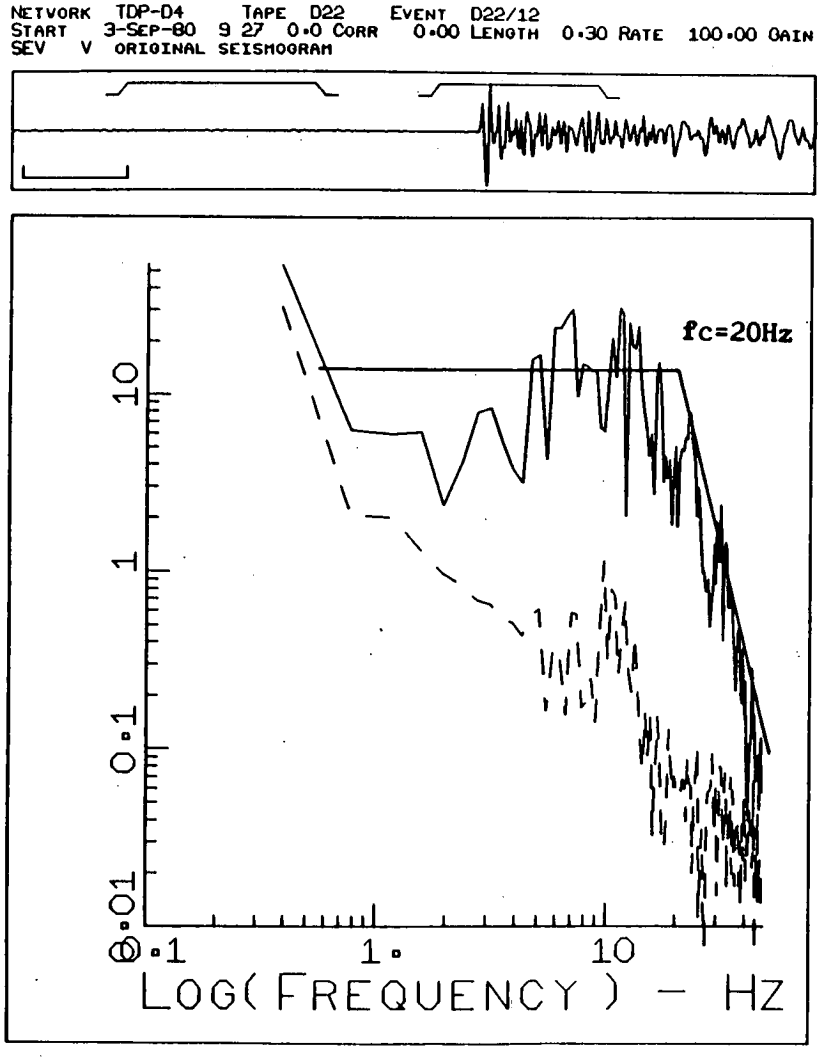

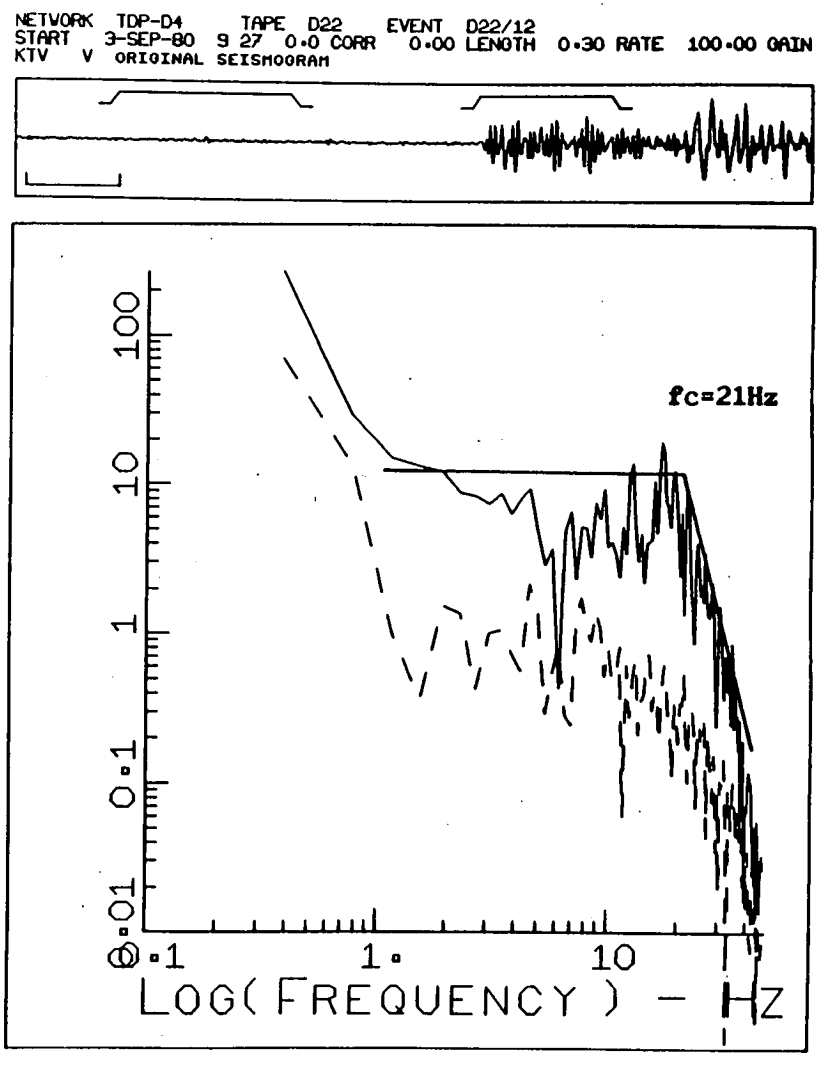

Fig. 5.7a,b - Two typical P-wave displacement spectra from Group 1 showing the estimated corner frequency (fc). The corresponding S-wave spectra are shown in fig. 5.6g,h. The noise spectra (dotted) is taken from a window prior to the first arrival.

Event	Station									
	TE	SE	AY	PB	IZ	DP	HF	DQ	KT	HI
TD0232.E46	17	10	-	12	9	-	-	-	-	8
TD0247.J27	14	12	12	-	12	-	13	-	11	-
TD0247.J38	-	14	13	-	13	-	11	14	-	-

Table 5.2 - S-wave corner frequency (f_c(S)) as measured at each station for three events from Group 1. All readings in Hz.

Event	Station									
	TE	SE	AY	PB	IZ	DP	HF	DQ	KT	HI
TD0247.J27	25	18	-	-	16	-	21	24	20	-

Table 5.3 - P-wave corner frequency (f_c(P)) as measured at each station for the Group 1 master event. All readings in Hz.

Event	Station									
	TE	SE	AY	PB	IZ	DP	HF	DQ	KT	HI
TD0247.J27	31	32	36	-	32	-	33	31	30	-

Table 5.4 - Values of f_{max} measured from the acceleration spectra of the Group 1 master event. All readings in Hz.

$r = 52 \pm 10$ m $r = 60 \pm 12$ m

This gives an average of $r = 56 \pm 11$ m.

Both models assume circular sources and so to obtain a source dimension comparable to the relocation result the above results need to be doubled. Hence, from spectral studies the source dimension would appear to lie in the range

$d = 112 \pm 16$ m to 212 ± 28 m

As explained in chapter 2 there may also be an upper frequency limit, referred to as f_{max}, due to source, path, recording site effects or a combination of all three (Hanks, 1982a and 1982b; Aki, 1987). f_{max} does not exist in all spectra but where it does it has been shown to have a value typically in the range 10-20Hz (Hanks, 1982a). If the same phenomena were to exist for the TDP data then it may affect the measurement of the corner frequency. As shown in fig. 2.2, f_{max} can be observed in the acceleration spectra and so, to check that our measurements of corner frequency lie below f_{max}, the acceleration spectra for two of the events were calculated. Typical spectra obtained from this are shown in fig. 5.8. A low frequency rise changes to a flat section at the corner frequency and then falls off at some higher frequency. Table 5.4 contains the measurements of this higher frequency for both events. The results are remarkably consistent with a mean value of 31 ± 2Hz. Since the system has a high frequency limit of 32Hz it would appear that it is this that we are measuring and that f_{max}, if it exists at all, is greater than 32Hz. We can therefore assume that our measurements of corner frequency are reliable.

Direct comparison of the spectral source dimension with that obtained from the relative location method is not easy. The spectral models of Brune and Madariaga both assume circular sources and hence only produce a single figure for the dimension. It is not known how this figure relates to the true dimensions of the source. It may be a measure of the longest dimension or just an average. From the relocation method three dimensions have been obtained although this is also a simplification since the maximum values in each direction

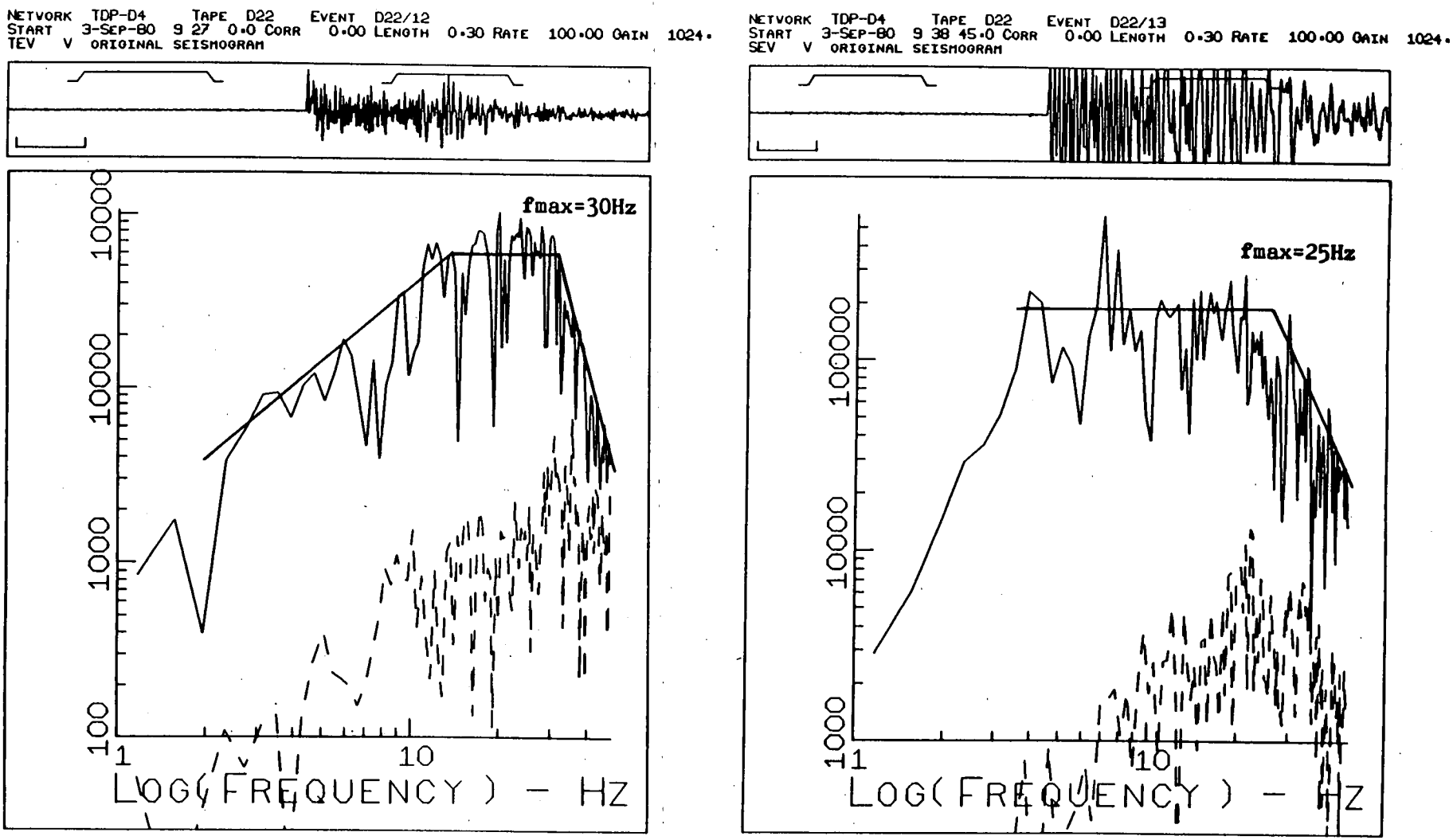

Fig. 5.8 - S-wave acceleration spectra from Group 1 with estimated values for fmax shown by the solid line. The noise spectra (dotted) is taken from a window prior to the first arrival.

were taken which does not convey the irregular shape that was outlined. A single representative dimension could be obtained by either taking an average of the three dimensions (d=245m) or by calculating the diameter of a sphere that has the same volume (d=264m). However, the comparison would still have little meaning since we have no way of knowing if similar measurements are being compared. It would, therefore, seem that the only valid comparison would be a general qualitative one.

It is encouraging that the two methods produce results that really are very close. The error in the relative location method is small and so the dimensions are likely to be accurate, assuming that the whole fault plane has been sampled. If this assumption is not true then the dimensions can be considered to be a minimum. On this basis the dimension obtained from the spectra is too small to be representative of the greatest dimension. The top end of the scale is very close to the average but from one set of results it is very difficult to draw valid conclusions.

5.4 Group Two

5.4.1 Introduction

Following the third phase of the Turkish Dilatancy Project (TDP-3) all earthquakes occurring in the vicinity of the network were located using HYP071 (Lee and Lahr, 1975). Chapter 1, which describes the project in detail, includes a plot of the epicentres (fig. 1.12) and this has been reproduced in fig. 5.9. Many of the events are clustered together, not only in space (as observed in fig. 5.9) but also in time, and a closer inspection of the seismograms of any one cluster shows just how similar most of the events are. These clusters would appear to be ideal for further analysis using the cross-correlation technique. The largest of these clusters is situated approximately 3km northwest of the station SE (at approximate coordinates $40^{o}39.5'$N, $29^{o}54'$E) and was selected for analysis as group 2. The cluster is ringed in fig. 5.9 by circle A.

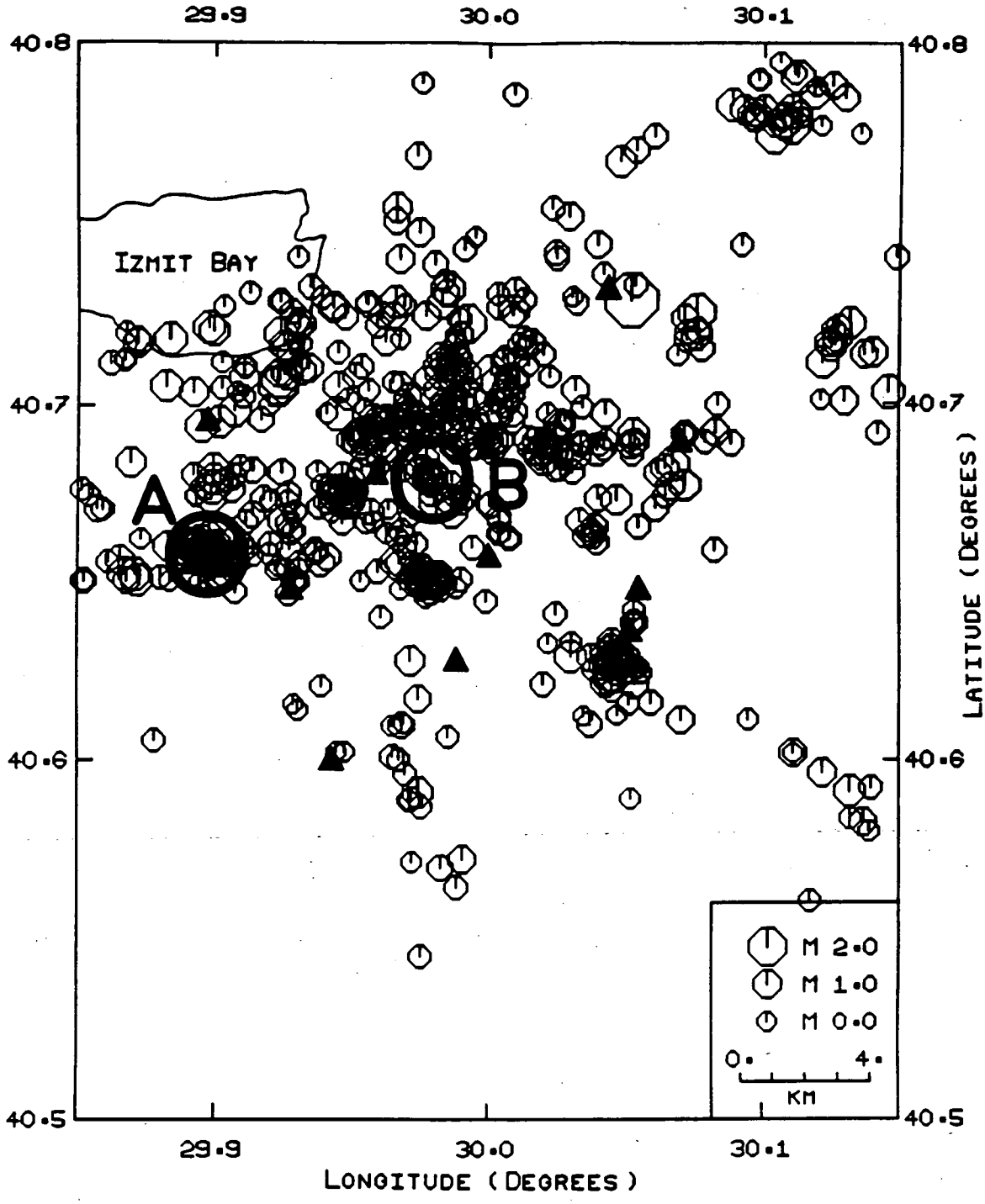

Fig. 5.9 - Epicentral plot of all local events recorded during TDP-3. The two clusters that are ringed contain Groups 2A, 2B (cluster A) and Group 3 (cluster B).

After weeding out dissimilar events, group 2 was found to contain 46 events occurring over a period of 4 days and at a depth of approximately 8kms. However, a closer inspection of the seismograms showed that the group could be further sub-divided into two smaller sub-groups based on differences in the relative amplitude of the P and S phases and in the motion of the first arrivals. These differences are relatively small and the seismograms still look very similar. Group 2A contains 26 events that occurred over a period of only 4 hours while group 2B contains 20 events that occurred at fairly regular intervals over the 4 day period.

5.4.2 Group 2A - Relative Location

The event codes and filenames of the 26 events comprising group 2A are listed in table 5.5 along with the HYP071 locations which are also plotted in fig. 5.10. Event G2A(8) was chosen to be the master event since it was well recorded at 6 stations (DP, AY, PB, TE, SE and KS) and the remaining 25 events have been relocated with respect to it. Fig. 5.11 is a plot of the relocated epicentres with two orthogonal cross-sections for velocities of V_p=6.0km/s and V_s=3.4km/s. As for group 1, it should be emphasised that the choice of velocity is only based on what is considered typical for these depths (8-12kms) and it is not deduced from any knowledge of the velocity structure in the area. The events plotted in fig. 5.11 have been numbered chronologically.

From the epicentral plot a clear alignment of the events can be seen in a WNW - ESE direction. The first cross-section (A-B) is taken in this preferred direction with section C-D at right angles to it. In section C-D the events are quite well constrained to a near-vertical plane while in section A-B there is some alignment of the events at an angle of around 30°. As for group 1 this finger-like distribution is interpreted as an elongated area of weakness on a fault rather than a magmatic intrusion. The actual plane is taken to be the one defined in cross-section C-D which has a strike of N102°E and a dip of somewhere between 85° to the south and 81° to the north.

		---------- Location (HYP071) ----------				
Event Code	Filename	Date	Time	Latitude (Deg/min)	Longitude (Deg/min)	Depth (km)
G2A(1)	TD4127.L40	840506	1140 17.94	40-39.58	29-53.77	7.54
G2A(2)	TD4127.L42	840506	1142 51.63	40-39.52	29-54.03	8.10
G2A(3)	TD4127.M11	840506	1211 5.24	40-39.26	29-54.30	8.65
G2A(4)	TD4127.M12	840506	1212 8.80	40-39.67	29-53.73	8.35
G2A(5)	TD4127.M14	840506	1214 33.54	40-39.58	29-53.67	8.71
G2A(6)	TD4127.M15	840506	1215 45.76	40-39.43	29-54.44	8.48
G2A(7)	TD4127.M17	840506	1217 27.64	40-39.31	29-54.33	8.72
G2A(8)	TD4127.M18	840506	1219 1.59	40-39.50	29-53.89	8.32
G2A(9)	TD4127.M21	840506	1221 34.81	40-39.51	29-54.26	8.03
G2A(10)	TD4127.M28	840506	1228 12.09	40-39.30	29-54.50	9.36
G2A(11)	TD4127.M45	840506	1245 2.62	40-39.57	29-54.11	8.47
G2A(12)	TD4127.M54	840506	1255 12.41	40-39.64	29-53.53	8.05
G2A(13)	TD4127.M56	840506	1257 0.84	40-39.55	29-53.69	8.02
G2A(14)	TD4127.NO1	840506	13 1 51.81	40-39.67	29-53.69	8.26
G2A(15)	TD4127.N13	840506	13 3 5.66	40-39.54	29-53.74	7.87
G2A(16)	TD4127.NO7	840506	13 7 20.85	40-39.40	29-54.54	8.71
G2A(17)	TD4127.N11	840506	1311 52.99	40-39.80	29-53.87	8.15
G2A(18)	TD4127.N13	840506	1313 47.62	40-39.53	29-53.83	7.68
G2A(19)	TD4127.N16	840506	1316 6.85	40-39.49	29-54.04	7.73
G2A(20)	TD4127.N19	840506	1319 7.20	40-39.66	29-54.06	8.45
G2A(21)	TD4127.N47	840506	1347 51.45	40-39.43	29-54.34	7.94
G2A(22)	TD4127.N48	840506	1348 50.82	40-39.47	29-54.37	8.79
G2A(23)	TD4127.000	840506	14 0 54.93	40-39.66	29-53.83	6.92
G2A(24)	TD4127.024	840506	1424 31.73	40-39.28	29-54.05	8.27
G2A(25)	TD4127.P14	840506	1514 43.22	40-39.46	29-54.25	8.95
G2A(26)	TD4127.P34	840506	1534 27.70	40-39.42	29-54.10	8.11

Table 5.5 - Group 2A. Event codes, filenames (GSRG standard files) and HYP071 locations (origin time and hypocentre).

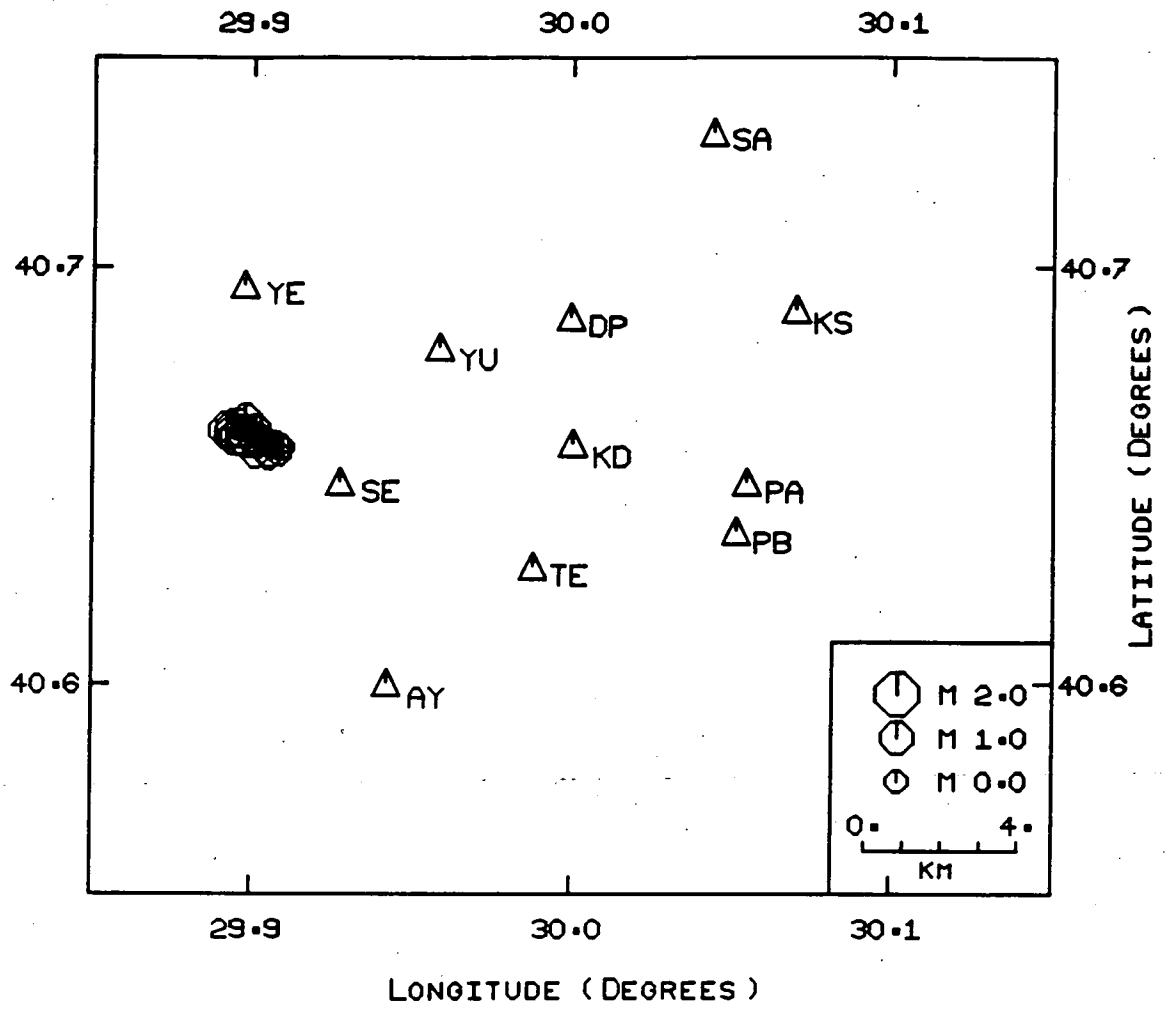

Fig. 5.10 - Epicentral plot of the Group 2A HYP071 locations (listed in table 5.5).

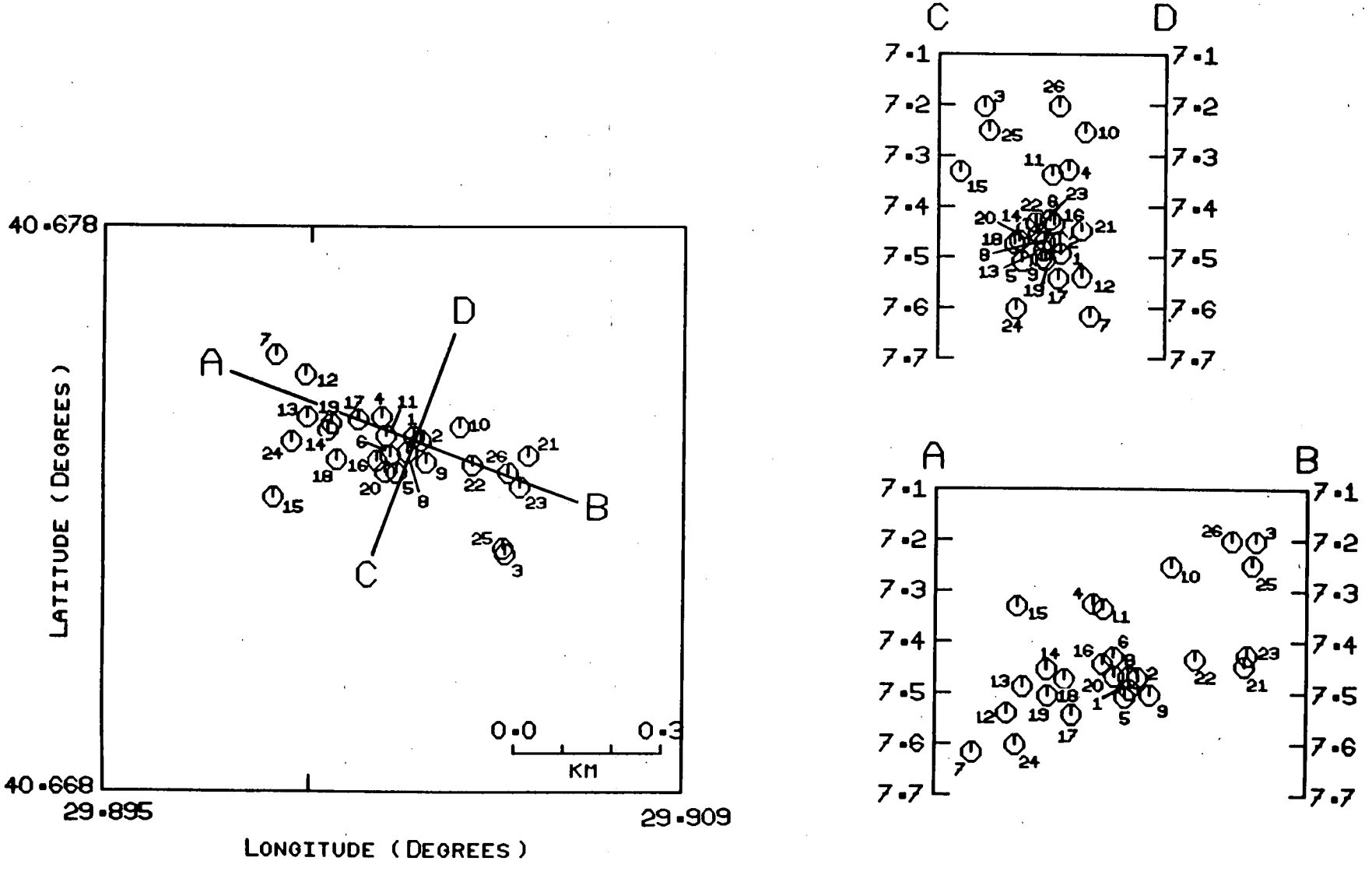

Fig. 5.11 - Epicentral plot and two orthogonal cross-sections of the events in Group 2A relocated at a velocity of Vp = 6.0km/s and Vs = 3.4km/s.

The ratio of the largest to the smallest amplitude at any one station is about 30 suggesting that the group can be modelled by a barrier-type model as discussed previously for group 1. In fig. 5.11 the temporal distribution of the events does appear to show some sort of pattern. The first eleven events (with the exception of G2A(3) and G2A(7)) and event G2A(20) all occur in a small volume at the centre of the cluster. The next eight events (G2A(12) - G2A(19)) and event G2A(24) are grouped together slightly further to the west and at a greater depth, while events G2A(21) - G2A(26) (except G2A(24)) occur further to the east in a less well defined group. This would seem to indicate the presence of several weaker barriers on the fault which lie between the stronger barriers that determine the nature of the group. There is no obvious change in waveform between these three sub-groups, indicating again that the weak barriers have no effect on the seismic waveforms.

The extreme dimensions of the group at a velocity V_p = 6.0km/s and V_s = 3.4km/s are 550m by 410m by 290m. Since the plane is near vertical the direction of elongation is that measured from section A-B (30^o from strike).

5.4.3 Group 2A - Fault Plane Solution

Using the relocation method a fault plane has been found that strikes N102^{o}E and dips somewhere around 90^o (section 5.4.2). To see if the fault plane solution is consistent with this plane, the first motion data has been plotted in fig. 5.12. Section 5.3.3 outlines the method used for obtaining strike and dip from such a diagram. The readings at all 8 stations are good and are taken from the whole group to form a composite picture (as opposed to just using the master event).

The distributions of compressions and dilations in fig. 5.12 is such that the complete fault plane solution cannot be properly defined. Only one of the nodal planes can be reasonably well constrained since it must separate the compressions to the north from the dilations to the south and, therefore, run in a roughly east-west direction. The two nodal readings at YU and KS would

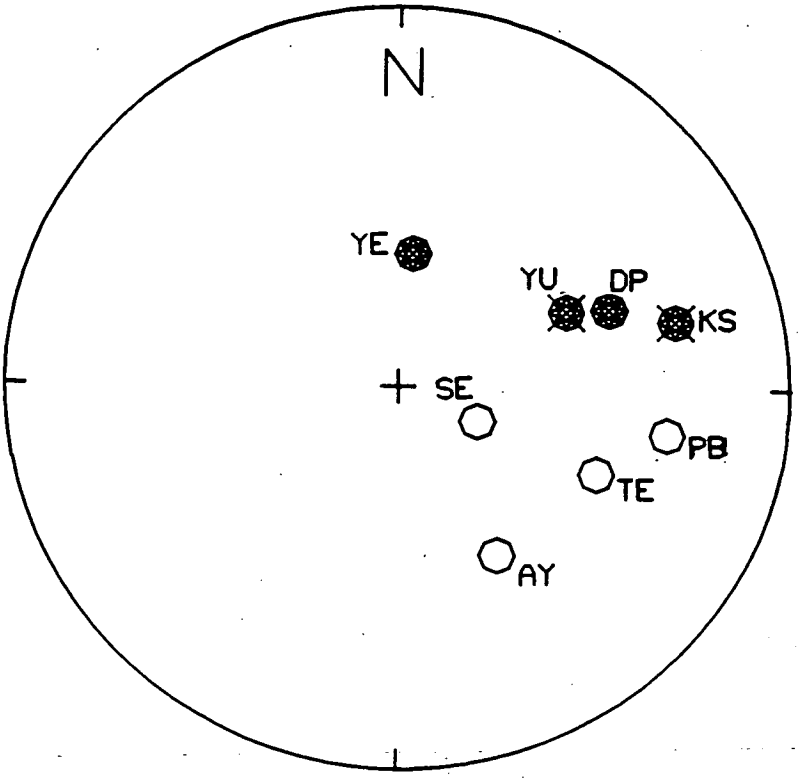

Fig. 5.12 - Equal area upper hemisphere projection of P-wave first motion for Group 2A, centred on the HYP071 location of the master event ($40^{o}39.50'$, $29^{o}53.89'$, 8.32km).

suggest that the solution is more likely to be south dipping although this is by no means certain since nodality is difficult to determine. In figs. 5.13a-d four examples of possible fault plane solutions are given. They show the extent to which the E-W trending nodal plane can be varied (with strikes ranging from N73^{o}E (properly expressed as N253^{o}E since it is north dipping) to N110^{o}E).

These solutions show that the range of fault planes obtained in the previous section and the range of fault plane solutions do overlap. The fault planes that do not fit the fault plane solution are those that dip northwards. These cannot be discounted, however, because of the error in the fault plane solution (due to the error in the absolute location of the master event) combined with the slight error in the relocations. We can, therefore, draw the conclusion that the fault plane derived by relocation is consistent with the fault plane solution (first motion data).

In fig. 5.13a-d two nodal planes are always shown but it is only the E-W trending plane that is well constrained. This means that the rake cannot be defined and comparison with the direction of elongation is not possible.

5.4.4 Group 2A - Spectral Determination of the Source Dimension

In section 5.4.2 a source dimension of approximately 550m by 410m by 290m was established. To see how this compares with the source dimension that can be obtained from spectral techniques (summarised in section 5.3.4), three events from group 2A were selected for spectral analysis (G2A(5), G2A(8) and G2A(15)). Fig. 5.14 contains a selection of the S wave spectra from these events showing the low frequency base level and the corner frequency. Table 5.6 contains the readings of the S wave corner frequency (f_c(S)) made at each station for all three events. To calculate the corner frequency ratio the P wave corner frequency (f_c(P)) was measured for event G2A(8) and these readings are listed in table 5.7.

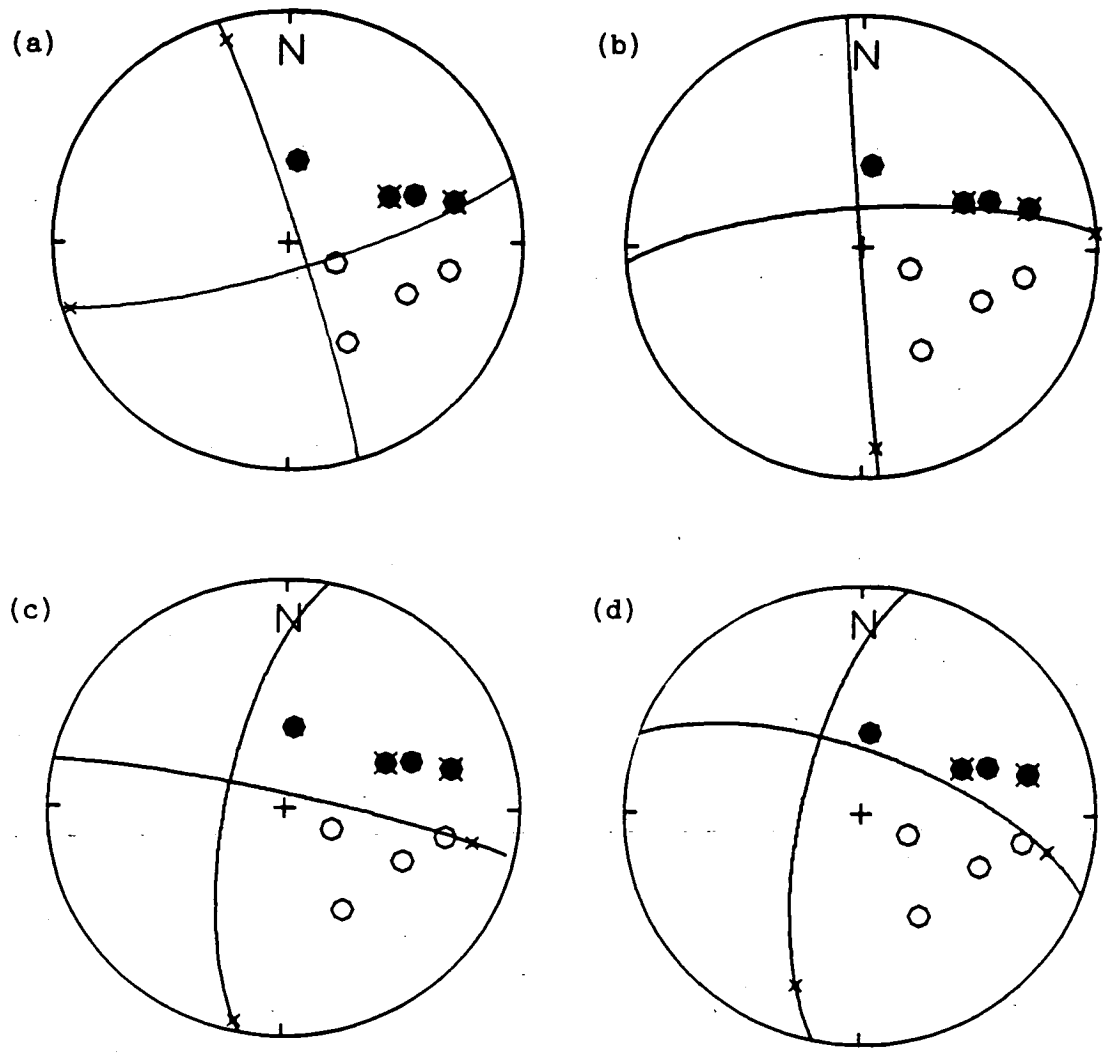

Fig. 5.13 - Possible fault plane solutions to fit the first motion data of fig. 5.12. Only one of the nodal planes is reasonably well constrained (E-W trending plane), the position of the other plane is fairly arbitrary. In (a) strike=253°, dip=80°, rake=4°, (b) strike=86°, dip=76°, rake=1°, (c) strike=102°, dip=85°, rake=-160° and (d) strike=110°, dip=68°, rake=-158°.

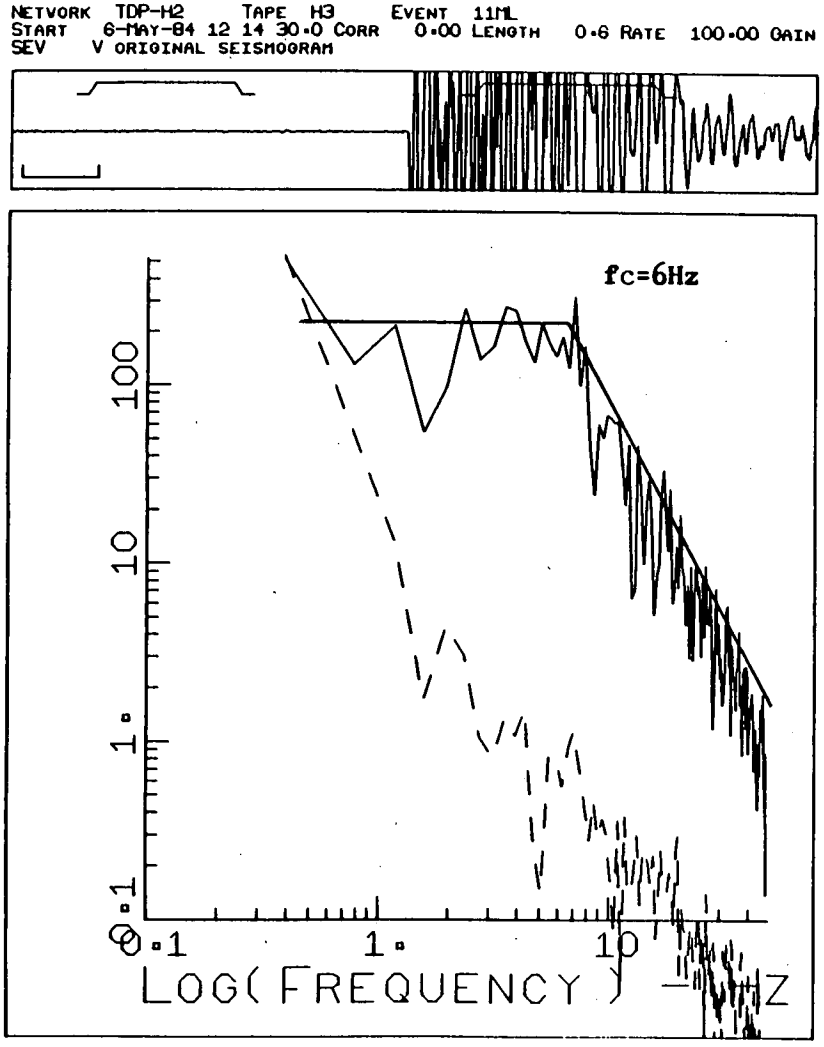

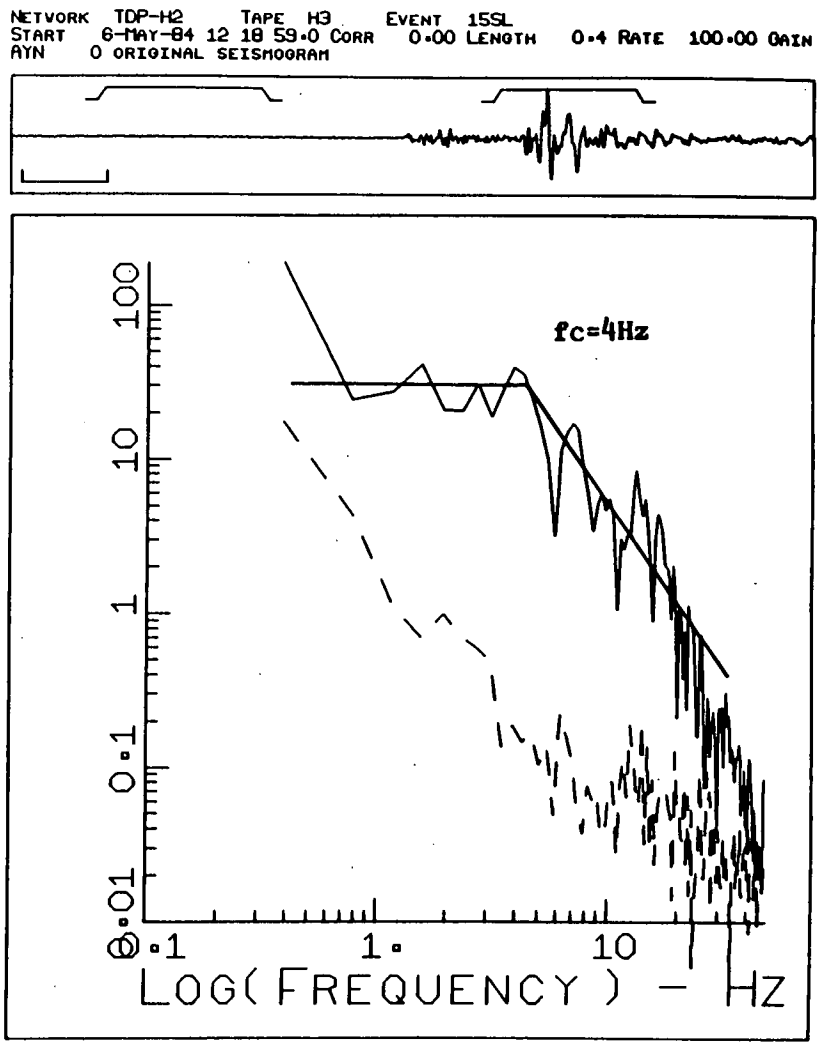

Fig. 5.14a,b - Corner frequency (fc) measurements for two typical S-wave displacement spectra from Group 2A. The noise spectra (dotted) is taken from a window prior to the first arrival.

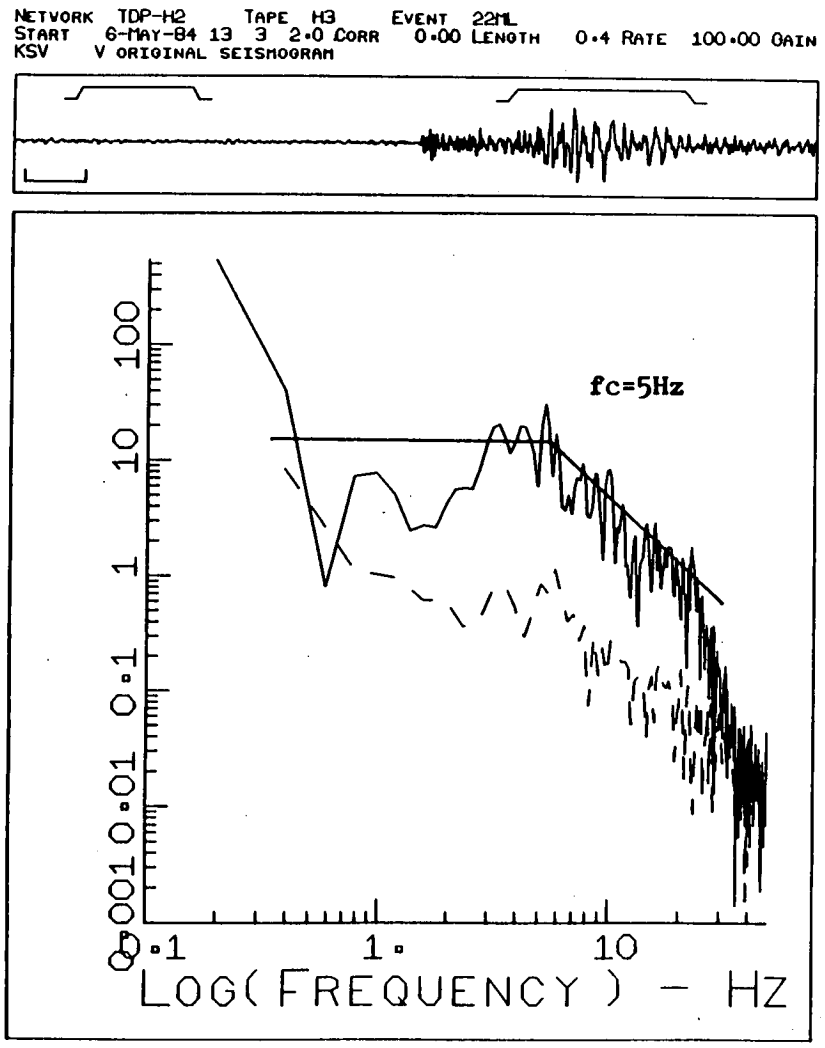

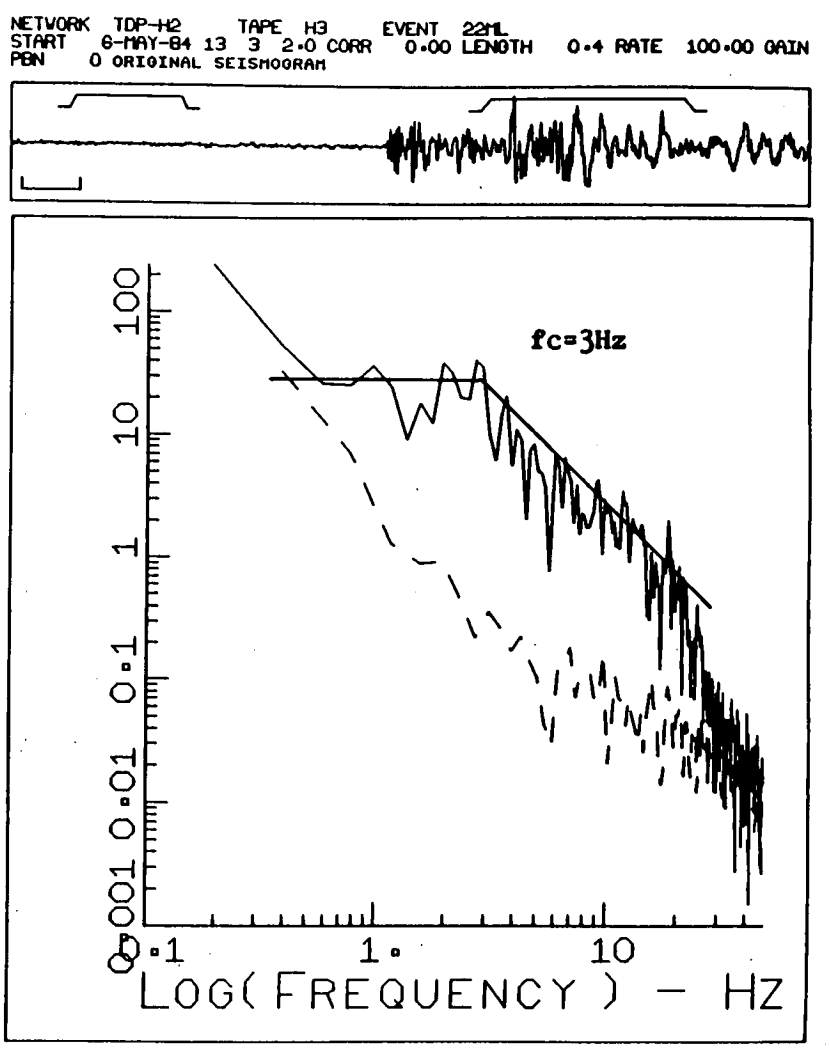

Fig. 5.14c,d - Corner frequency (fc) measurements for two typical S-wave displacement spectra from Group 2A. The noise spectra (dotted) is taken from a window prior to the first arrival.

Event	Station					
	KS	DP	AY	PB	TE	SE
TD4127.M14	4	7	6	3	6	6
TD4127.M18	5	-	4	3	5	6
TD4127.NO3	5	10	5	3	6	7

Table 5.6 - S-wave corner frequency (f_c(S)) as measured at each station for three events from Group 2A. All readings in Hz.

Event	Station					
	KS	DP	AY	PB	TE	SE
TD4127.M18	6	9	8	6	9	13

Table 5.7 - P-wave corner frequency (f_c(P)) as measured at each station for the Group 2A master event. All readings in Hz.

In section 5.3.4 the acceleration spectra for group 1 were examined to check that f_{max} (Hanks, 1982a; Aki, 1987), if it exists, is greater than the corner frequencies being measured. The results appeared to indicate that the spectra were only limited at 32Hz by the instruments, as would be expected, with no evidence of an f_{max} at any station. Hanks (1982a) suggests that where f_{max} exists it is station dependent. On this basis we could, therefore, assume that f_{max} would not have changed between projects since similar networks were being used. However, Aki (1987) is not so sure of the cause of f_{max} although he favours the idea of it being a source effect. For this reason the acceleration spectra for one of the events from group 3 were calculated and the upper frequency limit was measured. As for group 1, the only limit found was the recording system limit of 32Hz which does not affect the corner frequency measurements. It will also be assumed that for the remaining two groups (2B and 3) f_{max}, if it exists, is greater than 32Hz and will, therefore, have no effect.

Overall values for $f_c(S)$ and $f_c(P)$ are obtained by taking the mean and standard deviation from tables 5.6 and 5.7. This gives

$$f_c(S) = 5 \pm 2\text{Hz} \qquad f_c(P) = 9 \pm 2.5\text{Hz}$$

and a corner frequency ratio of

$$R_c = \frac{f_c(P)}{f_c(S)} = \frac{9 \pm 2.5}{5 \pm 2} = 1.80 \pm 0.88$$

The corner frequencies for group 2A are smaller than those for group 1 and as a result their errors are proportionally larger, even though the absolute values are no different. The effect of this on the corner frequency ratio is to give it a proportionally larger error. As for group 1 the corner frequency ratio would imply that the data would best fit the Brune model, but the error is such that it is not really possible to distinguish between the Brune and Madariaga models. Both models are therefore used to calculate the source dimension.

Using the Brune model, velocities of V_p = 6.0km/s and V_s = 3.4km/s and errors in the velocity of 10% we get

$$r = \frac{2.34\ V_p}{2\pi f_c(P)} \qquad \text{or} \qquad r = \frac{2.34\ V_s}{2\pi f_c(S)}$$

$$r = 253 \pm 104\text{m} \qquad r = 248 \pm 73\text{m}$$

Which gives an average of r = 251 ± 89m.

Using the Madariaga model we get

$$r = \frac{2.01\ V_s}{2\pi f_c(P)} \qquad \text{or} \qquad r = \frac{1.32\ V_s}{2\pi f_c(S)}$$

$$r = 143 \pm 59\text{m} \qquad r = 121 \pm 36\text{m}$$

Which gives an average of r = 132 ± 48m.

Since both models assume circular sources these figures are doubled in order to produce a dimension more comparable to the relative location results. Combining the two models gives a range for the spectral source dimension of

$$d = 264 \pm 68\text{m} \quad \text{to} \quad 502 \pm 126\text{m}$$

This range compares very favourably with the dimensions obtained in section 5.4.2 of 550m by 410m by 290m.

5.4.5 Group 2B - Relative Location

The event codes and file names of the 20 events comprising group 2B are listed in table 5.8 along with the HYP071 locations which are also plotted in fig. 5.15. Event G2B(14) was chosen to be the master event since it was well recorded at 6 stations (SE, DP, AY, TE, KS and PB) and the remaining 19 events have been relocated with respect to it. Fig. 5.16 is a plot of the relocated epicentres with two orthogonal cross-sections at velocities of V_p = 6.0km/s and V_s=3.4km/s. The events have been numbered chronologically.

		Location (HYP071)				
Event Code	Filename	Date	Time	Latitude (Deg/min)	Longitude (Deg/min)	Depth (km)
G2B(1)	TD4124.I42	84 503	842 18.40	40-39.36	29-53.86	8.05
G2B(2)	TD4124.P06	84 503	15 6 45.40	40-39.39	29-53.87	8.13
G2B(3)	TD4124.P25	84 503	1525 6.13	40-39.10	29-54.08	8.18
G2B(4)	TD4124.P27	84 503	1527 21.50	40-39.13	29-54.02	8.19
G2B(5)	TD4124.P40	84 503	1540 51.73	40-39.44	29-53.59	7.33
G2B(6)	TD4124.Q25	84 503	1625 27.09	40-39.49	29-53.70	8.25
G2B(7)	TD4124.W32	84 503	2232 53.84	40-39.28	29-54.15	8.22
G2B(8)	TD4125.A59	84 504	059 24.71	40-39.43	29-54.18	8.19
G2B(9)	TD4125.V29	84 504	2129 28.68	40-39.49	29-53.79	7.87
G2B(10)	TD4126.A35	84 505	035 33.08	40-39.50	29-54.10	6.76
G2B(11)	TD4126.K55	84 505	1055 48.26	40-39.44	29-53.80	8.12
G2B(12)	TD4126.L03	84 505	11 3 55.17	40-39.35	29-54.20	8.40
G2B(13)	TD4126.W04	84 505	22 4 19.11	40-39.49	29-53.72	7.89
G2B(14)	TD4126.X22	84 505	2322 29.96	40-39.57	29-53.71	8.09
G2B(15)	TD4127.D33	84 506	333 53.44	40-39.50	29-54.28	8.48
G2B(16)	TD4127.D50	84 506	350 51.42	40-39.36	29-54.52	8.53
G2B(17)	TD4127.H25	84 506	725 32.06	40-39.46	29-54.41	7.83
G2B(18)	TD4127.J25	84 506	925 57.39	40-39.54	29-53.88	8.42
G2B(19)	TD4127.V34	84 506	2154 38.60	40-39.42	29-53.81	7.81
G2B(20)	TD4128.H45	84 507	745 10.02	40-39.27	29-54.37	8.54

Table 5.8 - Group 2B. Event codes, filenames (GSRG standard files) and HYP071 locations (origin time and hypocentre).

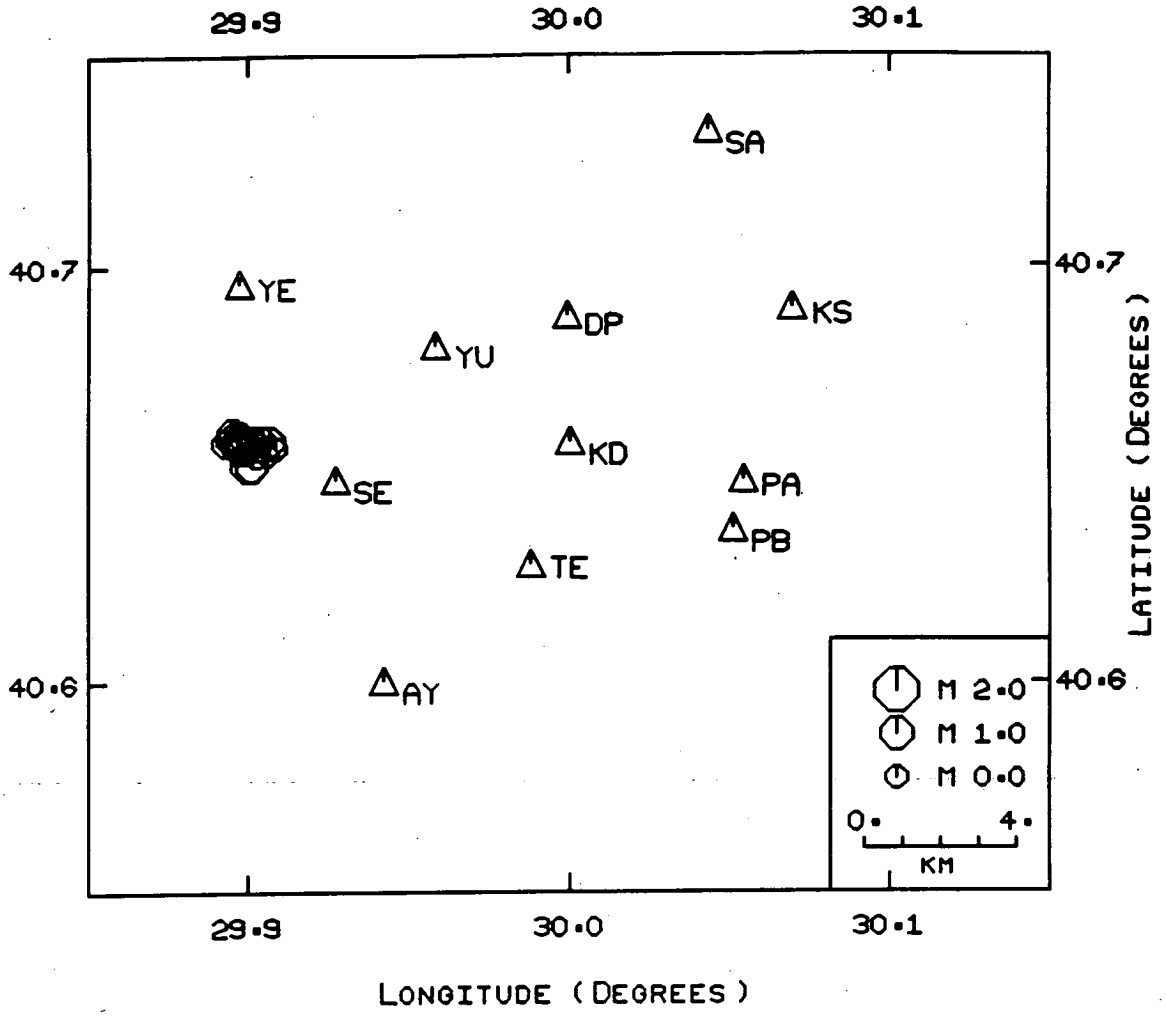

Fig. 5.15 - Epicentral plot of the Group 2B HYP071 locations (listed in table 5.8).

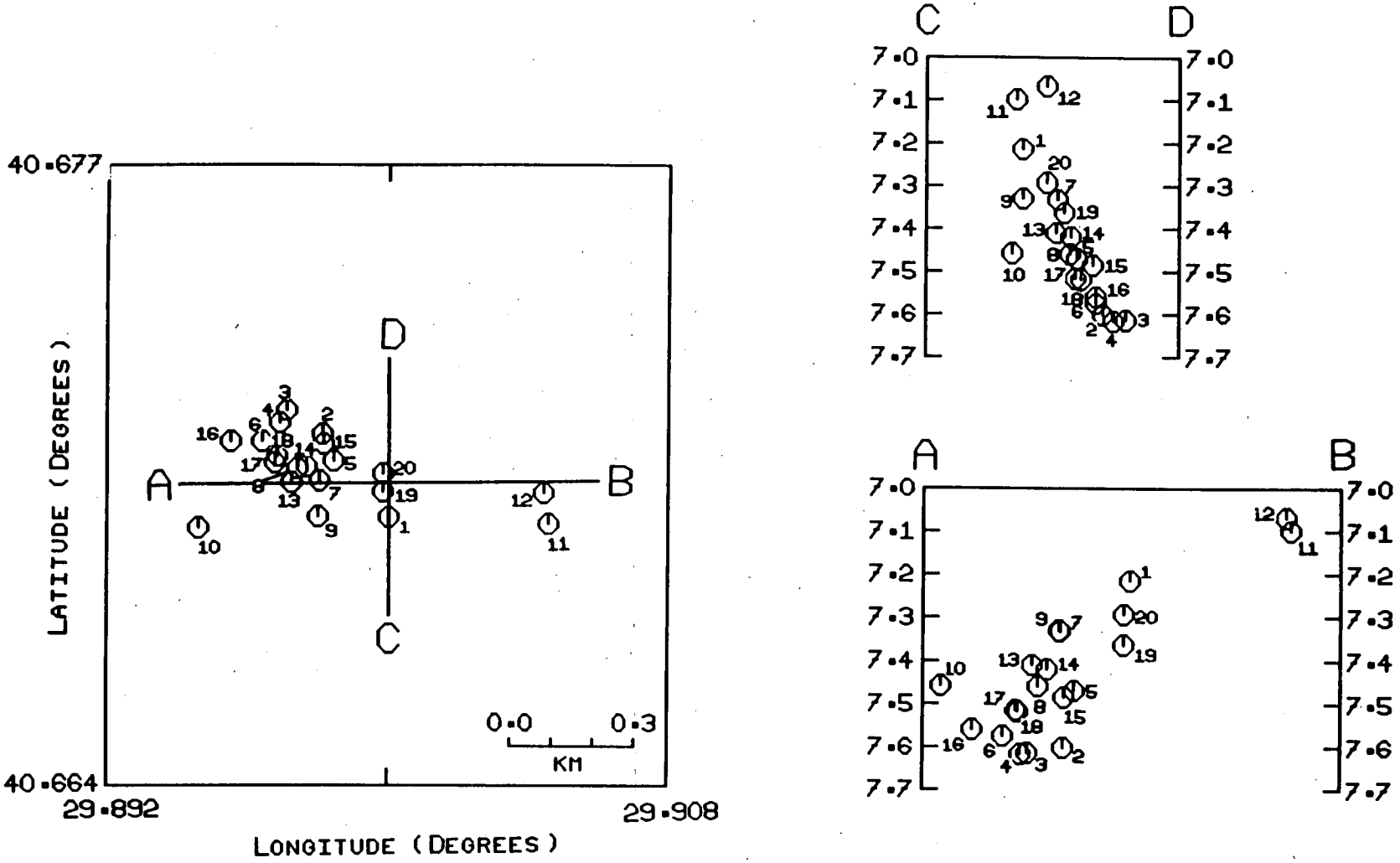

Fig. 5.16 - Epicentral plot and two orthogonal cross-sections of the events in Group 2B relocated at a velocity of Vp = 6.0km/s and Vs = 3.4km/s.

From the epicentral plot there appears to be a slight alignment of the events in an E-W direction. Section A-B is taken in this preferred direction with section C-D at right angles to it. Although there is a slight alignment of the events in section A-B (at an angle of approximately 34^{o} to the strike) by far the stronger alignment is in section C-D where a plane is clearly defined dipping at an angle of 69^{o} to the north. The strike of this plane is given as N270^{o}E since it is north dipping. The alignment seen in section A-B can again be interpreted as an elongation in the area of weaknesss on the fault.

The ratio of the largest to the smallest amplitude at any one station is about 10 which, like groups 1 and 2A, is consistent with the barrier-type model. The temporal distribution does not really show any clear pattern. Several of the events are clustered in small groups of 2 or 3 but this does not provide any real evidence of weaker barriers within the group. The majority of the events are clustered together in one large group but there are two smaller groups separated from it (G2B(1), G2B(19), G2B(20) and G2B(11), G2B(12)) and these may be separated by unbroken weaker barriers. There is no obvious difference in waveform between any members of group 2B.

The extreme dimensions of the group at a velocity of V_p = 6.0km/s and V_s = 3.4km/s are 820m by 584m by 160m. The direction of elongation quoted from section A-B must be corrected for the dip of the plane. Using equation 5.1 in section 5.3.2 with a = 69^{o} and c = 34^{o} we get the direction of elongation as 36^{o} to the strike.

5.4.6 Group 2B - Fault Plane Solution

In the previous section the relocation method found a fault plane that strikes N270^{o}E and dips 69^{o} north. The plot of the first motion data for this group is displayed in fig. 5.17. Readings were possible at six stations although those at AY and KS are not very reliable. Two of the stations show some degree of nodality (TE and KS).

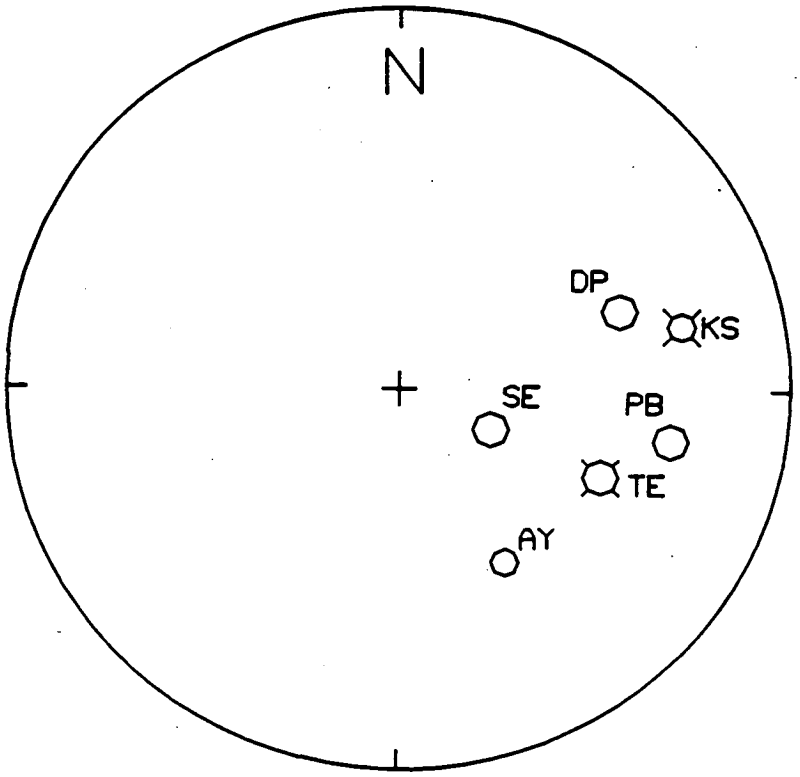

Fig. 5.17 - Equal area upper hemisphere projection of P-wave first motion for Group 2B, centred on the HYP071 location of the master event ($40^{o}39.57'$, $29^{o}53.71'$, 8.09km).

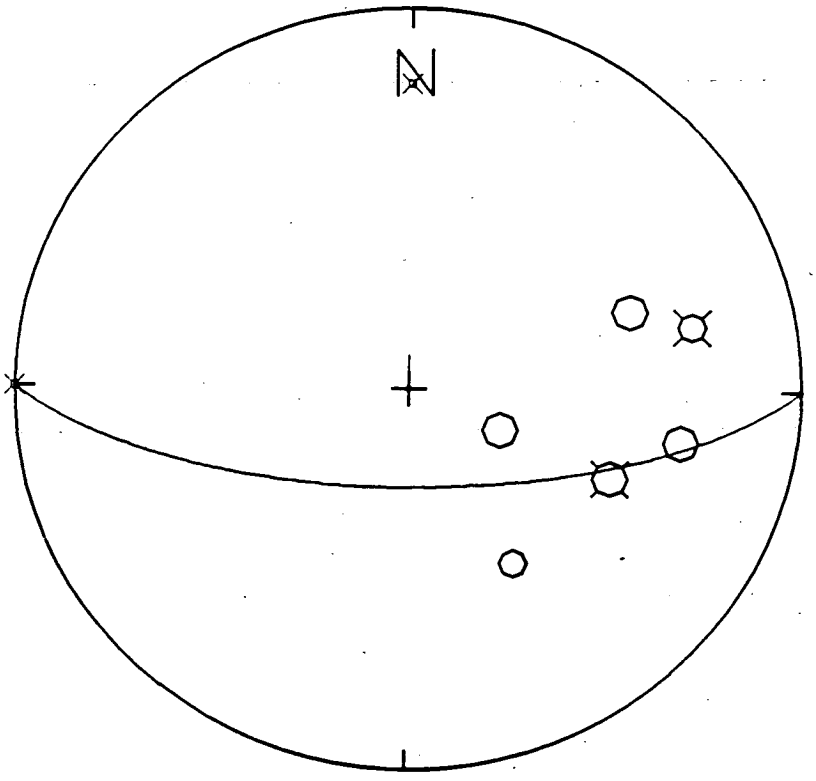

Fig. 5.18 - The relocated fault plane of section 5.4.5 superimposed upon the first motion data of fig. 5.17 (strike=270^{o}, dip=69^{o}).

Unfortunately, the determination of the fault plane solution from fig. 5.17 is almost impossible. All six stations have a dilational first motion which means that there is no constraint on either of the nodal planes. In addition, the nodal stations, which can often be used to help constrain the solution, were of little use. One of the nodal planes could pass close to station KS but it would not be very well constrained and station TE is surrounded by stations that are not nodal which does not make much sense.

Despite these problems a check can still be carried out to see if there is any consistency between the fault plane found in the previous section and the first motion data. In fig. 5.18 the fault plane (strike N270^{o}E, dip 69^{o}) is superimposed upon the first motion plot of fig. 5.17. As the data stands they are not consistent. However, if station AY is ignored then the fault plane is very close to agreeing with the first motion data. The dip of the fault plane only needs to be lessened by a few degrees, a difference that could be accounted for by the error in the absolute location of the master event that determines the position of the stations. Further more, the nodal station TE now sits in a much more sensible position.

To conclude, it would appear that the fault plane determined by the relative location method and the first motion data are consistent if the reading at station AY is removed. This is not an unreasonable step bearing in mind that the reading is unreliable as stated at the beginning of the section. Unfortunately no fault plane solution could be obtained from the first motion data which means that the rake cannot be measured and compared to the direction of elongation as measured in the previous section.

5.4.7 Group 2B - Spectral Determination of the Source Dimension

In section 5.4.5 a source dimension of approximately 820m by 584m by 160m was established. To see how this compares with the source dimension obtained using the corner frequency, three events from group 2B were selected for spectral analysis (G2B(2), G2B(13) and G2B(14)). Fig. 5.19 contains a selection of the S wave spectra from these events showing the low frequency base level and the

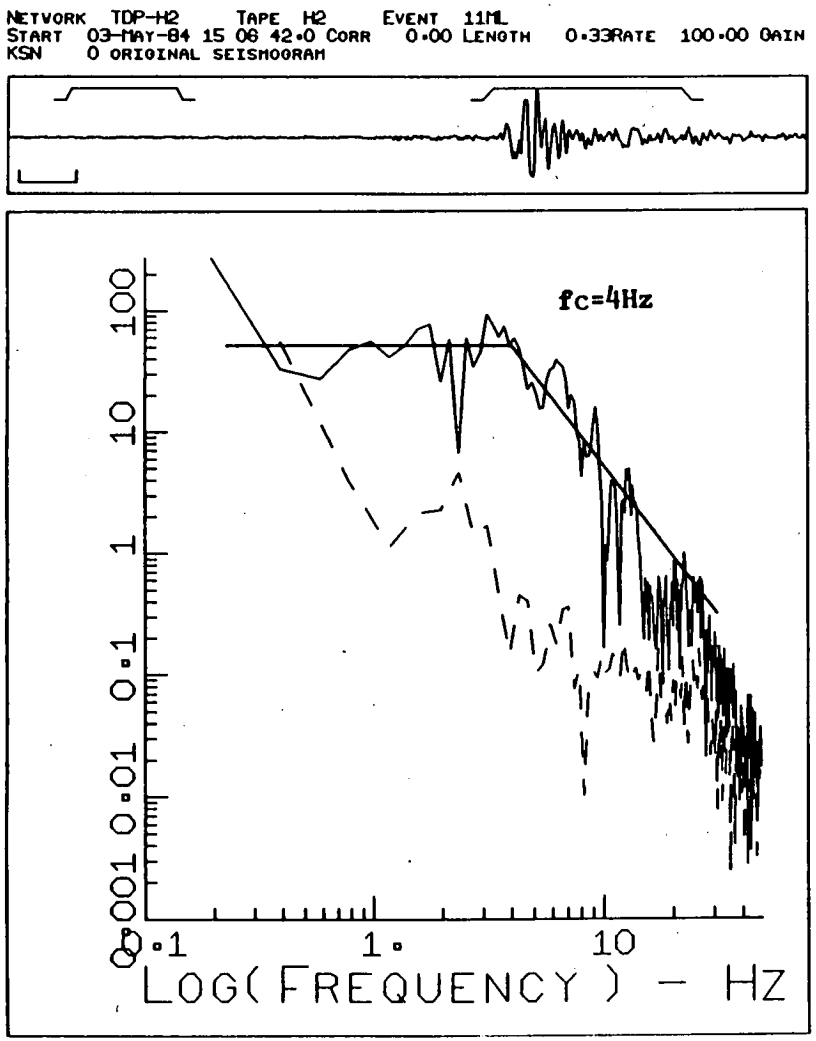

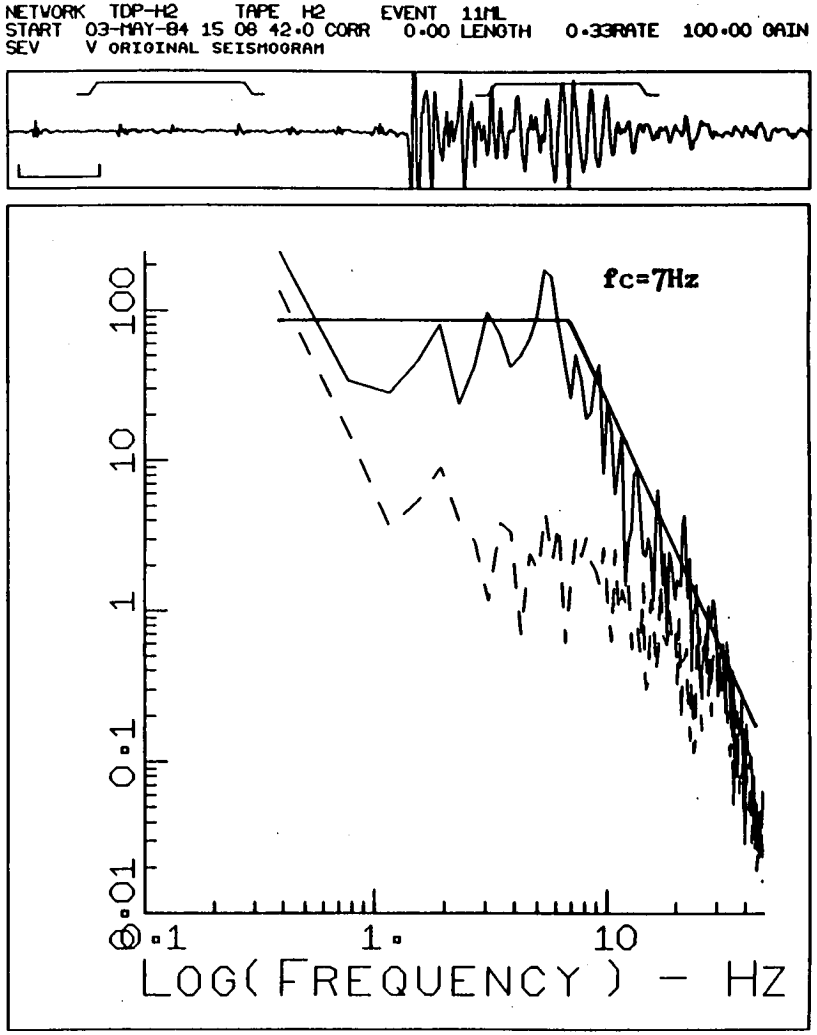

Fig. 5.19a,b - Corner frequency (fc) measurements for two typical S-wave displacement spectra from Group 2B. The noise spectra (dotted) is taken from a window prior to the first arrival.

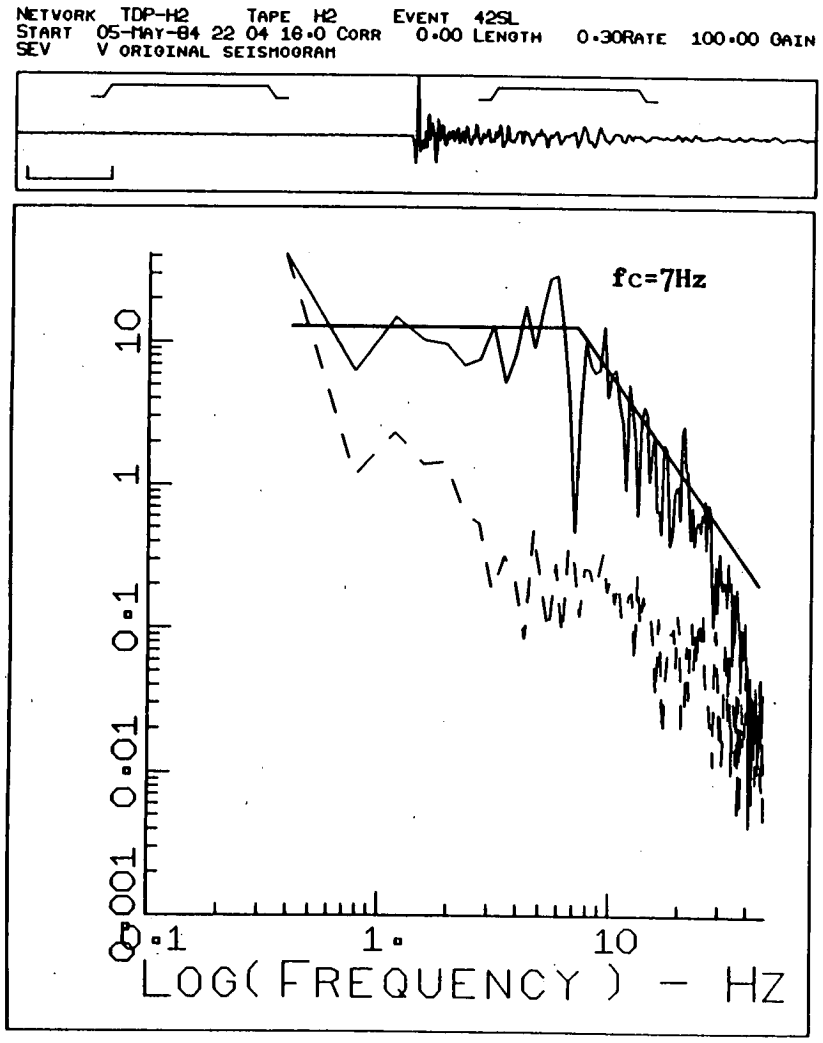

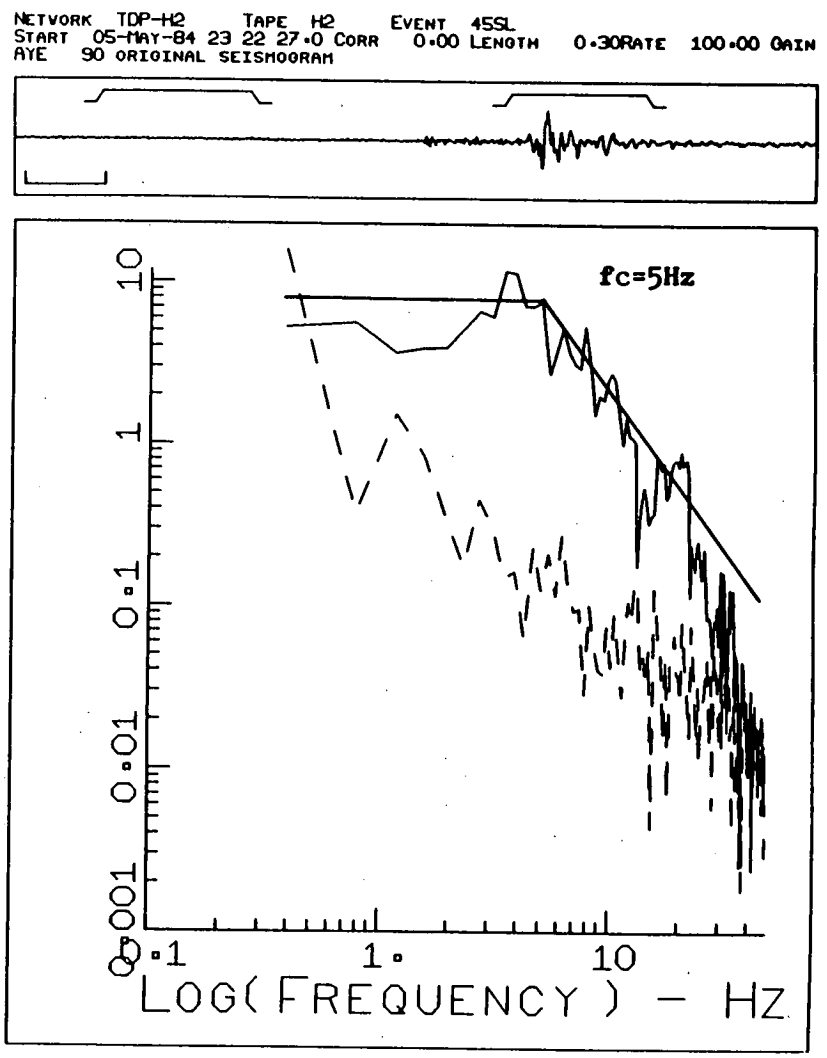

Fig. 5.19c,d - Corner frequency (fc) measurements for two typical S-wave displacement spectra from Group 2B. The noise spectra (dotted) is taken from a window prior to the first arrival.

corner frequency. Table 5.9 contains the readings of the S wave corner frequency ($f_c(S)$) made at each station for all three events. To calculate the corner frequency ratio the P wave corner frequency ($f_c(P)$) was measured for event G2B(14) and these readings are listed in table 5.10.

Overall values for $f_c(S)$ and $f_c(P)$ were obtained by taking the mean and standard deviation from tables 5.9 and 5.10. This gives

$$f_c(S) = 5 \pm 1.5 \text{ Hz} \qquad f_c(P) = 9 \pm 1.5 \text{ Hz}$$

and a corner frequency ratio of

$$R_c = \frac{f_c(P)}{f_c(S)} = \frac{9 \pm 1.5}{5 \pm 1.5} = 1.80 \pm 0.62$$

As for groups 1 and 2A the corner frequency ratio implies that the data would best fit the Brune model, but the error is such that it is not really possible to distinguish between the Brune and Madariaga models. Again both models are used to calculate the source dimension.

Using the Brune model, velocities of V_p = 6.0km/s and V_s = 3.4km/s and errors in the velocity of 10% we get

$$r = \frac{2.34\, V_p}{2\pi f_c(P)} \quad \text{or} \quad r = \frac{2.34\, V_s}{2\pi f_c(S)}$$

$$r = 253 \pm 80\text{m} \qquad r = 248 \pm 48\text{m}$$

Which gives an average of r = 251 ± 64m.

Using the Madariaga model gives

$$r = \frac{2.01\, V_s}{2\pi f_c(P)} \quad \text{or} \quad r = \frac{1.32\, V_s}{2\pi f_c(S)}$$

$$r = 143 \pm 45\text{m} \qquad r = 121 \pm 35\text{m}$$

Which gives an average of r = 132 ± 40m.

Event	Station					
	KS	DP	AY	PB	TE	SE
TD4124.P06	4	6	5	4	6	6
TD4126.W04	5	5	5	3	6	7
TD4126.X22	5	8	5	3	-	6

Table 5.9 - S-wave corner frequency (f_c(S)) as measured at each station for three events from Group 2B. All readings in Hz.

Event	Station					
	KS	DP	AY	PB	TE	SE
TD4126.X22	-	11	9	8	9	7

Table 5.10 - P-wave corner frequency (f_c(P)) as measured at each station for the Group 2B master event. All readings in Hz.

Since both models assume circular sources these radii are doubled in order to produce a dimension more comparable to the relocation results. Combining the two models gives a range for the spectral source dimension of

$$d = 264 \pm 57m \quad \text{to} \quad 502 \pm 91m$$

This range compares favourably with the dimensions obtained in section 5.4.5 of 820m by 584m by 160m.

5.4.8 Comparison of Groups 2A and 2B

Examination of the TDP-3 data set revealed the existence of a large group of apparently similar earthquakes on the edge of the network (group 2). Closer analysis showed that the 46 events of group 2 could be split into two smaller groups of 26 and 20 events (groups 2A and 2B respectively).

The relocation of group 2A revealed a fault plane striking N102^{o}E and dipping at approximately 90^{o}. The first motion fault plane solution was found to be consistent with this but suggested that the plane might be dipping slightly to the south. The dimensions obtained for the fault plane were in good agreement with the spectral source dimension. For group 2B a fault plane striking N270^{o}E and dipping 69^{o} north was found by the relative location method. From the first motion data a fault plane solution could not be obtained. However, with the elimination of one reading the fault plane was found to be consistent with the first motion plot. As for group 2A the dimensions of the fault plane were in good agreement with the spectral source dimension.

In fig. 5.20 the two master events, as recorded at two of the stations, are displayed for comparison. The similarity between the events is most striking in the S phase where the wavelengths are longer. The P phase and its coda are generally dissimilar. As mentioned in section 2.4.3, Geller and Mueller (1980) found that as the separation between two events increases the similarity between them is only retained at lower and lower frequencies. This would

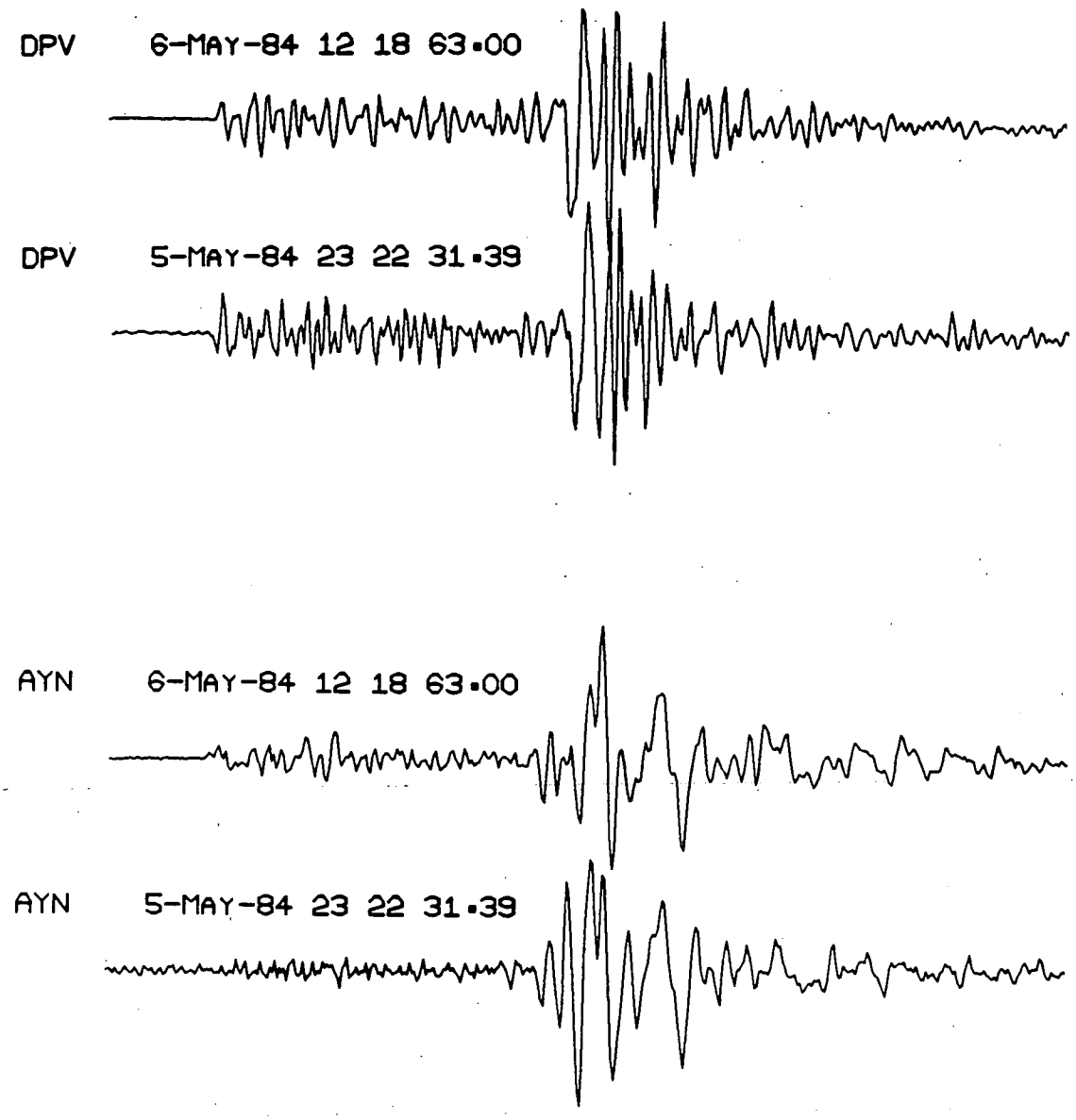

Fig. 5.20 - Comparison of the master events from Groups 2A and 2B as recorded at two of the stations (DP and AY).

suggest that groups 2A and 2B are in someway related but that they are not very close to each other.

So we appear to have two groups of earthquakes that are somehow related but that originate from two fault planes with markedly different dips, albeit similar strikes. To try and get some idea of how these fault planes are connected the two master events have been relocated with respect to each other. The error in this relative location is slightly greater than for the relocations within a group because there is only a small amount of similarity in the P phase resulting in a less well defined cross-correlation peak. In fig. 5.21 the relative locations of the two master events are shown and by superimposing each group on to its own master event fig. 5.22 is produced. The two groups do not overlap and are separated by approximately 300m.

In fig. 5.22 one cross-section has been taken along the strike and is plotted out twice. They show two possible interpretations of how the fault planes are related with dotted lines indicating where the fault planes might be. In cross-section (a) the planes are those described at the beginning of the section and it would appear that the fault planes are antithetic. This type of structure is often found in grabens or half-grabens where there has been a major slippage of one block of crust relative to another.

However, in section 5.4.2 it was not clear whether the fault plane dipped to the south (as in cross-section (a)) or to the north, although the fault plane solution favoured the south dipping plane. In cross-section (b) an alternative interpretation is shown with the two planes running parallel. A structure such as this is not consistent with the fault plane solutions but because of the high degree of uncertainty in fault plane solution analysis it should not be totally discounted.

In both (a) and (b) the two fault planes are connected by a block of crust approximately 300m across. It is the mutual effect of this block that produces the similarity between the groups but only at longer wavelengths because of the relatively large size of

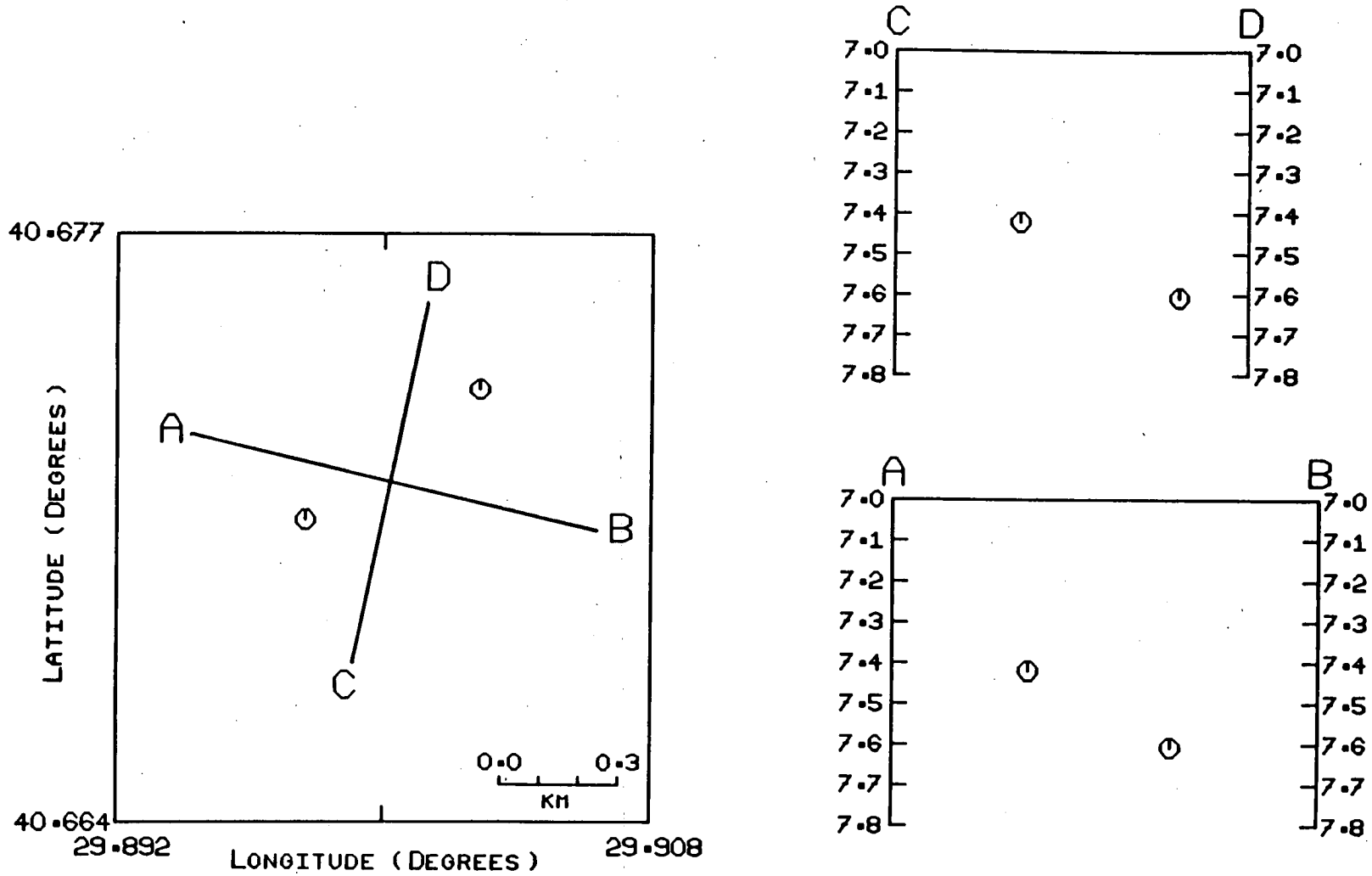

Fig. 5.21 - Epicentral plot and two cross-sections of the relative positions of the master events for Groups 2A and 2B as located using the relative relocation method.

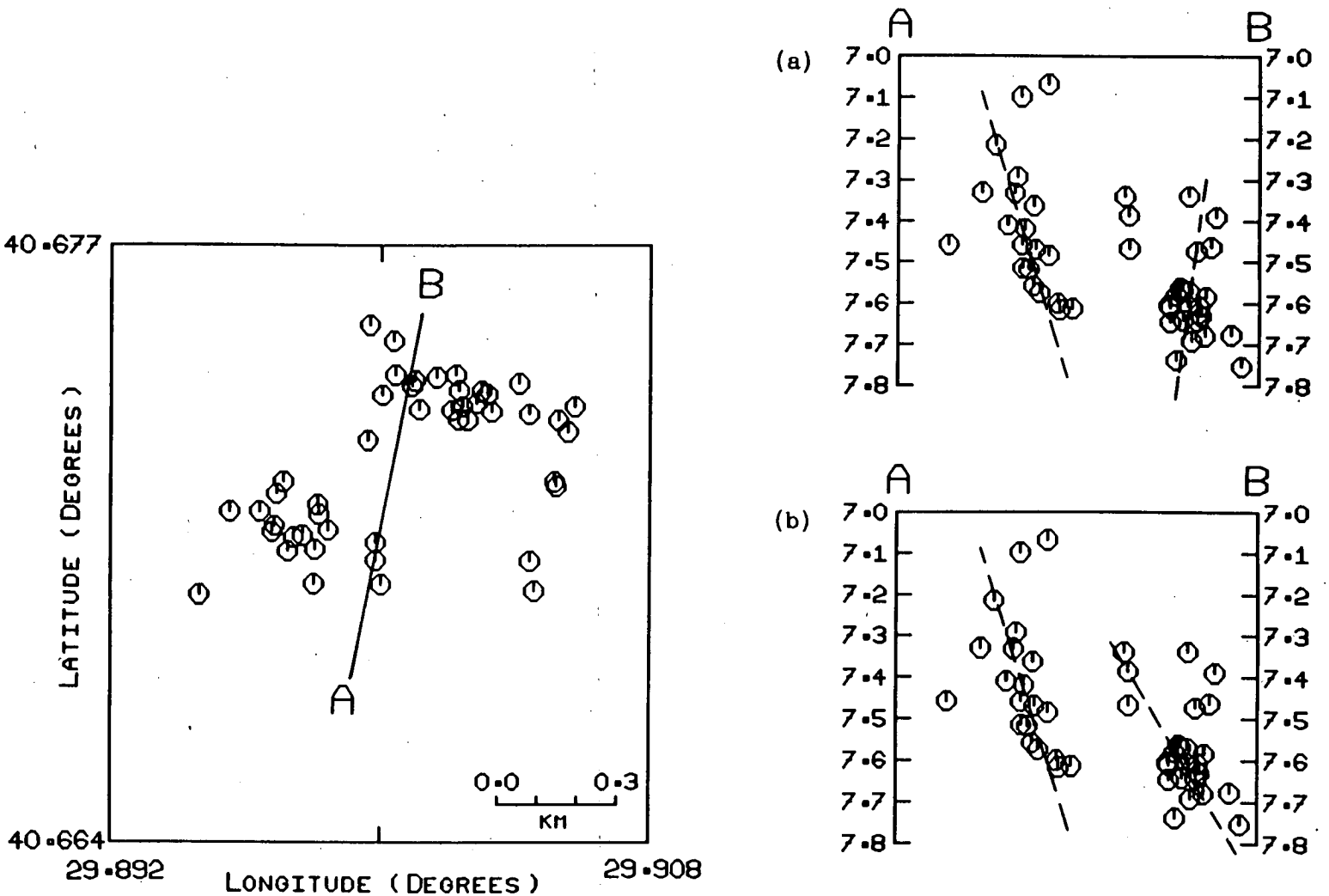

Fig. 5.22 - Epicentral plot and one cross-section repeated twice (showing two possible interpretations) of Groups 2A and 2B superimposed upon the relative positions of their master events as shown in fig. 5.21.

the block.

5.5 Group Three

5.5.1 Introduction

As for group 2 the third and final group was taken from the TDP-3 data set. In the introduction to group 2 (section 5.4.1) it was noted that the epicentral plot of all local events (fig. 5.9) shows the existence of several clusters, many of which are clustered in time as well as in space. Of these clusters two were selected for analysis and are circled in fig. 5.9. From cluster A the 46 events of group 2 were extracted and in this section a third group of similar earthquakes taken from cluster B will be analysed (group 3). Cluster B is situated approximately 2kms NNW of station KD (coordinates $40^{o}39'$N, $29^{o}59'$E) and it has the advantage of lying in a fairly central position within the network. However, despite careful examination of the waveforms in cluster B only 9 events, occurring over a period of 3 days, were found to be similar.

5.5.2 Group 3 - Relative Location

The event codes and filenames of the 9 events comprising group 3 are listed in table 5.11 along with the HYPO71 locations which are also plotted in fig. 5.23. Event G3(9) was chosen to be the master event since it was well recorded on all the components of all 8 stations in operation at the time (SA, KS, DP, AY, PB, TE, SE and YU). The remaining 8 events have been relocated with respect to the master event at velocities of V_p = 6.0km/s and V_s = 3.4km/s. In fig. 5.24 the epicentres have been plotted out and the events numbered chronologically.

From the epicentral plot it would appear that the events are aligned in a roughly E-W direction, although it should be noted that the scale is very small and the relocation errors of approximately 10m are therefore relatively large. The precise direction of the strike is not clear and so cross-sections (parallel and orthogonal to strike) were taken for various strikes around the E-W direction.

		Location (HYP071)					
Event Code	Filename	Date	Time	Latitude (Deg/min)	Longitude (Deg/min)	Depth (km)
G3(1)	TD4150.V32	84 529	2132 41.26	40-40.78	29-58.72	10.38
G3(2)	TD4150.W14	84 529	2214 57.97	40-40.89	29-58.11	10.43
G3(3)	TD4151.F17	84 530	517 49.28	40-40.86	29-58.65	10.22
G3(4)	TD4151.I02	84 530	8 2 8.72	40-40.80	29-58.77	10.31
G3(5)	TD4151.K20	84 530	1020 50.93	40-40.71	29-58.75	10.49
G3(6)	TD4151.K34	84 530	1035 0.23	40-40.73	29-58.74	10.46
G3(7)	TD4151.N10	84 530	1310 14.36	40-40.74	29-58.71	10.50
G3(8)	TD4152.C28	84 531	228 52.81	40-40.85	29-58.53	10.50
G3(9)	TD4153.T37	84 601	1937 20.73	40-40.84	29-58.79	10.48

Table 5.11 - Group 3. Event codes, filenames (GSRG standard files) and HYP071 locations (origin time and hypocentre).

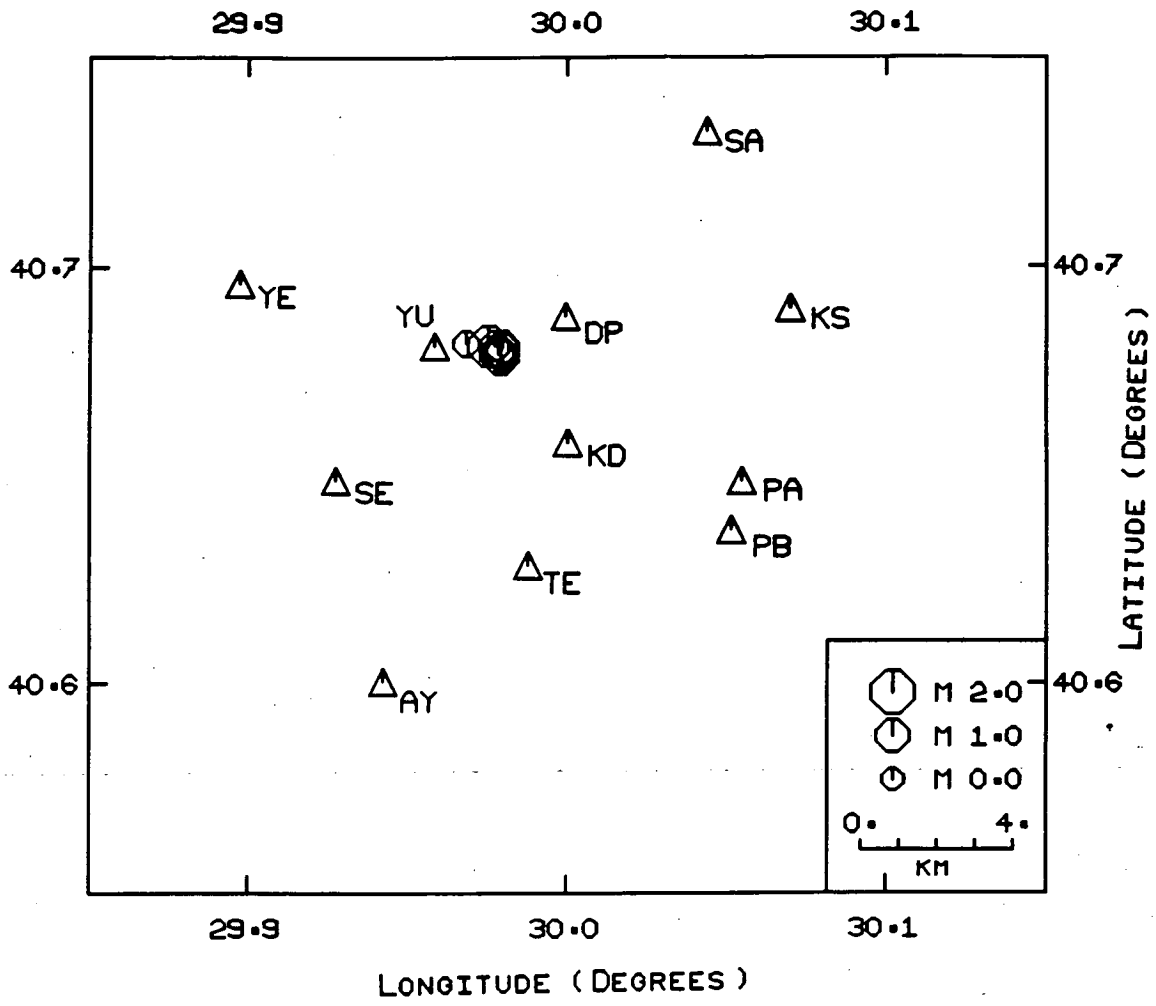

Fig. 5.23 - Epicentral plot of the Group 3 HYP071 locations (listed in table 5.11).

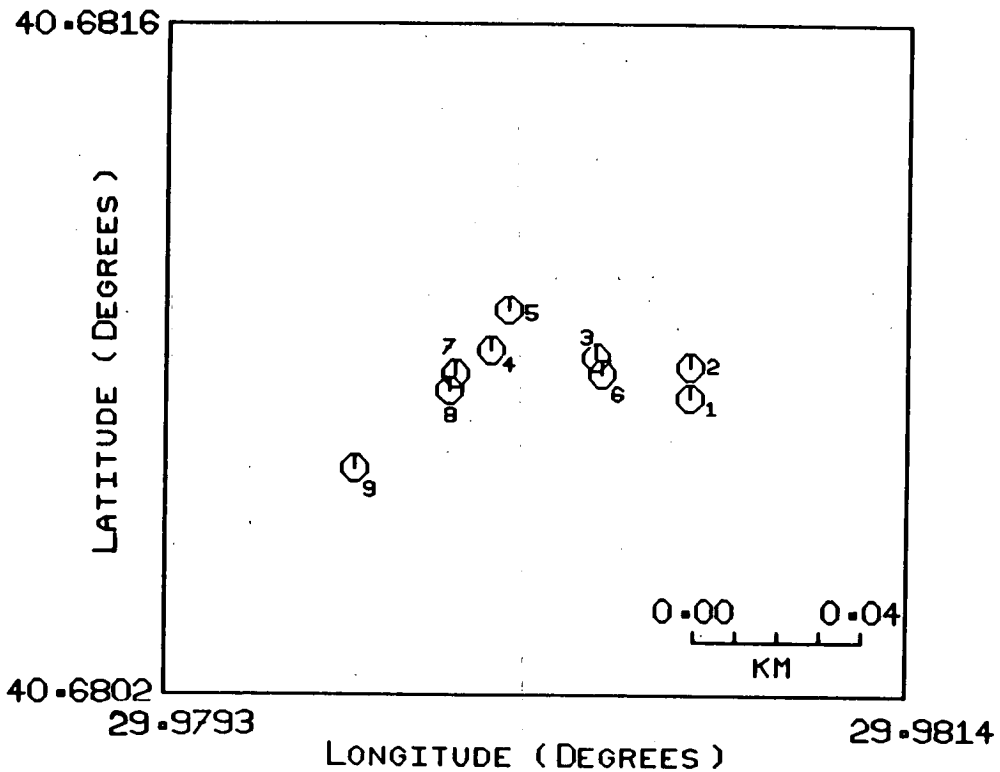

Fig. 5.24 - Epicentral plot of the Group 3 events relocated at a velocity of V_p=6.0km/s and V_s=3.4km/s.

As the orthogonal cross-section was rotated a planar structure was revealed. In fig. 5.25 the epicentral plot and cross-sections are shown for the orientation where the plane was best defined. This gives a strike N75°E with the plane dipping 81° south. The distribution of the events in the cross-section parallel to strike (A-B) outlines the direction of elongation of the area of weakness on the fault.

The ratio of the largest to the smallest amplitude at any one station is about 10 suggesting that the group could be modelled by a barrier-type model. The temporal distribution of the events does show a general westward migration but the error in the locations is such that any finer detail in the plots cannot be reliably interpreted.

The extreme dimensions of the group at velocities V_p = 6.0km/s and V_s = 3.4km/s are 84m by 53m by 33m. The direction of elongation measured in cross-section A-B must be corrected for the dip of the plane. Using equation 5.1 in section 5.3.2 with a = 81° and c = 31° we get the direction of elongation as 32° to the strike.

5.5.3 Group 3 - Fault Plane Solution

Using the relative location method a fault plane has been found that strikes N75°E and dips 81° to the south. To see if the fault plane solution is consistent with this plane the first motion data has been plotted in fig. 5.26. All 8 readings, taken from the group as a whole, are good. Section 5.3.3 outlines the method used for obtaining strike and dip from such a diagram.

Even though there is a good azimuthal distribution of the stations in fig. 5.26 the complete fault plane solution will be very dependent upon the one nodal reading at station AY and therefore will not be considered to be very well constrained. One of the nodal planes will separate the compressional reading (SA) from the dilational readings elsewhere and run in a roughly E-W direction dipping slightly to the south. The second nodal plane will run close to station AY and will hence give the first nodal plane a

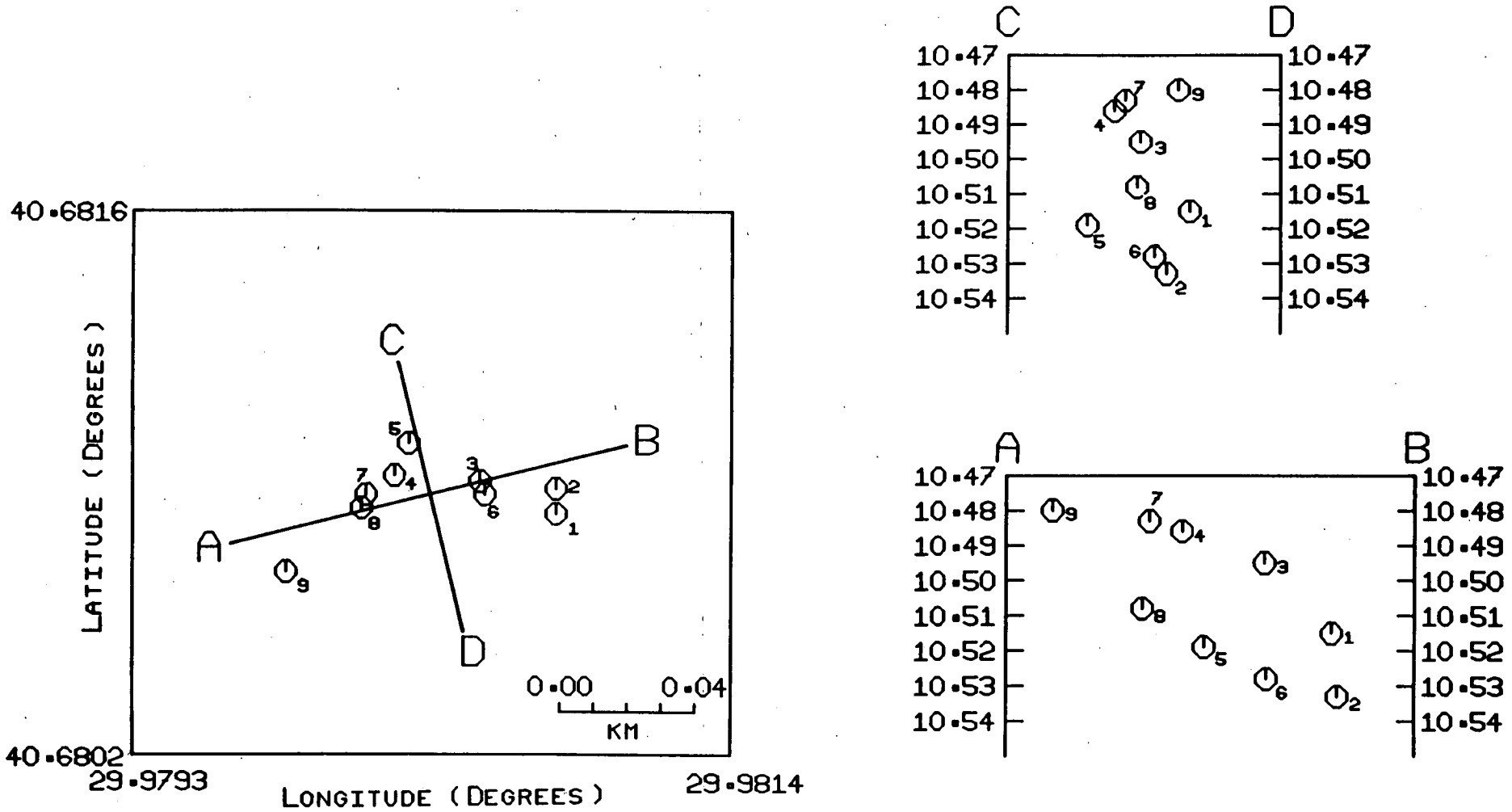

Fig. 5.25 - Epicentral plot and two orthogonal cross-sections of the events in Group 3 relocated at a velocity of Vp = 6.0km/s and Vs = 3.4km/s.

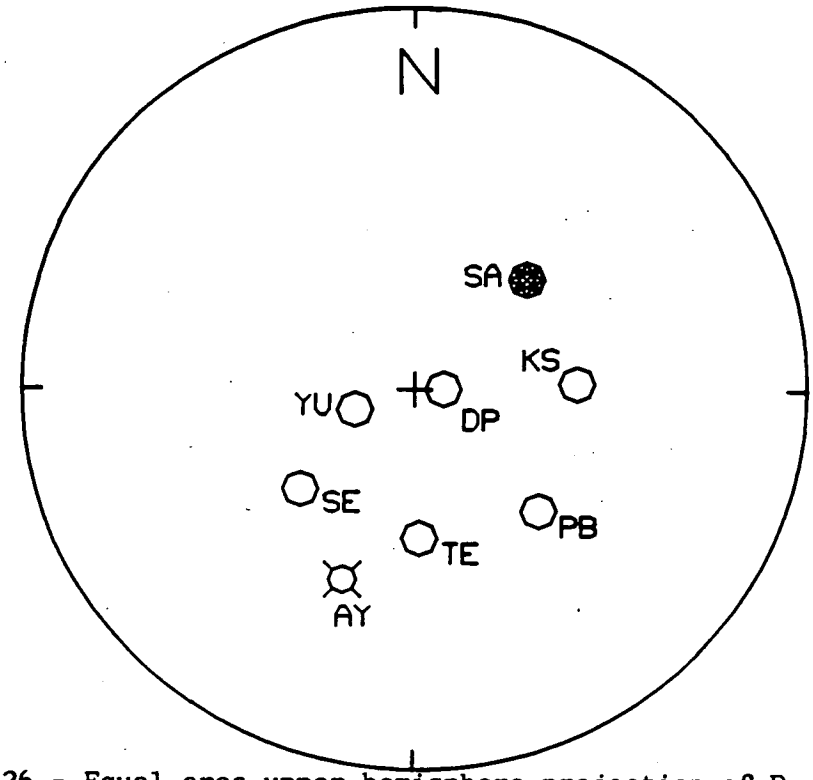

Fig. 5.26 - Equal area upper hemisphere projection of P-wave first motion for Group 3, centred on the HYP071 location of the master event ($40^{o}40.84'$, $29^{o}58.79'$, 10.48km).

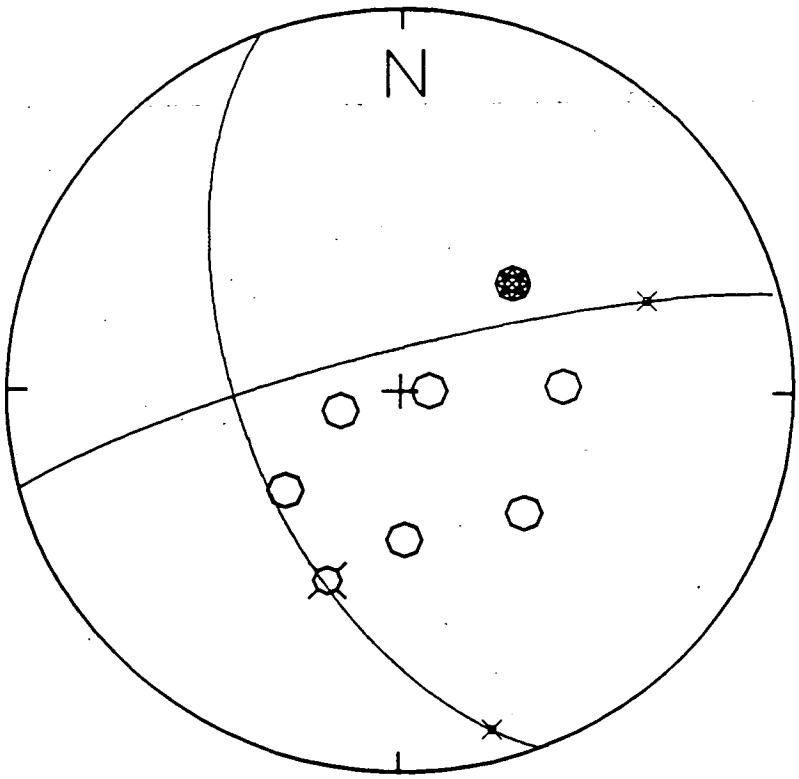

Fig. 5.27 - A fault plane solution using the fault plane found in section 5.5.3 (strike=75^{o}, dip=81^{o} and rake=-146^{o}).

slight ENE tilt. As usual there is no way of saying which of these nodal planes is the fault plane but since the one trending E-W is consistent with the plane revealed in the previous section it would seem reasonable to interpret it as the fault plane. Fig. 5.27 displays a fault plane solution with a plane striking N75^{o}E and dipping 81^{o} to the south.

In the previous section the area of weakness on the fault was found to be elongated at an angle of 32^{o} to the strike. In fig. 5.27 the rake of the assumed fault plane is -146^{o}, a difference of 66^{o}. It therefore seems unlikely that the direction of elongation is dependant upon the direction of slip.

5.5.4 Group 3 - Spectral Determination of the Source Dimension

In section 5.5.2 a source dimension of approximately 84m by 53m by 33m was established. To see how this compares with the source dimension that can be obtained from spectral techniques (summarised in section 5.3.3) three events from group 3 were selected for spectral analysis (G3(1), G3(7) and G3(9)). Fig. 5.28 contains a selection of the S wave spectra from these events. Table 5.12 contains the readings of the S wave corner frequency (f_c(S)) made at each station for all three events. To calculate the corner frequency ratio the P wave corner frequency (f_c(P)) was measured for event G3(9). However, on several of the components the corner frequency was difficult to measure because it was so high. The readings are generally in the low to mid twenties which on a log scale is quite close to the high frequency limit of 32Hz. For those stations where readings were possible the values were very consistent and they are listed in table 5.13.

By taking the mean and standard deviation from tables 5.12 and 5.13 overall values for f_c(S) and f_c(P) were obtained

$$f_c(S) = 16.5 \pm 2.0\text{Hz} \qquad f_c(P) = 24.5 \pm 1.5\text{Hz}$$

This gives a corner frequency ratio of

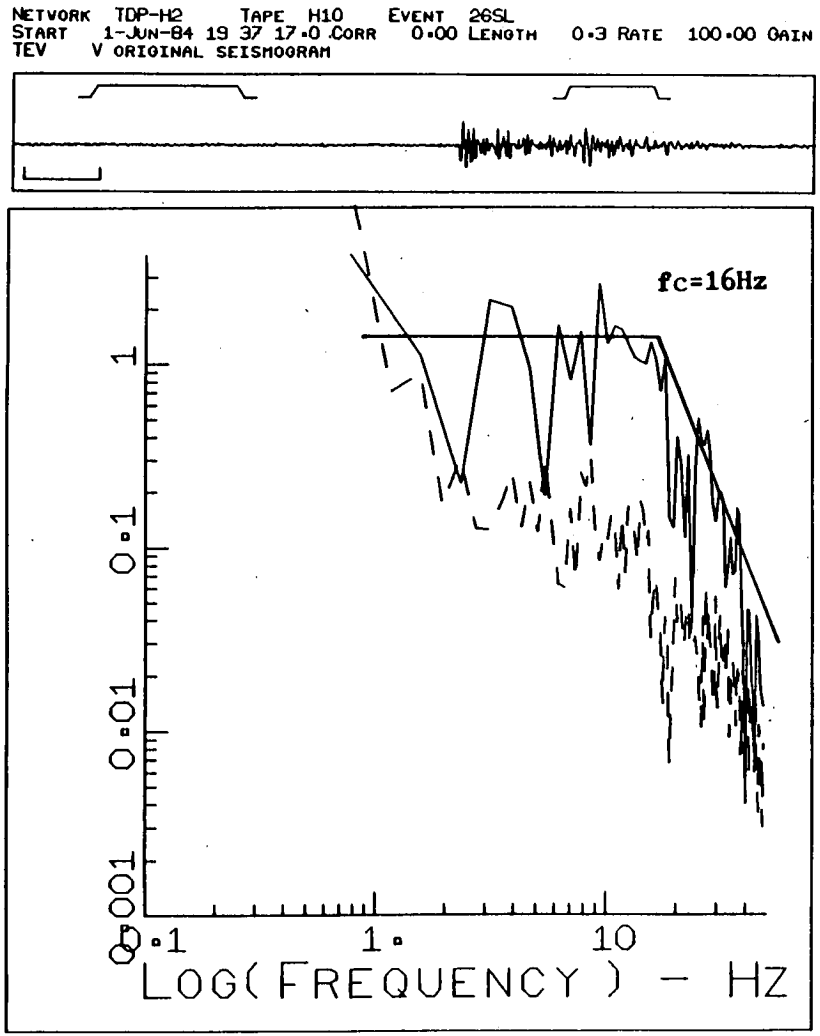

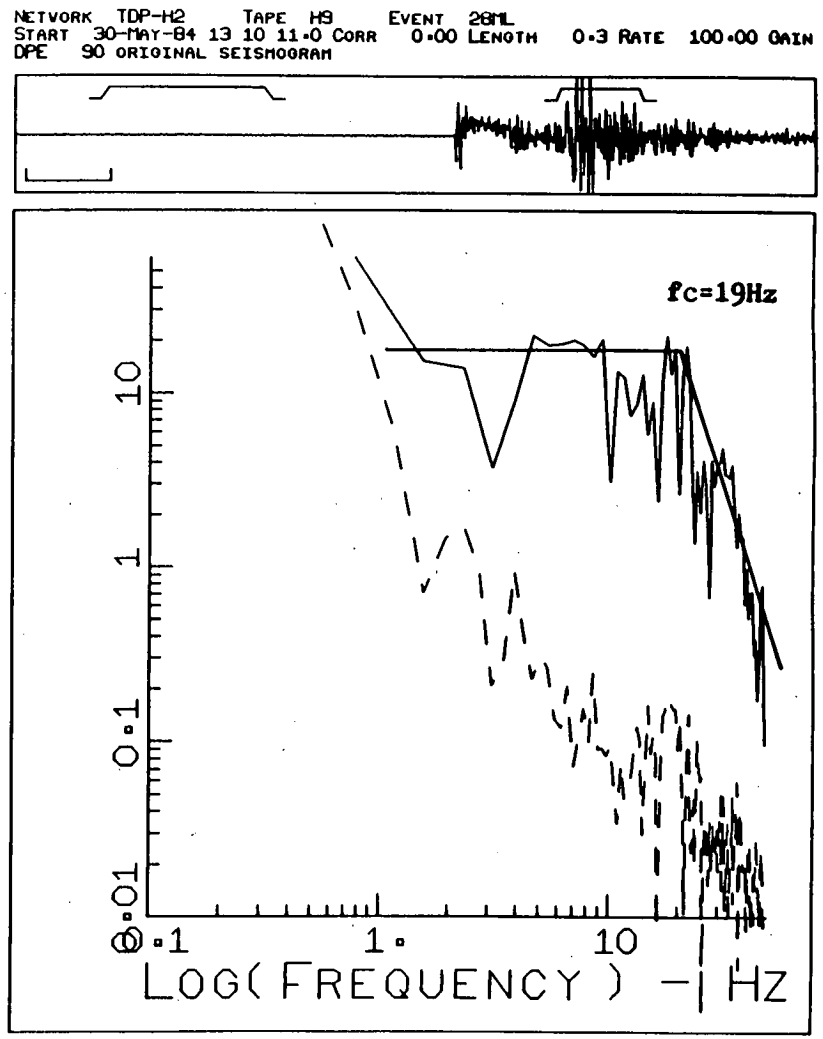

Fig. 5.28a,b - Corner frequency (fc) measurements for two typical S-wave displacement spectra from Group 3. The noise spectra (dotted) is taken from a window prior to the first arrival.

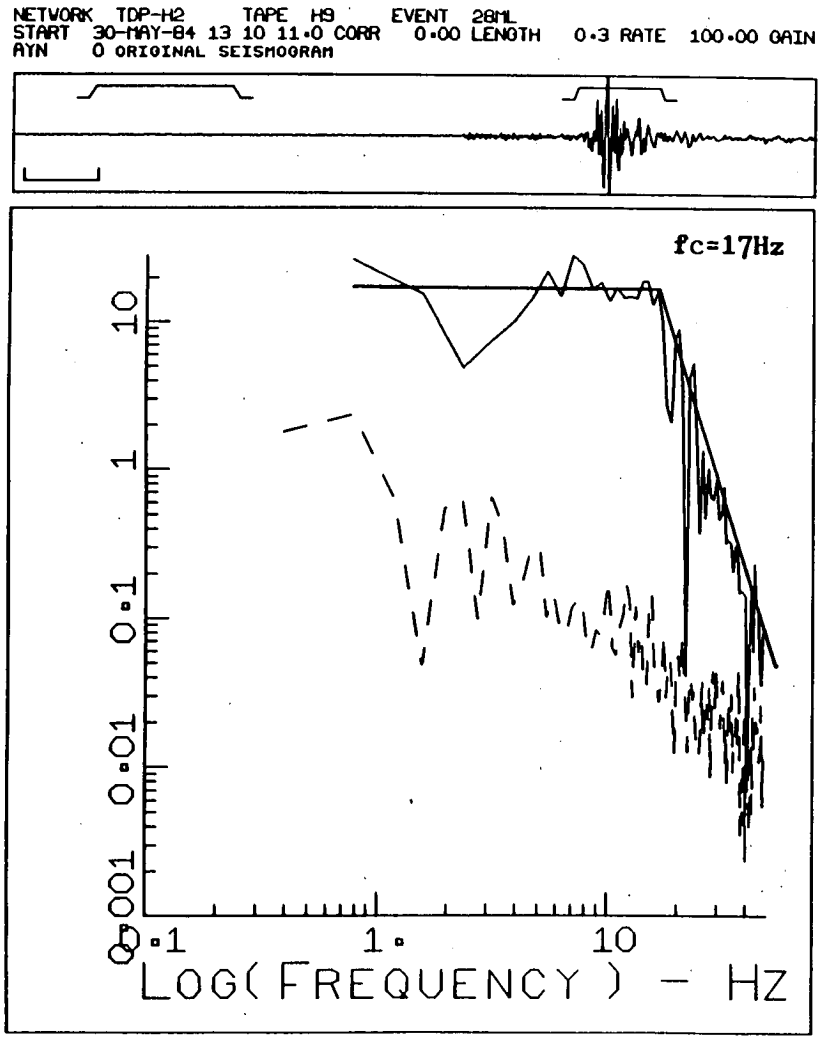

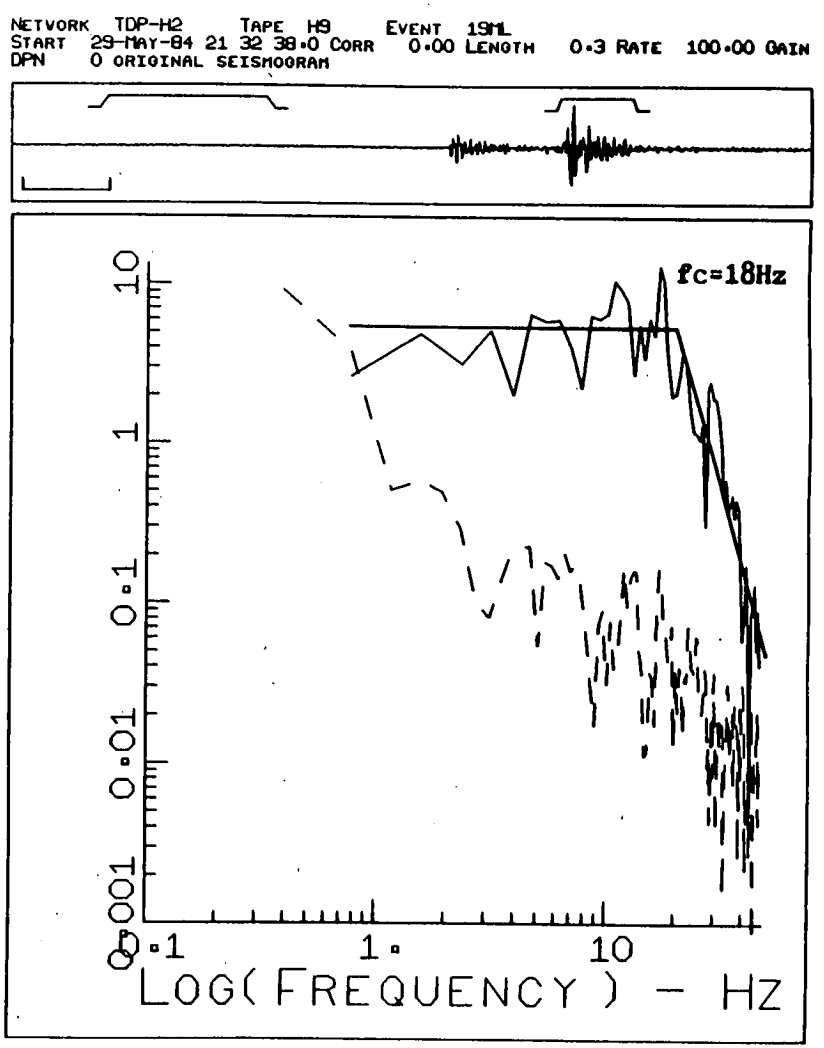

Fig. 5.28c,d - Corner frequency (fc) measurements for two typical S-wave displacement spectra from Group 3. The noise spectra (dotted) is taken from a window prior to the first arrival.

Event	Station							
	SA	KS	DP	AY	PB	TE	SE	YU
TD4150.V32	17	17	19	15	12	10	13	18
TD4151.N10	19	18	18	17	16	17	-	17
TD4153.T37	18	17	17	15	17	18	17	16

Table 5.12 - S-wave corner frequency (f_c(S)) as measured at each station for three events from Group 3. All readings in Hz.

Event	Station							
	SA	KS	DP	AY	PB	TE	SE	YU
TD4153.T37	24	24	27	24	24	26	23	23

Table 5.13 - P-wave corner frequency (f_c(P)) as measured at each station for the Group 3 master event. All readings in Hz.

$$R_c = \frac{f_c(P)}{f_c(S)} = \frac{24.5 \pm 1.5}{16.5 \pm 2.0} = 1.48 \pm 0.20$$

For this group the corner frequency ratio suggests that the data would best fit the Madariaga model, but, as for groups 1 and 2, the error is such that it is not really possible to distinguish between the Brune and Madariaga models. For this reason both models are used to calculate the source dimension.

For the Brune model, velocities of V_p = 6.0km/s and V_s = 3.4km/s and errors in the velocity of 10% we get

$$r = \frac{2.34\ V_p}{2\pi f_c(P)} \qquad \text{or} \qquad r = \frac{2.34\ V_s}{2\pi f_c(S)}$$

$$r = 76 \pm 12\text{m} \qquad\qquad r = 91 \pm 11\text{m}$$

which gives an average of r = 84 ± 11m.

For the Madariaga model

$$r = \frac{2.01\ V_s}{2\pi f_c(P)} \qquad \text{or} \qquad r = \frac{1.32\ V_s}{2\pi f_c(S)}$$

$$r = 44 \pm 5\text{m} \qquad\qquad r = 43 \pm 7\text{m}$$

which gives an average of r = 44 ± 6m.

Since both models assume circular sources these radii are doubled in order to produce a dimension more comparable to the relocation results. Combining the two models gives a range for the spectral source dimension of

$$d = 88 \pm 9\text{m} \quad \text{to} \quad 168 \pm 16\text{m}$$

This range is slightly larger that the dimensions obtained in section 5.5.2 (84m by 53m by 33m) but it is the right order of magnitude.

Chapter 6

Summary and Conclusions

6.1 Summary

In 1979 and 1980 the first two phases of the Turkish Dilatancy Project (TDP-1 and TDP-2) were carried out. The purpose of the project was to investigate crack induced seismic anisotropy, as a means to earthquake prediction, by monitoring shear-wave splitting in the records of local earthquakes. Both phases were successful and anisotropy was observed to occur over a wide area which led to the hypothesis of extensive dilatancy anisotropy (EDA). As a result a third phase was implemented (TDP-3) which was carried out during the summer of 1984. A closely spaced network of three-component stations was established over a section of the North Anatolian Fault in Northwestern Turkey and data was recorded for over six months. In total, 610 well located local earthquakes were recorded which have since been analysed giving results consistent with the first two phases. Further support for EDA was also given by a geoelectric study carried out over the same period. However, the idea of using EDA to predict earthquakes has still to be proven (chapter 1).

The epicentral plot of all local earthquakes recorded during TDP-3 revealed the existence of many clusters. A closer examination of some of these clusters found that several of them contained events that had very similar waveforms, a phenomena that would only occur if the events originated from a common source and followed near-identical propagation paths. Groups of similar earthquakes have been observed in most areas of the World and analysed in a variety of ways (chapter 2). In this study it was proposed to use

them in order to examine the source in detail by accurately locating the relative position of each event with respect to a master event within the same group. It is the waveform similarity that enables the necessary accuracy to be achieved.

The relative location method (chapter 3) calculates the position of one event relative to another using the change in the S-P time between the two events. It assumes that the propagation paths are identical and that the change in the S-P time is only caused by a difference in the location rather than a change in the velocity along the path. Small magnitude similar earthquakes occurring over a short period satisfy both assumptions.

The accuracy of the location is now dependent upon the precision with which the change in the S-P time can be measured. For similar earthquakes from the TDP data sets, arrival times are routinely read to a precision of 0.01 seconds but, with the aid of a cross-correlation technique, this can be improved by an order of magnitude to 0.001 seconds (chapter 4). In the technique a window is moved across a pair of seismograms and, at each point, the relative time delay is determined from the cross-correlation function and plotted against time along the seismogram. This is the time delay function and it can be calculated in either the time or frequency domain. In general, the results are not affected by the choice of domain. However, the time domain has the advantage that it is computationally simpler and produces a smoother time delay function. It is also less sensitive to changes in the size of the window or to the effects of noise and signal saturation. The size of the window is important since if it is too small the cross-correlation function will be unstable but if it is too large then resolution will be lost. Hence a compromise has to be made. The effects of noise or signal saturation are less drastic. Only in extreme cases is the time delay function badly affected.

Overall, the error in the location, determined using the relative location method and the cross-correlation technique, is no greater than 20-30m and will often be less. The two main sources of error are the timing precision and the choice of source velocity

used in the location.

In the data analysis (chapter 5) three groups of similar earthquakes were used. Group 1 was taken from the TDP-2 data set whilst groups 2 and 3 came from TDP-3. Slight differences in the waveform within group 2 meant that it could be further divided into two sub-groups (2A and 2B) which were then treated individually. First, for each group, the events were accurately located. The resultant event distributions all revealed planar structures from which source dimension, strike and dip were measured. Any temporal patterns within the groups were discussed in terms of the barriers that are assumed to control the release of stress on the fault (chapter 2). The event distributions also showed some degree of elongation in a particular direction. To see whether this was related to the rake (measured later) or controlled by the distribution of barriers, the direction of elongation was recorded.

The next stage was to plot out the first motion data and attempt a fault plane solution. This would give another measure of strike and dip, as well as rake, which could then be compared to the relative location results. For two of the groups the data was poorly constrained and so a complete solution was not possible. However, it was possible to check for consistency between the fault plane found by the relative location method and the first motion data. Where a solution was not possible the rake could not be measured for comparison with the direction of elongation.

Lastly, a spectral analysis of several events from each group was carried out. Both S and P corner frequencies were measured from displacement spectra and, using the theory put forward in chapter 2, the source dimension was determined. This could then be compared to the source dimension measured from the relative location method. In addition, the acceleration spectra were calculated to check that any upper frequency limit (f_{max}) did not interfere with the corner frequency measurement. The only limit that was found was the system cut-off at 32Hz.

The results for all the groups are listed in table 6.1.

To see how groups 2A and 2B are related to each other, the location of one master event relative to the other was calculated, although the slight dissimilarity between the waveforms meant that the error in the location was slightly higher than usual. The locations of both groups were then superimposed upon the positions of their respective master events. This showed that the groups were connected by a block approximately 300m across, which would explain the similarity between the groups at long wavelengths. However, the exact relationship between the two faults was unclear since they could be either antithetic or parallel, but the antithetic case is favoured since it is in better agreement with the first motion data.

6.2 Conclusions

The relative location method and the cross-correlation technique, when applied to groups of similar earthquakes, provide an excellent opportunity for examining the source. With a relative error of less than 20-30m in each location and typical source dimensions of several hundred metres, the examination should be quite detailed. The procedure has been shown to be robust for earthquakes with small event separations since these satisfy the assumptions made in the relative location method. The largest error was most likely to have occurred in the attempt to relate groups 2A and 2B to each other by the relative location of the two master events. The greater separation between the events meant a loss of similarity with errors, albeit small, being introduced by a breakdown in the assumptions of identical propagation paths and linearity and a greater uncertainty in the measurement of the change in the S-P time. Although the magnitude of the error cannot be reliably estimated it would not have increased by very much and the resultant interpretation is unlikely to have been affected.

In measuring the change in the S-P time a choice has to be made between using either the time domain or the frequency domain. Based on the results of chapter 4 the time domain has to be recommended.

	Relative Location Method				First Motion Data			Spectral Analysis
Group	Strike	Dip	Source Dimension	Direction of Elongation	Strike	Dip	Rake	Source Dimension
1	141°	45°	450m x 180m x 125m	27°-30°	141°-181°	44°-60°	-14°--22°	112-212m
2A	102°	85°S-81°N	550m x 410m x 290m	30°	(a)	(a)	-	264-502m
2B	270°	69°	820m x 584m x 160m	36°	(a)	(a)	-	264-502m
3	75°	81°	84m x 53m x 33m	32°	75° (b)	81° (b)	-146°	88-168m

Notes : (a) A fault plane solution is not possible although the data is consistent with the results obtained from the relative location method

(b) A wider range of solutions is possible

Table 6.1 - Summary of all the results obtained in chapter 5.

Theoretically, however, there should be no difference between the two domains and when using good data it can be seen that the results are nearly identical. The cause of the higher degree of scatter observed in the frequency domain must lie in the measurement of the slope of the phase. The slope is very sensitive to small changes in the phase at high frequencies and although a weighting system is used to compensate for this it is obviously not working adequately. To get around the problem, either a better weighting system must be devised or the slope must be measured by eye which, although time consuming, would readily be able to eliminate unwanted higher frequencies. Finally, it should again be pointed out that the program listed in appendix 2 does not incorporate a phase unwrapping routine. This will only affect the frequency domain since the seismograms will have to be closely aligned and, although this should not count against using the frequency domain since the problem could be solved, it does illustrate one of the computational difficulties involved.

The results produced by the analysis in chapter 5 have proved to be very encouraging. For each of the four groups the event distribution, as determined by the relative location method, showed some kind of structure. An interpretation in terms of a magmatic intrusion was discounted because no hot conductive bodies had been observed in the final geoelectric analysis. Therefore, each event distribution was interpreted as an elongated area of weakness on a fault. From a review of the theory of barriers and asperities included in chapter 2, this area of weakness is assumed to lie between, or be surrounded by, strong barriers that prevent further slippage on the fault and which determine the character of the earthquakes.

The position of these barriers can be deduced from the event distribution plots since the groups are confined by them. The actual position of each event is thought to be controlled by weaker barriers which are distributed between the stronger ones. However, in general, it is not possible to say where these barriers were positioned since they would have been broken during the sequence and so are not observable on the event distribution plots. However,

there are a couple of exceptions to this. In groups 1 and 2A some grouping of the events in time can be seen and this is interpreted as being due to weak barriers restricting the release of stress and preventing the group from spreading. These types of barriers are not strong or large enough to affect the character of the earthquakes.

The normal physical concept of a fault is of a single interface between two blocks of crust. If this were the case we might expect to see a very thin plane in the event distribution, but we do not, although it might be that the plane is distorted or perhaps curved, a feature that may not be very observable in the cross-sections that are taken. In table 6.1 three dimensions are given for the source which can be considered to be length, width and depth in order of decreasing magnitude. The measurements are fairly crude and are the extreme event separations in three orthogonal directions. Even when taking this into account the depth is still much larger than the error in the locations and, therefore, it would appear that the fault would be better described by a volume that somehow absorbs the movement of the blocks either side of it. The most obvious way it could do this is by fracturing. Such a model would explain why the events move around since different fractures may initiate different events and the interaction between the fractures would explain the presence of weaker barriers. In the event distribution plots for groups 1, 2A and, to a lesser extent, 2B it is possible to imagine some structure within the events, unrelated to time, which could be attributed to different fractures. If this were true it would imply a relatively small number of fractures but if the structure was coincidental then the volume could contain any number of them.

For all four groups the first motion data was plotted on an equal area projection and a fault plane solution attempted. Only for groups 1 and 3 was it possible to obtain a complete fault plane solution and in both cases the resultant strike and dip were found to agree with those obtained from the relative location method. For group 2A only one of the nodal planes could be determined but this was also found to be consistent with the relative location method. Only in group 2B was there any inconsistency but this was overcome

by eliminating one of the readings that was particularly dubious. Overall, the consistency shown between the two methods is encouraging for the relative location method since fault plane solutions from first motion data are widely used and considered to be fairly reliable.

The event distribution plots for all four groups showed some measure of elongation along the presumed fault plane and this has been recorded in table 6.1. For groups 1 and 3 a measure of the rake (direction of slip) was obtained from the complete fault plane solution and this is also recorded in table 6.1. As can be seen, the two measurements do not appear to be related. From this it was deduced that the direction of elongation is not determined by the direction of slip. It is more likely to be caused by the distribution of weak barriers over the fault.

For each of the four groups a measure of the source dimension was obtained from the relative location method. For comparison, it was also determined using an established spectral technique and both sets of results are listed in table 6.1. Unfortunately, the spectral technique only gives one dimension, since it is based on a simple circular model, and it is difficult to say how this relates to the three dimensions given by the relative location method. However, the results do show that they are of the same order and, more broadly, that the corner frequencies decrease as the dimensions increase, a relationship that would be expected in theory.

In conclusion, the main aim of the study was to develop a method that enables source dimension and geometry to be measured to a high degree of accuracy. The results that have been presented here would seem to indicate that the method has been successful in doing this although, as with all source studies, verification of the results is difficult. In the study, comparisons have been made with other methods and the results have been found to be consistent, although not necessarily equal. Many different methods have been developed for analysing the source and for any one parameter a wide range of results can be obtained. The errors are obviously large and, despite the increase in interest that has been shown in the subject

over the last few years, no one method has shown itself to be better than the others. Therefore, consistency between these methods and the method presented in this thesis is all that could be realistically hoped for.

The main advantages the relative location method has over the other methods is that it is not dependent upon having to find a model to describe the source and that most propagation path effects can be eliminated. As a result the accuracy is much higher and perhaps this will prove to be the way in which to obtain better information and to improve our knowledge of the source. Unfortunately, the method is limited to groups of similar earthquakes which restricts the extent to which the method can be deployed. However, recent increases in the popularity of microearthquake studies should ensure that there is no shortage of data and that most seismically important areas of the World will be examined.

In our attempt to understand the processes taking place within the Earth, and particularly the crust, it is important to have a thorough knowledge of the seismic source and perhaps this study will be able to make some contribution towards this goal.

6.3 Improvements and Suggestions for Further Work

The combination of the relative location method and cross-correlation technique shows a lot of promise as a method for examining the source in detail. Unfortunately, time has restricted the analysis, in this thesis, to only four groups of similar earthquakes, but, in order to fully test the method, many more should be analysed. The TDP data set alone contains numerous other groups and there are, no doubt, more examples to be found in other data sets. The analysis should include groups from different tectonic regimes or fault systems and groups in less well constrained situations (i.e. epicentre outside the network). This should help to show up the limits of the method and perhaps lead to some improvements of it. However, before proceeding with this, there are already two changes that could be made that might help to

improve the method in less well constrained groups.

In the relative location method the waves are assumed to travel direct to the station along straight paths and at a constant velocity. In reality, however, the crust contains many layers and velocities with the result that the waves will refract as they cross each layer interface and hence take a different route. For data, such as that used in this study, where the earthquakes lie directly below a compact network and with an incidence angle at the furthest station no greater than about 30^{o} from the vertical, then the effects will be negligible. However, if the method was to be used on shallower earthquakes or with a more widespread network, the refraction may have to be taken into account. Therefore, the method could be improved by adapting it to accept a multi-layered model through which the rays could be traced.

The one outstanding change that can be made to the cross-correlation program is to develop a reliable routine for unwrapping the phase. Although this would not change the results it would make the frequency domain a little easier to use. It would also be interesting to see what effect filtering the seismogram would have. For example, if the high frequencies are removed would it help to reduce the scatter in the frequency domain and/or improve the stability and, if so, how would this change be reflected in the time domain.

The data analysis, as carried out in chapter 5, has proved to be quite successful. However, the comparison of the source dimensions should be broadened to include several other methods, some of which have been mentioned in chapter 2. As discussed near the end of the previous section, no one method has shown itself to be any better than the others, but a broad comparison should reveal which of the methods are the nearest to being in agreement with the relative location method. Unfortunately, there is no other direct means of measuring the source dimension (or any other source parameter) which means that there will always be the problem of having to compare a single dimension (based on whatever type of model is being used) with the three dimensions of the relative location method.

Finally, it would be interesting to expand the area of study to include groups associated with large earthquakes. Foreshocks and aftershocks have often been observed to be similar, not just with each other but also with the main event. Perhaps, by calculating the relative locations of these events it might be possible to investigate source behaviour before and after a major earthquake. However, the method described in this thesis is not capable of carrying out the calculations in its present form. It is very likely that there will be some significant velocity changes associated with the occurrence of a large event. Hence, it will not be possible to say what proportion of any measured change in the S-P time would have been caused by a movement in the hypocentre. To get around the problem, a method that can measure the change in velocity between similar earthquakes (such as that employed by Poupinet (1984, 1985)) must be incorporated into the procedure.

References

Aki, K., 1967. Scaling law of seismic spectrum, *J. geophys. Res.*, 72, 1217-1231.

Aki, K., 1984. Asperities, barriers, characteristic earthquakes and strong motion prediction, *J. geophys. Res.*, 89, 5867-5872.

Aki, K., 1987. Magnitude-frequency relation for small earthquakes: a clue to the origin of f_{max} of large earthquakes, *J. geophys. Res.*, 92, 1349-1355.

Aki, K. and Richards, P.G., 1980. *Quantitative Seismology: Theory and Methods*, W.H.Freeman, San Francisco.

Ambraseys, N.N. and Zatopek, A., 1969. The Mudurnu Valley, West Anatolia, Turkey, earthquake of 22 July 1967, *Bull. Seismol. Soc. Am.*, 59, 521-589.

Anderson, D.L. and Whitcomb, J.H., 1975. Time-dependant seismology, *J. geophys. Res.*, 80, 1497-1503.

Andrews, D.J., 1976. Rupture velocity of plane strain shear cracks, *J. geophys. Res.*, 81, 5679-5687.

Anderson, J. and Hough, S.E., 1984. A model for the shape of the Fourier amplitude spectrum of acceleration at high frequencies, *Bull. Seismol. Soc. Am.*, 74, 1969-1993.

Asada, T., 1953. On the relation between the predominant period and maximum amplitude of earthquake motions, *J. Seismol. Soc. Japan, Ser. 2*, 6, 69-73.

Atkinson, B.K., 1979. A fracture mechanics study of subcritical tensile cracking of quartz in wet environments, *Pure appl. Geophys.*, 117, 1011-1024.

Atkinson, B.K., 1982. Subcritical crack propagation in rocks: theory, experimental results and applications, *J. struct. Geol.*, 4, 41-56.

Atkinson, B.K., 1984. Subcritical crack growth in geological materials, *J. geophys. Res.*, **89**, 4077-4114.

Backus, G. and Mulcahy, M., 1976a. Moment tensors and other phenomenological descriptions of seismic sources - I. Continuous displacements, *Geophys. J. R. astr. Soc.*, **46**, 341-361.

Backus, G. and Mulcahy, M., 1976b. Moment tensors and other phenomenological descriptions of seismic sources - II. Discontinuous displacements, *Geophys. J. R. astr. Soc.*, **47**, 301-329.

Bakun, W.H., Bufe, C.G. and Stewart, R.M., 1976. Body wave spectra of central California earthquakes, *Bull. Seismol. Soc. Am.*, **66**, 363-384.

Bakun, W.H. and Lindh, A.G., 1977. Local magnitudes, seismic moments and coda duration for earthquakes near Oroville, California, *Bull. Seismol. Soc. Am.*, **67**, 615-629.

Beamish, D., 1982. A geomagnetic precursor to the 1979 Carlisle earthquake, *Geophys. J. R. astr. Soc.*, **68**, 531-543.

Berckhemer, H., 1962. Die Ausdehnung der Bruchflache im Erdbebenherd und ihr Einfluss auf das seismische Wellenspektrum, *Gerlands Beitr. Geophys.*, **71**, 5-26.

Boatwright, J., 1978. Detailed spectral analysis of two small New York state earthquakes, *Bull. Seismol. Soc. Am.*, **68**, 1117-1131.

Boatwright, J., 1980. A spectral theory for circular seismic sources; simple estimates of source dimension, dynamic stress drop and radiated seismic energy, *Bull. Seismol. Soc. Am.*, **70**, 1-27.

Boatwright, J., 1982. A dynamic model for far-field acceleration, *Bull. Seismol. Soc. Am.*, **72**, 1049-1068.

Boatwright, J., 1984. Seismic estimates of stress release, *J. geophys. Res.*, **89**, 6961-6968.

Boore, D.M., Lindh, A.G., McEvilly, T.V. and Talmachoff, W.W., 1975. A search for travel-time changes associated with the Parkfield, California, earthquake of 1966, *Bull. Seismol. Soc. Am.*, **65**, 1407-1418.

Booth, D.C. and Crampin, S., 1985. Shear-wave polarizations on a curved wavefront at an isotropic free surface, *Geophys. J. R. astr. Soc.*, **83**, 31-45.

Brune, J.N., 1970. Tectonic stress and the spectra of seismic shear waves from earthquakes, *J. geophys. Res.*, **75**, 4997-5009.

Brune, J.N., 1971. Correction, *J. geophys. Res.*, **76**, 5002.

Brune, J.N., 1976. The physics of earthquake strong motion, *Seismic risk and engineering decisions*, Ch. 5, 140-177, C. Lomnitz and E. Rosenbleuth, editors, Elsevier, Amsterdam.

Buchbinder, G.G.R. and Keith, C.M., 1979. Stability of P travel times in the region of La Malbaie, Quebec, *Bull. Seismol. Soc. Am.*, **69**, 463-481.

Burridge, R., 1973. Admissible speeds for plane-strain self-similar shear cracks with friction but lacking cohesion, *Geophys. J. R. astr. Soc.*, **35**, 439-455.

Clymer, R.W. and McEvilly, T.V., 1981. Travel-time monitoring with Vibroseis, *Bull. Seismol. Soc. Am.*, **71**, 1903-1927.

Crampin, S., 1978. Seismic-wave propagation through a cracked solid: polarization as a possible dilatancy diagnostic, *Geophys. J. R. astr. Soc.*, **53**, 467-496.

Crampin, S., Evans, J.R. and Atkinson, B.K., 1982. A new physical basis for prediction, *EOS*, **63**, 370 (abstract).

Crampin, S., Evans, J.R. and Atkinson, B.K., 1984. Earthquake prediction: a new physical basis, *Geophys. J. R. astr. Soc.*, **76**, 147-156.

Crampin, S., Evans, J.R. and Ucer, S.B., 1985. Analysis of records of local earthquakes: the Turkish Dilatancy Projects (TDP1 and TDP2), *Geophys. J. R. astr. Soc.*, **83**, 1-16.

Crampin, S., Jacob, A.W.B., Miller, A. and Neilson, G., 1970. The LOWNET radio-linked seismometer network in Scotland, *Geophys. J. R. astr. Soc.*, **21**, 207-216.

Das, S. and Aki, K., 1977a. A numerical study of two-dimensional spontaneous rupture propagation, *Geophys. J. R. astr. Soc.*, **50**, 643-668.

Das, S. and Aki, K., 1977b. Fault plane with barriers: a versatile earthquake model, *J. geophys. Res.*, **82**, 5658-5670.

Day, S.M., 1982. Three-dimensional simulation of spontaneous rupture: The effect of non-uniform prestress, *Bull. Seismol. Soc. Am.*, **72**, 1881-1902.

Dewey, J.W., 1976. Seismicity of Northern Anatolia, *Bull. Seismol. Soc. Am.*, **66**, 843-868.

Dewey, J.F., Pittman, W.C., Ryan, W.B.F. and Bonnin, J., 1973. Plate tectonics and the evolution of the Alpine system, *Geol. Soc. Am. Bull.*, **84**., 3137-3180.

Dewey, J.F. and Sengor, A.M.C., 1979. Aegean and surrounding regions: complex multiplate and continuum tectonics in a convergent zone, *Geol. Soc. Am. Bull.*, **90**, 84-92.

Ellsworth, W.L., 1975. Bear Valley, California, earthqauke sequence of February-March 1982, *Bull. Seismol. Soc, Am.*, 65, 483-506.

Evans, J.R., 1980. ADC: a program for digitising seismic records into a format suitable for automatic processing, *Brit. Geol. Surv. Glob. Seismol. Rep. No. 136.*

Evans, J.R., 1984. Effects of the free surface on shear wavetrains, *Geophys. J. R. astr. Soc.*, 76, 165-172.

Evans, J.R., 1986a. A user's guide to ADC and NETFIL, computer programs for use in digitising Geostore tapes, *British Geological Survey Global Seismology Research Group Reports*, in preparation.

Evans, J.R., 1986b. PICK: an interactive program for identifying the arrival times of seismic phases, *British Geological Survey Global Seismology Research Group Report*,in preparation.

Evans, J.R., Asudeh, I., Crampin, S. and Ucer, S.B., 1985. Tectonics of the Marmara Sea region of Turkey: new evidence from micro-earthquake fault plane solutions, *Geophys. J. R. astr. Soc.*, 83, 47-60.

Florensov, N.A. and Solonenko, V.P., 1963. The Gobi-Altai earthquake, *Akademiya Nauk SSSR*, Moscow.

Frankel, A., 1982. Precursors to a Magnitude 4.8 earthquake in the Virgin Islands: Spatial clustering of small earthquakes, anomalous focal mechanisms, and earthquake doublets, *Bull. Seismol. Soc. Am.*, 72, 1277-1294.

Geller, R.J. and Mueller, C.S., 1980. Four similar earthquakes in central California, *Geophys. Res. Lett.*, 7, 821-824.

Glangeaud, F., 1981. Signal processing for magnetic pulsations, *J. Atmos. Terr. Phys.*, 43, 981-998.

Gutenberg, B. and Richter, C.F., 1954. Seismicity of the Earth and associated phenomena, *Princeton University Press*, Princeton N.J., 310pp..

Gutenberg, B. and Richter, C.F., 1956. Earthquake magnitude, intensity, energy and acceleration, 2, *Bull. Seismol. Soc. Am.*, 46, 105-145.

Hamaguchi, H. and Hasegawa, A., 1975. Recurrent occurence of the earthquakes with similar waveforms and its related problems, *Jishin*, 28, 152-170.

Hanks, T.C., 1977. Earthquake stress drops, ambient tectonic stresses and stresses that drive plate motions, *Pure Appl. Geophys.*, 115, 441-458.

Hanks, T.C., 1979. b values and ω^{-} seismic source models: implications for tectonic stress variations along active crustal fault zones and the estimation of high-frequency strong ground motion, *J. geophys. Res.*, 84, 2235-2242.

Hanks, T.C., 1981. The corner frequency shift, earthquake source models and Q, *Bull. Seismol. Soc. Am.*, 71, 597-612.

Hanks, T.C., 1982a. f_{max}, *Bull. Seismol. Soc. Am.*, 72, 1867-1879.

Hanks, T.C., 1982b. f_{max}, Proceedings of Workshop XVI, The Dynamic Characteristics of Faulting Inferred from Recordings of Strong Ground Motions, *U.S. Geol. Surv., Open-file Rept., 82-591*, 405-436.

Hanks, T.C. and Wyss, M., 1972. The use of body-wave spectra in the determination of seismic-source parameters, *Bull. Seismol. Soc. Am.*, 62, 561-589.

Honda, H. and Ito, H., 1939. On the period of P waves and the magnitude of the earthquake, *Geophys. Mag.*, 13, 155-160.

Ida, Y., 1973. The maximum acceleration of seismic ground motion, *Bull. Seismol. Soc. Am.*, **63**, 959-968.

Ishida, M. and Kanamori. H., 1978. The foreshock activity of the 1971 San Fernando earthquake, California, *Bull. Seismol. Soc. Am.*, **68**, 1265-1279.

Ishida, M. and Kanamori, H., 1980. Temporal variation of seismicity and spectrum of small earthquakes preceding the 1952 Kern County, California, earthquake, *Bull. Seismol. Soc. Am.*, **70**, 509-527.

Johnson, L.R., 1979. Seismic source theory, *Rev. Geophys. Space Phys.*, **17**, 328-336.

Kanai, K., Osada, K. and Yoshizawa, S., 1953. The relation between the amplitude and the period of earthquake motion, *Bull. Earthquake Res. Inst. Tokyo Univ.*, **31**, 45-56.

Kanamori, H. and Fuis, G., 1976. Variation of P-wave velocity before and after the Galway Lake earthquake (M_L=5.2) and the Goat Mountain earthquakes (M_L=4.7, 4.7) in the Mojave Desert, *Bull. Seismol. Soc. Am.*, **66**, 2017-2037.

Karnik, V., 1971. *Seismicity of the European Area, Part 2*, Reidel, Dordrecht.

Kaufman, K. and Burdick, L.J., 1980. The reproducing earthquakes of the Galapogos Islands, *Bull. Seismol. Soc. Am.*, **70**, 1759-1770.

Lay, T. and Kanamori, H., 1980. Earthquake doublets in the Solomon Islands, *Phys. Earth Planet. Interiors*, **21**, 283-304.

Le Pichon, X. and Angelier, J., 1979. The Hellenic arc and trench system: a key to the neotectonic evolution of the Eastern Mediterranean area, *Tectonophysics*, **60**, 1-42.

Le Pichon, X. and Angelier, J., 1981. The Aegean Sea, *Phil. Trans. R. Soc. Lond.*, A300, 357-372.

Leary, P.C., Malin, P.E., Phinney, R.A., Brocher, T. and VonColln, R., 1979. Systematic monitoring of millisecond travel time variations near Palmdale, California, *J. geophys. Res.*, 84, 659-666.

Lee, W.H.L. and Lahr, J.C., 1975. HYP071 (Revised): a computer program for determining hypocentre, magnitude and fault motion patterns of local earthquakes, *U. S. Geological Survey Open File Report*, 75-311.

Madariaga, R., 1976. Dynamics of an expanding circular fault, *Bull Seismol. Soc. Am.*, 66, 639-666.

Makris, J., 1976. A dynamical model of the Hellenic arc deduced from geophysical data, *Tectonophysics*, 36, 339-346.

Main, I.G., 1985. Seismotectonics and seismic hazard in areas of differing crustal deformation rates, *Ph.D. Thesis*, University of Edinburgh.

Marrow, P.C. and Walker, A.B., 1986. The aftershock sequence of the 19th July 1984 Lleyn earthquake, *Brit. Geol. Surv. Glob. Seismol. Rep. No. 288.*

Matamoto, T., 1960. On the spectral structure of earthquake waves, *Bull. Earthquake Res. Inst. Tokyo*, 38, 13-27.

McGarr, A., Green, R.W.E. and Spottiswoode, S.M., 1981. Strong ground motion of mine tremors: some implications for near-source ground motion parameters, *Bull. Seismol. Soc. Am.*, 71, 295-319.

McKenzie, D., 1972. Active tectonics of the Mediterranean region, *Geophys. J. R. astr. Soc.*, 30, 109-185.

McKenzie, D., 1978. Active tectonics of the Alpine-Himalayan belt: the Aegean Sea and surrounding regions, *Geophys. J. R. astr. Soc.*, 55, 217-254.

Mogi, K., 1967. Earthquakes and fractures, *Tectonophysics*, 5, 35-55.

Molnar, P., Tucker, B.E. and Brune, J.N., 1973. Corner frequencies of P and S waves and models of earthquake sources, *Bull. Seismol. Soc. Am.*, 63, 2091-2104.

Okada, H., Watanabe, H., Yamashita, H. and Yokoyama, I., 1981. Seismological significance of the 1977-1978 eruptions and magma intrusion process of Usu Volcano, Hokkaido, *J. Volcanol. Geotherm. Res.*, 9, 311-344.

Pamir, H.N., 1944. Kuzey Anadolu'da bir deprem cizgisi, *Istanbul. Univ. Fen Fak. Mecm. A*, 9, 143-158.

Papageorgiou, A.S. and Aki, K., 1983a. A specific barrier model for the quantitative description of inhomogenous faulting and the prediction of strong ground motion. I. Description of the model, *Bull. Seismol. Soc. Am.*, 73, 693-722.

Papageorgiou, A.S. and Aki, K., 1983b. A specific barrier model for the quantitative description of inhomogenous faulting and the prediction of strong ground motion. Part II. Applications of the model, *Bull. Seismol. Soc. Am.*, 73, 953-978.

Peake, L.G., Healy, J.H. and Roller, J.C., 1977. Time variance of seismic velocity from multiple explosive sources southeast of Hollister, California, *Bull. Seismol. Soc. Am.*, 67, 1339-1354.

Pechmann, J.C. and Kanamori, H., 1982. Waveforms and spectra of preshocks and aftershocks of the 1979 Imperial Valley, California, earthquake: Evidence for fault heterogeneity?, *J. geophys. Res.*, 87, 10579-10597.

Pointing, A.J., 1985. Seismicity and lithospheric structure of Northern Kenya, *Ph.D. Thesis*, University of Leicester.

Poupinet, G., Glangeaud, F. and Cote, P., 1982. P-time delay measurement of a doublet of microearthquakes, *Proc. IEEE ICASSP82*, Paris, May 3-5, 1516-1519.

Poupinet, G., Ellsworth, W.L. and Frechet, J., 1984. Monitoring velocity variations in the crust using earthquake doublets: an application to the Calaveras Fault, California, *J. geophys. Res.*, **89**, 5719-5731.

Poupinet, G., Frechet, J., Ellsworth, W.L., Fremont, M.J. and Glangeaud, F., 1985. Doublet analysis: improved accuracy for earthqauke prediction studies, *Earthq. Predict. Res.*, **1**, 147-159.

Randall, M.J., 1973. The spectral theory of seismic sources, *Bull. Seismol. Soc. Am.*, **63**, 1133-1144.

Rikitake, T., 1976. *Earthquake Prediction*, Elsevier, Amsterdam, 357pp.

Russell, M., 1987. Electromagnetic induction studies in a region of active crustal dislocation, *Ph.D. Thesis*, University of Edinburgh.

Scholz, C.H., Sykes, L.R. and Aggarwal, Y.P., 1973. Earthquake Prediction: A physical basis, *Science*, **181**, 803-810.

Schwartz, D.P. and Coppersmith, K.J., 1984. Fault behaviour and charateristic earthquakes: examples from the Wasatch and San Andreas fault zones, *J. geophys. Res.*, **89**, 5681-5698.

Semenov, A.M., 1969. Variations in the travel time of transverse and longitudinal waves before violent earthquakes, *Izv. Acad. Sci., Earth Phys.*, English translation, **4**, 245.

Sengor, A.M.C., 1984. The Cimmeride orogenic system and the tectonics of Eurasia, *Geol. Soc. Am. Special paper 195.*

Silver, P., 1983. Retrieval of source-extent parameters and the interpretation of corner frequency, *Bull. Seismol. Soc. Am.*, 73, 1499-1511.

Silver, P. and Masuda, T., 1985. A source extent analysis of the Imperial Valley earthquake of October 15, 1979 and the Victoria earthquake of June 9, 1980, *J. geophys. Res.*, 90, 7639-7651.

Spottiswoode, S.M. and McGarr, A., 1975. Source parameters of tremors in a deep-level gold mine, *Bull. Seismol. Soc. Am.*, 65, 93-112.

Takeo, M., 1983. Source mechanisms of Usu Volcano, Japan, earthquakes and their tectonic implications, *Phys. Earth Planet. Inter.*, 32, 241-264.

Toksoz, M.N., Shakel. A.F. and Michael, A.J., 1979. Space-time migration of earthquakes along the North Anatolian Fault zone and seismic gaps, *Pure appl. Geoph.*, 117, 1258-1270.

Tsujiura, M., 1980. Earthquake swarm activity in the Northern Tokyo Bay, *Bull. Earthquake Res. Inst.*, 55, 601-619.

Tsujiura, M., 1981. Activity mode of the 1980 earthquake swarm off the east coast of the Izu Peninsula, *Bull. Earthquake Res. Inst.*, 56, 1-24.

Tsujiura, M., 1983a. Waveform and spectral features of earthquake swarms and foreshocks in special reference to earthquake prediction, *Bull. Earthquake Res. Inst. Univ. Tokyo*, 58, 65-134.

Tsujiura, M., 1983b. Characteristic frequencies for earthquake families and their tectonic implications: evidence from

earthquake swarms in the Kanto District, Japan, *Pure Appl. Geophys.*, **121**, 573-600.

Turbitt, T. (editor), 1985. Catalogue of British earthquakes recorded by the BGS seismograph network, 1982, 1983, 1984, *Brit. Geol. Surv. Glob. Seismol. Rep. No. 260.*

Ucer, S.B., Crampin, S., Evans, J.R., Miller, A. and Kafadar, N., 1985. The MARNET radiolinked seismometer network spanning the Marmara Sea and the seismicity of Western Turkey, *Geophys. J. R. astr. Soc.*, **83**, 17-30.

Wesson, R.L., Robinson, R., Bufe, C.G., Ellsworth, W.L., Pfluke, J.H., Steppe, J.A. and Seekins, L.C., 1977. Search for seismic forerunners to earthquakes in Central California, *Tectonophysics*, **42**, 111-126.

Appendix 1

[The program listed in this appendix does not include the error analysis of chapter 3.]

```
C*******************************************************************************
C
C     RELOC V2.00
C
C     Relocates a family of events with respect to a master event
C     from the same family. Input(channel 1) comprises of a station
C     list(name,longitude,latitude,height),location of the master
C     event(longitude,latitude,depth) and observed data necessary
C     for relocation(one line for event code,one line for each
C     station and its observed difference in S-P time - taken from
C     cross-correlation function). Output(channel 2) is comprised
C     of new location(code,longitude,latitude,depth) and its
C     residual(sum of square of diffrerences/number of samples).
C     Channel 3 is output file for EQANAL.
C
C     Alan Logan     March 1985
C
C*******************************************************************************
C
C     Constants
C     CHARACTER*4 BLANKS, DOL
C     PARAMETER ( BLANKS = '    ' )
C     PARAMETER ( DOL = '$$$$' )
C     REAL PI, FMTKM
C     PARAMETER ( PI = 3.1415926 )
C     PARAMETER ( FMTKM = 1.853167 )
C
C     Variables
      CHARACTER*6 CODE(30)
      INTEGER LTD(10), LGD(10), IHT(10),
      INTEGER LTNWD(30), LGNWD(30), HTNW(30)
      INTEGER MAT(3,10), MATTRA(10,3), MATPRO(3,3)
      REAL FLTM(10), FLGM(10)
      REAL DELLT(10), DELLG(10), DELHT(10), DIST(10), DELSP(10)
      REAL ALPHA(3)
      REAL FNWLT(30), FNWLG(30), FNWHT(30)
      REAL EXSP(10), EXMSSP(10)
      REAL STNM1(10), STNM2(10)
      REAL FLTNWM(30), FLGNWM(30)
      REAL SMTINV(3,3), SMTFIN(10,3)
C
C     Assign one input file (channel 1) and two output files (channels 2 and 3)
C
      WRITE(7,101)
  101 FORMAT('  Assign input and output files'/ 7X,'Input :',$)
      CALL ASSIGN(1,,-1)
      WRITE(7,102)
  102 FORMAT(7X,'Output 1 (degrees and minutes) :',$)
      CALL ASSIGN(2,,-1)
      WRITE(7,103)
  103 FORMAT(7X,'Output 2 (EQANAL format) :',$)
      CALL ASSIGN(3,,-1)
C
C     Type in P and S velocities and calculate the velocity factor
C
      CALL ASKR(VP,'P-Velocity ?',7.0)
      CALL ASKR(VS,'S-Velocity ?',4.0)
      FV=(VP-VS)/(VP*VS)
C
C     Write out header for channel 2
C
      WRITE(2,49)VP,VS
   49 FORMAT('VP = ',F4.2/'VS = ',F4.2//)
      WRITE(2,50)
   50 FORMAT('CODE      LAT.      LONG.    HT.
     1STN.  DOBS     DCALC  '/)
C
C     Read in station list which must end with a blank line
C
      I=0
  110 I=I+1
      READ(1,10)STNM1(I),LGD(I),FLGM(I),LTD(I),FLTM(I),IHT(I)
   10 FORMAT(A4,2(1X,I2,F5.2),1X,I3)
      IF (STNM1(I).NE.BLANKS) THEN
```

```
      GO TO 110
      ENDIF
  100 ITNS=I-1
C
C     Read in location of master event
C
      READ(1,20)MELGD,FMELGM,MELTD,FMELTM,FMEDEP
   20 FORMAT(2(I2,F5.2,1X),F6.3)
      WRITE(3,90)MELTD,FMELTM,MELGD,FMELGM,FMEDEP
C
C     Calculate coordinates of stations (in kms) with the master event at the origin, and
C     the distance from the master event to each station.
C
C
      FLGMTK=FMTKM*COS((40.66667*PI)/180.0)
      DO 120 I=1,ITNS
      DELLG(I)=(FLOAT(LGD(I)-MELGD)*60.0+(FLGM(I)-FMELGM))*FLGMTK
      DELLT(I)=(FLOAT(LTD(I)-MELTD)*60.0+(FLTM(I)-FMELTM))*FMTKM
      DELHT(I)=FMEDEP+(FLOAT(IHT(I))*0.001)
  120 DIST(I)=SQRT(DELLG(I)*DELLG(I)+DELLT(I)*DELLT(I)+DELHT(I)*
     1DELHT(I))
C
C     Relocate each event in turn. First reading in the data for each event.
C
      DO 1000 N=1,32
      IF (N.EQ.32) GO TO 1003
      READ(1,70,END=1001)CODE(N)
   70 FORMAT(A6)
      I=0
  140 I=I+1
      READ(1,30)STNM2(I),DELSP(I)
   30 FORMAT(A4,1X,F6.3)
      IF (STNM2(I).NE.DOL) THEN
      GO TO 140
      ENDIF
  130 NMST=I-1
C
C     Calculate expected change in S-P times at each station for hypocentre movements of
C     100m East,North and up and put into a matrix MAT(3,3)
C
      DO 150 I=1,NMST
      DO 160 J=1,ITNS
      IF (STNM2(I).EQ.STNM1(J)) GO TO 170
  160 CONTINUE
      WRITE(7,80)CODE(N)
   80 FORMAT(' STATION MISSING IN',1X,A6)
      GO TO 1000
  170 DELLG1=DELLG(J)-0.1
      DSTEST=SQRT(DELLG1*DELLG1+DELLT(J)*DELLT(J)+DELHT(J)*DELHT(J))
      DELDS1=DSTEST-DIST(J)
      MAT(1,I)=IFIX((ABS(DELDS1)*FV*1000.0)+0.5)
      IF (DELDS1.LT.0.0) MAT(1,I)=-MAT(1,I)
      DELLT1=DELLT(J)-0.1
      DSTNOR=SQRT(DELLG(J)*DELLG(J)+DELLT1*DELLT1+DELHT(J)*DELHT(J)) DELDS2=DSTNOR-DIST(J)
      MAT(2,I)=IFIX((ABS(DELDS2)*FV*1000.0)+0.5)
      IF (DELDS2.LT.0.0) MAT(2,I)=-MAT(2,I)
      DELHT1=DELHT(J)-0.1
      DSTUP=SQRT(DELLG(J)*DELLG(J)+DELLT(J)*DELLT(J)+DELHT1*DELHT1)
      DELDS3=DSTUP-DIST(J)
      MAT(3,I)=IFIX((ABS(DELDS3)*FV*1000.0)+0.5)
      IF (DELDS3.LT.0.0) MAT(3,I)=-MAT(3,I)
  150 CONTINUE
C
C     Transpose
C
      DO 180 I=1,3
      DO 180 J=1,NMST
  180 MATTRA(J,I)=MAT(I,J)
C
C     Multiply MATxMATTRA
C
      DO 190 I=1,3
      DO 190 K=1,3
      ISUM1=0
```

```
      DO 200 J=1,NMST
      IPP1=MAT(I,J)*MATTRA(J,K)
  200 ISUM1=ISUM1+IPP1
      MATPRO(I,K)=ISUM1
  190 CONTINUE
C
C     Invert MATPRO - output SMTINV
C
      CALL MATIN3(MATPRO,SMTINV)
C
C     Multiply transpose by inverse
C
      DO 210 I=1,NMST
      DO 210 K=1,3
      SUM2=0.0
      DO 220 J=1,3
      PP2=MATTRA(I,J)*SMTINV(J,K)
  220 SUM2=SUM2+PP2
      SMTFIN(I,K)=SUM2
  210 CONTINUE
C
C     Multiply this matrix by a row vector of
C     observed changes in S-P.
C
      DO 230 I=1,3
      SUM3=0.0
      DO 240 J=1,NMST
      PP3=(DELSP(J)*1000.0)*SMTFIN(J,I)
  240 SUM3=SUM3+PP3
      ALPHA(I)=SUM3
  230 CONTINUE
C
C     New coordinates (in kms from coordinates of master event).
C
      FNWLG(N)=ALPHA(1)*0.1
      FNWLT(N)=ALPHA(2)*0.1
      FNWHT(N)=ALPHA(3)*0.1
C
C     Calculate expected change in S-P times for the new location
C     for each station.
C
      DO 250 I=1,NMST
      DO 260 J=1,ITNS
      IF (STNM2(I).EQ.STNM1(J)) GO TO 270
  260 CONTINUE
  270 DELNW1=DELLG(J)-FNWLG(N)
      DELNW2=DELLT(J)-FNWLT(N)
      DELNW3=DELHT(J)-FNWHT(N)
      DISTNW=SQRT(DELNW1*DELNW1+DELNW2*DELNW2+DELNW3*DELNW3)
      DELDS=DISTNW-DIST(J)
      EXSP(I)=DELDS*FV
  250 CONTINUE
C
C     Write out code,location and residual for each event.
C
      WRITE(2,60)CODE(N),FNWLT(N),FNWLG(N),FNWHT(N)
   60 FORMAT(A6,3(3X,F6.3))
C
C     Write out observed and calculated S-P times for each station
C
      DO 300 I=1,NMST
      WRITE(2,61)STNM2(I),DELSP(I),EXSP(I)
   61 FORMAT(42X,A4,3X,F6.3,2X,F6.3)
  300 CONTINUE
C     Calculate and write out expected S-P delays for
C     stations not in data set.
C
      DO 400 I=1,ITNS
      DO 410 J=1,NMST
      IF (STNM1(I).EQ.STNM2(J)) GO TO 400
  410 CONTINUE
      DLLG=DELLG(I)-FNWLG(N)
      DLLT=DELLT(I)-FNWLT(N)
      DLHT=DELHT(I)-FNWHT(N)
```

```
      DST=SQRT(DLLG*DLLG+DLLT*DLLT+DLHT*DLHT)
      DLDST=DST-DIST(I)
      EXMSSP(I)=DLDST*FV
      WRITE(2,62)STNM1(I),EXMSSP(I)
   62 FORMAT(42X,A4,3X,'******',2X,F6.3)
  400 CONTINUE
C
C     Convert lat. and long. into degrees and minutes.
C
      LGNW=INT((FNWLG(N)/FLGMTK)/60.0)
      FLGNW=(FNWLG(N)/FLGMTK)-(FLOAT(LGNW)*60.0)
      LGNWD(N)=LGNW+MELGD
      FLGNWM(N)=FLGNW+FMELGM
      IF (FLGNWM(N).LT.0.0) THEN
         FLGNWM(N)=FLGNWM(N)+60.0
         LGNWD(N)=LGNWD(N)-1
      ENDIF
      LTNW=INT((FNWLT(N)/FMTKM)/60.0)
      FLTNW=(FNWLT(N)/FMTKM)-(FLOAT(LTNW)*60.0)
      LTNWD(N)=LTNW+MELTD
      FLTNWM(N)=FLTNW+FMELTM
      IF (FLTNWM(N).LT.0.0) THEN
         FLTNWM(N)=FLTNWM(N)+60.0
         LTNWD(N)=LTNWD(N)-1
      ENDIF
      HTNW(N)=FNWHT(N)+FMEDEP
C
C     Write out location coordinates to channel 3
C
      WRITE(3,90)LTNWD(N),FLTNWM(N),LGNWD(N),FLGNWM(N),HTNW(N)
   90 FORMAT(18X,I2,1X,F6.3,I3,1X,2F6.3,24X)
C
 1000 CONTINUE
      GO TO 1002
 1003 WRITE(7,40)
   40 FORMAT('  N=31, INCREASE DIMENSIONS')
 1001 WRITE(2,65)
   65 FORMAT('$')
      STOP 'END OF INPUT FILE'
 1002 STOP 'ERROR'
      END
C
C
C
C
C
C
C**********************************************************************************************
C
C     SUBROUTINE MATIN3(N,Y)
C
C     SYMMETRIC 3X3 MATRIX INVERSION
C
C**********************************************************************************************
      SUBROUTINE MATIN3(N,Y)
      DIMENSION A(20),B(20),N(3,3),Y(3,3)
      DO 1 I=1,3
      DO 1 J=1,3
    1 A((I-1)*3+J)=FLOAT(N(J,I))
      B(1)=1.0/A(1)
      DO 2 I=2,9
    2 B(I)=0.0
      MM=1
      KN=0
      DO 3 M=2,3
      K=M-1
      MM=MM+4
      KN=KN+3
      EK=A(MM)
      MI=M-3
      DO 4 I=1,K
      MI=MI+3
      IJ=I-3
      JM=KN
```

```
      DO 4 J=1,K
      IJ=IJ+3
      JM=JM+1
    4 EK=EK-A(MI)*B(IJ)*A(JM)
      B(MM)=1.0/EK
      MI=M-3
      IM=KN
      DO 5 I=1,K
      IM=IM+1
      IJ=I-3
      JM=KN
      DO 6 J=1,K
      IJ=IJ+3
      JM=JM+1
    6 B(IM)=B(IM)-B(IJ)*A(JM)*B(MM)
      MI=MI+3
    5 B(MI)=B(IM)
      IM=KN
      DO 3 I=1,K
      IM=IM+1
      MJ=M-3
      IJ=I-3
      DO 3 J=1,K
      MJ=MJ+3
      IJ=IJ+3
    3 B(IJ)=B(IJ)+B(IM)*B(MJ)*EK
      DO 7 I=1,3
      DO 7 J=1,3
    7 Y(J,I)=B((I-1)*3+J)
      END
C*******************************************************************************************
```

INPUT FILE

A typical input file (channel 1) for program RELOC (as listed above). The station list must end with a blank line and the delay times for each event are separated by four dollar signs ($$$$).

```
SE 2955.65 4038.91 614          !
TE 2959.28 4037.70 648          !
AY 2956.55 4036.03 995          !   Station name and coordinates
PB 3003.09 4038.21 847          !
DP 2959.97 4041.29 190          !
KS 3004.20 4041.40 140          !

2954.14 4040.44 07.47           !   Master event coordinates
A1                              !   Event code
DP -0.003                       !
AY  0.001                       !   Station name and delay
PB -0.003                       !     in milliseconds
SE -0.003                       !
$$$$
A2
DP -0.003
AY  0.001
PB -0.002
SE  0.000
$$$$
A3
DP  0.010
AY  0.000
SE  0.018
$$$$
A4
DP  0.016
AY  0.021
PB  0.019
SE  0.022
TE  0.018
$$$$
A5
DP -0.001
AY -0.008
PB  0.000
SE -0.005
TE -0.003
KS -0.001
$$$$
```

OUTPUT FILES

The two files listed below are the corresponding output files created by the program RELOC on channels 2 and 3 for the input file listed above. In the first file (channel 2) the location of each event is given as the difference between it and the master event in kilometres. For each station the observed and calculated time delays are shown. The second file contains one line for each event, starting with the master event, giving the epicentre in degrees and minutes and the depth in kilometres (all locations are relative to the master event).

Channel 2 :

VP = 6.00
VS = 3.40

CODE	LAT.	LONG.	HT.	STN.	DOBS	DCALC
A1	0.030	0.013	0.024			
				DP	-0.003	-0.004
				AY	0.001	0.000
				PB	-0.003	-0.002
				SE	-0.003	-0.002
				TE	******	-0.001
				KS	******	-0.003
A2	0.022	0.026	0.001			
				DP	-0.003	-0.003
				AY	0.001	0.001
				PB	-0.002	-0.002
				SE	0.000	0.000
				TE	******	-0.001
				KS	******	-0.003
A3	-0.200	0.200	-0.267			
				DP	0.010	0.009
				AY	0.000	0.000
				SE	0.018	0.018
				TE	******	-0.002
				PB	******	-0.009
				KS	******	-0.003
A4	0.068	-0.052	-0.143			
				DP	0.016	0.016
				AY	0.021	0.020
				PB	0.019	0.017
				SE	0.022	0.021
				TE	0.018	0.020
				KS	******	0.013
A5	-0.041	-0.023	0.039			
				DP	-0.001	-0.001
				AY	-0.008	-0.006
				PB	0.000	-0.002
				SE	-0.005	-0.006
				TE	-0.003	-0.004
				KS	-0.001	0.001

Channel 3 :

```
40 40.440 29 54.140 7.470
40 40.456 29 54.149 7.494
40 40.452 29 54.159 7.471
40 40.332 29 54.282 7.203
40 40.477 29 54.103 7.327
40 40.418 29 54.124 7.509
```

Appendix 2

```
C*******************************************************************************
C
C     SERDEL V3.00
C
C     SERDEL computes the apparent delay between two time series in either the time domain
C     or frequency domain.  The window size is set at 0.64 seconds and 5 seconds of data
C     taken from GSRG standard data files is analysed.  The files must be input in
C     chronological order.
C
C     The program must be linked with the GSRG seismogram handling library SGMLIB.NV, the
C     INTLIB library and a plotting library :
C
C          LINK SERDEL,LIB:(SGMLIB.NV,INTLIB,TK4014) for terminal XK1 or Tektronix 4014
C
C          LINK SERDEL,LIB:(SGMLIB.NV,INTLIB,TK4112) for tektronix terminal 4112
C
C          LINK SERDEL,LIB:(SGMLIB.NV,INTLIB),L:LASLIB,LIB:TK4014 for the laser printer
C                                                  (LASLIB can be found in DP:LASER.DSK)
C
C     Alan Logan     22-MAR-87
C
C*******************************************************************************
C
C     Constants
      CHARACTER*5 VERSION
      PARAMETER ( VERSION= 'V3.00' )
      INTEGER INTERVAL
      PARAMETER ( INTERVAL= 2 )
      INTEGER MAIN LENGTH, SUB LENGTH
      PARAMETER ( MAIN LENGTH= 436, SUB LENGTH= 64 )
      INTEGER NO POINTS
      PARAMETER ( NO POINTS= MAIN LENGTH + SUBLENGTH )
      INTEGER NO DELAYS
      PARAMETER ( NO DELAYS= MAIN LENGTH / INTERVAL + 1 )
      REAL X ORIGIN, Y S1 ORIGIN, Y S2 ORIGIN, Y ORIGIN DELAY
      PARAMETER ( X ORIGIN= 1.0, Y S1 ORIGIN= 9.0, Y S2 ORIGIN= 6.8, Y ORIGIN DELAY= 2.9 )
      REAL Y T1 ORIGIN, Y T2 ORIGIN
      PARAMETER ( Y T1 ORIGIN= 10.5, Y T2 ORIGIN= 0.4 )
      REAL X LENGTH
      PARAMETER ( X LENGTH= 6.5 )
      REAL TICK HEIGHT
      PARAMETER ( TICK HEIGHT= 0.07 )
C
C     Variables
      CHARACTER*27 HEAD1, HEAD2      ! Label for series 1, 2 respectively
      LOGICAL SCALE HEAD
      INTEGER DOMAIN CHOICE, END CHOICE
      REAL RATE, RATE1, RATE2        ! Sampling rate of both series (if same), first series,
     1                                 second series
C
C     Arrays
      INTEGER S1 (NO POINTS), S2 (NO POINTS) ! Hold the two time series
      REAL DELAY (NO DELAYS) ! Holds apparent time delay
C
C     Initialize plotter
C
      CALL PLOTS
      CALL FACTOR (1.0)
C
C     Input file names, extract data and select either time or frequency domain
C
      WRITE (7,'(/2A//A/A//)') ' SERDEL Version ', VERSION,
     1                      '    Performs either time domain or frequency domain method of',
     2                      ' analysis for measuring the time delay between similar
     3                        seismograms'
C
30    WRITE (7,'(A/)') ' *****  Files must be input in chronological order ***** '
10    WRITE (7,'(A/)') ' First File :'
      CALL GET SERIES (S1, HEAD1, RATE1)
      WRITE (7,'(A/)') ' Second File :'
      CALL GET SERIES (S2, HEAD2, RATE2)
C
C     Check that sampling rates are equal (program will prompt for new file names if they
C     are not)
```

```
C
      IF (RATE1 .NE. RATE2) THEN
         WRITE (7,'(A,F6.1,A,F6.1)') ' Error ; sampling intervals are unequal. RATE1=',
     1                               RATE1, ' RATE2=', RATE2
         GO TO 10
         ENDIF
      RATE= RATE1
20    WRITE (7,'(/A/A/A//)') ' In which domain do you wish to calculate the time delay :',
     1                       '     1  Frequency','     2  Time'
      CALL ASKI (DOMAIN CHOICE, 'Select : ')
C
C     Calculate time delay according to the domain selected
C
      IF (DOMAIN CHOICE .EQ. 1) THEN
         CALL GET DELAY (S1, S2, DELAY, RATE, NO POINTS, NO DELAYS, INTERVAL, SUB LENGTH)
         ELSE IF (DOMAIN CHOICE .EQ. 2) THEN
         CALL GET TIME DELAY (S1, S2, DELAY, RATE, NO POINTS, NO DELAYS, INTERVAL,
     1                                                                  SUB LENGTH)
         ELSE
         WRITE (7,'(/A/)') ' You must select either 1 or 2, try again'
         GO TO 20
         ENDIF
C
C     Plot time scales at the top and bottom of the page
C
      SCALE HEAD= .FALSE.
      CALL TIME SCALE (X ORIGIN, Y T1 ORIGIN, RATE, X LENGTH, NO POINTS, -TICK HEIGHT,
     1                                                  SCALE HEAD, DOMAIN CHOICE)
      SCALE HEAD= .TRUE.
      CALL TIME SCALE (X ORIGIN, Y T2 ORIGIN, RATE, X LENGTH, NO POINTS, TICK HEIGHT,
     1                                                  SCALE HEAD, DOMAIN CHOICE)
C
C     PLot original seismograms
C
      CALL PLOT SEISMOGRAM (S1, NO POINTS, HEAD1, X ORIGIN, Y S1 ORIGIN, X LENGTH)
      CALL PLOT SEISMOGRAM (S2, NO POINTS, HEAD2, X ORIGIN, Y S2 ORIGIN, X LENGTH)
C
C     Plot size of window used
C
      CALL PLOT WINDOW (SUB LENGTH, X LENGTH, NO POINTS)
C
C     Plot time delay below seismograms
C
      CALL PLOT DELAY (DELAY, NO DELAYS, SUB LENGTH, INTERVAL, RATE, X ORIGIN,
     1                                                  Y ORIGIN DELAY, X LENGTH)
C
C     Select whether to recalculate the time delay in a different domain, analyse new series
C     or exit the program
C
      WRITE (7,'(/A/A/A/A//)') ' Do you wish to :','    0  Exit',
     1'    1  Recalculate time delay in different domain','    2  Start with new series'
      CALL ASKI (END CHOICE, 'Select : ')
      IF (END CHOICE .EQ. 1) THEN
         CALL NEWPAGE
         GO TO 20
         ELSE IF (END CHOICE .EQ. 2) THEN
         CALL NEWPAGE
         GO TO 30
         ENDIF
      CALL PLOT (0., 0., 999)
      CALL EXIT
      END
C
C
C
C
C
C
```

```
C*******************************************************************************
C
C     SUBROUTINE GET SERIES (S, HEAD, RATE)
C
C     Gets a time series S of length LENGTH (parameter), a CHARACTER*10 descriptor, HEAD,
C     and the digitising rate, RATE.
C
C*******************************************************************************
      SUBROUTINE GET SERIES (S, HEAD, RATE)
C
C     Constants
      INTEGER LENGTH, MAX AMP
      PARAMETER ( LENGTH= 500 )     ! Length of time series
      PARAMETER ( MAX AMP = 2100 ) ! Saturation level
C
C     Arguments
      INTEGER S (LENGTH)
      CHARACTER*27 HEAD
      REAL RATE
C
C     Variables
      CHARACTER*15 FILE NAME        ! Name of data file
      CHARACTER*11 TIME STRING      ! ASCII string representation of arrival time
      CHARACTER*9  DATE STRING      ! Date of event (dd-mmm-yy)
      CHARACTER*5  STRING           ! Temporary storage
      CHARACTER*4  STATION NAME, OLD STATION NAME
      DATA OLD STATION NAME /' '/
      INTEGER CHANNEL               ! Indicates channel number of statrion required
      INTEGER HOUR, MINUTE          ! Hour and minute of arrival time
      INTEGER AMP FACTOR
      INTEGER NOISY (LENGTH)
      INTEGER ICODE
      INTEGER START HOUR, START MINUTE ! Hour & minute of start time
      REAL START SECOND             ! Second of record start time
      REAL SECOND                   ! Second of arrival time
      REAL START POINT              ! First point required from file
      REAL REC LENGTH               ! Length of record in minutes
      REAL START DELAY              ! Offset of segment start from beginning of record
     1                                in minutes
      LOGICAL AMPLIFY, NOISE
C
C     Common blocks
      CHARACTER*80 HEADER
      CHARACTER*2  DUMMY
      COMMON /HDR/ DUMMY, HEADER (51)
      INTEGER  TITLE, NETWORK, RECORD, END, STCARD (40)
      COMMON /CARDS/ TITLE, NETWORK, RECORD, END, STCARD
C
C     Input file name and check that it exists
C
100   CALL ASKFN (FILE NAME , '      File Name ? ')
      ICODE= IGTHDR (1, FILE NAME)
            IF (ICODE .LT. 0) THEN
               WRITE (7,'(3A/)') '      Sorry, can''t find ', FILE NAME, '. Try again.'
               GO TO 100
               ENDIF
C
C     Extract date, time, record length and rate from the file header
C
      STRING= HEADER (RECORD) (50:54)
      READ (STRING,'(F5.2)', ERR=190 ) REC LENGTH
      STRING= HEADER (RECORD) (62:66)
      READ (STRING,'(F5.1)', ERR=190 ) RATE
      DATE STRING= HEADER (RECORD) (10:18)
      TIME STRING= HEADER (RECORD) (20:30)
      IF (READ TIME (TIME STRING, START HOUR, START MINUTE, START SECOND) .LT. 0) THEN
            WRITE (7,'(2A/)') '       Failed to decode record start time - ', TIME STRING
            GO TO 100
            ENDIF
      WRITE (7,'(3A,F5.2,A/)') '       Start time of record is ', TIME STRING, ' and length
     1                          is ', REC LENGTH, ' minutes.'
C
C     Input station required and check that it exists
C
```

```
105   CALL ASKS (STATION NAME, '      Which station do you want ? ', OLD STATION NAME, , 4)
      I= 1
108   IF (HEADER (STCARD(I)) (13:16) .NE. STATION NAME) THEN
         I= I+1
         IF (I .GT. 40) THEN
            WRITE (7,'(3A/)') '       Can''t find a station called ', STATION NAME,
     1                        '.  Try again'
            GO TO 105
            ENDIF
         GO TO 108
         ENDIF
      OLD STATION NAME= STATION NAME
      CHANNEL= I
C
C     Select start time from which 5 seconds of data will be extracted and check that it is
C     consistent with the file start time and length
C
110   CALL ASKS (TIME STRING, '      Start time of analysis ? [Format - hh:mm:ss.ss] ', ,
     1                                                                              8, 11)
      IF (READ TIME (TIME STRING, HOUR, MINUTE, SECOND) .LT. 0) GO TO 110
      START DELAY= (HOUR - START HOUR) * 60. + (MINUTE - START MINUTE) + (SECOND -
     1                                                                  STARTSECOND)/60.
      SEG LENGTH= LENGTH / RATE / 60.
      IF (START DELAY .LE. 0. .OR. START DELAY + SEG LENGTH .GT. REC LENGTH) THEN
            WRITE (7,'(A/)') '       Mismatch between time requested and available record.
     1                                                                        Try again'
            GO TO 110
            ENDIF
      START POINT= NINT (START DELAY * RATE * 60.)
C
C     Extract data from file and put it into series S
C
      ICODE= IGTDAT (1, CHANNEL, START POINT, LENGTH, 1, S)
            IF (ICODE .LT. 0) THEN
               WRITE (7,'(A,I3,A/)') '       Fatal error (Code=', ICODE, ') on reading data'
               CALL EXIT
               ENDIF
C
C     Remove any DC bias from series S
C
      CALL REMOVE MEAN (S, LENGTH)
C
C     Amplify series S if required.  The signal will saturate at a value of 2100 (MAX AMP)
C
      CALL ASK (AMPLIFY, ' Do you wish to amplify this signal ?', .FALSE. )
      IF (AMPLIFY) THEN
         CALL ASKI (AMP FACTOR, ' Factor:')
         I=1
  120    IF (I .LE. LENGTH) THEN
            S(I) = S(I) * AMP FACTOR
            IF (ABS(S(I)) .GT. MAX AMP) THEN
               S(I) = MAX AMP * (S(I)/ABS(S(I)))
            ENDIF
            I=I+1
            GO TO 120
         ENDIF
      ENDIF
C
C     Add noise to series S if required.  The noise is taken from either the start or the
C     end of the file (depending on arrival time) and may be amplified
C
      CALL ASK (NOISE, ' Do you wish to add noise ?', .FALSE.)
      IF (NOISE) THEN
         IF (START DELAY .LE. 5.0/60.0) THEN
            WRITE (7, '(A/)') ' Using last five seconds of data file'
            START DELAY = REC LENGTH - 6.1/60.0
            START POINT = NINT(START DELAY * RATE * 60.0)
         ELSE
            WRITE (7, '(A/)') ' Using first five seconds of data file'
            START POINT = 0.0
         ENDIF
         ICODE = IGTDAT (1, CHANNEL, START POINT, LENGTH, 1, NOISY)
         IF (ICODE .LT. 0) THEN
            WRITE (7, '(A,I3,A/)') '      Fatal error ( code = ', ICODE, ') on reading data'
```

```
            CALL EXIT
         ENDIF
         CALL REMOVE MEAN (NOISY, LENGTH)
         CALL ASKI (AMP FACTOR, ' Noise Scale Factor: ')
         I=1
  130    IF (I .LE. LENGTH) THEN
            S(I) = S(I) + NOISY(I) * AMP FACTOR
            I=I+1
            GO TO 130
         ENDIF
      ENDIF
C
C     Read station name, date and time into variable HEAD
C
      HEAD= ' '
      HEAD (1:4)= STATION NAME
      HEAD (7:15)= DATE STRING
      HEAD (17:27)= TIME STRING
C
      RETURN
C
190      WRITE (7,'(2A/)') '       Failed to decode field ', STRING
         GO TO 100
      END
C
C
C
C
C
C
C*****************************************************************************************
C
C     INTEGER FUNCTION READ TIME (STRING, HOUR, MINUTE, SECOND)
C
C     Decodes the CHARACTER*11 ASCII STRING of format hh:mm:ss.ss into INTEGER HOUR, MINUTE
C     and REAL SECOND
C
C*****************************************************************************************
      INTEGER FUNCTION READ TIME (STRING, HOUR, MINUTE, SECOND)
C
C     Arguments
      CHARACTER*11 STRING
      INTEGER HOUR, MINUTE
      REAL SECOND
C
C
      CALL ERRSET (56, .TRUE., .FALSE., .TRUE., .FALSE.)
      READ (STRING, '(I2,X,I2,X,F5.2)', ERR=210) HOUR, MINUTE, SECOND
      READ TIME= 1
      RETURN
210      READ TIME= -1
         RETURN
      END
C
C
C
C
C
C
```

```
C*******************************************************************************
C
C     SUBROUTINE GET TIME DELAY (S1, S2, DELAY, RATE, NO POINTS, NO DELAYS,
C                                                              INTERVAL, SUB LENGTH)
C
C     Computes relative time delay (in the time domain) between series S1 and S2 (sampling
C     rate = RATE, number of data points = NO POINTS) as a function of time along the
C     series.  A window of length SUB LENGTH is used at intervals determined by INTERVAL.
C     The time delay is stored in a series DELAY (sampling rate = RATE, number of data
C     points = NO DELAYS)
C
C*******************************************************************************
      SUBROUTINE GET TIME DELAY (S1, S2, DELAY, RATE, NO POINTS, NO DELAYS,
     1                           INTERVAL, SUB LENGTH)
C
C     Arguments:
      INTEGER NO POINTS, NO DELAYS
      INTEGER INTERVAL, SUB LENGTH
      INTEGER S1 (*), S2 (*)
      REAL DELAY (*)
      REAL RATE
C
C     Constants
      INTEGER MAX SUB LENGTH
      PARAMETER ( MAX SUB LENGTH= 64 )
      INTEGER FIRST
      PARAMETER ( FIRST= 4 )
      INTEGER DOUBLE LENGTH
      PARAMETER ( DOUBLE LENGTH = 2 * MAX SUB LENGTH )
C
C     Variables:
      INTEGER ZERO POINT
      INTEGER START OFFSET
      REAL SUB1 (MAX SUB LENGTH), SUB2 (MAX SUB LENGTH)
      REAL CROSSC (DOUBLE LENGTH)
      REAL PEAK, FACTOR
C
C     Check that the window length is not too long for the series being analysed
C
      IF (SUB LENGTH .GT. MAX SUB LENGTH) THEN
         WRITE (7,'(A)') ' SUB LENGTH too long.  Increase MAX SUB LENGTH in subroutine GET
     1DELAY and GET TIME DELAY.'
         ENDIF
      START OFFSET= 0
      J=1
C
C     Extract sub-series determined by the position and size of the window (START OFFSET and
C     SUB LENGTH)
C
410   IF (START OFFSET .LE. NO POINTS - SUB LENGTH) THEN
            DO 420 I= 1, SUB LENGTH
            SUB1 (I)= S1 (START OFFSET + I)
420         SUB2 (I)= S2 (START OFFSET + I)
C
C     Cosine taper sub-series to reduce edge effects
C
         CALL CSTPR (SUB1, SUB LENGTH, 50.)
         CALL CSTPR (SUB2, SUB LENGTH, 50.)
C
C     Calculate the cross-correlation function (CROSSC)
C
         CALL X CORRELATION (SUB1, SUB2, SUB LENGTH, CROSSC, FACTOR)
         ZERO POINT = SUB LENGTH
C
C     Measure the position of the central peak (PEAK) of the cross-correlation function
C
         CALL GET PEAK (CROSSC, SUB LENGTH, PEAK, FACTOR, ZERO POINT)
         DELAY (J) = PEAK
         J=J+1
         START OFFSET= START OFFSET + INTERVAL
         GO TO 410
         ENDIF
      RETURN
      END
```

```
C*****************************************************************************
C
C     SUBROUTINE CSTPR (RDATA, NPTS, PERCNT)
C
C     Cosine tapers a time series RDATA of NPTS, where PERCNT is the percentage to be
C     tapered at each end
C
C     Mod of one of Russ Evans' routines
C
C     Bob McGonigle
C
C*****************************************************************************
      SUBROUTINE CSTPR (RDATA, NPTS, PERCNT)
C
C     Arguments
      INTEGER NPTS
      REAL PERCNT
      REAL RDATA (1)
C
C     Variables
      INTEGER ICOS1, ICOS2, IA, IB, INC, IEND, FI
      REAL PI, F, X
C
C
      PI=3.141592654
      ICOS1=FLOAT(NPTS)*PERCNT/100.
      IF(ICOS1.LE.1)RETURN
      ICOS2=NPTS-ICOS1+1
      IA=1
      IB=ICOS1
      INC=1
      IEND=1
      J=1
      F=PI/FLOAT(ICOS1-1)
110      DO 120 I=IA,IB,INC
         FI=I-1
         X=RDATA(J)
         RDATA(J)=X*(1.-COS(FI*F))*0.5
120      J=J+1
      IF(IEND.EQ.2)RETURN
      IEND=2
      IA=ICOS1
      IB=1
      INC=-1
      J=ICOS2
      GO TO 110
      END
C
C
C
C
C
C
```

```
C*******************************************************************************
C
C     SUBROUTINE REMOVE MEAN (SERIES, LENGTH)
C
C     Subtracts the mean from integer series SERIES (length LENGTH). Uses first 100 points
C     only to avoid any possible distortion by the signal
C
C*******************************************************************************
      SUBROUTINE REMOVE MEAN (SERIES, LENGTH)
C
C     Arguments
      INTEGER LENGTH
      INTEGER SERIES (LENGTH)
C
C     Variables
      REAL TOTAL
      INTEGER MEAN
C
C
      TOTAL= 0.0
         DO 810 I= 1, 100
810      TOTAL= TOTAL + FLOAT(SERIES (I))
      MEAN= NINT(TOTAL / 100)
         DO 820 I= 1, LENGTH
820      SERIES (I)= SERIES (I) - MEAN
      RETURN
      END
C
C
C
C
C
C
C*******************************************************************************
C
C     SUBROUTINE PLOT SEISMOGRAM (SERIES, NO POINTS, HEAD, XO, YO, X LENGTH)
C
C     Plots seismogram SERIES of length NO POINTS (no. of points) at rate RATE with the
C     origin at (XO, YO).  X LENGTH is the length of plot in inches.  The date time and
C     station name are encoded in HEAD
C
C*******************************************************************************
      SUBROUTINE PLOT SEISMOGRAM (SERIES, NO POINTS, HEAD, XO, YO, X LENGTH)
C
C     Arguments
      INTEGER NO POINTS
      INTEGER SERIES (NO POINTS)
      CHARACTER*27 HEAD
      REAL RATE, XO, YO
      REAL X LENGTH
C
C     Constants:
      CHARACTER*1 ZERO
      PARAMETER ( ZERO= '0' )
      REAL TICK
      PARAMETER ( TICK= 0.05 )
C
C     Variables
      CHARACTER*5 MAX,MIN
      CHARACTER*10 TITLE
      DATA TITLE / 'SEISMOGRAM' /
      INTEGER MAX AMPLITUDE, MIN AMPLITUDE
      REAL SCALE FACTOR
      REAL TICK1
      REAL X, Y
C
C     Calculate the scaling factor from the maximum amplitude of SERIES
C
      MAX AMPLITUDE= 0
      I=1
910   IF (I .LE. NO POINTS) THEN
         IF (IABS(SERIES(I)) .GT. MAX AMPLITUDE) THEN
            MAX AMPLITUDE= IABS(SERIES(I))
            ENDIF
```

```
         I=I+1
         GO TO 910
         ENDIF
      MIN AMPLITUDE= - MAX AMPLITUDE
      SCALE FACTOR= 1.0 / MAX AMPLITUDE
C
C     Plot axes
C
      I= 1
      Y= YO
      X= XO + X LENGTH + 0.1
      TICK1= -TICK
915   IF (I .LE. 2) THEN
         CALL PLOT (X+TICK1, Y-1.0, 3)
         CALL PLOT (X, Y-1.0, 2)
         CALL PLOT (X, Y, 2)
         CALL PLOT (X+TICK1, Y, 2)
         CALL PLOT (X, Y, 3)
         CALL PLOT (X, Y+1.0, 2)
         CALL PLOT (X+TICK1, Y+1.0, 2)
         TICK1= TICK
         X= XO - 0.1
         I= I + 1
         GO TO 915
         ENDIF
C
C     Label axes
C
      WRITE (MAX, '(I5)') MAX AMPLITUDE
      WRITE (MIN, '(I5)') MIN AMPLITUDE
      CALL SYMBOL (X-0.5, Y+1.0-0.05, 0.10, MAX, 0.0, 5)
      CALL SYMBOL (X-0.2, Y-0.05, 0.10, ZERO, 0.0, 1)
      CALL SYMBOL (X-0.5, Y-1.0-0.05, 0.10, MIN, 0.0, 5)
      CALL SYMBOL (X-0.5, Y-0.75, 0.15, TITLE, 90.0, 10)
      CALL SYMBOL (XO+0.1, YO+1.0, 0.10, HEAD, 0.0, 27)
C
C     Plot seismogram
C
      X= XO
      CALL SPLT (X, Y, SERIES, NO POINTS, SCALE FACTOR, X LENGTH)
      RETURN
      END
C
C
C
C
C
C
```

```
C*******************************************************************************
C
C     SUBROUTINE SPLTR (XO, YO, DAT, NPTS, YSF, XLEN)
C
C     Plots real arrays
C
C*******************************************************************************
      SUBROUTINE SPLTR (XO, YO, DAT, NPTS, YSF, XLEN)
C
C     Arguments
      INTEGER NPTS
      REAL XO, YO, YSF, XLEN
      REAL DAT (1)
C
C     Variables
      INTEGER IP
      REAL D, X, Y
C
C
      IP=3
      D= XLEN / (NPTS - 1 )
      X=XO
      DO 36 I=1,NPTS
      Y= DAT (I) * YSF + YO
      CALL PLOT (X, Y, IP )
      IP=2
   36 X=X+D
      CALL PLOT (X, Y, 3 )
      RETURN
      END
C
C
C
C
C
C
C*******************************************************************************
C
C     SUBROUTINE PLOT DELAY (DELAY, LENGTH, SUB LENGTH, INTERVAL, RATE, XO, YO, X LENGTH)
C
C     Plots delay DELAY (length LENGTH) calculated using windows of length SUB LENGTH and at
C     a spacing determined by INTERVAL.  Windows digitised at RATE samples / second.  Axis
C     origin at (XO, YO).  X LENGTH is length of plot in inches.
C
C
C*******************************************************************************
      SUBROUTINE PLOT DELAY (DELAY, LENGTH, SUB LENGTH, INTERVAL, RATE, XO, YO, X LENGTH)
C
C     Arguments
      INTEGER LENGTH, INTERVAL, SUB LENGTH
      REAL DELAY (LENGTH)
      REAL XO, YO
      REAL X LENGTH
      REAL RATE
C
C     Constants
      CHARACTER*21 AXIS LABEL
      PARAMETER ( AXIS LABEL= 'DELAY IN MILLISECONDS' )
      REAL HEIGHT
      PARAMETER ( HEIGHT= 4. )
      REAL AMP FACTOR
      PARAMETER ( AMP FACTOR= 1.0 )
      REAL TICK SIZE
      PARAMETER ( TICK SIZE= 0.07 )
      REAL PROPORTION
      PARAMETER ( PROPORTION= 15.0 )
C
C     Variables
      CHARACTER*6 LABEL
      INTEGER NO POINTS, X POINT
      INTEGER TICK NUMBER
      LOGICAL TAG
      LOGICAL OK1, OK2
      REAL MAXIMUM, RESET MAX
```

```
      REAL MAX AMPLITUDE
      REAL TICK STEP, Y FACTOR
      REAL X INCREMENT
      REAL WHOLE SECONDS
      REAL X,Y
C
C     Convert delay from seconds to milliseconds.
C
         DO 940 I=1, LENGTH
940      DELAY(I)= 1000. * DELAY(I)
C
C     Calculate absolute maximum value of delay.
C
      MAX AMPLITUDE= SCALE REAL ARRAY (DELAY, LENGTH, PROPORTION)
      MAXIMUM= AMP FACTOR * MAX AMPLITUDE
C
C     If delays all zero set MAXIMUM to 10.0.
C
      IF (MAXIMUM .LT. 10.0) THEN
         MAXIMUM= 10.0
         ENDIF
C
C     Calculate axis scale
C
      CALL GET INCREMENT (MAXIMUM, TICK STEP, TICK NUMBER)
C
C     RESET MAX is the new maximum value to be drawn on the axes.
C
      RESET MAX= TICK STEP * TICK NUMBER
C
C     RESET MAX may be altered if desired
C
      WRITE (7,'(A,I2,A,F4.1/A,F6.2/)') ' Delay plot scale will be comprised
     1 of ', TICK NUMBER, ' increments of ', TICK STEP, ' up to a scale
     2 maximum of ', RESET MAX
C
      CALL ASK (OK1, 'Do you wish to reset these values ?')
      IF (OK1) THEN
  990    CALL ASKR (TICK STEP, 'New incremental step :')
         CALL ASKI (TICK NUMBER, 'Number of steps :')
         RESET MAX= TICK STEP * TICK NUMBER
         WRITE (7,'(A,F6.2/)') ' New scale maximum= ', RESET MAX
         CALL ASK (OK2, 'Is this OK ?')
         IF (.NOT. OK2) THEN
            GO TO 990
            ENDIF
         ENDIF
C
C     Set scale factor
C
      Y FACTOR= HEIGHT / 2. / RESET MAX
      TAG= .TRUE.
C
C     Plot axes
C
      CALL PLOT AXIS (XO-0.1, YO, TICK STEP, Y FACTOR, TICK NUMBER, TICK SIZE, TAG)
      CALL PLOT AXIS (XO-0.1, YO, -TICK STEP, Y FACTOR, TICK NUMBER, TICK SIZE, TAG)
      TAG= .FALSE.
      CALL PLOT AXIS (XO+X LENGTH+0.1, YO, TICK STEP, Y FACTOR, TICK NUMBER, -TICK SIZE,
     1                TAG)
      CALL PLOT AXIS (XO+X LENGTH+0.1, YO, -TICK STEP, Y FACTOR, TICK NUMBER, -TICK SIZE,
     1                TAG)
      CALL SYMBOL (XO-0.65, YO-1.50, 0.15, AXIS LABEL, 90.0, 21)
      X= XO
      Y= YO
      CALL PLOT (X, Y, 3)
      X= X + 0.2
975   IF (X .LE. (X LENGTH + XO)) THEN
         CALL PLOT (X, Y, 2)
         X= X + 0.2
         CALL PLOT (X, Y, 3)
         X= X + 0.2
         GO TO 975
         ENDIF
```

```
      IF (X .LT. (X LENGTH + XO + 0.2)) THEN
         X= XO + X LENGTH
         CALL PLOT (X, Y, 2)
         ENDIF
C
C     Plot data
C
      NO POINTS= (LENGTH * INTERVAL) + SUB LENGTH
      X INCREMENT= X LENGTH / NO POINTS
      X POINT= SUB LENGTH / 2
      I=1
980   IF (I .LE. LENGTH) THEN
         X= XO + (X POINT * X INCREMENT)
         IF (ABS (DELAY (I)) .LE. RESET MAX) THEN
            Y= YO + (DELAY (I) * Y FACTOR)
            CALL SYMBOL (X, Y, 0.07, 3, 0.0, -1)
         ELSE IF (DELAY(I) .GT. 0.0) THEN
            IF (ABS (DELAY (I-1)) .LE. RESET MAX) THEN
               Y = YO + (DELAY (I-1) * Y FACTOR) + 0.15
               CALL SYMBOL (X, Y, 0.07, 2, 0.0, -1)
               CALL PLOT (X, Y, 3)
               CALL PLOT (X, Y-0.12, 2)
            ENDIF
            IF (ABS (DELAY (I+1)) .LE. RESET MAX) THEN
               Y = YO + (DELAY (I+1) * Y FACTOR) + 0.03
               CALL SYMBOL (X, Y, 0.07, 2, 180.0, -1)
               CALL PLOT (X, Y, 3)
               CALL PLOT (X, Y+0.12, 2)
            ENDIF
         ELSE
            IF (ABS (DELAY (I-1)) .LE. RESET MAX) THEN
               Y = YO + (DELAY (I-1) * Y FACTOR) -0.15
               CALL SYMBOL (X, Y, 0.07, 2, 180.0, -1)
               CALL PLOT (X, Y, 3)
               CALL PLOT (X, Y+0.12, 2)
            ENDIF
            IF (ABS (DELAY (I+1)) .LE. RESET MAX) THEN
               Y = YO + (DELAY (I+1) * Y FACTOR) -0.03
               CALL SYMBOL (X, Y, 0.07, 2, 0.0, -1)
               CALL PLOT (X, Y, 3)
               CALL PLOT (X, Y-0.12, 2)
            ENDIF
         ENDIF
         X POINT= X POINT + INTERVAL
         I= I+1
         GO TO 980
      ENDIF
      RETURN
      END
C
C
C
C
C
C
```

```
C*******************************************************************************
C
C     SUBROUTINE GET INCREMENT (MAXIMUM, TICK STEP, TICK NUMBER)
C
C     Given the maximum value of an array (MAXIMUM), the increment for the y - axis is
C     calculated (TICK STEP) and the number of ticks (TICK NUMBER) needed to cover the
C     array.
C
C*******************************************************************************
      SUBROUTINE GET INCREMENT (MAXIMUM, TICK STEP, TICK NUMBER)
C
C     Arguments
      INTEGER TICK NUMBER
      REAL MAXIMUM, TICK STEP
C
C     Variables
      INTEGER TRUNCATED LOG
      REAL LOG MAX, RATIO
C
      LOG MAX= ALOG10 (MAXIMUM)
      TRUNCATED LOG= INT (LOG MAX)
      IF (LOG MAX .GT. 0.0) THEN
         TICK STEP= 10. ** TRUNCATED LOG
         ELSE
         TICK STEP= 10. ** (TRUNCATED LOG - 1)
         ENDIF
      RATIO= MAXIMUM / TICK STEP
      TICK NUMBER= INT (RATIO + 1.0)
      IF (TICK NUMBER .LE. 3) THEN
         TICK STEP= TICK STEP / 2.
         TICK NUMBER= TICK NUMBER * 2
         ENDIF
      RETURN
      END
C
C
C
C
C
C*******************************************************************************
C
C     SUBROUTINE PLOT AXIS (XO, YO, TICK STEP, FACTOR, TICK NUMBER, TICK SIZE, TAG)
C
C     Plots y-axis with origin (XO, YO), steps of value TICK STEP (TICK NUMBER in total) and
C     scaling factor FACTOR
C
C*******************************************************************************
      SUBROUTINE PLOT AXIS (XO, YO, TICK STEP, FACTOR, TICK NUMBER, TICK SIZE, TAG)
C
C     Arguments
      INTEGER TICK NUMBER
      REAL XO, YO, TICK STEP, TICK SIZE, FACTOR
      LOGICAL TAG
C
C     Variables
      CHARACTER*5 LABEL
      INTEGER Y INTEGER VALUE
      REAL Y VALUE, MAXIMUM
      REAL X, Y
C
      Y VALUE= 0.0
      MAXIMUM= TICK STEP * TICK NUMBER
      CALL PLOT (XO, YO, 3)
      X= XO
960   IF (ABS(Y VALUE) .LE. ABS(MAXIMUM))THEN
         IF ((TICK STEP .LT. 0.0) .AND. (Y VALUE .EQ. 0.0)) THEN
            Y VALUE= Y VALUE + TICK STEP
            GO TO 960
            ENDIF
         Y= YO + (Y VALUE * FACTOR)
         CALL PLOT (X, Y, 2)
         CALL PLOT (X+TICK SIZE, Y, 2)
         IF (TAG) THEN
```

```
            Y INTEGER VALUE= Y VALUE
            WRITE (LABEL, '(I5)') Y INTEGER VALUE
            CALL SYMBOL (X-0.5, Y-0.05, 0.10, LABEL, 0.0, 5)
            ENDIF
         CALL PLOT (X, Y, 3)
         Y VALUE= Y VALUE + TICK STEP
         GO TO 960
         ENDIF
      RETURN
      END
C
C
C
C
C
C
C*************************************************************************************
C
C     SUBROUTINE TIME SCALE (XO, YO, RATE, X LENGTH, NO POINTS, TICK HEIGHT, SCALE HEAD,
C                                                                          DOMAIN CHOICE)
C
C     Marks time scale at the top and bottom of the page with tick marks every second.
C
C*************************************************************************************
      SUBROUTINE TIME SCALE (XO, YO, RATE, X LENGTH, NO POINTS, TICK HEIGHT, SCALE HEAD,
     1                       DOMAIN CHOICE)
C
C     Arguments
      INTEGER NO POINTS
      INTEGER DOMAIN CHOICE
      REAL XO, YO, RATE, X LENGTH, TICK HEIGHT
      LOGICAL SCALE HEAD
C
C     Constants
      CHARACTER*7 SCALE LABEL
      PARAMETER ( SCALE LABEL= 'SECONDS' )
      CHARACTER*26 TITLE1
      CHARACTER*42 TITLE2
      CHARACTER*47 TITLE3
      PARAMETER ( TITLE1= 'RELATIVE DELAY MEASURED BY' )
      PARAMETER ( TITLE2= 'CROSS-CORRELATION IN TIME DOMAIN' )
      PARAMETER ( TITLE3= 'CROSS-CORRELATION IN FREQUENCY DOMAIN' )
C
C     Variables
      REAL X INCREMENT, WHOLE SECONDS, X, Y
C
      IF (SCALE HEAD) THEN
         GO TO 980
         ENDIF
C
C     Write title at the top of the page
C
      CALL SYMBOL (XO, YO+0.35, 0.15, TITLE1, 0.0, 26)
      IF (DOMAIN CHOICE .EQ. 1) THEN
         CALL SYMBOL (XO, YO+0.15, 0.15, TITLE3, 0.0, 47)
         ELSE
         CALL SYMBOL (XO, YO+0.15, 0.15, TITLE2, 0.0, 42)
         ENDIF
C
C     Plot axis with tick marks
C
 980  X INCREMENT= X LENGTH / NO POINTS
      WHOLE SECONDS= AINT(NO POINTS / RATE)
      CALL PLOT (XO, YO, 3)
      CALL PLOT (XO, YO + TICK HEIGHT, 2)
      CALL PLOT (XO, YO, 3)
      Y= YO
      I= 1
970   IF (I .LE. WHOLE SECONDS) THEN
         X= XO + (I * RATE * X INCREMENT)
         CALL PLOT (X, Y, 2)
         CALL PLOT (X, Y + TICK HEIGHT, 2)
         CALL PLOT (X, Y, 3)
         I= I + 1
```

```
         GO TO 970
         ENDIF
      X= XO + X LENGTH
      CALL PLOT (X, Y, 2)
      IF (SCALE HEAD) THEN
         CALL SYMBOL (XO+X LENGTH/2-0.45, YO-0.25, 0.15, SCALE LABEL, 0.0, 7)
         ENDIF
      RETURN
      END
C
C
C
C
C
C
C**********************************************************************************************
C
C     REAL FUNCTION   SCALE REAL ARRAY (DATA, SAMPLES, PROPORTION)
C
C     Returns scale value such that
C       return = minimum ( scale |
C         number { data(i) | abs [data(i)] >= scale } < proportion * samples )
C                                          (Note strict inequality !)
C     Note limitation on DATA that abs [ data (i) ] .le. MAXIMUM
C
C**********************************************************************************************
      REAL FUNCTION   SCALE REAL ARRAY (DATA, SAMPLES, PROPORTION)
C
C     Arguments :
      REAL    DATA (*)      ! Array of data points to be scaled
      INTEGER SAMPLES       ! Length of array DATA
      REAL PROPORTION       ! Limit of samples allowed to lie outside scale
                            !    0.0 le PROPORTION lt 1.0
C
C     Common block:
      INTEGER SCRATCH, MAXIMUM
      PARAMETER ( MAXIMUM= 50 ) ! Largest maximum value anticipated in DATA ...
      COMMON /SCRATCH/ SCRATCH (0:MAXIMUM) ! Array used for scratch storage
C
C     Variables:
      INTEGER SUBTOTAL      ! number { data (i) | abs [ data (i) ] >= I }
      INTEGER LIMIT         ! = PROPORTION * SAMPLES
C
C
C     .. zero SCRATCH ..
710                 DO 720 I= 0, MAXIMUM
720                    SCRATCH (I)= 0
      I= 1
730   IF (I .LE. SAMPLES) THEN
         J= MIN0 (INT (ABS (DATA(I))), MAXIMUM)
         SCRATCH (J)= SCRATCH (J) + 1
         I= I+1
         GO TO 730
         ENDIF
C
      SUBTOTAL= 0
      I= MAXIMUM
      LIMIT= (PROPORTION * SAMPLES) / 100
740   SUBTOTAL= SUBTOTAL + SCRATCH (I)
      IF (SUBTOTAL .LT. LIMIT) THEN
         I= I-1
         GO TO 740
         ENDIF
C
      SCALE REAL ARRAY= FLOAT (I + 1)
      RETURN
      END
C
C
C
C
C
C
```

```
C*****************************************************************************
C
C     SUBROUTINE PLOT WINDOW (SUB LENGTH, X LENGTH, NO POINTS)
C
C     Plots window size between the seismogram and the time delay plot
C
C*****************************************************************************
      SUBROUTINE PLOT WINDOW (SUB LENGTH, X LENGTH, NO POINTS)
C
C     Arguments
      INTEGER SUB LENGTH, NO POINTS
      REAL X LENGTH
C
C     Variables
      CHARACTER*13 TITLE
      PARAMETER ( TITLE= 'WINDOW LENGTH' )
      REAL XO, YO, MARK
      PARAMETER ( XO= 2.0, YO= 5.5, MARK= 0.1 )
      REAL X, X INCREMENT
C
      X INCREMENT= X LENGTH / NO POINTS
      CALL PLOT (XO, YO-MARK, 3)
      CALL PLOT (XO, YO+MARK, 2)
      CALL PLOT (XO, YO-(MARK/4), 3)
      X= XO + (SUB LENGTH * X INCREMENT)
      CALL PLOT (X, YO-(MARK/4), 2)
      CALL PLOT (X, YO-MARK, 3)
      CALL PLOT (X, YO+MARK, 2)
      CALL PLOT (X, YO+(MARK/4), 3)
      CALL PLOT (XO, YO+(MARK/4), 2)
C
      CALL SYMBOL (X+0.2, YO-(MARK/2.), 0.15, TITLE, 0.0, 13)
      RETURN
      END
C
C
C
C
C
C
C*****************************************************************************
C
C     SUBROUTINE X CORRELATION (SUB1, SUB2, SUB LENGTH, CROSSC, FACTOR)
C
C     Computes cross-correlation function (CROSSC) from two sub-sections (SUB1, SUB2, length
C     SUB LENGTH).  FACTOR governs the starting position of the calculation.
C
C*****************************************************************************
      SUBROUTINE X CORRELATION (SUB1, SUB2, SUB LENGTH, CROSSC, FACTOR)
C
C     Arguments:
      INTEGER SUB LENGTH
      REAL FACTOR
      REAL SUB1 (*), SUB2 (*)
      REAL CROSSC (*)
C
C     Variables:
      INTEGER TOTAL, START, FINISH
      REAL INCREMENT
C
      FACTOR = 0.75
      TOTAL = 2 * SUB LENGTH
      START = SUB LENGTH - SUB LENGTH * FACTOR
      FINISH = SUB LENGTH + SUB LENGTH * FACTOR
C
         DO 100 L = START, FINISH
         CROSSC (L) = 0.0
C
            DO 100 K = 1, SUB LENGTH
            M=L+K
            IF ((M.GT.SUB LENGTH) .AND. (M.LE.TOTAL)) THEN
               M= M - SUB LENGTH
               INCREMENT = SUB1 (M) * SUB2 (K)
               CROSSC (L) = CROSSC (L) + INCREMENT
```

```
               ENDIF
C
  100     CONTINUE
C
       RETURN
       END
C
C
C
C
C
C
C**********************************************************************************************
C
C      SUBROUTINE GET PEAK (CROSSC, SUB LENGTH, PEAK, FACTOR, ZERO POINT)
C
C      Measures the position of the peak (PEAK) in function CROSSC which is derived from
C      sub-sections of length SUB LENGTH, cut by FACTOR. ZERO POINT marks the middle of the
C      function.
C
C**********************************************************************************************
       SUBROUTINE GET PEAK (CROSSC, SUB LENGTH, PEAK, FACTOR, ZERO POINT)
C
C      Arguments:
       INTEGER SUB LENGTH, ZERO POINT
       REAL CROSSC (*)
       REAL FACTOR, PEAK
C
C      Variables:
       INTEGER START, FINISH, MAX POINT
       REAL MAX AMPLITUDE, MAX POSITION, X ZERO
       REAL DIFFERENCE (2)
C
       START= SUB LENGTH - SUB LENGTH*FACTOR
       FINISH= SUB LENGTH + SUB LENGTH*FACTOR
C
C      First finds the maximum value of CROSSC
C
       MAX AMPLITUDE= 0.0
          DO 100 I= START,FINISH
          IF (CROSSC (I) .GT. MAX AMPLITUDE) THEN
             MAX AMPLITUDE= CROSSC (I)
             MAX POINT= I
             ENDIF
  100     CONTINUE
C
C      Determines the differences either side of the maximum point and calculates the true
C      peak
C
       DIFFERENCE (1) = CROSSC (MAX POINT) - CROSSC (MAXPOINT - 1)
       DIFFERENCE (2) = CROSSC (MAX POINT + 1) - CROSSC (MAXPOINT)
       X ZERO = DIFFERENCE (1) / (DIFFERENCE (1) - DIFFERENCE (2))
       MAX POSITION= (FLOAT(MAX POINT) - 0.5) + X ZERO
       PEAK = (ZERO POINT - MAX POSITION) * 0.01
       RETURN
       STOP ' No peak in cross-correlation function '
       END
C
C
C
C
C
C
```

```
C*******************************************************************************
C
C     SUBROUTINE GET DELAY (S1, S2, DELAY, RATE, NO POINTS, NO DELAYS, INTERVAL, SUB LENGTH)
C
C     Computes the relative time delay (in the frequency domain) between series S1 and S2
C     (sampling rate = RATE, number of data points = NO POINTS) as a function of time along
C     the series.  A window of length SUB LENGTH is used at intervals determined by
C     INTERVAL.  The time delay is stored in a series DELAY (sampling rate = RATE, number of
C     data points = NO DELAYS)
C
C*******************************************************************************
      SUBROUTINE GET DELAY (S1, S2, DELAY, RATE, NO POINTS, NO DELAYS, INTERVAL, SUB LENGTH)
C
C     Arguments:
      INTEGER NO POINTS, NO DELAYS
      INTEGER INTERVAL, SUB LENGTH
      INTEGER S1 (*), S2 (*)
      REAL DELAY (*)
      REAL RATE
C
C     Constants
      INTEGER MAX SUB LENGTH
      PARAMETER ( MAX SUB LENGTH= 64 )
      INTEGER FIRST
      PARAMETER ( FIRST= 4 )
C
C     Variables:
      INTEGER POWER
      INTEGER LAST
      INTEGER START OFFSET
      REAL SUB1 (MAX SUB LENGTH), SUB2 (MAX SUB LENGTH)
      REAL XSPECTRUM (MAX SUB LENGTH)
      REAL PHASE (MAX SUB LENGTH/2)
      REAL COHERENCE (MAX SUB LENGTH / 2)
      REAL A XY (MAX SUB LENGTH / 2), A XX (MAX SUB LENGTH / 2), A YY (MAX SUB LENGTH / 2)
      REAL WEIGHT, SQ COHERENCE
      REAL SUM PHASE, SUM FREQUENCY, SLOPE
C
C     Check that the window length is not too long for the series being analysed
C
      IF (SUB LENGTH .GT. MAX SUB LENGTH) THEN
         WRITE (7,'(A)') ' SUB LENGTH too long.  Increase MAX SUB LENGTH in subroutine GET
     1DELAY and GET TIME DELAY.'
         ENDIF
      START OFFSET= 0
      J=1
C
C     Extract sub-series determined by the position and size of the window (START OFFSET
C     and SUB LENGTH)
C
410   IF (START OFFSET .LE. NO POINTS - SUB LENGTH) THEN
            DO 420 I= 1, SUB LENGTH
            SUB1 (I)= S1 (START OFFSET + I)
420         SUB2 (I)= S2 (START OFFSET + I)
C
C     Cosine taper sub-series to reduce edge effects
C
         CALL CSTPR (SUB1, SUB LENGTH, 50.)
         CALL CSTPR (SUB2, SUB LENGTH, 50.)
C
C     Fourier transform the sub-series
C
         POWER= NINT (ALOG10(FLOAT(SUB LENGTH)) / ALOG10(2.0))
         CALL RFFT  (POWER, SUB1, +1.)
         CALL RFFT  (POWER, SUB2, +1.)
C
C     Calculate the cross-spectrum
C
         CALL GET X SPECTRUM (SUB1, SUB2, XSPECTRUM, SUB LENGTH)
C
C     Calculate the phase and unwrap it
C
         CALL GET PHASE (XSPECTRUM, PHASE, SUB LENGTH)
C         CALL UNWRAP PHASE (PHASE, SUB LENGTH / 2)
```

```
C
C     Smooth the phase
C
         CALL SMOOTH (PHASE, SUB LENGTH / 2)
         I= 1
C
C     Calculate the amplitude of the cross-spectrum and the two sub-series and smooth them
C
430      IF (I .LE. SUB LENGTH / 2) THEN
            A XY(I)= SQRT (AMPLITUDE (XSPECTRUM (2*I-1), XSPECTRUM (2*I)))
            A XX(I)= AMPLITUDE (SUB1 (2*I-1), SUB1 (2*I))
            A YY(I)= AMPLITUDE (SUB2 (2*I-1), SUB2 (2*I))
            I= I+1
            GO TO 430
            ENDIF
         CALL SMOOTH (A XX, SUB LENGTH / 2)
         CALL SMOOTH (A YY, SUB LENGTH / 2)
         CALL SMOOTH (A XY, SUB LENGTH / 2)
         I=1
C
C     Calculate the coherence
C
435      IF (I .LE. SUB LENGTH / 2) THEN
            COHERENCE (I)=  A XY(I) / SQRT (A XX(I) * A YY(I))
            I=I+1
            GO TO 435
            ENDIF
C
C     Calculate the slope of the phase weighted by the coherence
C
         SUM PHASE= 0.0
         SUM FREQUENCY= 0.0
         I= FIRST
         LAST= SUB LENGTH / 3
431      IF (I .LE. LAST) THEN
            IF (COHERENCE(I) .GE. 1.0) COHERENCE(I)= 0.999999
            SQ COHERENCE= COHERENCE(I) * COHERENCE(I)
            WEIGHT= (SQ COHERENCE * SQ COHERENCE)/(1. - (SQ COHERENCE * SQ COHERENCE))
            SUM PHASE= SUM PHASE + (PHASE (I) * WEIGHT)
            SUM FREQUENCY= SUM FREQUENCY + (WEIGHT * (I-1))
            I= I+1
            GO TO 431
            ENDIF
         SLOPE= SUM PHASE / SUM FREQUENCY
C
C     Determine the delay from the slope of the phase
C
         DELAY (J)= (SLOPE * SUB LENGTH) / (2. * 3.1415 * RATE)
         J=J+1
         START OFFSET= START OFFSET + INTERVAL
         GO TO 410
         ENDIF
            RETURN
      END
C
C
C
C
C
C
```

```
C*******************************************************************************
C
C     SUBROUTINE GET X SPECTRUM (S1, S2, XSPECTRUM, LENGTH)
C
C     Computes cross spectrum of spectra S1, S2 of LENGTH (compacted) points and places
C     result in XSPECTRUM
C
C*******************************************************************************
      SUBROUTINE GET X SPECTRUM (S1, S2, XSPECTRUM, LENGTH)
C
C     Arguments
      INTEGER LENGTH
      REAL S1 (LENGTH), S2 (LENGTH), X SPECTRUM (LENGTH)
C
C
      X SPECTRUM (1)= S1(1) * S2(1)
      X SPECTRUM (2)= S1(2) * S2(2)
      I= 3
510   IF (I .LT. LENGTH) THEN
         X SPECTRUM (I)=   S1(I) * S2(I) + S1(I+1) * S2(I+1)
         X SPECTRUM (I+1)= S1(I) * S2(I+1) - S1(I+1) * S2(I)
         I=I+2
         GO TO 510
         ENDIF
      RETURN
      END
C
C
C
C
C
C
C*******************************************************************************
C
C     SUBROUTINE GET PHASE (SERIES, PHASE, LENGTH)
C
C     Calculates phase of (complex) spectrum SERIES, of length LENGTH and places result in
C     the (real) series PHASE of length LENGTH/2
C
C*******************************************************************************
      SUBROUTINE GET PHASE (SERIES, PHASE, LENGTH)
C
C     Arguments
      INTEGER LENGTH
      REAL SERIES (LENGTH), PHASE (LENGTH/2)
C
C
      PHASE (1)= 0.
      I= 2
610   IF (I .LE. LENGTH / 2) THEN
         PHASE (I)= ATAN2 (SERIES (I*2), SERIES (I*2-1))
         I= I+1
         GO TO 610
         ENDIF
      RETURN
      END
C
C
C
C
C
C
```

```
C*****************************************************************************
C
C     SUBROUTINE SMOOTH (SERIES, LENGTH)
C
C     Applies a 5-point triangular filter to SERIES of length LENGTH
C
C*****************************************************************************
      SUBROUTINE SMOOTH (SERIES, LENGTH)
C
C     Arguments
      INTEGER LENGTH
      REAL SERIES (LENGTH)
C
C     Arrays
      REAL MEMORY (-2:2)
C
C
         DO 710 I= -2, 2
710      MEMORY(I)= SERIES(I+3)
      SERIES(1)= 0.5 * (MEMORY(-2) + 0.667 * MEMORY(-1) + 0.333 * MEMORY(0))
      SERIES(2)= 0.375 * (MEMORY(-1) + 0.667 * (MEMORY(-2) + MEMORY(0)) + 0.333 * MEMORY(1))
      I= 3
720   IF (I+2 .LE. LENGTH) THEN
            DO 730 J= -2, 1
730         MEMORY(J)= MEMORY(J+1)
         MEMORY(2)= SERIES(I+2)
         SERIES(I)= 0.333 * (MEMORY(0) + 0.667 * (MEMORY(-1) + MEMORY(1)) + 0.333 *
     1              (MEMORY(-2) + MEMORY (2)))
         I= I+1
         GO TO 720
         ENDIF
      SERIES(LENGTH-1)= 0.375 * (MEMORY(1) + 0.667 * (MEMORY(2) + MEMORY(0)) + 0.333 *
     1                  MEMORY(-1))
      SERIES(LENGTH)= 0.5 * (MEMORY(2) + 0.667 * MEMORY(1) + 0.333 * MEMORY(0))
      RETURN
      END
C
C
C
C
C
C
C*****************************************************************************
C
C     FUNCTION AMPLITUDE (X, Y)
C
C     Calculates the amplitude of the complex number X + iY
C
C*****************************************************************************
      FUNCTION AMPLITUDE (X, Y)
C
C     Arguments
      REAL X, Y
C
C
      AMPLITUDE=  X*X + Y*Y
      RETURN
      END
C
C
C
C
C
C
```

```
      SINTH = SIN(THETA/2.0)
      WSTPR = -2.0*SINTH*SINTH
      WSTPI = SIN(THETA)
      WR = 1.0
      WI = 0.0
      DO 9 M = 1,MMAX,2
      DO 8 I = M,N,ISTEP
      J = I + MMAX
      TEMPR = WR*DATA(J) - WI*DATA(J+1)
      TEMPI = WR*DATA(J+1) + WI*DATA(J)
      DATA(J) = DATA(I) - TEMPR
      DATA(J+1) = DATA(I+1) - TEMPI
      DATA(I) = DATA(I) + TEMPR
 8    DATA(I+1) = DATA(I+1) + TEMPI
      TEMPR = WR
      WR = WR*WSTPR - WI*WSTPI + WR
 9    WI = WI*WSTPR + TEMPR*WSTPI + WI
      MMAX = ISTEP
      GO TO 6
 10   RETURN
      END
C
C
C
C
C
C
C*******************************************************************************************
C
C     SUBROUTINE UNWRAP PHASE  (PHASE, LENGTH)
C
C     Corrects the phase (PHASE) for any wrap-over.
C
C*******************************************************************************************
      SUBROUTINE UNWRAP PHASE  (PHASE, LENGTH)
C
C     Constants
      REAL PI
      PARAMETER ( PI= 3.1415 )
C
C     Arguments
      INTEGER LENGTH
      REAL PHASE (LENGTH)
C
C     Variables
      INTEGER FACTOR
      REAL DIFFERENCE
C
      I=2
910   IF (I .LE. LENGTH) THEN
         DIFFERENCE= PHASE (I) - PHASE (I-1)
         FACTOR= NINT (DIFFERENCE / (2. * PI))
         PHASE (I)= PHASE (I) - FACTOR * 2. * PI
         I= I+1
         GO TO 910
         ENDIF
      RETURN
      END
C*******************************************************************************************
```

Appendix 3

A.3.1 Introduction

Time delay measurements can be carried out in either the time domain or the frequency domain and in section 4.3.2 a comparison is made of the two different methods. The aim of this appendix is to explain the frequency domain method in more detail and to illustrate it throughout. It is also shown, by using a weighting system comparible with that implicitly used in the time domain method, that the two methods can produce very similar results.

A.3.2 Frequency Domain Method

The main principles of how the frequency domain is used to evaluate the time delay are contained in section 4.2.4.

After taking the Fourier transform of the windowed signals, the cross-spectrum is calculated, an example of which is shown in fig. A-1. To measure the time delay, the phase, as a function of frequency, is extracted from the cross-spectrum and its gradient is estimated using a least squares procedure. The phase of the cross-spectrum in fig. A-1 is plotted out in fig. A-2. It can be seen that as the frequency increases the phase begins to oscillate and lose its stability. If the gradient estimation were to use all frequencies equally such unstable values could greatly distort the result. For this reason a weighting system is used to discriminate against such instability. It is based upon the coherence, as given in equation 4.7, with a weighting function as given in equation 4.8. In fig. A-3 the coherence corresponding to the cross-spectrum of fig. A-1 is plotted. As can be seen, the coherence stays at, or close to, 1 from 5-30Hz but then it also begins to oscillate and in comparing fig. A-2 and fig. A-3 it can be seen that the phase instability roughly corresponds with these oscillations. However, the correspondence is not perfect, with the result that the some of the less stable phase values will receive a relatively high weighting value and thus distort the gradient estimation. This is the main cause of the scatter observed in section 4.3.2.

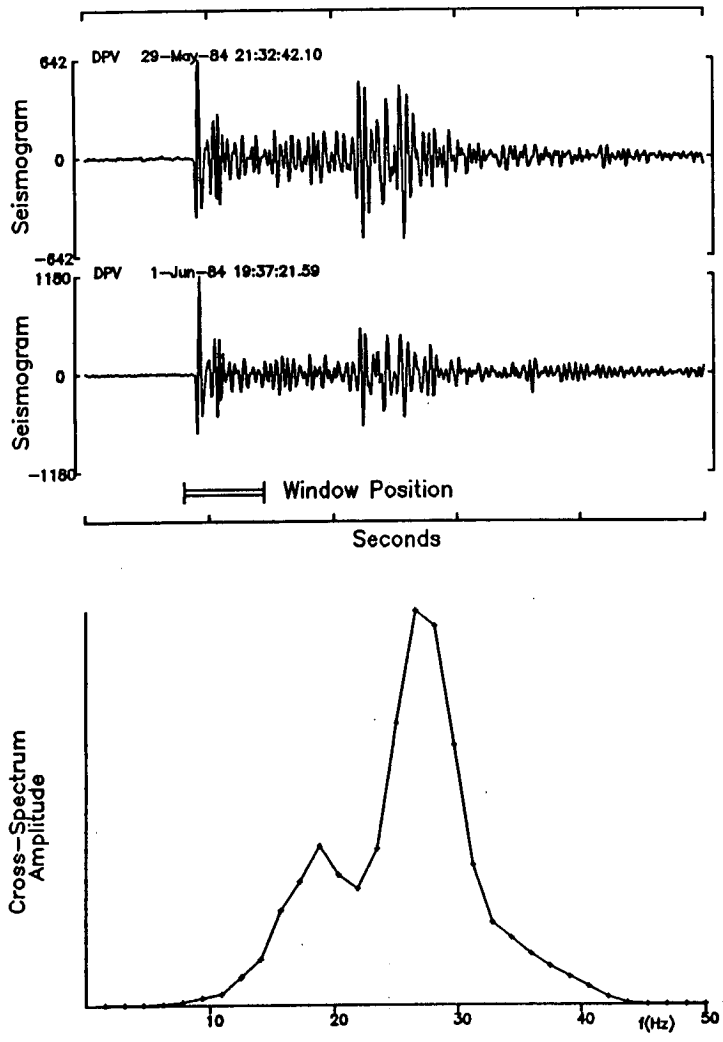

Fig. A-1 - Cross-spectrum amplitude as a function of frequency.

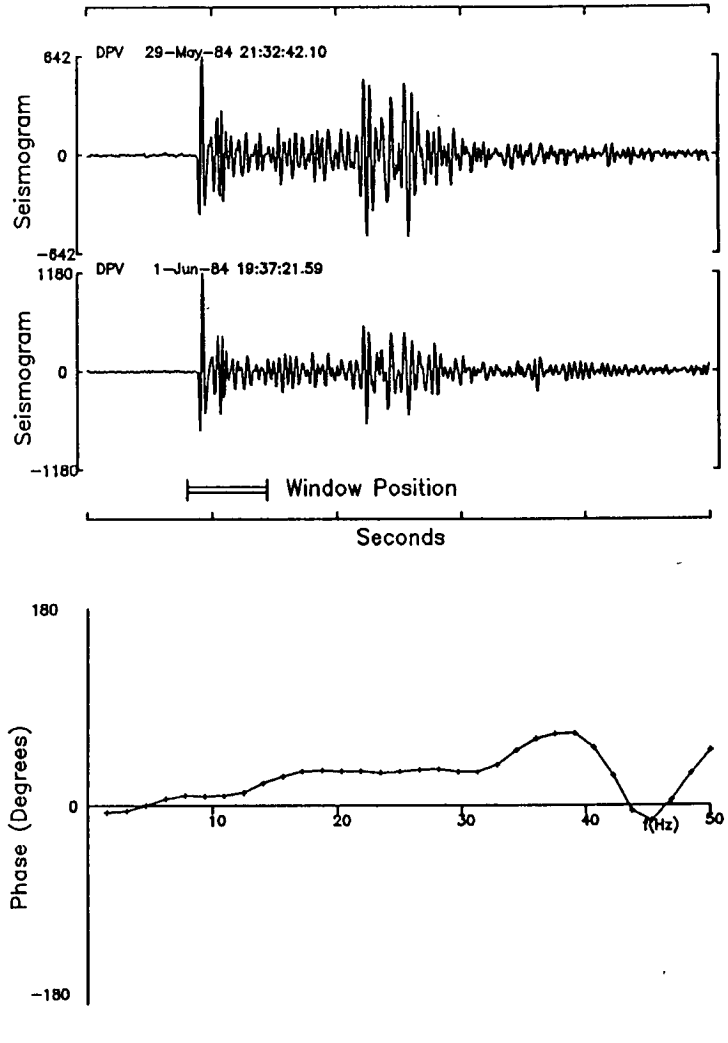

Fig. A-2 - Phase component of the cross-spectrum of fig. A-1.

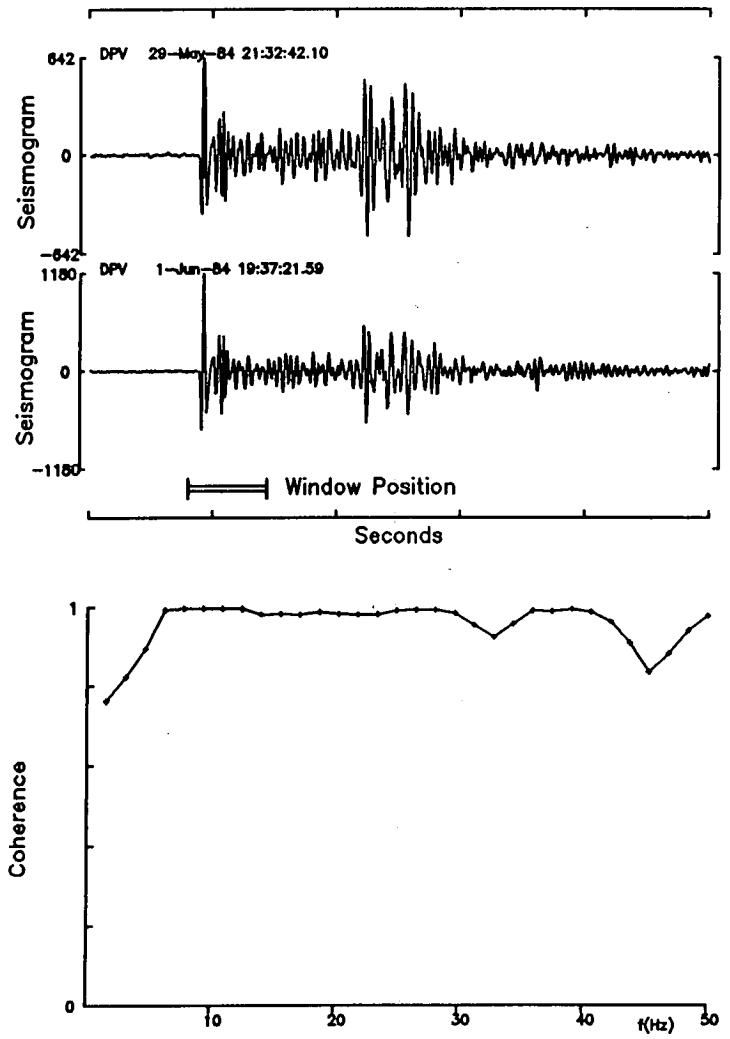

Fig. A-3 - Coherence as a function of frequency calculated using a five-point smoothing function.

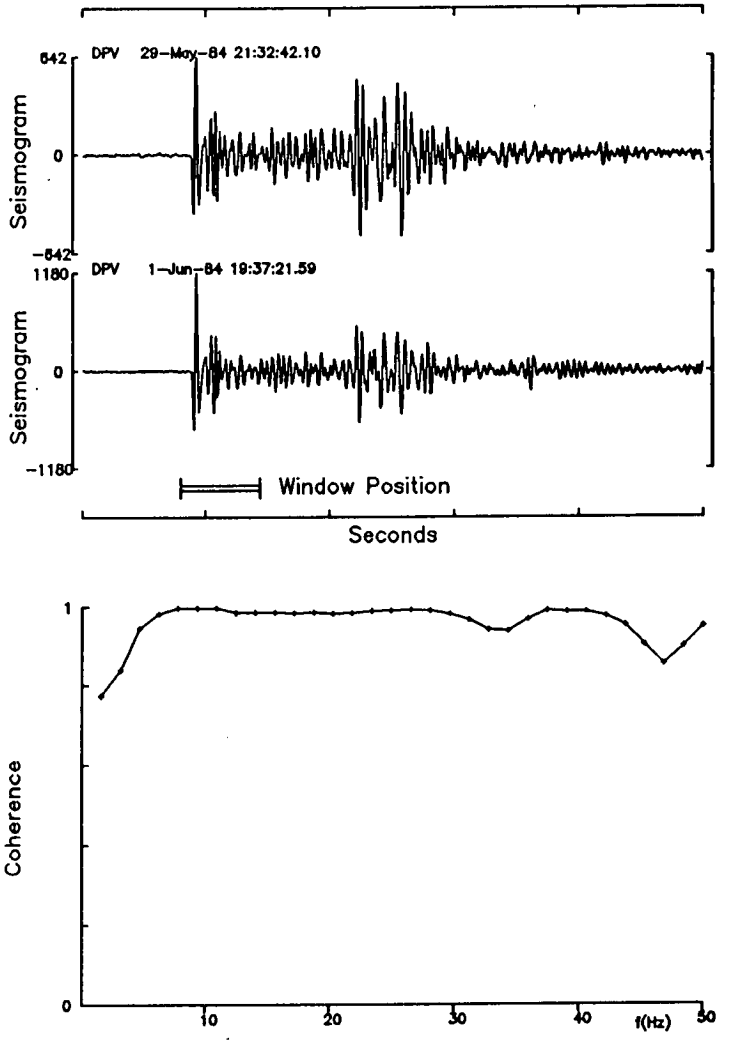

Fig. A-4 - Coherence as a function of frequency calculated using a seven-point smoothing function.

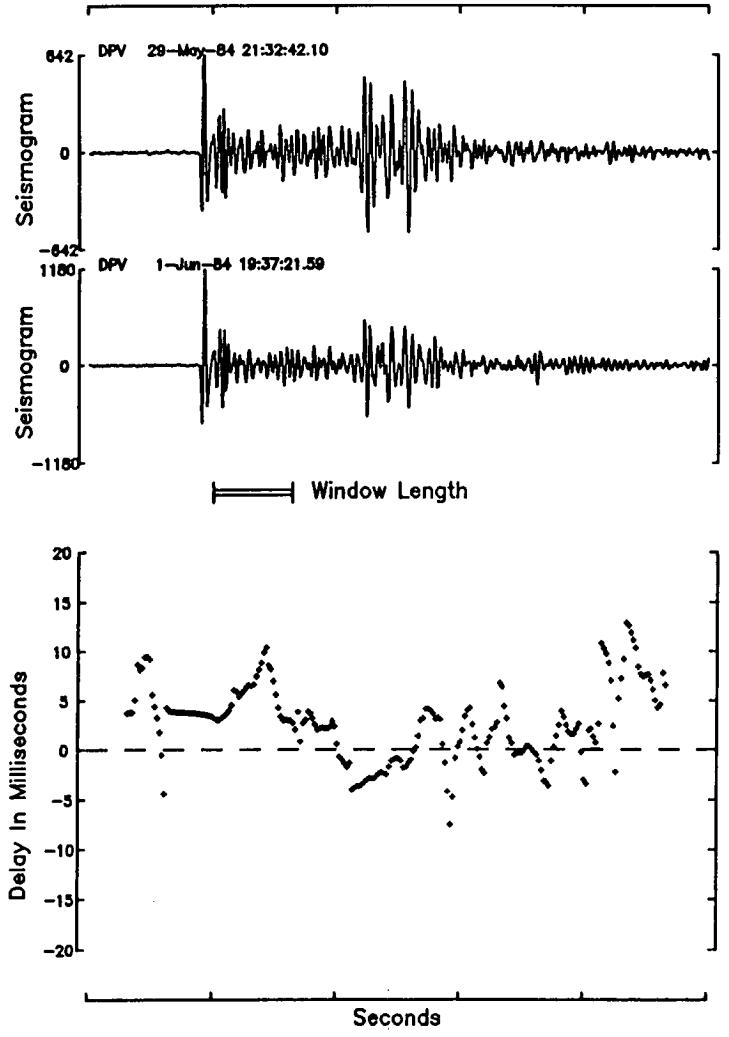

Fig. A-7 - Time delay function calculated in the frequency domain using a seven-point smoothing function.

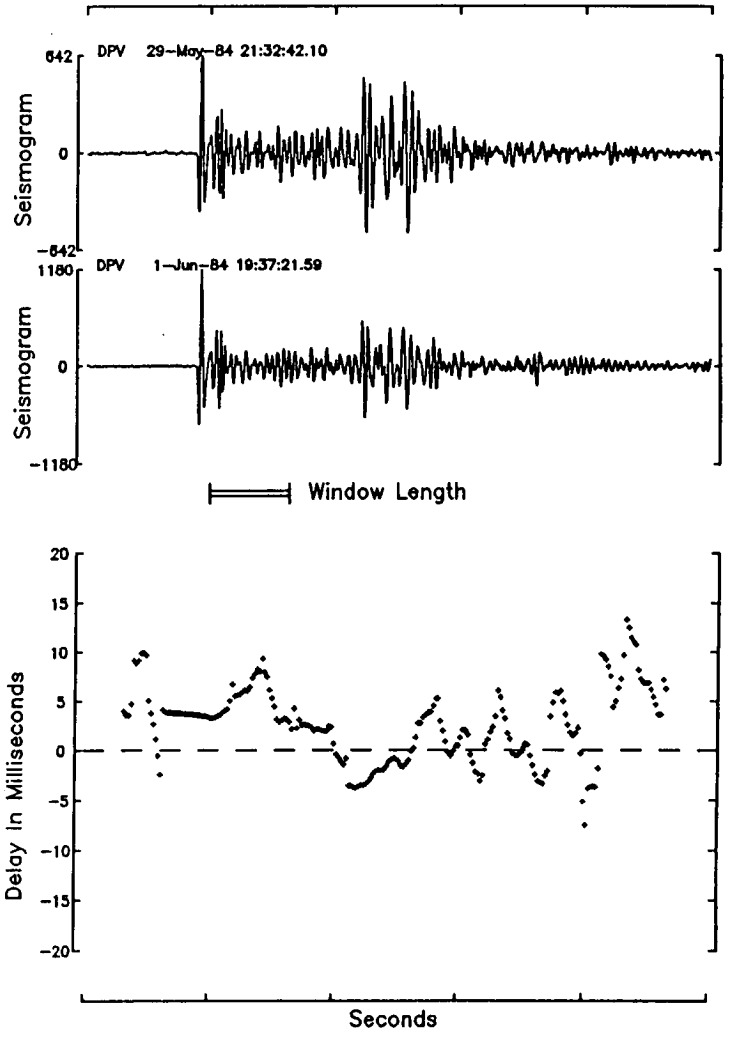

Fig. A-8 - Time delay function calculated in the frequency domain using a nine-point smoothing function.

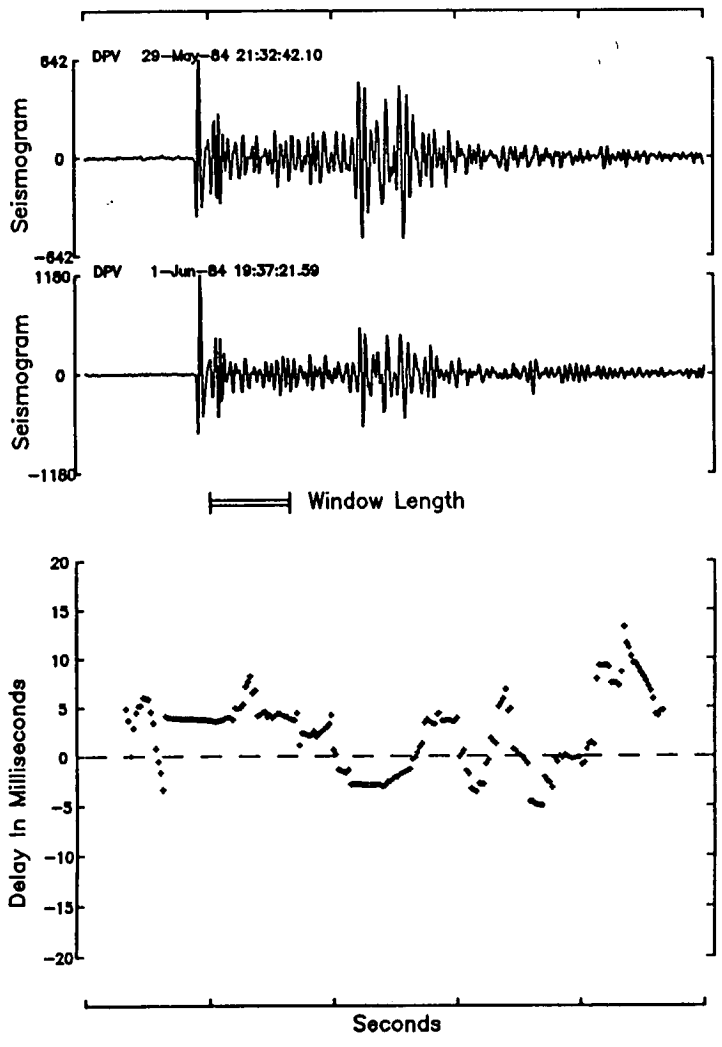

Fig. A-9 - Time delay function calculated in the frequency domain using an amplitude weighting function.

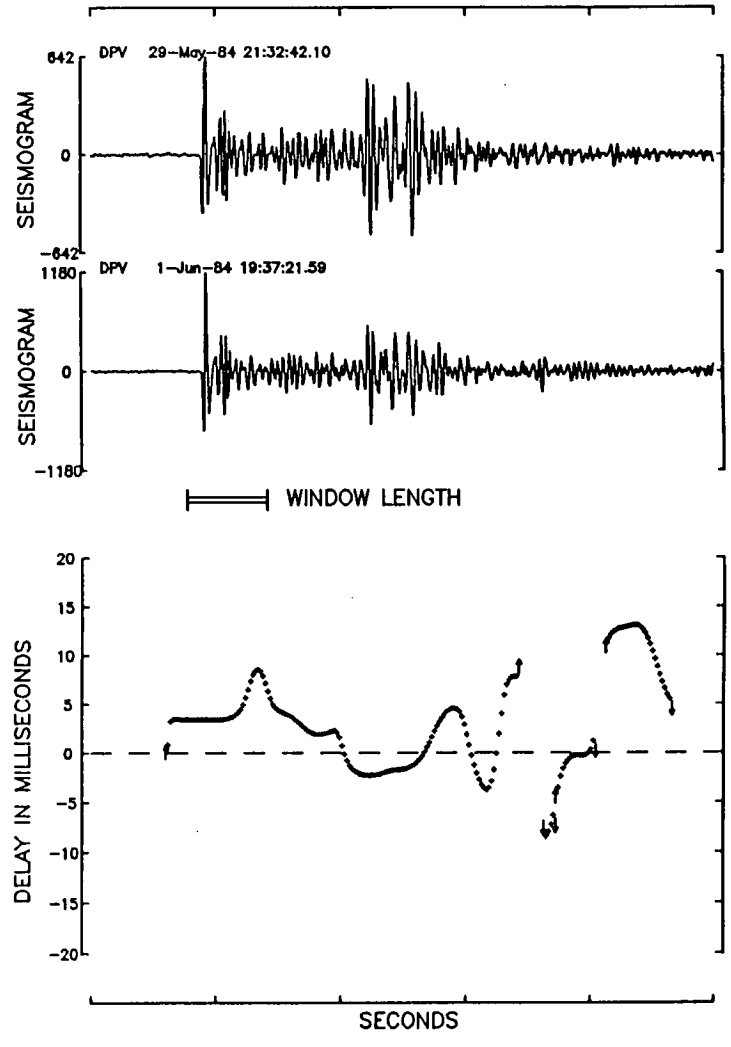

Fig. A-10 - Time delay function as calculated in the time domain.